N7678029

DEVELOPMENT OF A FAIL SAFE DESIGN OXIDATION RESISTANT REINFORCED CARBON SYSTEM FOR THE WING LEADING EDGE OF A SPACE SHUTTLE VEHICLE

NASA-JSC CONTRACT NAS9-12763

PHASE III FINAL REPORT

VOLUME IV

APPENDIX B

STRUCTURAL AND DYNAMIC ANALYSES

VOUGHT SYSTEMS DIVISION
LTV AEROSPACE CORPORATION
P.O. BOX 5907 · DALLAS, TEXAS 75222

APPENDIX B

STRUCTURAL AND DYNAMICS DESIGN INFORMATION RELEASES (DIR)

CONTENTS

T143-DIR-2-02	Comparison of VMSC NASTRAN Leading Edge Thermoelastic Equilibrium vs NASA/MSC NASTRAN
T143-DIR-2-06	Phase III "Fail Safe" Leading Edge Material Design Allowables
T143-DIR-2-08	Phase III Oxidized Leading Edge Structural Analysis
T143-DIR-2-09	Phase III Fail Safe Leading Edge Strucutral Analysis
T143-DIR-2-12	Ultimate Static Loads Distribution and Preliminary Canted H/S Panel Analysis - Leading Edge Support Structure
T143-DIR-2-17	Leading Edge Support Structure Strucutral Analysis
T143-DIR-3-1	Dynamic Analyses and Testing of the Shuttle Wing Leading Edge Thermal Insulation System

SEP 1976
RECEIVED
NASA STI FACILITY
INPUT BRANCH

DESIGN INFORMATION [redacted] – RELEASE X74-10173

ODEL (S) AND EFF. COMPARISON OF VMSC NASTRAN LEADING EDGE THERMOELASTIC EQUILIBRIUM VS. NASA/MSC NASTRAN SOLUTION - PHASE II	SYSTEM	DIR. NO. T143-DIR-2-02	REV.
		DATE 5-16-72	PAGE 1 OF 7
		REF. G. O. NUMBER 3357-AA-1160	

Fill in block below for Information Request

O _____ GROUP _____

EQ. BY _____ GROUP _____

EASON _____

TV ONLY ☐ BWR ☐ BUWEPS ☐ ☐ _____

Fill in block below for Information Release

IN REPLY TO DIR. NUMBER _____

REL. TO D. M. While GROUP 3-52000

PREPARED BY	DATE	CHECKED BY	DATE
R. D. Bennett	5/18/72	W C Agan	5/19/72
GROUP APP.	DATE	PROJ OFFICE	DATE
J. E. Brougham	5/22/72	A. Lang for D. While	5/22/72

C B. A. Forcht (3), G. B. Whisenhunt

ESIGN INFORMATION:

Ref. (A): DIR No. T143-DIR-2-01, "Verification of NASTRAN Leading Edge Thermoelastic Equilibrium - Phase II", dated 3 May 1972.

PURPOSE: The purpose of this DIR is to show a comparison between a VMSC NASTRAN Leading Edge solution and a NASA/MSC NASTRAN solution to the same problem. VMSC is currently using Level 11.1.4 NASTRAN and MSC is using Level 12.1 NASTRAN. Level 11.1.4 NASTRAN is a MacNeal-Schwendler Corp. development and is approximately two years newer than Level 12.1.

SUMMARY: The Level 11.1.4 solution shows external equilibrium (Ref. A, Sheets 3 and 4 of this DIR). The Level 12.1 solution does not yield a balanced solution (ref. sheets 5,6,& 7 of this DIR).

A similar comparison of a static load problem, with no thermal loadings, yields the identical results for both levels of NASTRAN, NASA/MSC's 12.1 and VMSC's 11.1.4.

52042 R1

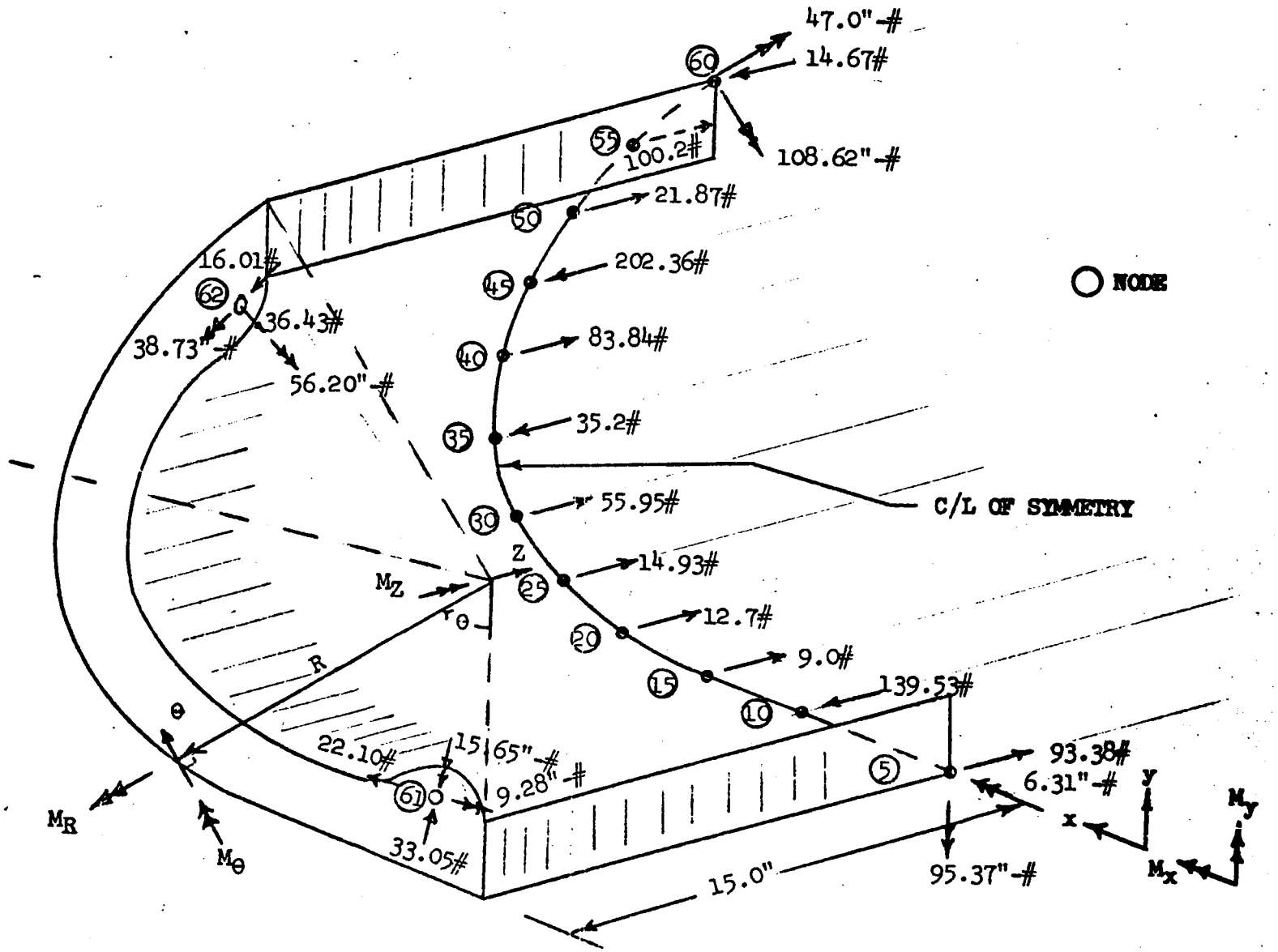

FIGURE 1 LEADING EDGE - THERMOELASTIC REACTIONS
VMSC NASTRAN LEVEL 11.1.4 SOLUTION (REF. A)

TABLE I

VMSC-NASTRAN LEVEL 11.1.4 SOLUTION (REF. A)

RPP LEADING EDGE STRESS ANALYSIS CONFIGURATION C-THERMOELASTIC AUGUST 3, 1971 PAGE 1

MAX TEMPERATURES - 400 SEC.

SUBCA

FORCES OF SINGLE-POINT CONSTRAINT

POINT ID.	TYPE	T1 (R) -lbs	T2 (θ) -lbs	T3 (Z) -lbs	R1 (Mr) -in-lbs	R2 (Mθ) -in-lbs	R3 (Mz) -in-lbs
5	G	0.0	0.0	9.338220E 01	9.537025E 01	6.312739E 00	0.0
10	G	0.0	0.0	-1.395276E 02	-8.936155E-02	-1.552689E 00	0.0
15	G	0.0	0.0	8.998474E 00	-5.324613E-01	-1.433645E 00	0.0
20	G	0.0	0.0	1.270053E 01	-2.553616E-01	-4.758933E-01	0.0
25	G	0.0	0.0	1.493031E 01	2.635300E-03	5.882251E-02	0.0
30	G	0.0	0.0	5.594893E 01	2.540344E-02	5.315495E-02	0.0
35	G	0.0	0.0	-3.520456E 01	-8.261496E-02	-4.371037E-01	0.0
40	G	0.0	0.0	8.384256E 01	1.701343E-02	-8.857174E-01	0.0
45	G	0.0	0.0	-2.023564E 02	1.622203E-01	-8.119450E-01	0.0
50	G	0.0	0.0	2.187326E 01	5.014896E-02	-3.979540E-01	0.0
55	G	0.0	0.0	1.001979E 02	6.719798E-02	-2.616141E-01	0.0
60	G	0.0	0.0	-1.469336E 01	-1.086173E 02	4.700349E 01	0.0
61	G	-3.335132E 01	2.209766E 01	0.0	1.564713E 01	-9.288818E 00	0.0
62	G	-3.643164E 01	-1.601563E 01	0.0	-5.620084E 01	-3.872653E 01	0.0

FORCE BALANCE Ref. Table II for angles.

ΣF_x = R61 sin 6.25 + θ61 cos 6.25 + R62 sin 51 - θ62 cos 51 =-33.351(.109) + 22.098 (.994) - 36.432 (.778) + 16.016(.629)
= -3.635 + 21.965 - 28.344 + 10.074 =
ΣF_x = 0.060 lbs
ΣF_y = -R61 cos 6.25 + θ61 sin 6.25 + R62 cos51 +θ62 sin51 = 33.351(.994) + 22.098(.109) - 36.432(.629) - 16.016(.778)
= 33.151 + 2.409 - 22.916 - 12.460 =
ΣF_y = 0.184 lbs
ΣF_z = 0.090 lbs (sum column T3)

TABLE II - FORCE AND MOMENT EQUILIBRIUM

(Ref. Figure 1 and Table I)

VMSC NASTRAN LEVEL 11.1.4 SOLUTION (REF. A)*

NODE	FORCE Lbs.	Y In.	M_x In/Lbs	M_R M_θ In/Lbs	θ deg	M_{R_x} M_{θ_x} In/Lbs	M_{T_x} In/Lbs	X In.	M_y In/Lbs	M_R M_θ In/Lbs	θ deg	M_{R_y} M_{θ_y} In/Lbs	In
5	93.38	0	0	6.3	0	6.31	6.	0	0	-95.37	0		
10	-139.53	1.31	-183.				-183.	4.82	673.				
15	9.0	3.06	28.				28.	9.52	-86.				
20	12.7	4.68	59.				59.	12.61	-160.				-
25	14.93	6.55	98.				98.	14.95	-223.				-
30	55.95	8.88	497.				497.	16.88	-944.				-
35	-35.20	11.18	-394.				-394.	17.82	627.				
40	83.84	13.68	1147.				1147.	18.03	-1511.				-1
45	-202.36	16.12	-3262.				-3262.	17.61	3563.				3
50	21.87	18.37	402.				402.	16.64	-364.				-
55	100.2	20.77	2081.				2081.	14.83	-1486.				-1
60	-14.69	23.95	-352.	-47.	sin 45.5	-33.5	-386.	11.01	162.	47.0	cos 45.5	32.9	
				-108.6	cos 45.5	-76.1	-76.			-108.6	sin 45.5	-77.5	-
61*	(1) 33.1	15.0	498.	-9.28	cos 6.25	-9.22	489.	(5)	54.0	-9.3	sin 6.25	-1.0	
	(2)	15.0	36.	15.65	sin 6.25	1.7	38.	(6)	-329.	-15.7	cos 6.25	-15.6	-
62*	(3) -12.5	15.0	-188.	38.73	sin 51°	30.1	-158.	(7)	344.	-38.7	cos 51°	-24.4	
	(4) -22.9	15.0	-344.	-56.20	cos 51°	-35.4	-309.	(8)	-187.	-56.	sin 51°	-43.7	-

ΣF_y = 0.3 Lbs.

ΣM_{T_X} (+) 4845
(-) 4768
87.

ΣM_{T_Y} (-) (+)

(1) -(-33.35) cos 6.25 = 33.1
(2) 22.10 (sin 6.25) = 2.4
(3) (-16.01) sin 51° = -12.5
(4) (-36.43) cos 51° = -22.9
(5) 33.35 sin (6.25) (15.0) = 54.0
(6) -22.1 (cos 6.25) (15.0) = -329.0
(7) 36.43 (cos 51°) (15.0) = 344.0
(8) -16.01 (sin 51°) (15.0) = -187.0

ΣF_{NODES} (5 thru 60) = +.09#

(% ERROR) M_{T_X} = $\left(\frac{87}{4885}\right)$ = 1.8%

(% ERROR) M_{T_y} = $\left(\frac{93}{5523}\right)$ = 1.7%

* Minor corrections have been incorporated since release of Ref. (A)

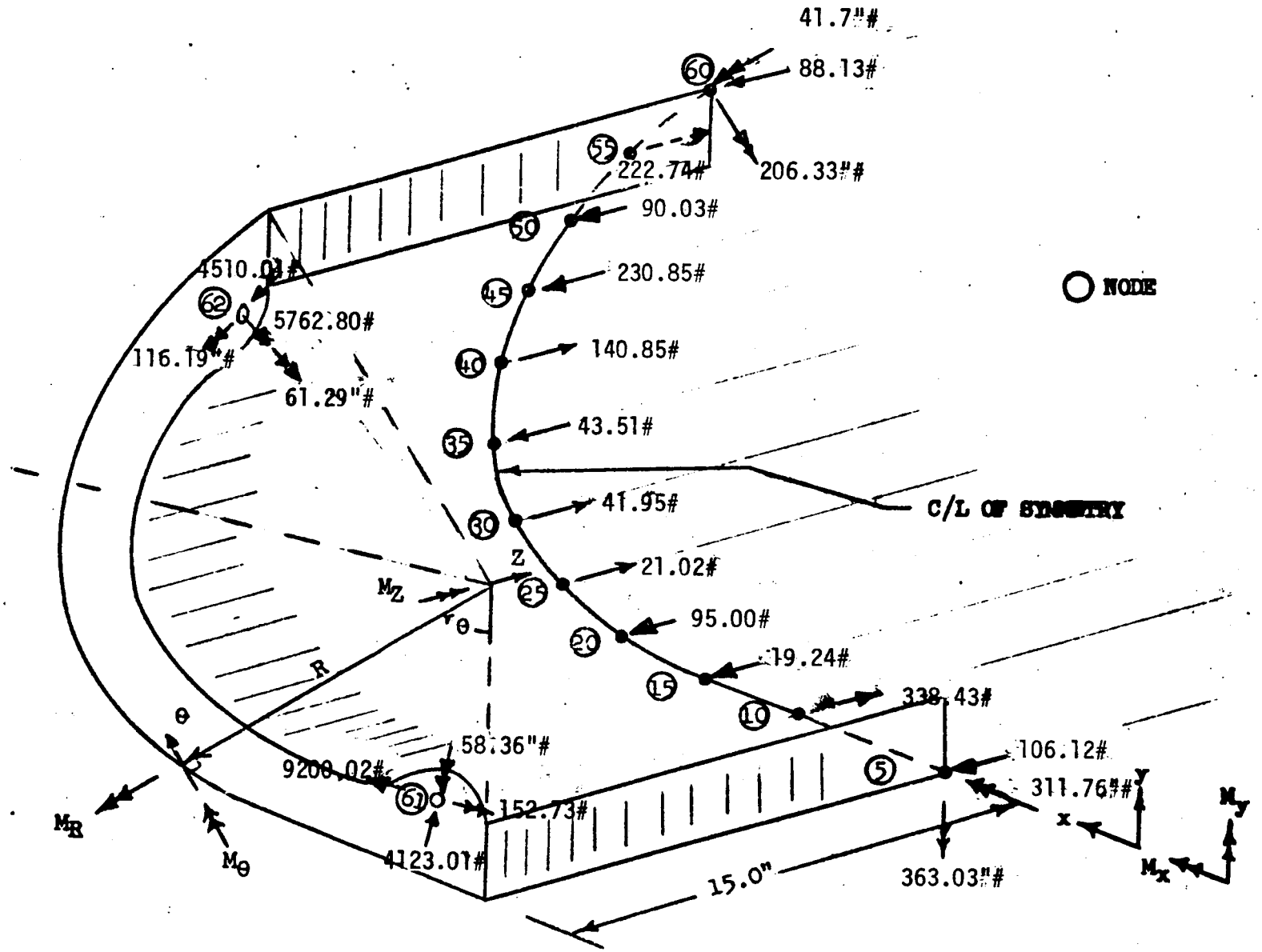

FIGURE 2 LEADING EDGE - THERMOELASTIC REACTIONS
NASA/MSC NASTRAN LEVEL 12.1 SOLUTION

TABLE III
NASA/MSC NASTRAN LEVEL 12.1 SOLUTION

'P LEADING EDGE STRESS ANALYSIS CONFIGURATION C-THERMOELASTIC MAY 12, 1972 PAGE
IX TEMPERATURES - 400 SEC.

SUB

F O R C E S O F S I N G L E - P O I N T C O N S T R A I N T

INT ID.	TYPE	T1 (R~lbs)	T2 (θ~lbs)	T3 (Z~lbs)	R1 (M_R~inlbs)	R2 (M_θ~inlbs)	R3 (M_Z
5	G	.0	.0	-1.061180+02	3.630332+02	3.117655+02	.0
10	G	.0	.0	3.384271+02	-2.546645-01	-2.782865+00	.0
15	G	.0	.0	-1.923742+02	1.149358+00	2.853845+00	.0
20	G	.0	.0	-9.500304+01	5.637488-01	8.412060-01	.0
25	G	.0	.0	2.102379+01	-1.478079-01	-2.945202-01	.0
30	G	.0	.0	4.195383+01	8.001149-02	7.611407-01	.0
35	G	.0	.0	-4.351381+01	3.117055-01	1.579575+00	.0
40	G	.0	.0	1.408469+02	-2.807097-01	3.034585+00	.0
45	G	.0	.0	-2.308502+02	-5.614398-01	2.760750+00	.0
50	G	.0	.0	-9.002701+00	-1.126701+00	5.645289+00	.0
55	G	.0	.0	2.227401+02	-3.711374-01	2.348213+00	.0
60	G	.0	.0	-8.813245+01	-4.167957+01	2.063281+02	.0
61	G	4.123013+03	9.200245+03	.0	5.835608+01	-1.527312+02	.0
62	G	-5.762802+03	-4.510092+03	.0	-6.129068+01	-1.161886+02	.0

FORCE BALANCE Ref. Table IV for angles.

ΣF_x = R61 sin 6.25 + θ61 cos6.25 +R62 sin51 - θ62 cos51 = 4123.01(.109)+9200.24(.994) -5762.80(.778) +4510109(.629) =
= 449.41 + 9145.04 - 4483.46 + 2836.85 =
ΣF_x = 7947.84 lbs.

ΣF_y = -R61 cos6.25 + θ61 sin6.25 + R62 cos51 + θ62 sin51 = -4123.01(.994) + 9200.24(.109) - 5762.80(.629) -4510.01(.778) =
= -4098.27 + 1002.83 - 3624.80 - 3508.79 =
ΣF_y =-10,229.03 lbs.

ΣF_z = -1.708 lbs. (sum of column T3)

TABLE IV - FORCE AND MOMENT EQUILIBRIUM

(Ref. Figure 2 and Table III)

MSC NASTRAN LEVEL 12.1 SOLUTION

NODE	FORCE Y LBS.	Y In.	Mx In/Lbs.	M_R M_θ In/Lbs.	θ	M_{Rx} $M_{\theta x}$ In/Lbs.	M_{Tx} In/Lbs.
5	-106.11	0	0	311.76			311.8
10	338.43	1.31	443.34				443.3
15	-192.37	3.06	-588.65				-588.7
20	-95.0	4.68	-444.6				-444.6
25	21.02	6.55	137.68				137.7
30	41.95	8.88	372.52				372.5
35	-43.51	11.18	-486.44				-486.4
40	140.85	13.68	1926.8				1926.8
45	-230.85	16.12	-3721.3				-3721.3
50	-9.0	18.37	-165.3				-165.3
55	222.74	20.77	4626.3				4626.3
60	-88.13	23.95	-2110.7	-206.0	sin 45.5°	-146.9	-2257.6
			0	-41.6	cos 45.5°	-29.2	-29.2
61	(1) -4098.3	15.0	-61,474.0	-152.7	cos 6.25°	-151.8	-61,626
	(2) 1002.8	15.0	15,042.0	-58.36	sin 6.25°	6.4	15,048
62	(3) -3508.8	15.0	-52,500.	116.2	sin 51°	90.3	-52,410.
	(4) -3624.8	15.0	-54,500.	-6129	cos 51°	-38.6	-54,539

ΣF_y = -10,229 LBS.

(+) 22,916
(-) 176,268

ΣM_{Tx} = -153,352 In Lbs.

(1) -(4123.0) cos6.25 = -4098.3
(2) (9200) sin6.25 = 1002.8
(3) (-4510) sin 51 = -3508.8
(4) (-562) cos 51 = -3624.8

DESIGN INFORMATION [redacted] – RELEASE

6-20-

DEL (S) AND EFF. PHASE III "FAIL SAFE" LEADING EDGE MATERIAL	DIR. NO. T143-DIR-2-06		REV.
DESIGN ALLOWABLES	DATE June 9,1972	PAGE 1	OF 10
SYSTEM	REF. G. O. NUMBER 3357 AA 1160		

Fill in block below for Information Request	Fill in block below for Information Release
~~GROUP~~	IN REPLY TO DIR. NUMBER --
Q. BY ~~GROUP~~	REL. TO D. M. While GROUP 3-52000
ASON	PREPARED BY W. E. Agan DATE / CHECKED BY W E Agan DATE 6/19/7
V ONLY ☑ BWR ☐ BUWEPS ☐ ☐	GROUP APP. A.E. Brougham DATE 6/19/72 / PROJ OFFICE DATE 6/20/72

I. E. Harder, T. K. Henry, E. C. Matza, H. I. Knight, B. A. Forcht, G. B. Whisenhunt

SIGN INFORMATION:

REFERENCE: (A) Phase II Test Data from Southern Research - unpublished to date.

(B) VMSC Materials & Processes Laboratory notebook - unpublished.

(C) VMSC Final Oral Presentation at NASA/MSC on 20 April 1972.

(D) Determination of Shear Modulus, In-Plane for RPP-3, T143-TRA-028, dated 5/11/72.

(E) Results of Determination of Shear Modulus, In-Plane for RPP-3, T143-TIR-20001, dated 6/8/72.

(F) Phase II Final Report VMSC No. T143-5R-00124 dated 30 April 1972.

PURPOSE: The purpose of this DIR is to release RPP-3 material design allowables to be used in the Phase III "Fail Safe" Leading Edge structural analysis. The philosophy of a "Fail Safe" Leading Edge requires data on both coated and bare material.

DISCUSSION:

The enclosed material properties are the results of Phase II Leading Edge testing done both at VMSC and Southern Research Institute. The data points are based upon one to three tests of 13 ply thickness only. RPP properties vary with thickness. Extrapolation of material properties above and below the 13 ply thickness is based upon engineering judgment gained through numerous characterization tests prior to

and during Phases I and II. Accordingly, the data published herein is preliminary but, based on a limited statistical analysis, Reference (C), conservatively representative of final statistical design allowables that will be used in actual flight hardware design.

A list and discussion of the enclosed figures is given below.

FIGURE 1 - Elastic Moduli versus No. of Ply - Bare RPP-3

These curves present typical room temperature Young's Modulus for compression, tension, and flexure in the warp direction for 13 ply bare RPP-3. The single data points were obtained by Southern Research Institute (SRI) as control specimens during Phase II Leading Edge testing, Reference (A) and (F). The shape of th curves were determined from modulus data which was previously generated from several data points by in-house testing, Reference (B). The in-plane shear modulus was determined by in-house testing, Reference (D) and (E). The shear test specimen was coated 13 ply RPP-3 and the shear modulus was increased for the bare material by the ratio between bare and coated Young's Modulus in both tension and compression which is 1.30. Poisson's ratio was determined by SRI for coated 13 ply RPP-3 and is estimated to be the same for both coated and bare material. The elastic properties in the fill direction are approximately 75% of the warp direction properties, except the shear modulus which, because of its matrix dependency, is the same in either direction. The 75% relationship for elastic properties was derived from the SRI test data.

FIGURE 2 - Elastic Moduli versus No. of Ply - Coated RPP-3

These curves present typical room temperature Young's Modulus for compression, tension, and flexure in the warp direction for 13 ply coated RPP-3. The data points are based on three tests each and were obtained by SRI, except in-plane shear, during Phase II Leading Edge testing, References (A) and (F). The shape of the curves were determined by ratio of the bare modulus data of Figure 1 which was previously generated from several data points by in-house testing, Reference (B).

The in-plane shear modulus was determined for 13 ply coated RPP-3 by in-house testing, Reference (D) and (E). Poisson's ratio was determined by SRI for coated 13 ply RPP-3. Similar to the bare data, the fill direction properties are equal to 75% of the warp direction properties, except shear modulus.

FIGURE 3 - Coated and Bare Strength versus No. of Ply

The data for the strength curves were obtained from SRI Phase II Leading Edge testing, References (A) & (F)and early in-house testing, Reference (B). All curves and data are based on typical room temperature values divided by 1.5. The 1.5 reduction factor provides a design allowable approximately 10% lower than a "99/95" statistical design allowable projected from preliminary, but representative, flexure data gathered during Phase II characterization testing, Reference (C). The bare flexure data points at 5 and 9 ply were obtained during early in-house Phase II RPP inventory testing, Reference (B). These data along with SRI data at 13 ply were used to establish the shape of the flexure strength versus number of ply curve. This shape was ratioed to obtain the strength curves. For all strength data, except in-plane shear, the fill direction properties are equal to 60% of the warp direction properties. The 60% relationship for strength properties was derived from the SRI test data. The bare in-plane shear strength was not determined by test but was increased from the coated test data by the minimum ratio of bare to coated strength for tension and flexure, which was 1.2.

FIGURE 4 - Elastic Moduli versus Temperature

These curves show typical value elastic moduli in compression, tension, and flexure for coated RPP-3 as a function of temperature. The test data, References (A) and (F), is for warp direction material 13-ply thick. The fill direction moduli are equal to 75% of the warp direction moduli. For thicknesses other than 13-ply, the data in Figure 4 may be ratioed by the thickness-modulus relationship in Figure 2.

FIGURE 5 - Strength versus Temperature

Curves showing warp direction flexure, compression and tension strengths versus temperature are presented in Figure 5 for 13-ply coated RPP-3. Similar to the data in Figure 3, these data, References (A) and (F), have been divided by 1.5 to account for strength reductions required to achieve "99/95" design allowables. The fill direction strengths are equal to 60% of the warp direction strengths. For thicknesses other than 13-ply, the data in Figure 5 may be ratioed by the thickness-strength relationship in Figure 3.

FIGURE 6 - Interlaminar Strength versus Temperature

Interlaminar shear and tension strength at room and elevated temperature is presented in Figure 5. Again, all data are typical values divided by 1.5. The 13 ply RPP-3 coated specimens were tested by SRI, Reference (A). Because of the single plane interlaminar mode of failure within the matrix material, these data are applicable to all thicknesses of RPP-3, coated or bare.

FIGURE 1

ELASTIC MODULI Vs No. of PLY

MAT'L: BARE RPP-3
WARP DIRECTION
70°F

△ CURVE FIT DATA (TYPICAL VALUES), BASED ON ONE TEST EACH POINT - REF (A)

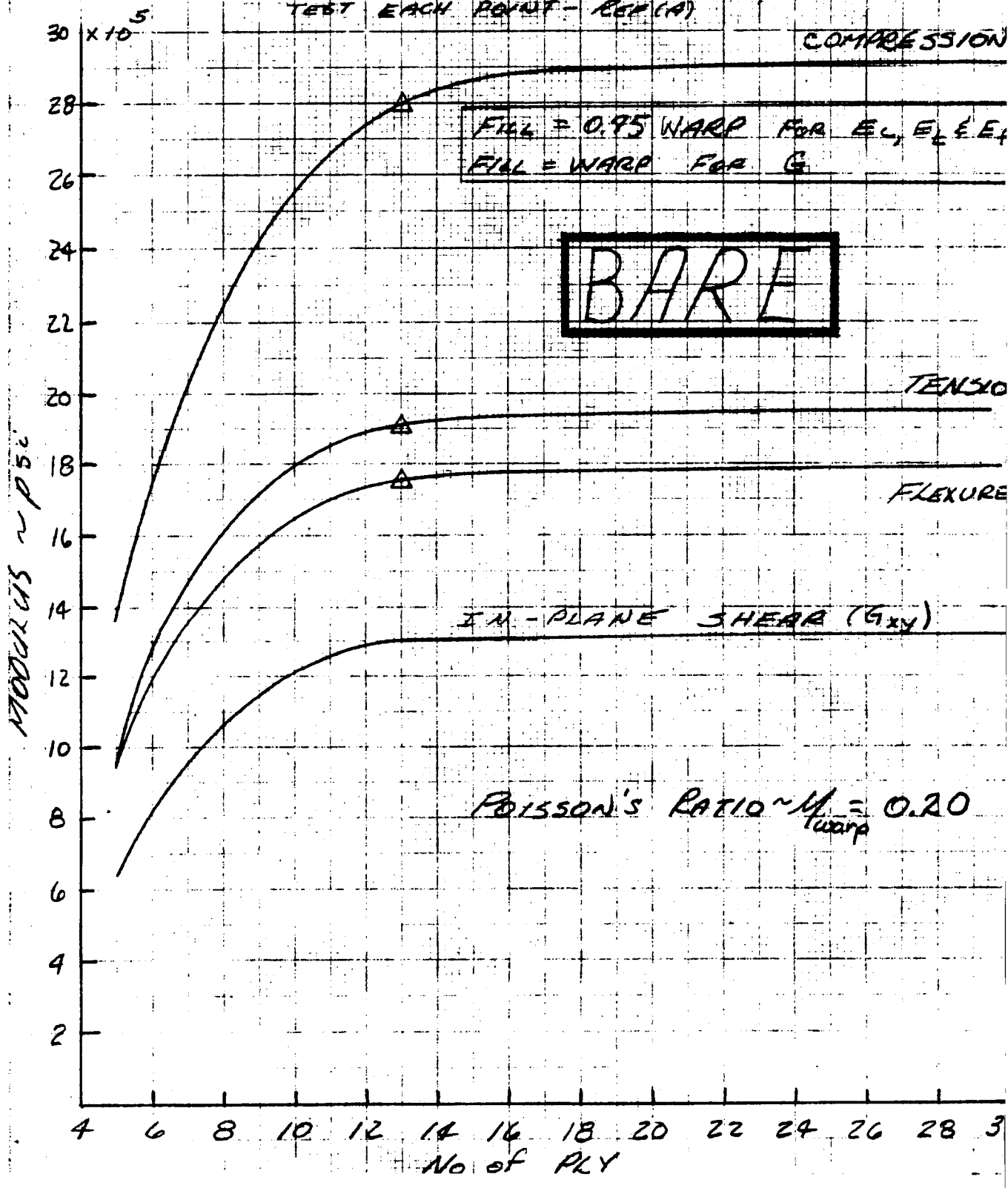

FIGURE 2

ELASTIC MODULI vs No. of PLY

MAT'L: 10/30/60 COATED RPP-3
WARP DIRECTION
70°F

△ CURVE FIT DATA (TYPICAL VALUES), BASED O
THREE TESTS EACH POINT, REF (A) & (C)

FILL = .75 WARP FOR E_c, E_t, & E_f
FILL = WARP FOR G

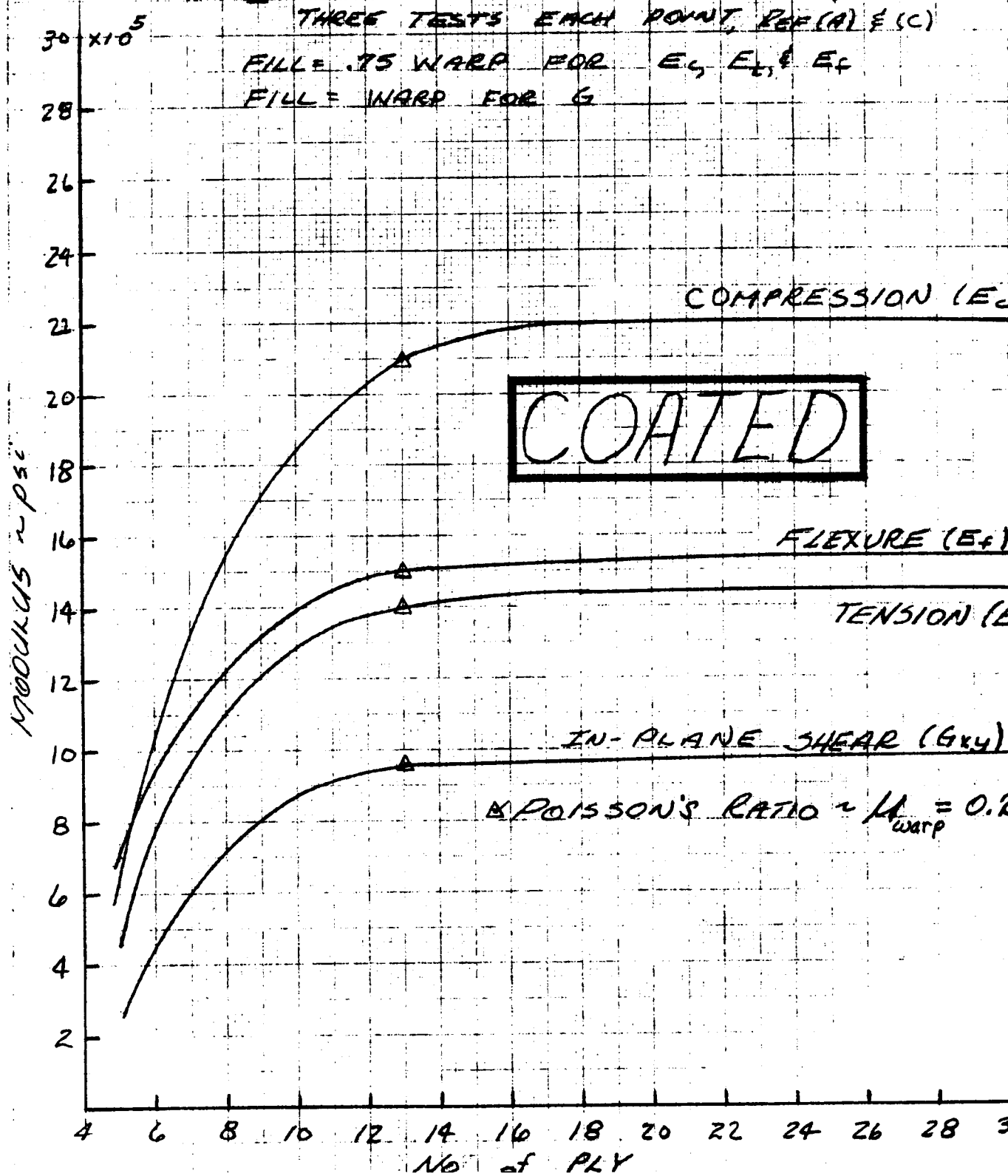

FIGURE 3

COATED & BARE STRENGTH VS No. of PLY

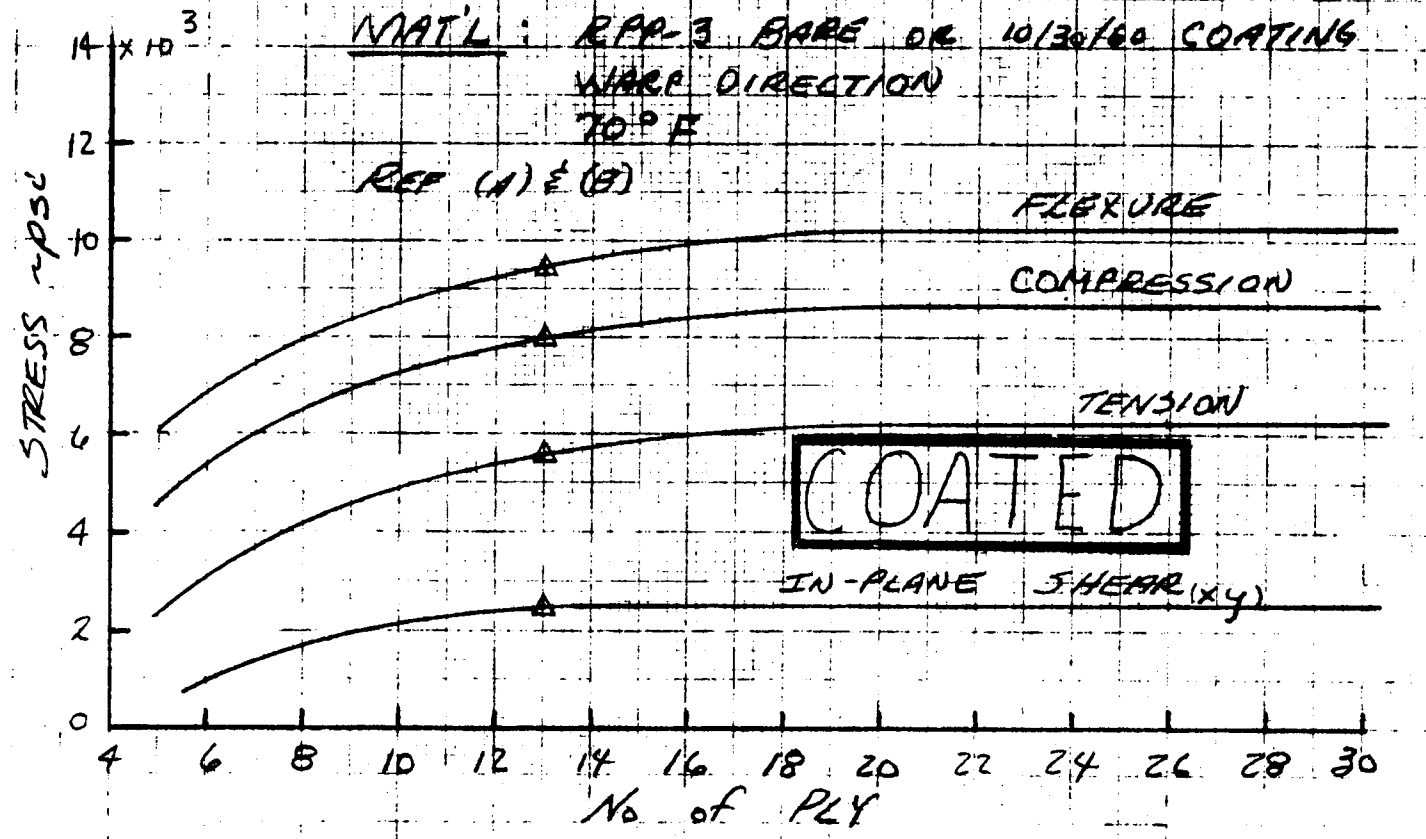

△ CURVE FIT DATA ÷ 1.5, BASED ON THREE TESTS EACH POINT, UNLESS DIFFERENT NUMBER of TESTS NOTED

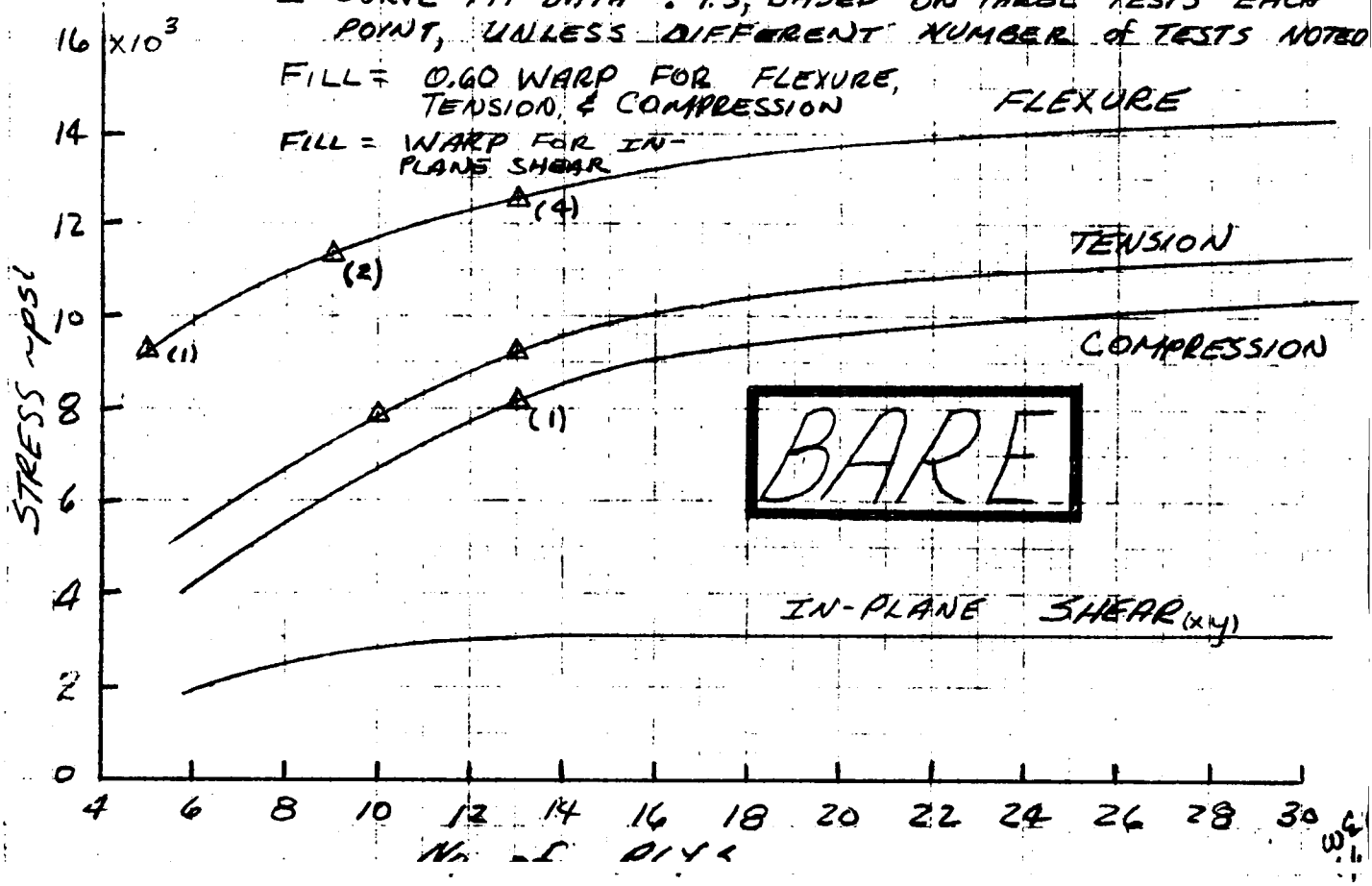

FIGURE 4

ELASTIC MODULI VS TEMPERATURE

MAT'L: 10/30/60 COATED RPP-3
WARP DIRECTION
13 PLY

△ : CURVE FIT DATA (TYPICAL VALUES), BASED ON THREE TESTS EACH POINT REF (A)

FILL = 0.75 WARP

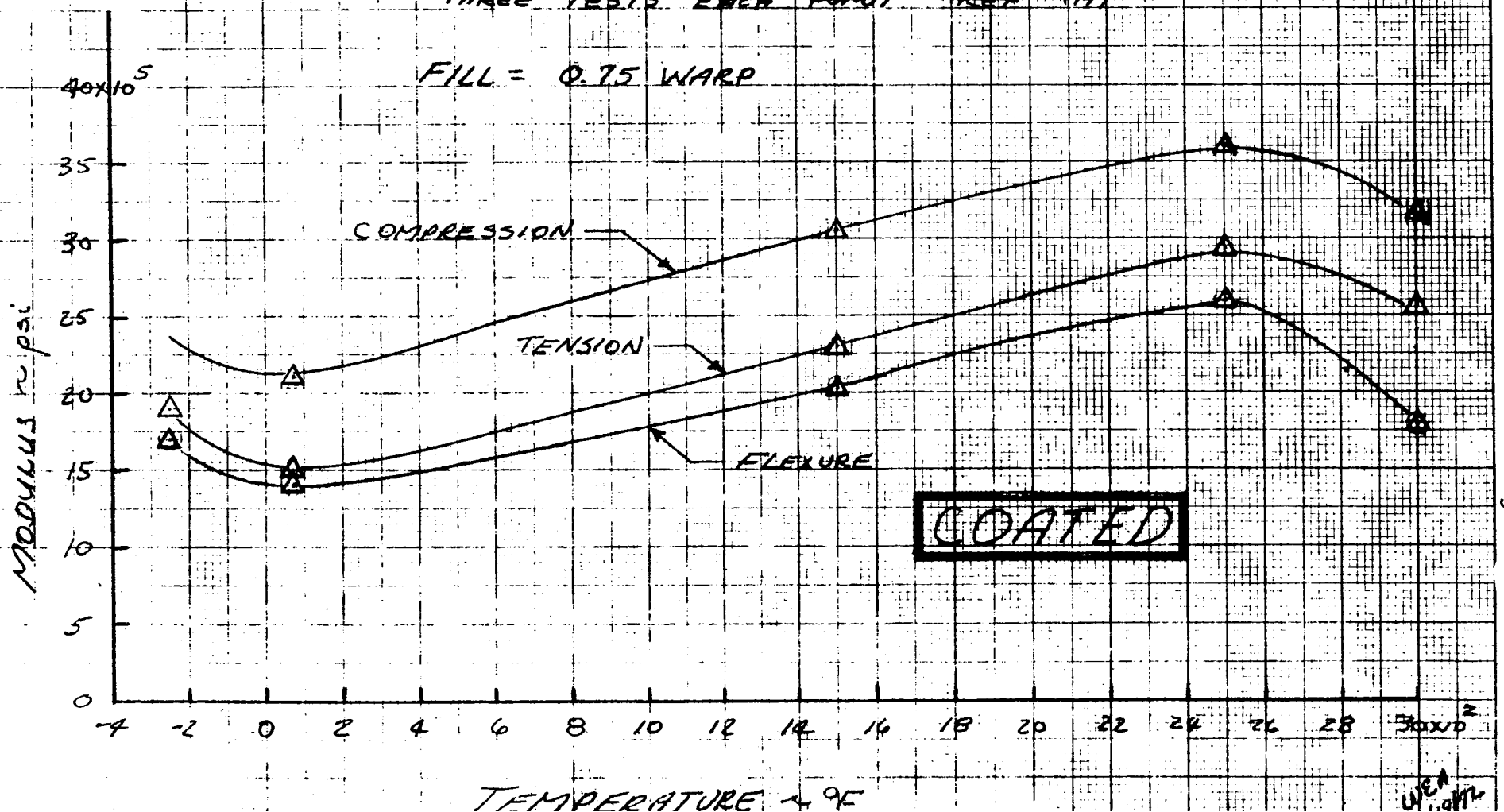

FIGURE 5

STRENGTH VS TEMPERATURE

MAT'L: 10/30/60 COATED RPP-3
WARP DIRECTION
13 PLY

△ : CURVE FIT DATA ± 1.5 BASED ON THREE TESTS EACH POINT REF (A)

FILL = 0.60 WARP

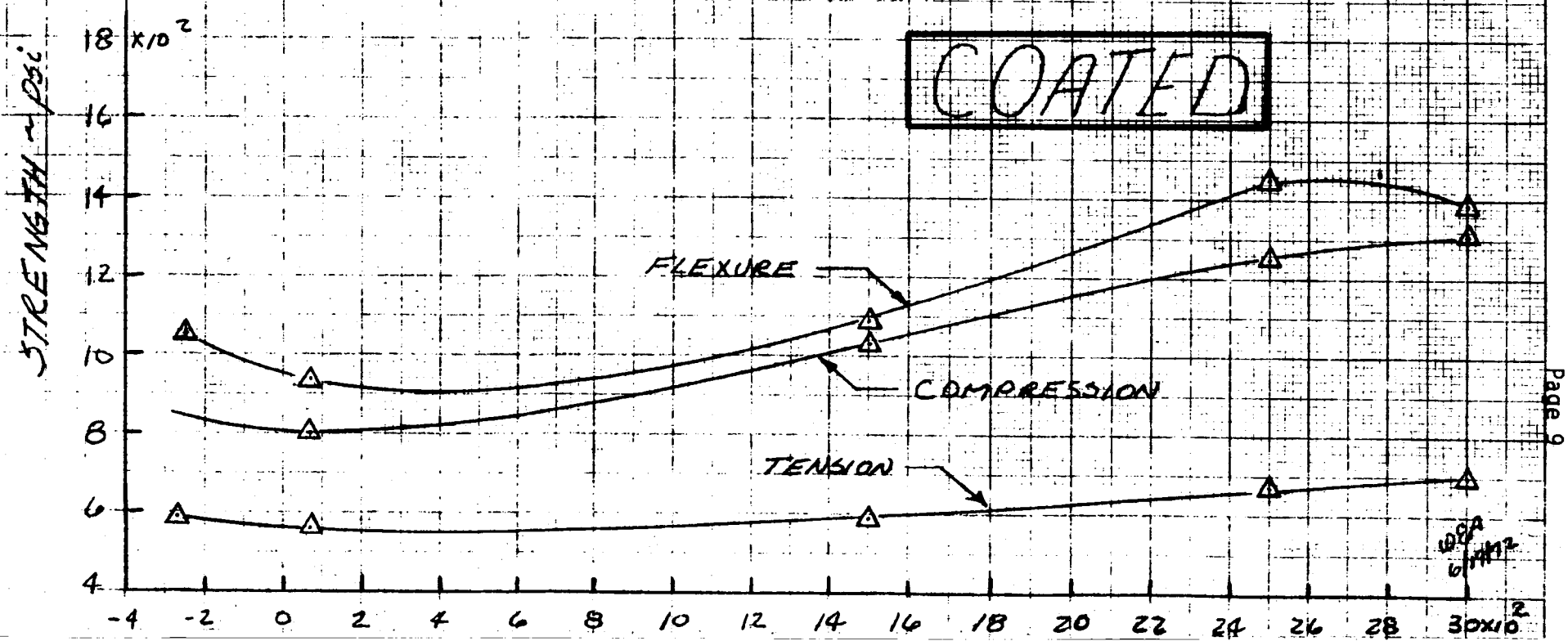

FIGURE 6

INTERLAMIAR STRENGTH VS TEMPERATURE

MAT'L: 10/30/60 COATED RPP-3

DATA IS APPLICABLE TO ALL THICKNESS, COATED OR BARE

△ CURVE FIT DATA ÷ 1.5, BASED ON THREE TESTS EACH POINT

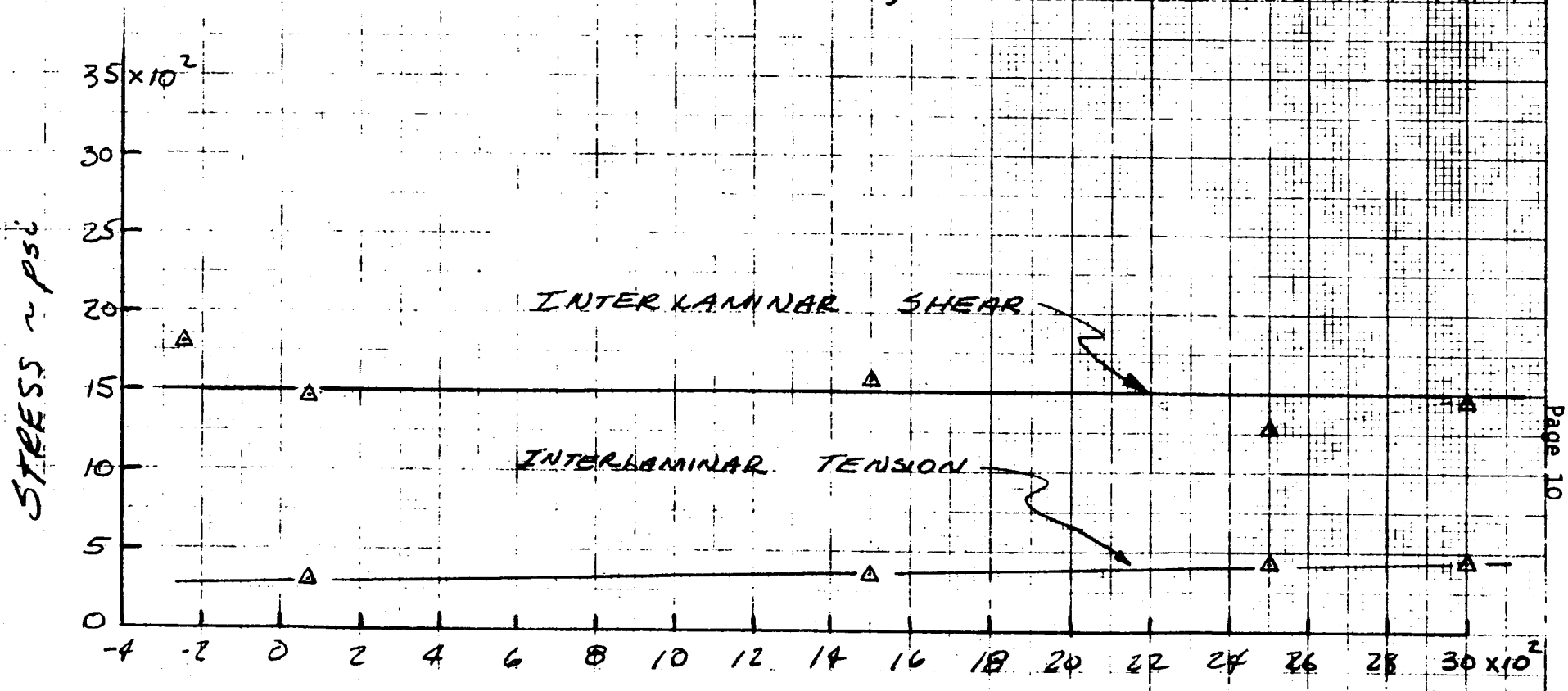

DESIGN INFORMATION ~~REQUEST~~ – RELEASE

7-28-

MODEL (S) AND EFF.	DIR. NO.	REV.
PHASE III OXIDIZED LEADING EDGE STRUCTURAL ANALYSIS	T143-DIR-2-08	
	DATE: 24 July 72	PAGE: 1 OF 22
SYSTEM:	REF. G. O. NUMBER: 3357 AA 1160	

Fill in block below for Information Request	Fill in block below for Information Release
TO _____ GROUP _____	IN REPLY TO DIR. NUMBER _____
REQ. BY _____ GROUP _____	REL. TO D. M. While GROUP 3-52000
REASON _____	PREPARED BY P. R. Bagwell DATE 7/24 · CHECKED BY WE Agan DATE 7/24
LTV ONLY ☐ BWR ☐ BUWEPS ☐ ☐ _____	GROUP APP. DATE 7/28 · PROJ OFFICE DATE 7/28/7

CC E. C. Matza, B. A. Forcht, H. I. Knight, G. B. Whisenhunt

DESIGN INFORMATION:

REFERENCE: (A) Phase III "Fail Safe" Leading Edge Material Design Allowables, T143-DIR-2-06, dated 9 June 1972.

(B) Phase III "Fail Safe" Leading Edge Structural Analysis, T143-DIR-2-09, dated 28 July 1972.

(C) Space Shuttle Wing Leading Edge Design Criteria, Phase III, T143-5R-00060, dated 19 May 1972.

(D) Ablation Analysis of Bare RPP Shuttle Wing Leading Edge, T143-DIR-2-03, dated 5 June 1972.

PURPOSE: The purpose of the DIR is to document the static and buckling analysis for the "oxidized" leading edge panel for cruise load conditions. The "Fail Safe" leading edge is evaluated in Reference (B).

SUMMARY: The leading edge is an oxidation "Fail Safe" design capable of satisfactory performance, without the aid of the oxidation protective coating for one complete mission of maximum heat load and structural load trajectories. Thus, the thick laminate leading edge is sized such that oxidation during entry will reduce the panels to a minimu effective uniform 8 ply thickness. Therefore, one design condition is to insure that the "oxidized" panel is capable of withstanding the maximum cruise loads occurring after entry.

LOCATION	MATERIAL	NO. OF PLIES	t (in)	E_w (psi)	E_f (psi)	G (psi)	V_w	V_f
Rib	Coated RPP-3	12	.156	1.38×10^6 (1.48×10^6)	1.04×10^6 (1.11×10^6)	0.94×10^6 (0.94×10^6)	.20 (.20)	.15 (.15)
Spars	Coated RPP-3	20	.260	1.44×10^6 (1.54×10^6)	1.08×10^6 (1.155×10^6)	0.97×10^6 (0.97×10^6)	.20 (.20)	.15 (.15)
Skin	Bare RPP-3	8	.104	1.62×10^6 (1.48×10^6)	1.22×10^6 (1.11×10^6)	1.06×10^6 (1.06×10^6)	.20 (.20)	.15 (.15)

t = thickness (inches)
w = warp direction
f = fill direction
V = Poisson's ratio
E_w, E_f, G = membrane properties. Flexure properties shown in parenthesis.

The maximum loads, to which the "oxidized" panels will be exposed, occur f a 2.5 g pullout maneuver while operating in the aircraft mode, Reference (C). To account for the venting lag effects while ascending or descending, + 0.5 psi and - 0. were added to the maneuver pressure loads, Reference (C), to produce two load cases. Case I refers to the + 0.5 psi venting lag condition and results in an overall collap load. Load Case II refers to the - 0.5 psi venting lag condition and results in an overall burst load. Pictorial plots of the applied loads appear in Figure 1.

The leading edge was modeled and analyzed using the NASTRAN computer rout Figures 2 and 3 are computer plots showing the overall model geometry. The model is comprised of quadrilateral membrane and bending elements. Figure 4 shows the load ar stress capability of the elements. The skin elements are nominally 1 inch square whi the rib and spar elements are an average 1 inch by 0.4 inch. The elements themselves comprised of superimposed membrane and bending elements. The membrane elements are a tropic allowing both warp and fill properties to be used. The properties used are th membrane tension properties from Reference (A). The bending elements are also aniso and use the flexure material properties from Reference (A). In both cases, fill elas properties are 75% of the warp elastic properties.

Panel deflection at limit load was arbitrarily limited to the net loca thickness. Using this limitation as a design criterion, the structure is deflecti rather than stress, critical. This accounts for the high margins in all areas. Plots of the deflected shapes at the rib and at the panel centerline appear in Fig The maximum panel deflection occurs at the panel centerline just forward of the lo spar, and is equal to .050" at limit load. The local thickness is 0.104 inches (8 An estimate of the deflection at 7 and 6 plies indicated a minimum thickness of 7 may be achieved; however, the additional analyses for one ply (0.095 lb/ft^2) was n warranted.

Table I summarizes the maximum stresses, their locations, and their associated margins of safety. The maximum rib tensile stress, Reference Figure 6, 540 psi. This stress occurs at the junction of the rib and the skin just forward the lower lug area. The maximum rib compression stress of 500 psi occurs at the s point just forward of the upper lug area. The rib tension allowable, Reference (A is 5400 psi.

$$M.S. = \frac{5400}{540} - 1 \qquad M.S. = +9.0 \text{ ULT}$$

The upper spar critical stress is a compressive stress of -950 psi, Reference Figure 7, and occurs at the inside edge of the spar at the panel center Reference Page 13. The allowable compressive stress is 8700 psi, Reference (A).

$$M.S. = \frac{8700}{950} - 1 \qquad M.S. = +8.16 \text{ ULT}$$

Critical stress for the lower spar is tensile, Reference Figure 7, and at the inside edge at the panel centerline, Reference Page 13. This stress is 119 The tension allowable for the 20 ply, coated spars is 6100 psi, Reference (A).

$$M.S. = \frac{6100}{1190} - 1 \qquad M.S. = +4.13 \text{ ULT}$$

The maximum skin tensile stress occurs at the panel centerline 0.3 in. for of the lower spar and acts in the spanwise direction, Reference Figure 8. The stres is 581 psi, which for a membrane tension allowable of 6700 psi, Reference (A), gives a margin of safety of:

$$M.S. = \frac{6700}{581} - 1 \qquad M.S. = +10.5 \text{ ULT}$$

The maximum skin axial+flexure stress, Reference Figure 9, occurs at a point just ahead of the maximum tensile stress, Reference Page 13, and has a value of - 840 psi. The flexure strength for 8 ply bare material is 11,000 psi and the compression allowable is - 5500 psi, Reference (A).

$$M.S. = \left(\frac{1}{\frac{592}{11,000} + \frac{248}{5500}}\right) - 1.0 \qquad M.S. = +9.2 \text{ ULT}$$

The maximum skin shear stress of 960 psi, Reference Figure 10, occurs adjacent to the lower spar and the lower lug area, Reference Page 13. The in-plane shear strength for 8 ply, bare RPP-3 is 2400 psi, Reference (A).

$$M.S. = \frac{2400}{960} - 1 \qquad M.S. = +1.50 \text{ ULT}$$

Margins of safety for the upper and lower lug areas are not shown since the reactions due to cruise flight loads are small compared to those encountered dur boost. Since the material conditions and thicknesses in the lug areas are not affec by panel oxidation, the boost loads on the "Fail Safe" design are the critical desig loads and are analyzed in Reference (B). Figure 1 shows the magnitudes of the react

loads for both subcases. External equilibrium is verified by a separate computer routine which uses the NASTRAN generated load, constraint forces, and model geometr as input. Table II contains the results of that analysis and shows that external equilibrium is satisfied.

Buckling Analysis - The oxidized leading edge has been analyzed for buckling with t NASTRAN routine. The math model is shown in Figure 11 and is comprised of anisotrc membrane and bending elements. A full model is required to obtain proper buckling and mode shapes. The mesh size shown is larger than the static analysis model but provides proper representation of the stiffness which is the most important bucklir parameter. Stress recovery is not needed and therefore does not dictate mesh size.

The material properties used in the buckling analysis are from Referer The 8 ply bare compression and flexure moduli were used for skin membrane and bendi elements respectively. The 12 ply coated tension and flexure moduli were used for rib membrane and bending elements respectively.

Load Case I, Figure 4, is the critical cruise load for buckling. This condition occurs during a 2.5 g maneuver and includes an 0.5 psi collapse venting l

NASTRAN performs the buckling analysis by solving for the roots or eigenvalues of the characteristic equation:

$$[Kaa + \lambda Kaa^d] \{u\} = 0$$

where,

Kaa = elastic stiffness matrix

Kaa^d = differential stiffness matrix

$\{u\}$ = displacement vector

λ_i = eigenvalues, factors by which the static load condition must be multiplied to produce buckling

The three eigenvalues that were calculated for the oxidized leading edge are:

$$\lambda_1 = 3.43$$

$$\lambda_2 = 3.92$$

$$\lambda_3 = 6.41$$

The minimum margin of safety for buckling is:

$$M.S. = \frac{3.43}{1.0} - 1 = + 2.43 \text{ ULT}$$

The centerline buckle mode shapes for λ_1 and λ_2 are shown in Figure 12. The full lower panel buckle mode shape for λ_1 is presented in Figure 13. This first mode shape is a full sine wave which is typical of a radially loaded arch or cylinder

A classical buckling problem was evaluated using NASTRAN and the results compared favorably. A simply supported 6" x 12" flat aluminum sheet loaded in edgewise compression was evaluated using NASTRAN and found to have a minimum eigenvalue of 0.9 and a full sine buckle mode shape. Classical theory predicts an eigenvalue of 1.05 and a full sine buckle mode shape.

ULT. LOADS.

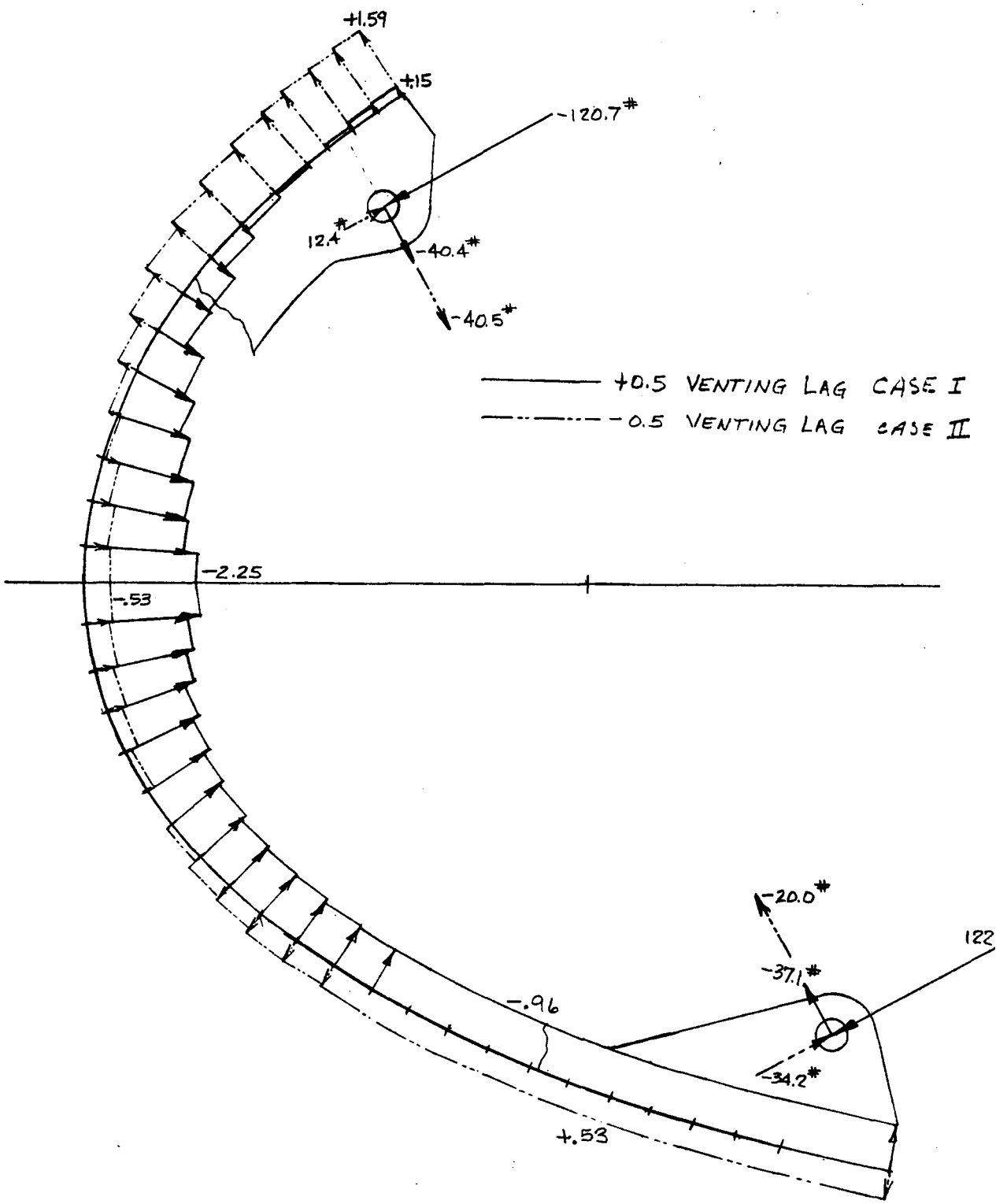

FIGURE 1 APPLIED CRUISE LOADS

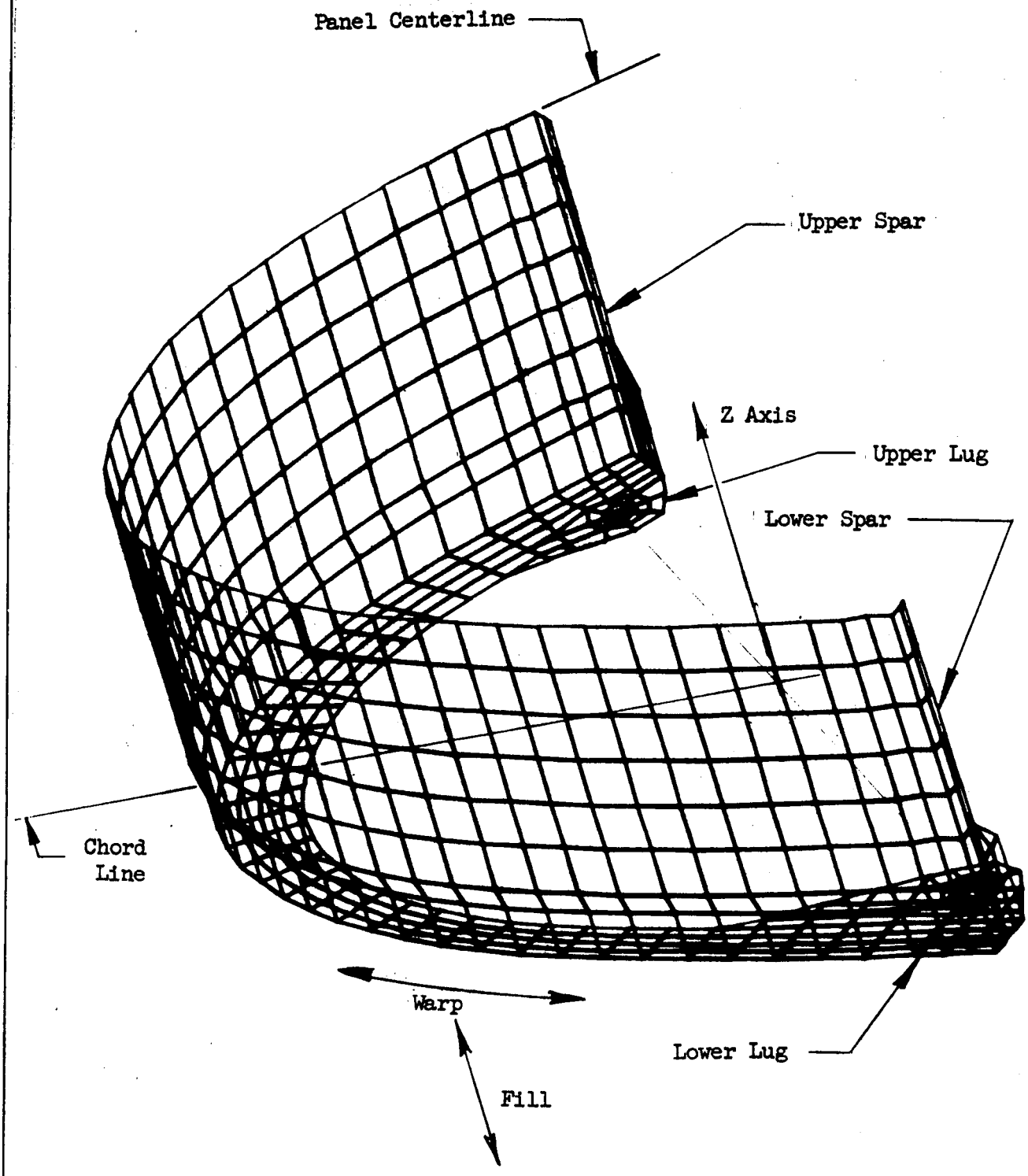

Figure 2 Perspective of NASTRAN Leading Edge Model

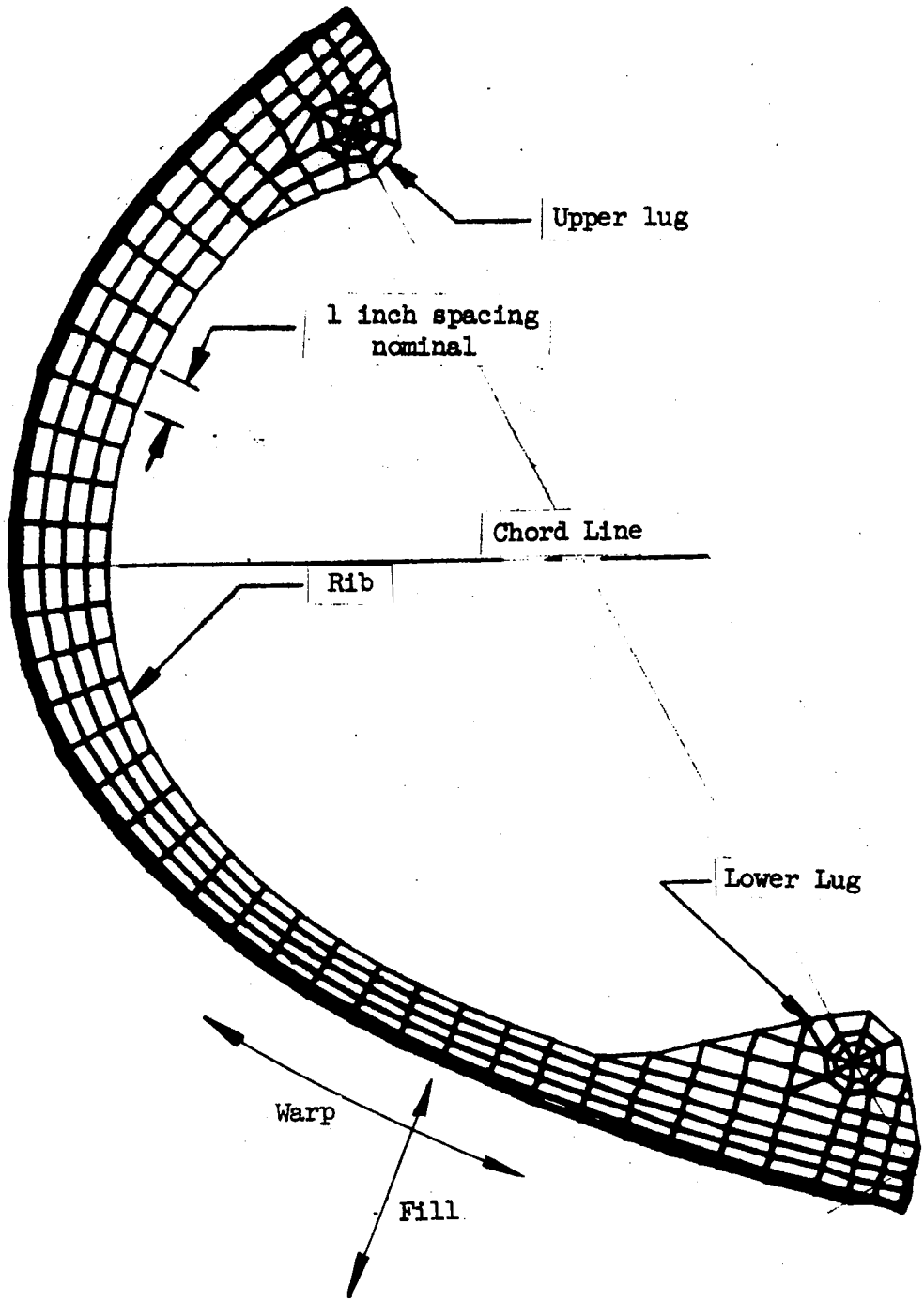

Figure 3 Side View of NASTRAN Rib Model

BENDING ELEMENT

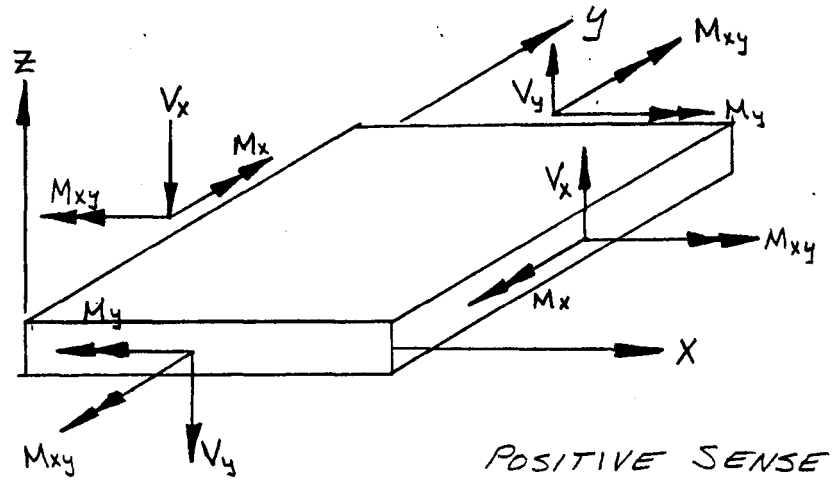

POSITIVE SENSE SHOWN FOR ALL FORCES AND STRESSES

MEMBRANE ELEMENT

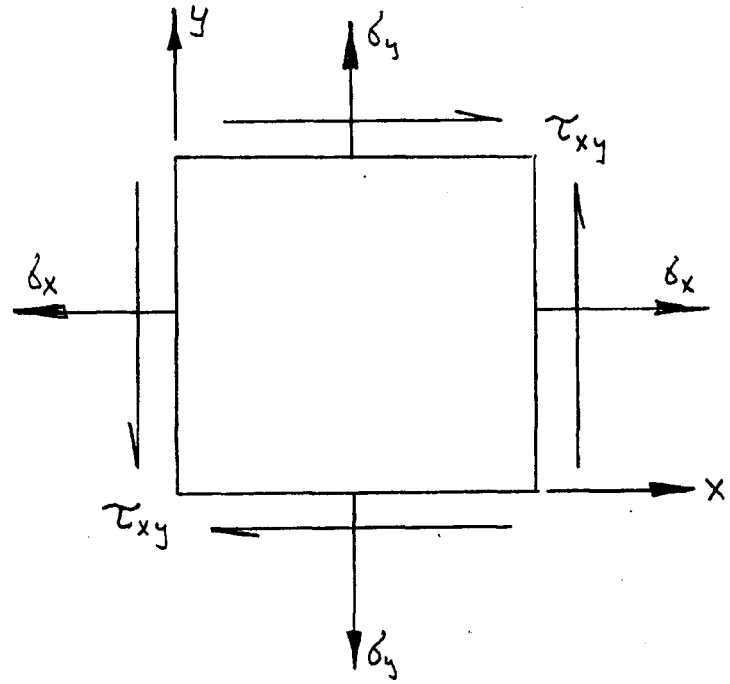

FIGURE 4 FORCE AND STRESS CAPABILITY FOR QUADRILATERAL ELEMENTS

LIMIT LOADS

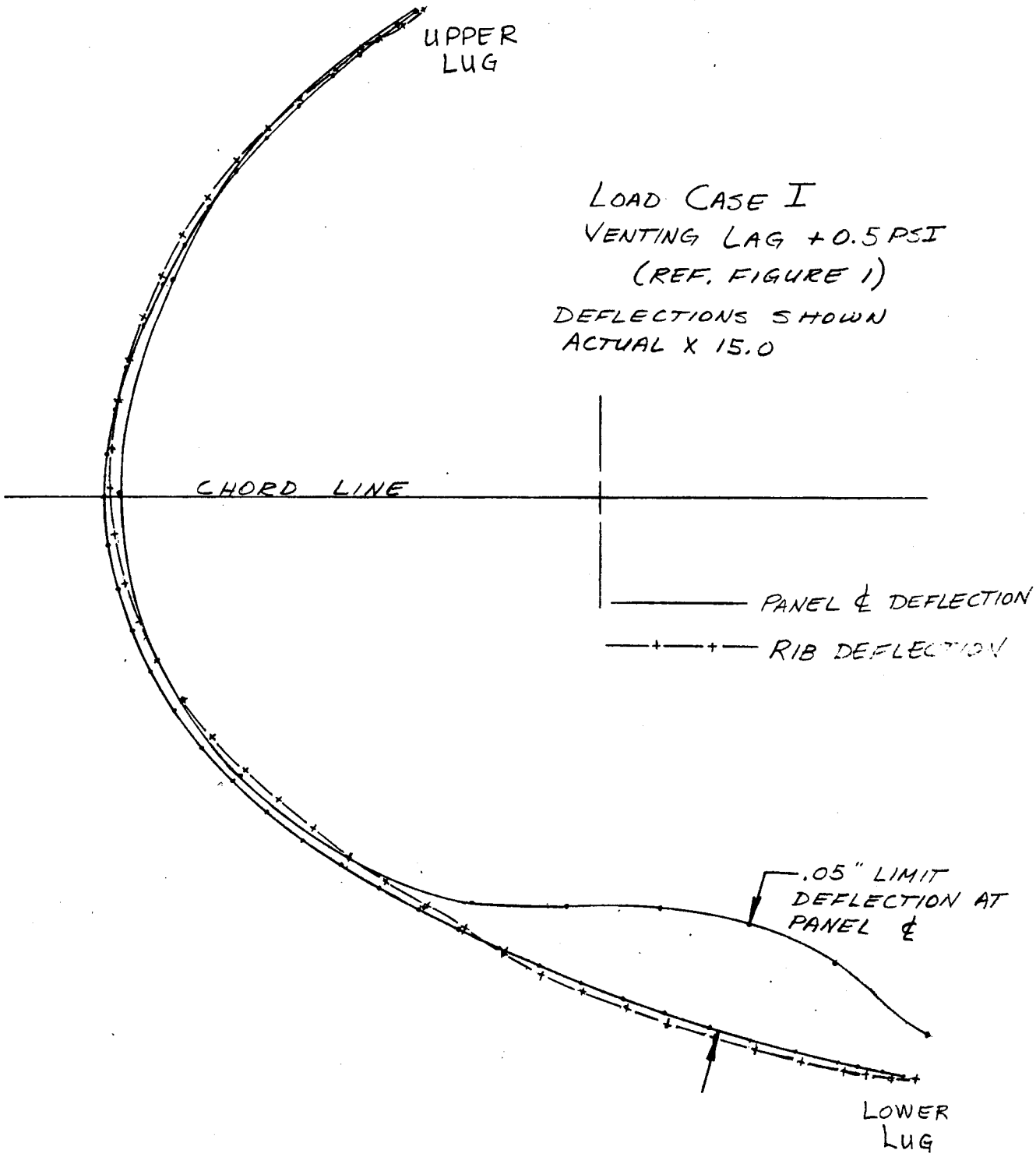

FIGURE 5 RIB AND CENTERLINE DEFLECTED SHAPES

ULT. LOADS

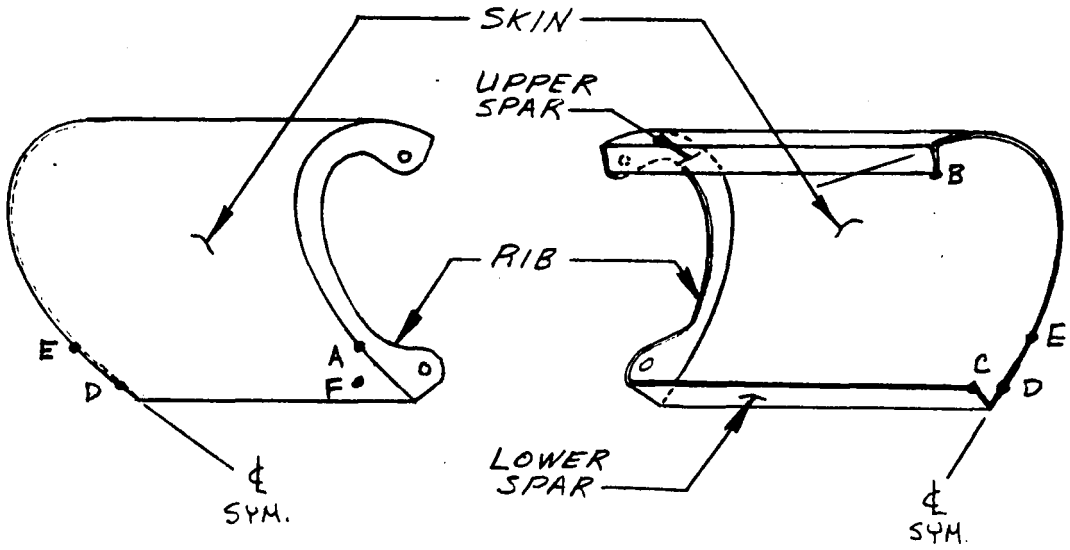

TABLE I
SUMMARY of MARGINS of SAFETY

LOCATION	STRUCTURE	TYPE STRESS	MAX. STRESS	ALLOW.* STRESS	LOAD CASE	M.S. (ULT.)	REF. FIG.
A	RIB	TENSION	540	5400	1	HIGH	6
B	UPPER SPAR	COMPRESSION	-950	-8700	2	HIGH	7
C	LOWER SPAR	TENSION	1190	6100	1	4.13	7
D	SKIN	TENSION	731	6700	1	HIGH	8
E	SKIN	FLEXURE + AXIAL	-840	11,000	1	HIGH	9
F	SKIN	SHEAR	960	2400	1	1.50	10

* REFERENCE A

NOTE:

1) RIB ALLOWABLE STRESS BASED ON 12 PLY COATED MATERIAL
2) SPAR ALLOWABLE STRESS BASED ON 20 PLY COATED MATERIAL
3) SKIN ALLOWABLE STRESS BASED ON 8 PLY BARE MATERIAL

CLEARPRINT PAPER CO. No. 539 MILLIMETERS BOTH WAYS PRINTED IN U.S.A. CLEARPRINT TECHNICAL PAPER NO. 1018
CLEARPRINT CHARTS

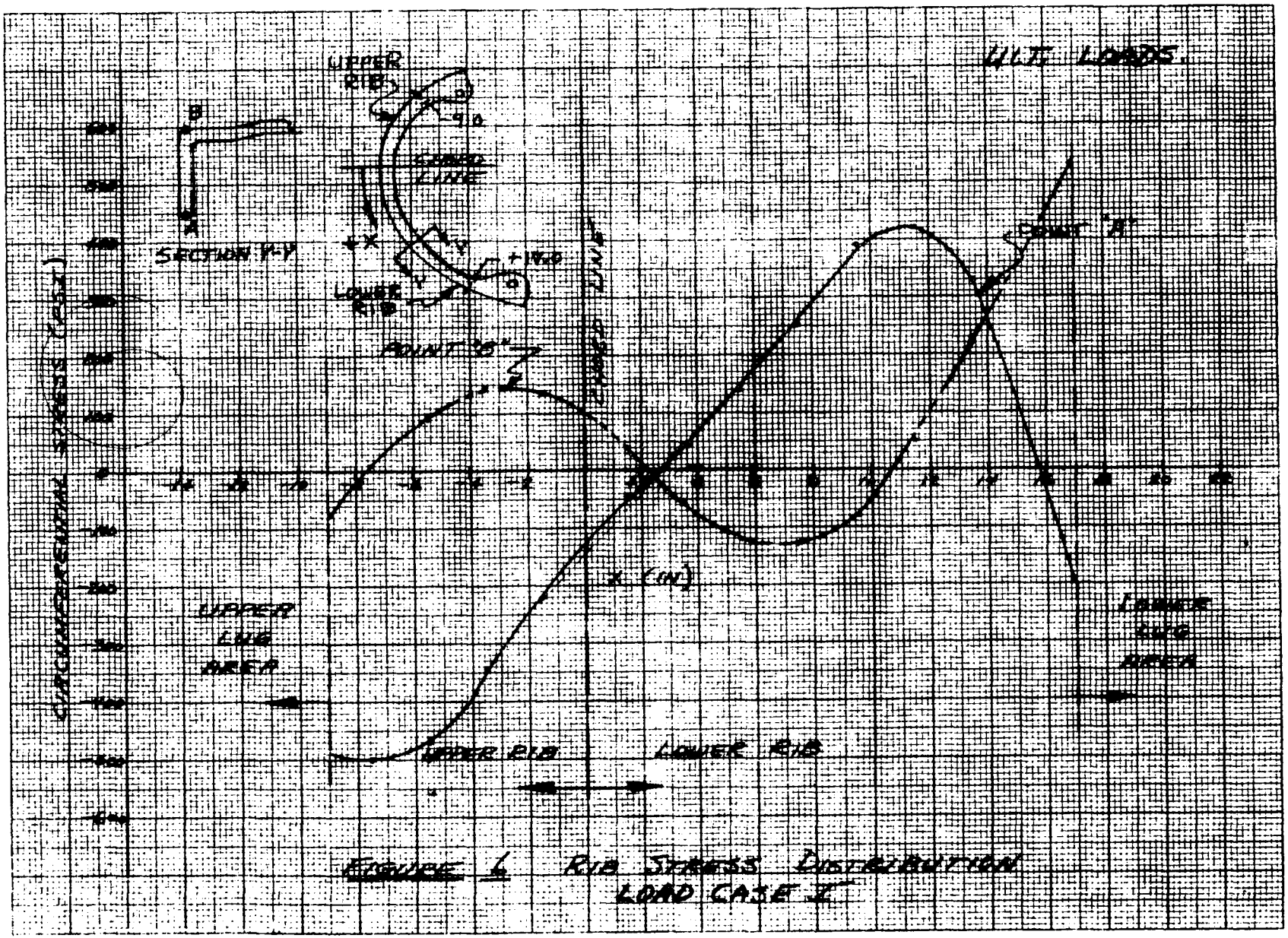

FIGURE 6 RIB STRESS DISTRIBUTION
LOAD CASE I

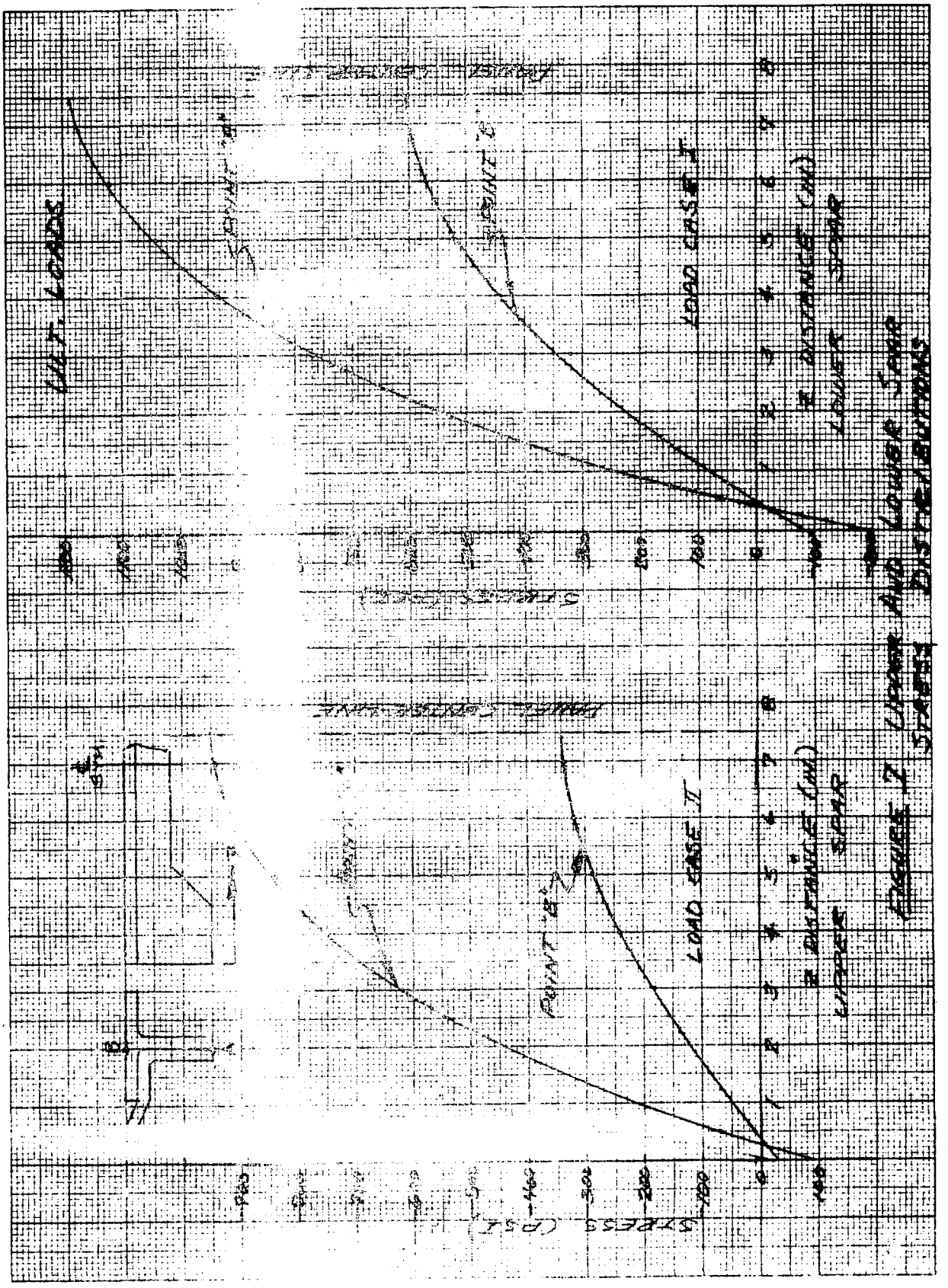

FIGURE 7 UPPER AND LOWER SPAR DISTRIBUTIONS

CLEARPRINT PAPER CO NO. C39 MILLIMETERS BOTH WAYS 160 X 220 DIVISIONS; PRINTED IN U.S.A. ON CLEARPRINT TECHNICAL PAPER NO. 1015

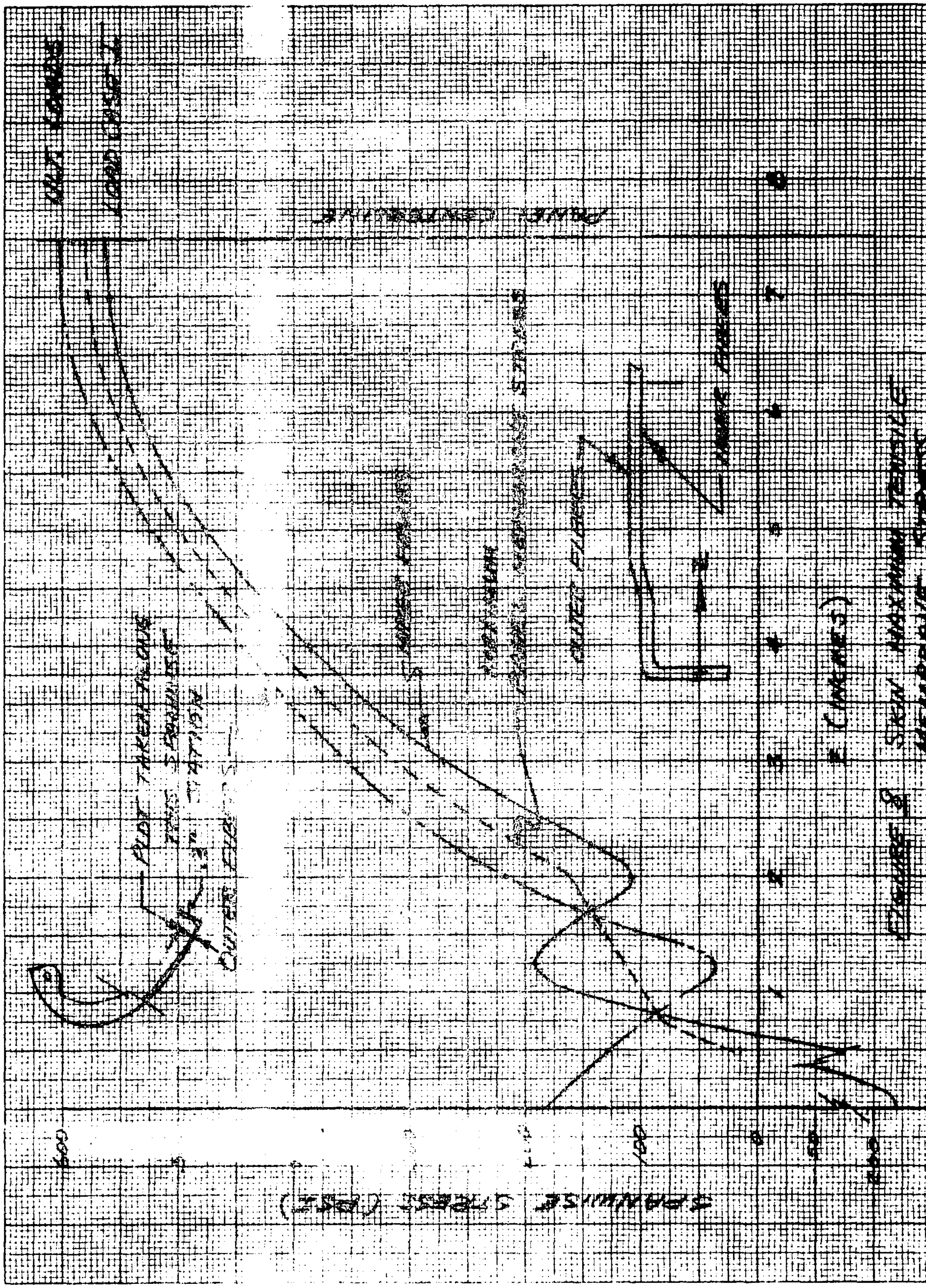

FIGURE 9 SKIN MAXIMUM TENSILE MEMBRANE STRESS

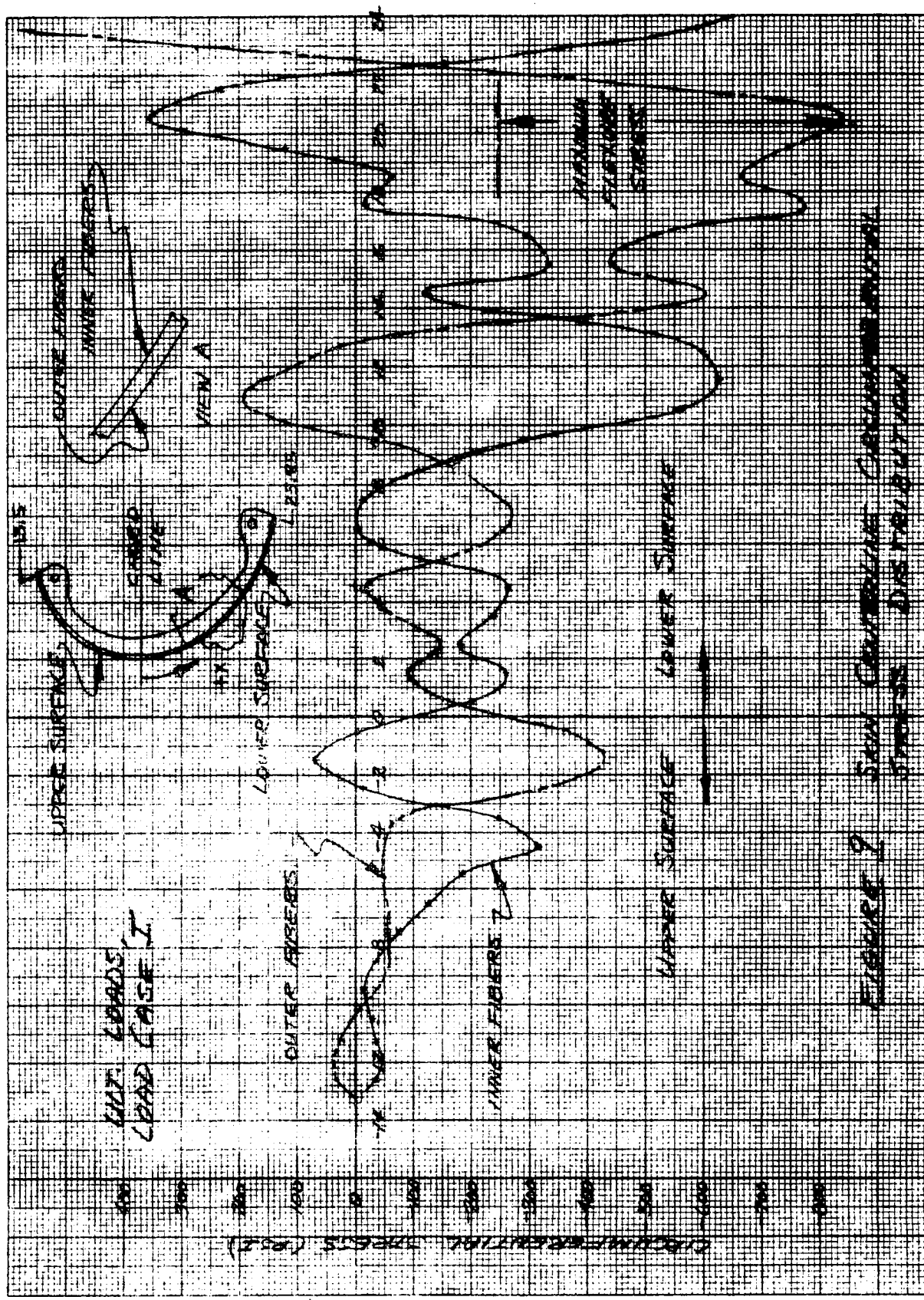

FIGURE 9 SKIN CIRCUMFERENTIAL STRESS DISTRIBUTION

CLEARPRINT PAPER CO. NO. 219 MILLIMETERS BOTH WAYS 180 / 220 DIVISIONS
PRINTED IN U.S.A. ON CLEARPRINT TECHNICAL PAPER NO. 1015

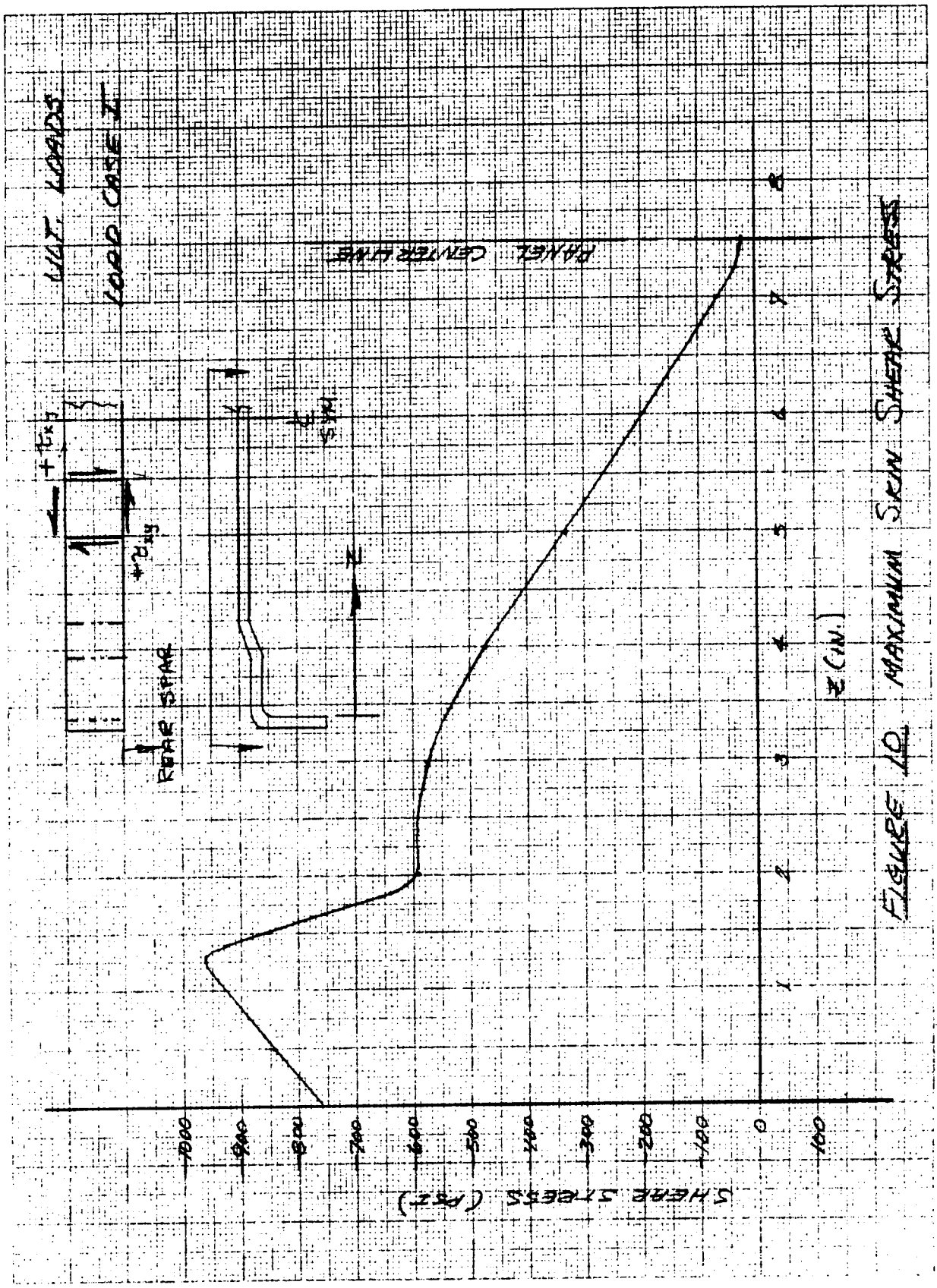

FIGURE 10 MAXIMUM SKIN SHEAR STRESS

TABLE II

EXTERNAL BALANCE

OXIDIZED LEADING EDGE/STATIC ANALYSIS CRUISE/LOAD CASE 1

TYPE	FF(Lbs)	FU (Lbs)	FO(Lbs)	MF(In-Lbs)	MU (In-Lbs)	MO(I
1	0.804E 00	0.143E 03	0.624E 01	0.102E 03	0.335E 01	0.139E
1	-0.214E 03	-0.256E 02	-0.190E-01	-0.566E 03	-0.848E 03	-0.383E
2	0.213E 03	0.0	0.399E 03	0.410E 04	0.259E 04	0.141E
2	0.0	-0.117E 03	-0.405E 03	-0.364E 04	-0.175E 04	-0.115E
3				0.0	0.0	0.0
3				0.0	0.0	0.0
4				0.260E 01	0.225E 01	0.150E
4				-0.266E 00	-0.120E 01	-0.159E
TOTALS	0.282E-02	-0.119E-02	-0.668E-04	0.430E 00	0.140E 00	-0.772E

TYPE 1= BALANCE FROM APPLIED POINT LOADS
2= BALANCE FROM CONSTRAINT POINT LOADS
3= BALANCE FROM APPLIED MOMENTS
4= BALANCE FROM CONSTRAINT MOMENTS

NOTE- WHEN ONLY THERMAL LOADING IS PRESENT, TYPES 1 AND 3 ARE NOT CONSIDERED IN THE BALANCE

FF,MF - FORCE AND MOMENT FORWARD
FU,MU - FORCE AND MOMENT UP
FO,MO - FORCE AND MOMENT OUTBOARD

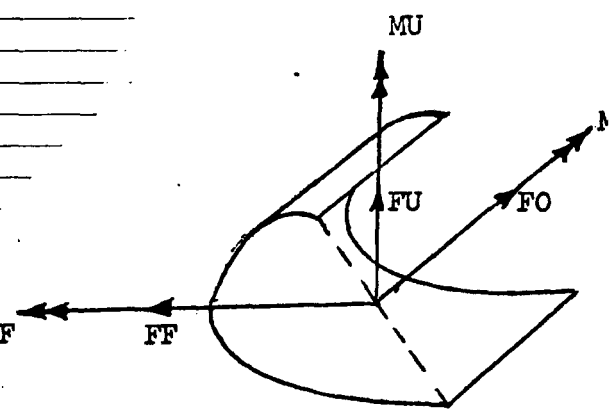

SIGN CONVENTION

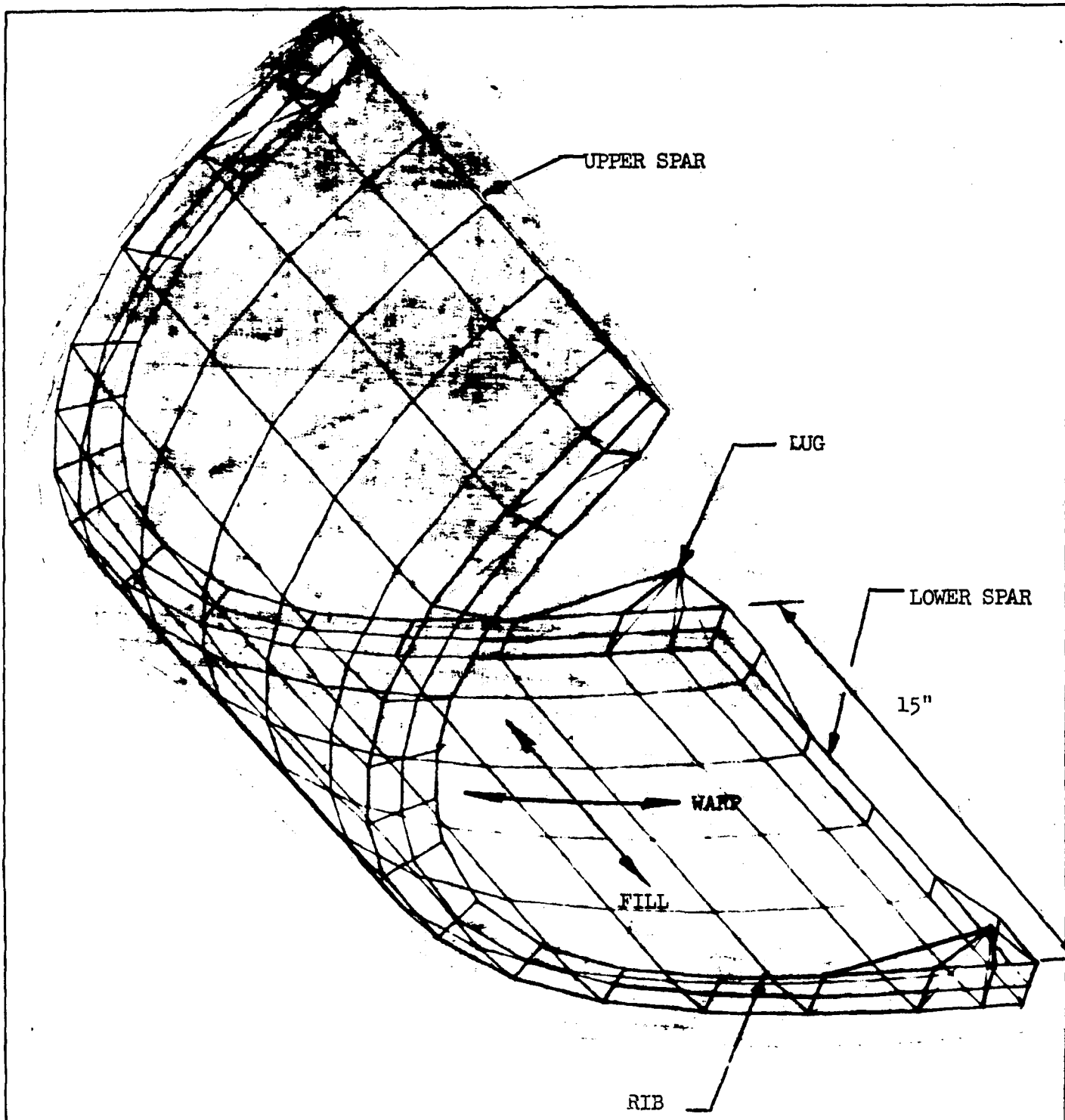

FIGURE 11

LEADING EDGE NASTRAN BUCKLING MODEL

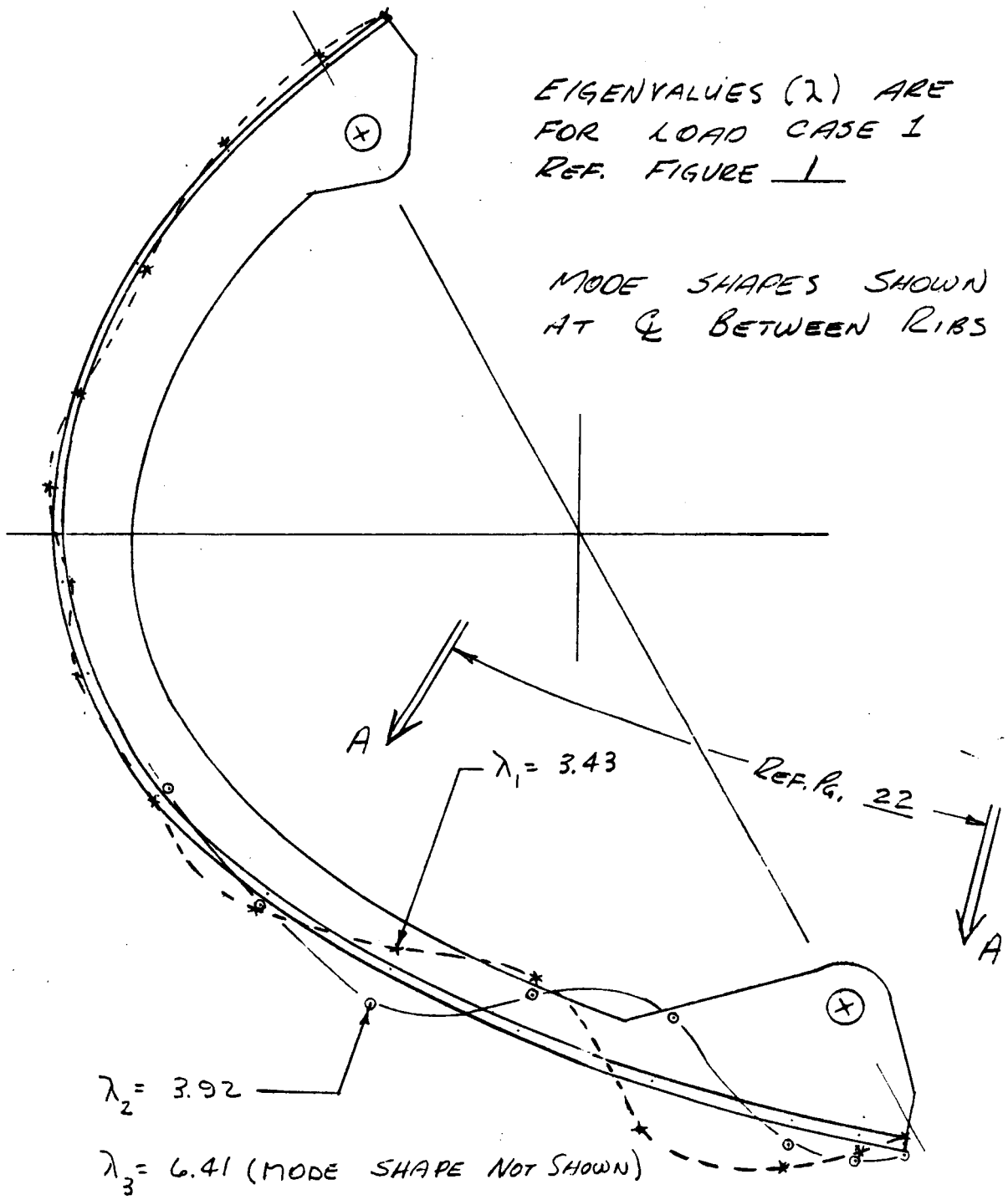

FIGURE 12 BUCKLE MODE SHAPES

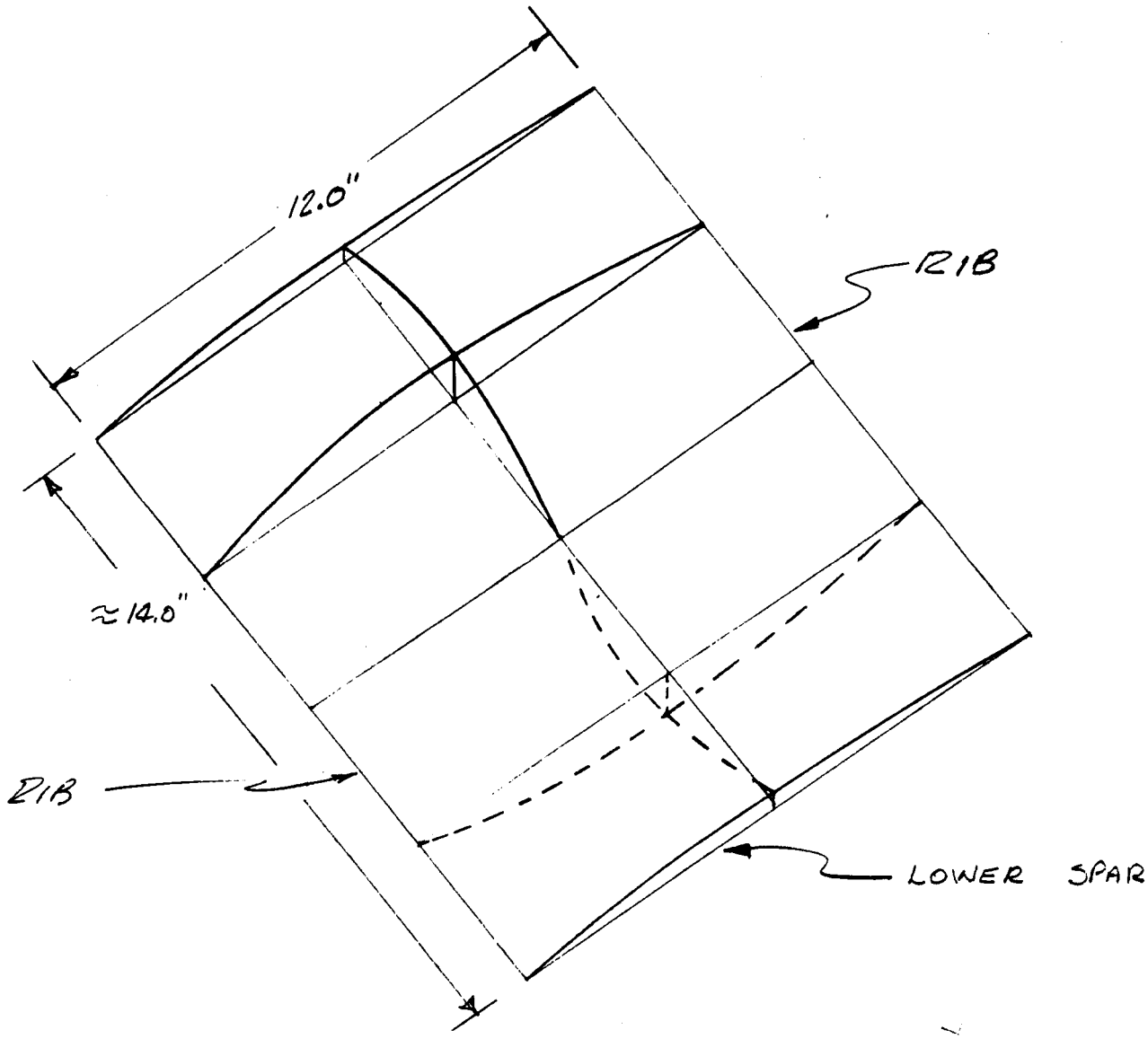

VIEW A-A REF. PG. 21

LEADING EDGE LOWER PANEL FULL BUCKLE MODE SHAPE FOR $\lambda_1 = 3.43$

FIGURE 13 FIRST BUCKLE MODE SHAPE

DESIGN INFORMATION [redacted] – RELEASE

8-

MODEL (S) AND EFF.	DIR. NO.	REV.
PHASE III FAIL SAFE LEADING EDGE STRUCTURAL ANALYSIS	T143-DIR-2-09	
	DATE: 28 July 1972	PAGE: 1 OF
SYSTEM	REF. G. O. NUMBER: 3357 AA 1160	

Fill in block below for Information Request	Fill in block below for Information Release
TO _____ GROUP _____	IN REPLY TO DIR. NUMBER _____
REQ. BY _____ GROUP _____	REL. TO D. M. While GROUP 3-52000
REASON _____	PREPARED BY P.R. Bagwell [signature] 8/2/72; T.K. Henry [signature] 8/2/72 — CHECKED BY W E Agan 8/
LTV ONLY ☐ BWR ☐ BUWEPS ☐ ☐	GROUP APP. [signature] DATE 8/4/72 — PROJ OFFICE [signature] 8/

CC

E. C. Matza, B. A. Forcht, H. I. Knight, G. B. Whisenhunt

DESIGN INFORMATION:

REFERENCES: (A) Phase III "Fail Safe" Leading Edge Material Design Allowables, T143-DIR-2-06, dated 9 June 1972.

(B) Phase III "Oxidized" Leading Edge Structural Analysis, T143-DIR-2-08, dated 24 July 1972.

(C) Space Shuttle Wing Leading Edge Design Criteria, Phase III, T143-5R-00060, dated 19 May 1972.

(D) Ablation Analysis of Bare RPP Shuttle Wing Leading Edge, T143-DIR-2-03, dated 5 June 1972.

(E) Predicted Temperature Distribution for the Wing Leading Edge Skin and Rib, T143-DIR-2-07, dated 13 July 1972.

(F) Seely, F. B. and Smith, J. O., Advanced Mechanics of Materials, John Wiley & Sons, Inc., New York, New York, 1962, pp. 164-166.

(G) Gatewood, B. E., Thermal Stresses, McGraw-Hill, 1957, page 10.

(H) Fail Safe Leading Edge Panel, VMSC Drawing T143T0000T.

PURPOSE: The purpose of this DIR is to document the static boost, side load, and thermoelastic analyses for the "Fail Safe" leading edge panel, Ref. (H). The "oxid panel analysis is documented in Reference (B).

0-52042 R1

SUMMARY: The "fail safe" leading edge is designed to enable the panels to provide satisfactory performance for one complete mission of maximum heat load and structural load trajectories, without the aid of the oxidation inhibiting coating. The panel thickness is sized such that if ablation occurs during entry the panels will reduce to an effective 8 ply uniform thickness. Allowing for variation in ablation over the surface, the "fail safe" leading edge panel skin thickness varies between 16 and 34 plies. One design requirement is to provide adequate margins of safety during the boost phase of the mission. Further, the thermally induced stresses which are critical during entry, must not be excessive for the "fail safe" (un-oxidized) thick laminate panel.

The following minimum margins of safety exist for the thick-laminate panels during the boost phase.

LOCATION	ULT M.S.	BASED ON	LOAD CONDITION	REF. PAGE
Upper Lug	+ 0.31	Shear	32 "g" side load	5
Rib	+ 0.40	Tension	α = -5.8°, vent. lag	5
Upper Spar	+ 4.60	Compression	α = 4.0°, vent. lag	6
Lower Spar	+ 2.73	Compression	α = -5.8°, vent. lag	6
Skin	+ 4.1	Compression	α = -5.8°, vent. lag	6
Skin	High	Tension	α = -5.8°, vent. lag	7
Skin	High	Flexure	α = -5.8°, vent. lag	7
Skin	+ 2.33	Shear	α = -5.8°, vent. lag	7
Lower Lug	+ 1.40	Flexure	32 "g" side load	8
Upper Lug	+ 2.12	Shear	α = 4.0°, total vent.	7

The following minimum margins of safety exist for the thick-laminate panels during entry.

LOCATION		BASED ON	REF. PAGE
Skin	+ 2.52	Tension	34
Skin	+ 1.34	Shear	35
Upper Spar	+ 3.00	Tension	35
Lower Spar	High	Compression	35
Rib	+ 1.74	Tension	36
Skin	+ 2.5	Tension	36

Maximum panel deflection occurs at the panel centerline six inches forward of the lower spar during boost and is .072" (limit).

DISCUSSION OF RESULTS: The boost static analysis is discussed below. The entry thermoelastic analysis discussion begins on Page 33.

Boost Static Analysis - The "fail safe" leading edge panel is designed to ablate to an effective 8 ply thickness without the aid of the oxidation protective coating. Since the amount of ablation varies with position on the leading edge, Reference (D), the thickness distribution shown in Figure 1 was used. The rib is 12 ply, coated RPP-3 and the upper and lower spars are 20 ply, coated RPP-3. From Reference (A), the following material properties were used.

LOCATION	MAT'L	NO.of PLIES	t (in)	E_w (psi)	E_f (psi)	G (psi)	V_w	V_f	α in/in/°F	ρ lbs/in^3
Rib	Coated RPP-3	12	.156	1.38×10^6 (1.48×10^6)	1.04×10^6 (1.11×10^6)	0.94×10^6 (0.94×10^6)	.20 (.20)	.15 (.15)	1.5×10^{-6} (1.5×10^{-6})	.051 (.051)
Spars	Coated RPP-3	20	.260	1.44×10^6 (1.53×10^6)	1.08×10^6 (1.15×10^6)	0.97×10^6 (0.97×10^6)	.20 (.20)	.15 (.15)	1.5×10^{-6} (1.5×10^{-6})	.051 (.051)
Skin	Coated RPP-3	Over 16	.208	$.143\times10^6$ (1.52×10^6)	1.07×10^6 (1.14×10^6)	0.96×10^6 (0.96×10^6)	.20 (.20)	.15 (.15)	1.5×10^{-6} (1.5×10^{-6})	.051 (.051)

t = thickness (inches)
w = warp direction
f = fill direction
V = Poisson's Ratio
ρ = density (lbs/in^3)
α = coefficient of thermal expansion (in/in/°F)
xxx = membrane properties
(xxx) = flexure properties

The four pressure load conditions shown in Figures 2 and 3 occur during the boost phase, Reference (C). These curves account for a 1.0 psi burst venting lag for both a 4° and a -5.8° angle of attack. In addition to the pressure loads, 32 "g" RMS vibration loads are also generated during lift off, Reference (C). For the purposes of this analysis, the vibration induced loads were applied as static loads.

The leading edge was modeled and analyzed using the NASTRAN computer routine. The model used for the boost load conditions is shown in Figures 4 and 5. Due to symmetry of applied loads and panel constraints, only one-half of one panel was modeled. For the side load analysis however, the panel constraints are not symmetric about the panel centerline. As a result, the full 15" panel was modeled. Plots of this model are shown in Figures 6 and 7. Both models consist of quadrilateral and triangular membrane-bending elements. The grid size for the boost load model is a nominal 1-inch square on the skin and an average 1-inch by 0.4 inch on the rib. As can be seen in Figure 7, the side load model has a variable grid size. Since more accurate stresses were desired in and around the lug areas, a finer grid was used in these areas. To hold the total degrees of freedom, and hence the computer execution times to reasonable levels, larger elements were used for the balance of the panel. The larger elements do not adversely affect the mass or stiffness of the model.

The elements themselves consist of super-imposed membrane and bending elements. Both type of elements are anisotropic, and warp and fill properties were used. The membrane elements used the membrane tension properties from Reference (A), and the bending elements used the flexure properties. In all cases, the fill properties are 75% of the warp properties.

Maximum panel deflection occurs during boost for $\alpha = -5.8°$ (load case II), venting lag. The maximum deflection occurs at the panel centerline six in. forward of the lower spar and is .072" (limit). The maximum rib deflection of .058" (limit) occurs at rib station 13, Fig. 5. Plots of the deflected shapes for the rib and the panel centerline are shown in Figure 8.

Table I summarizes stresses, locations, and associated margins of of safety which occur during boost (Reference page 18). The minimum margin of safety occurs in the rib due to a shearing stress developed by the 32 "g" side load. Figure 9 shows the location of this stress and Figure 10 shows the shear stress distribution on a cut through this point. The maximum shear stress is 1905 psi. The allowable for the 23 ply lug area from Reference (A) is 2500 psi.

$$M.S. = \frac{2500}{1905} - 1 \qquad M.S. = +0.31 \text{ ULT}$$

As can be seen in Figure 10, there is virtually no membrane shear stress. The stiffness of the spar and the skin effectively prevent membrane shearing action. However, as can be seen in the deflected shape in Figure 11, the elements are twisted, creating the high shear stresses. The maximum flexure stress is shown in Figure 19 and will be discussed later.

Maximum rib tension stresses, shown in Figure 12, occur at rib station -5.5, refer to Figure 5, at the outer edge of the flange. The maximum stress developed is +3850 psi. The tension allowable from Reference (A) for 12 ply, coated RPP-3 is 5400 psi.

$$M.S. = \frac{5400}{3850} - 1 \qquad M.S. = +0.40 \text{ ULT}$$

The maximum stress for the upper spar occurs during boost for load case IV, Reference Figure 3. As shown in Figure 13, the stress is compressive and acts at the outside edge of the up-standing flange. The stress generated is

-1570 psi, which, with an allowable from Reference (A) of -8800 psi, gives a margin of safety of:

$$M.S. = \frac{8800}{1570} - 1 \qquad M.S. = +4.60 \text{ ULT}$$

Figure 13 also shows the maximum stress for the lower spar which acts during load case II, Reference Figure 2. The stress generated acts at the outside edge of the up-standing flange and has a value of -2360 psi. The compression allowable for the 20 ply spar is -8800 psi.

$$M.S. = \frac{8800}{2360} - 1 \qquad M.S. = +2.73 \text{ ULT}$$

Figure 14 shows a plot of the spanwise stress distribution for the skin at the point of maximum compressive stress. Maximum compression in the skin occurs at the panel centerline immediately ahead of the lower spar. The stress of -1075 psi consists of a membrane compressive stress of -665 psi and a flexure stress of 410 psi. The local panel thickness is 20 ply, Reference Figure 1, which possesses a fill flexure strength of 6,120 psi and a fill compression strength of -5160 psi, Reference (A).

$$M.S. = \frac{1}{\frac{665}{5160} + \frac{410}{6120}} - 1 \qquad M.S. = +4.1 \text{ ULT}$$

Figure 15 is a plot of the circumferential stress distribution along the panel centerline, and shows not only the point of maximum tensile membrane stress for the panel, but also the point of maximum flexure stress. The maximum panel membrane tensile stress of 340 psi occurs at rib station 17, Reference Figure 5. The flexure stress acting at that point is 460 psi, giving a maximum outer fiber stress of 800 psi. The local panel thickness is 22 ply, giving a flexure strength of 10,200 psi and a tension strength of 6300 psi.

$$M.S. = \frac{1}{\frac{340}{6300} + \frac{460}{10,200}} - 1 \qquad M.S. = +9.00 \text{ ULT}$$

The maximum flexure stress of 580 psi occurs at rib station 20, Reference Figure 5. The membrane stress at that point is tensile and equal to 220 psi, giving a mximum outer fiber stress of 800 psi. The local panel thickness is 21 ply, however, the flexure and tension allowables are the same as those given for 22 ply above, Reference (A).

$$M.S. = \frac{1}{\frac{580}{10,200} + \frac{220}{6300}} - 1 \qquad M.S. = +9.90 \text{ ULT}$$

The maximum skin shear stress is shown in Figure 16. The stress of 750 psi occurs at the junction of the rib and the skin at rib station 17.5, Reference Figure 5. The shear strength, for the local panel thickness of 22 ply, is 2500 psi, Reference (A).

$$M.S. = \frac{2500}{750} - 1 \qquad M.S. = +2.33 \text{ ULT}$$

The maximum stresses computed by NASTRAN for the upper and lower lugs due to boost loads are summarized in Figures 17 and 18. Critical load case for the upper lug is load case III, Reference Figure 3. The minimum margin of safety occurs for the "shear-out" failure mode and is +2.12. The shear stress developed is 800 psi and the shear strength for the 23 ply lug is 2500 psi. The minimum allowable margin for in-plane lug loads is +1.0, Reference (C).

$$M.S. = \frac{2500}{800} - 1 \qquad M.S. = +2.12 \text{ ULT}$$

Critical boost load stresses are developed in the lower lug for load case II, Reference Figure 2. Again, the shear stresses produce the minimum margin of safety. The maximum shear stress developed is 760 psi.

$$M.S. = \frac{2500}{760} - 1 \qquad M.S. = +2.29 \text{ ULT}$$

These margins apply only to the in-plane loads due to boost pressures which attempt to "pull-out" or "shear-out" the material immediately around the bolt hole. A lower margin of safety exists in the lower lug due to flexure stresses created as a result of the 32 "g" side load condition. The point at which the maximum flexure stresses occur is shown in Figure 9 as cut "A-A". Figure 19 is a plot of the inner and outer fiber stresses occurring along the line "A-A". The membrane stresses are essentially zero and the flexure stress is $\pm$ 4250 psi. For the 23 ply lug, the flexure strength is 10,200 psi.

$$M.S. = \frac{10,200}{4,250} - 1 \qquad M.S. = +1.40 \text{ ULT}$$

The upper lug is not critical for the side load induced flexure stresses because of its closer proximity to the skin and the upper spar. Figure 7 shows the lower bolt hole to be well outside the "box" created by the rib, lower spar, and skin. As a result, the lug acts as a cantilever plate in resisting side loads. However, the upper bolt hole falls within the "box" formed by the rib, upper spar, and skin and has the additional stiffness of the spar and the rib with which to react the side loads. Figure 11 is a plot of the deflected shape of the lower lug and shows the bending deformation responsible for the high flexure stresses.

Due to the "curved beam" effect, moments applied to corners create radial stresses. When the moment tends to open the angle, radial tension stresses are created which, for laminate materials such as RPP-3, are carried as interlaminar tension stresses. The interlaminar tension strength is small in comparison to the in-plane tension strength, 375 psi versus 5600. Figure 20 is a plot of the allowable moment for thicknesses from 8 to 25 plies. The curve is

based on a .16 inch inside radius with a mean radius equal to the inside radius plus one-half the thickness of the material. Spotted on the graph are the points corresponding to the maximum joggle moment and the maximum rib-skin or spar-skin moment. As can be seen, the corner moments are very low and high margins of safety exist. The allowable moment, where the thickness changes around the corner such as a 34 ply skin mating with a 12 ply rib, is based on the smaller thickness.

To verify that static equilibrium exists, a separate computer routine was written which accepts NASTRAN load, constraint force, and geometry data as input. The load and constraint forces for the boost load conditions are shown in Figures 2 and 3. External equilibrium is satisfied and the results for load case II are shown in Table II on page 31. Figure 21 shows the reactions due to the 32 "g" limit side load. Equilibrium is also shown.

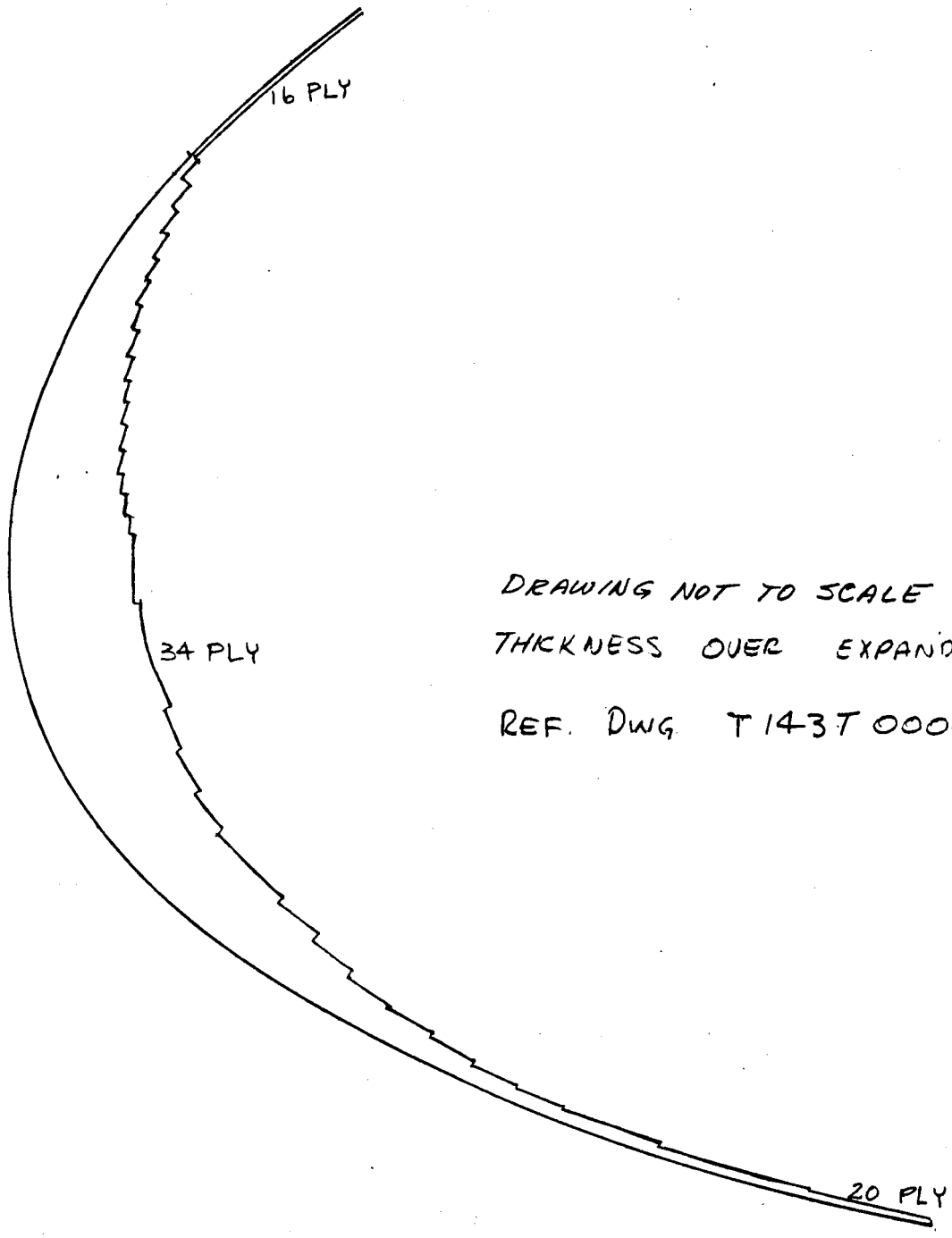

DRAWING NOT TO SCALE
THICKNESS OVER EXPANDED
REF. DWG T143T00007

FIGURE 1 "FAIL SAFE" SKIN THICKNESS DISTRIBUTION

ULT. LOADS

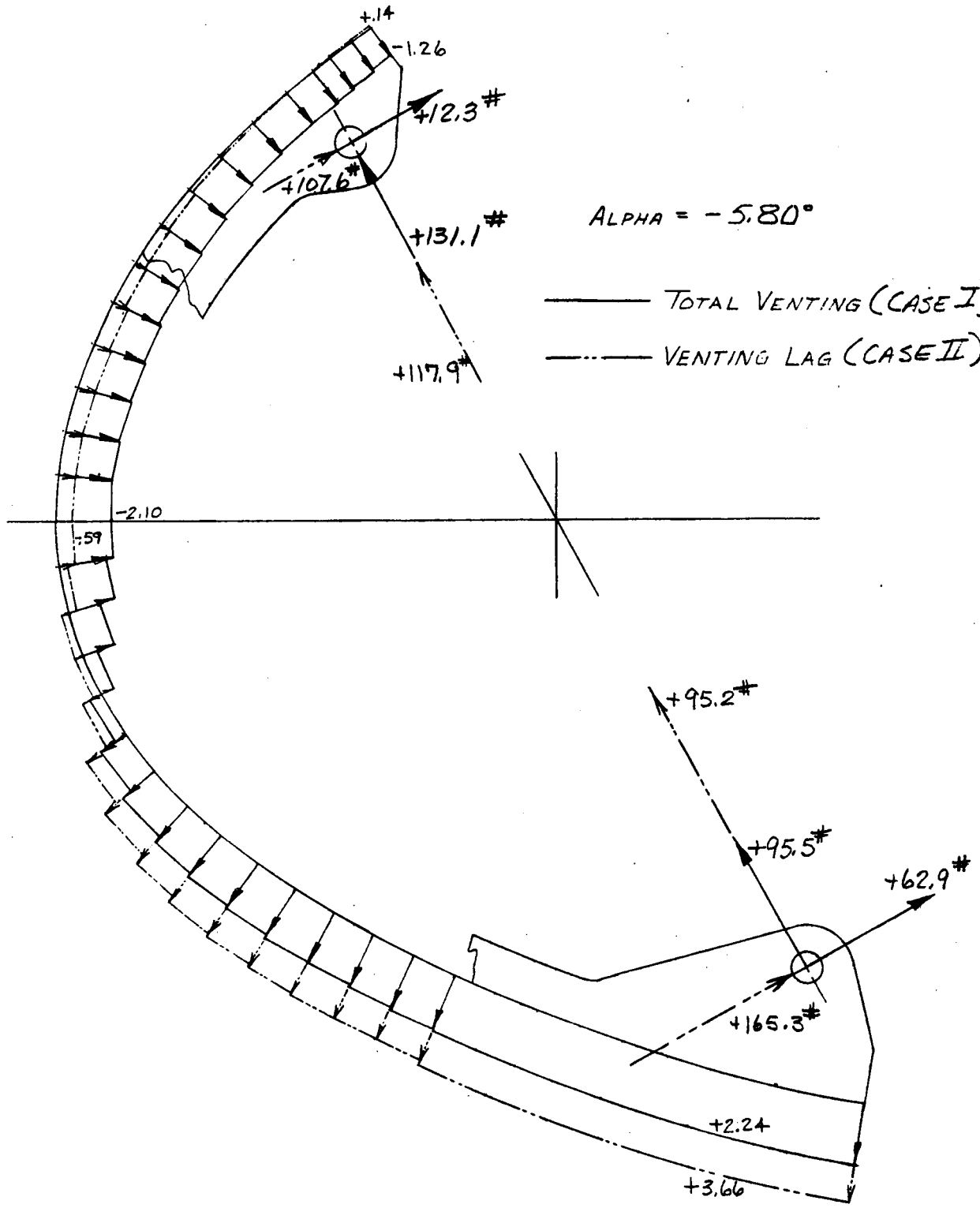

FIGURE 2. ULT. BOOST PRESSURE LOADS

ULT. LOADS

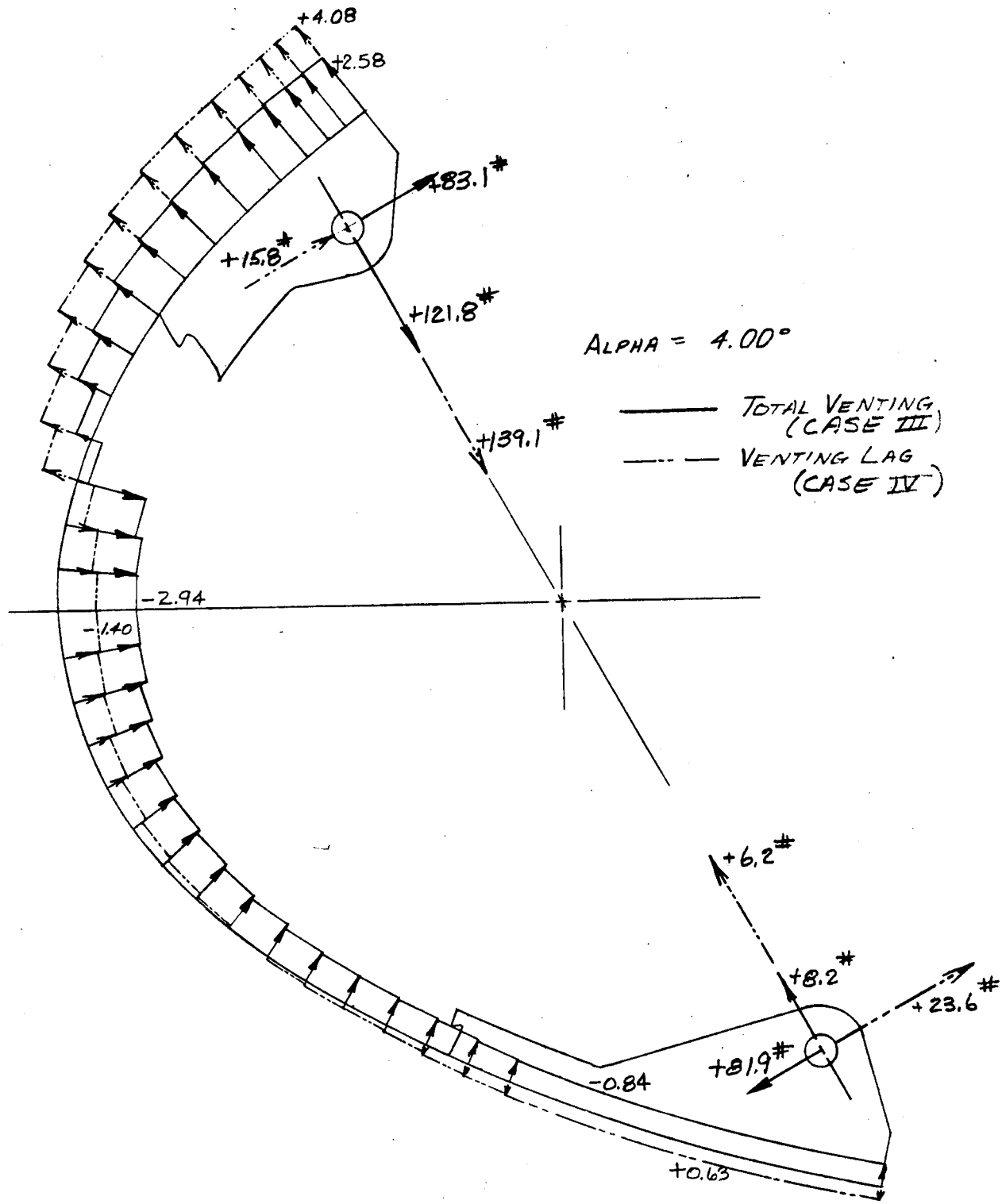

FIGURE 3. ULT. BOOST PRESSURE LOADS

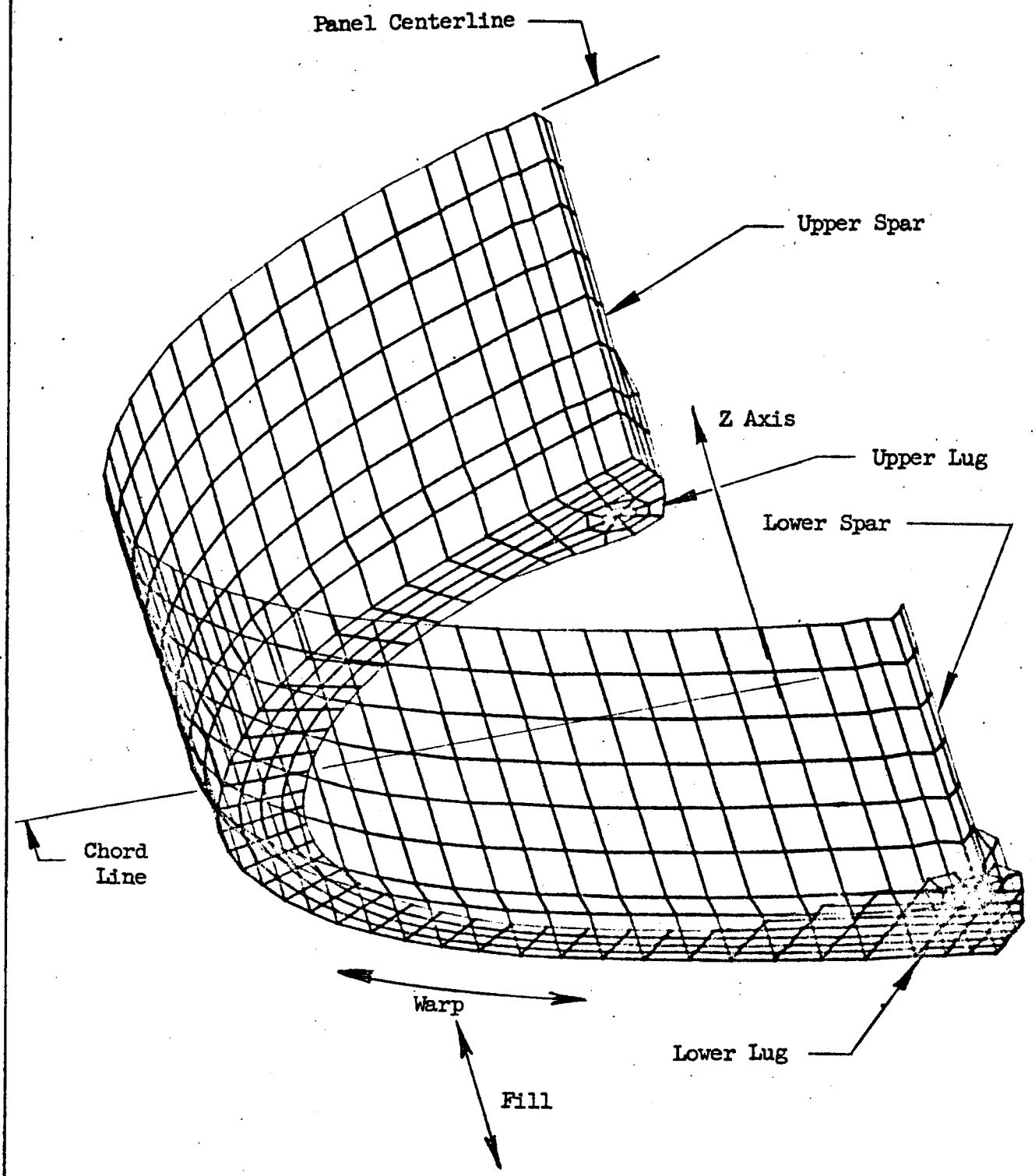

Figure 4 Perspective of NASTRAN Leading Edge Model

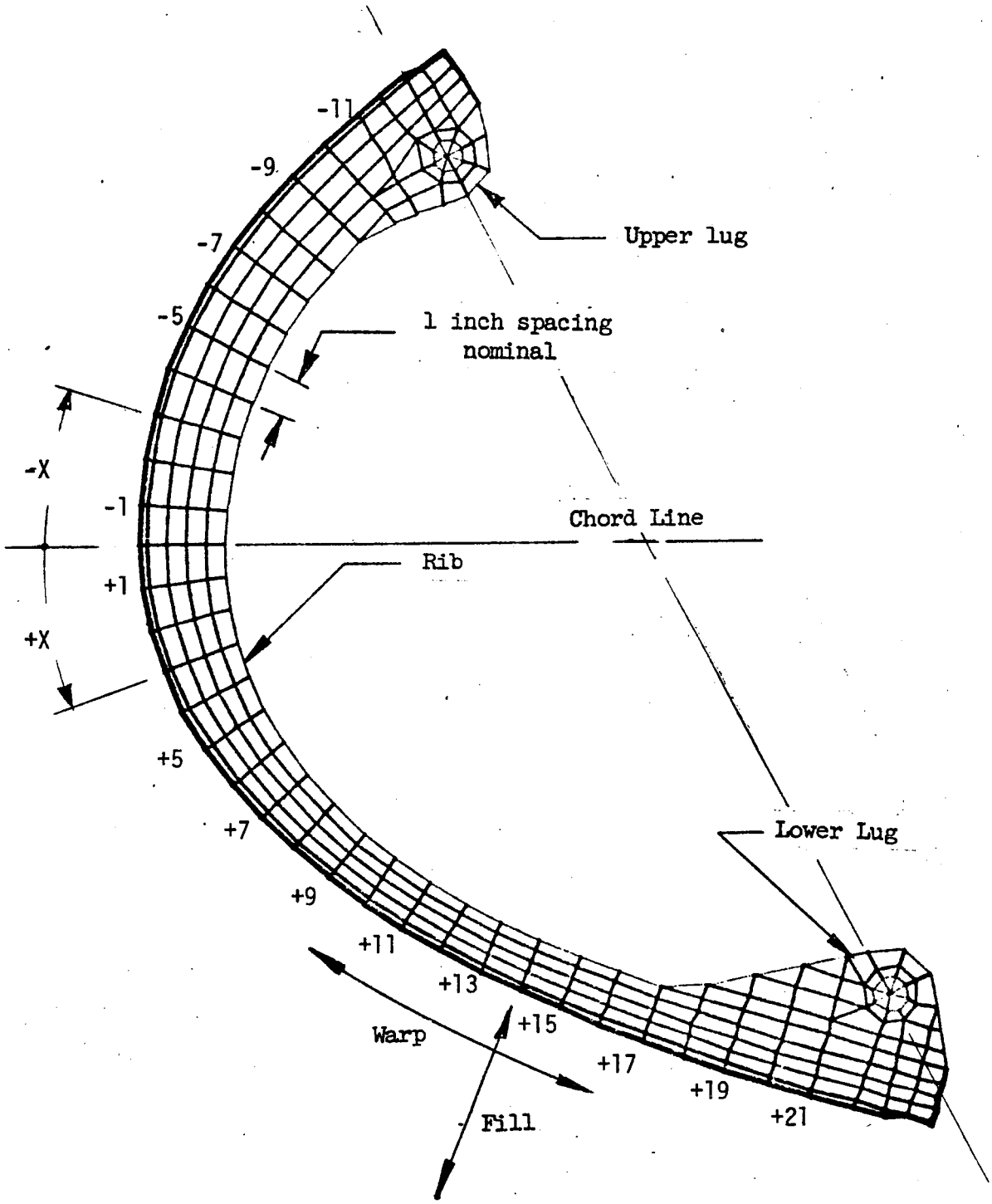

Figure 5 Side View of NASTRAN Rib Model

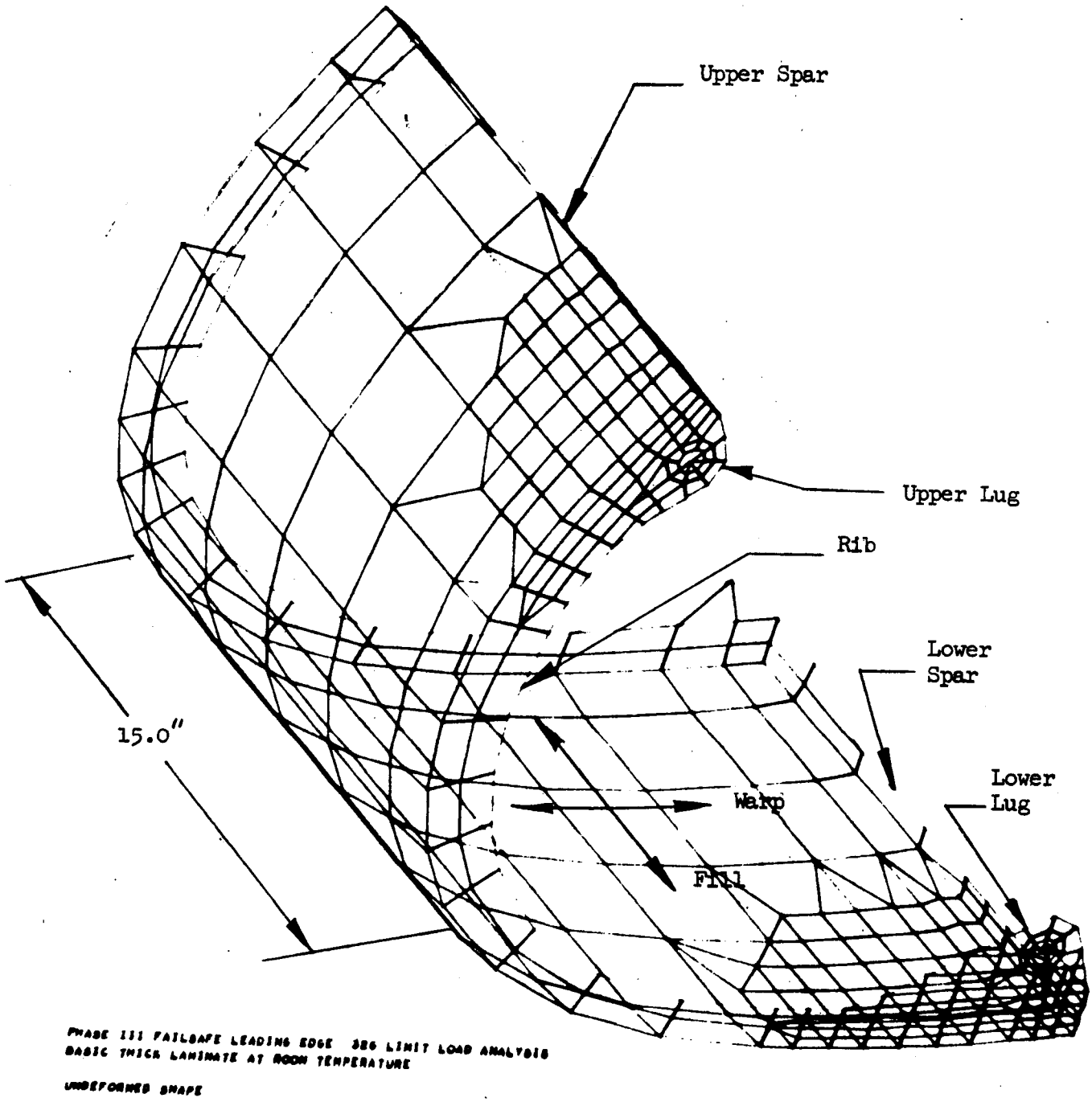

Figure 6 - Perspective view of the NASTRAN side load model

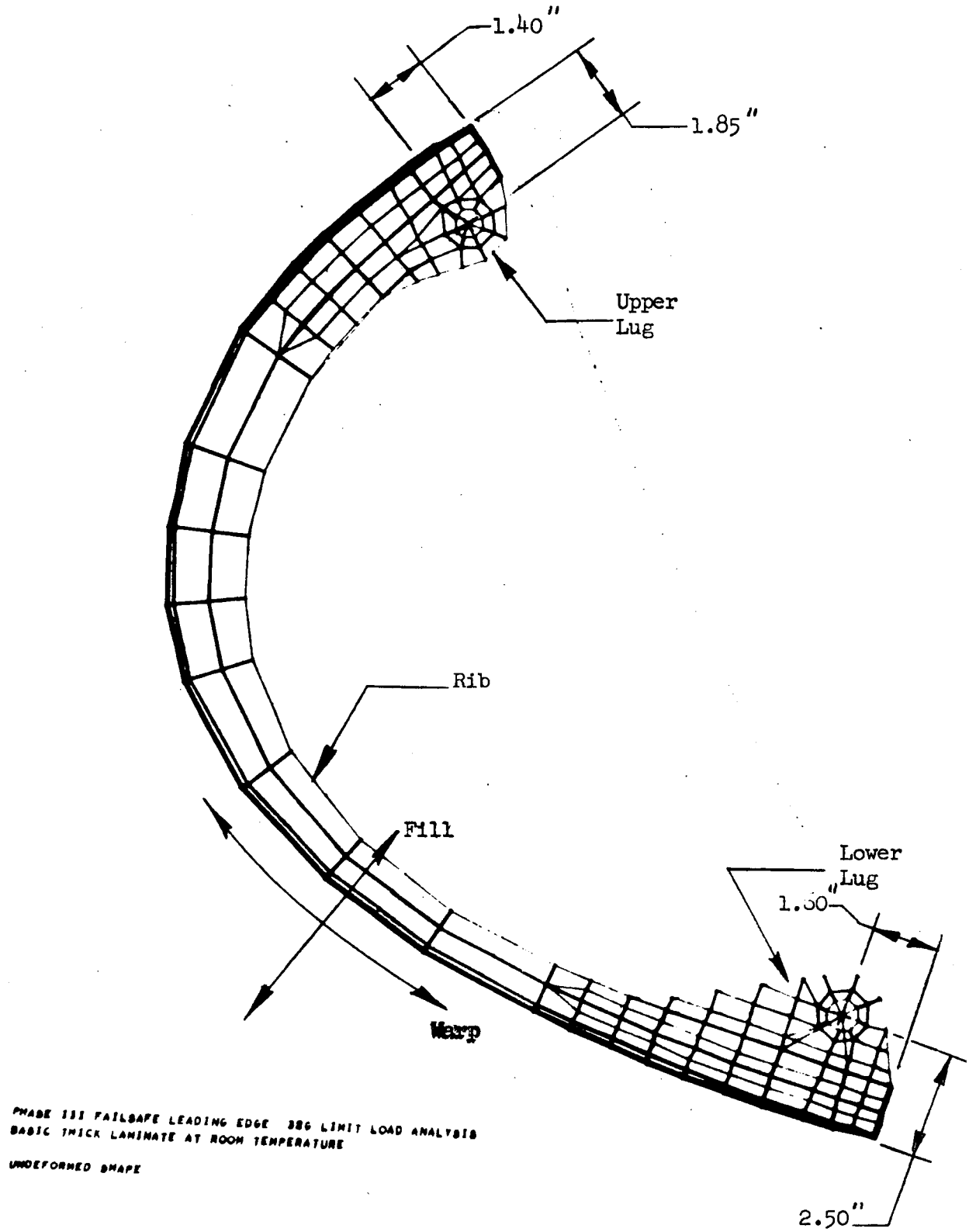

Figure 7 - Side view of the NASTRAN side load model

LIMIT LOADS

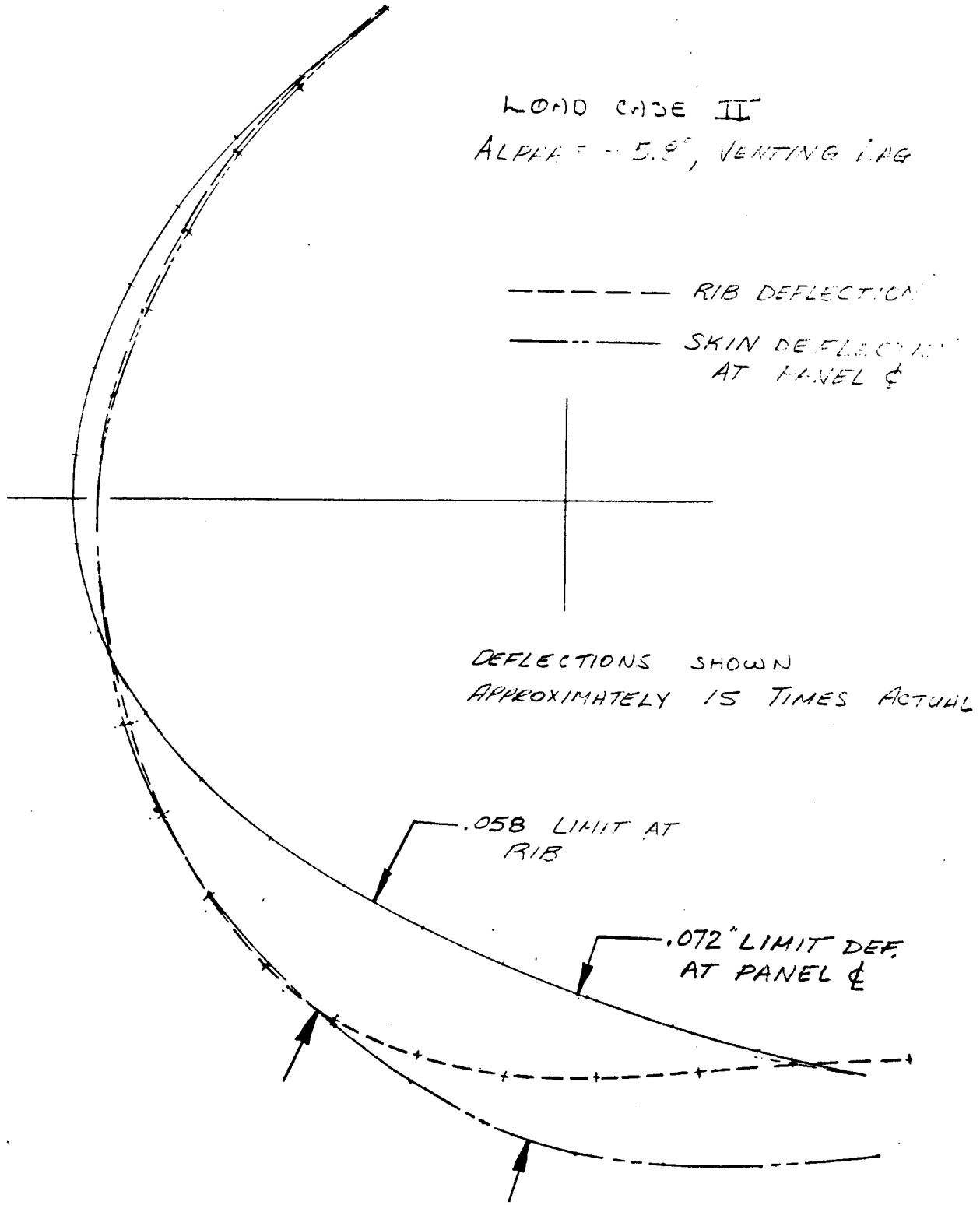

FIGURE 8. LIMIT PANEL DEFLECTIONS

ULT. LOADS

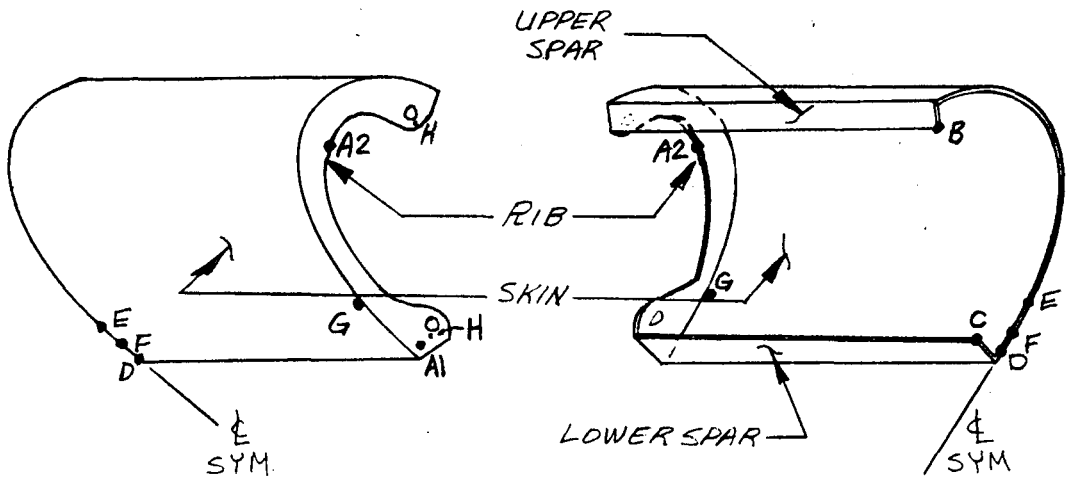

TABLE I - M.S. SUMMARY (BOOST)

POSITION	STRUCTURE	MATERIAL SPECS.	TYPE OF STRESS	MAXIMUM STRESS	ALLOW. STRESS *	M.S.	REF. FIG.
A1	LUG	23 PLY	SHEAR	1905	2500	0.31	10
A2	RIB	12 PLY	TENSION	3850	5400	0.40	12
B	UPPER SPAR	20 PLY COATED	COMPRESSION	-1570	-8800	4.60	13
C	LOWER SPAR	20 PLY COATED	COMPRESSION	-2360	-8800	2.73	13
D	SKIN	20 PLY COATED	MAXIMUM COMPRESSION	-1075	-5160 COMP. 6120 FLEXURE	+4.1	14
E	SKIN	22 PLY COATED	MAXIMUM MEMBRANE TENSION	+800	6300 TENSION 10,200 FLEXURE	HIGH	15
F	SKIN	21 PLY COATED	MAXIMUM FLEXURE	+800	6300 TENSION 10,200 FLEXURE	HIGH	15
G	SKIN	22 PLY COATED	SHEAR	750	2500	2.33	16
H	UPPER LUG	23-PLY	SHEAR	800	2500	2.12	17
	LOWER LUG	23-PLY	FLEXURE	4250	10,200	1.40	19

* FROM REF. A

ALL STRESSES ARE FOR LOAD CASE II EXCEPT "A1" AND "H" WHICH ARE FOR 32 "g" SIDE LOAD, AND B WHICH IS FOR LOAD CASE IV.

ULT LOADS

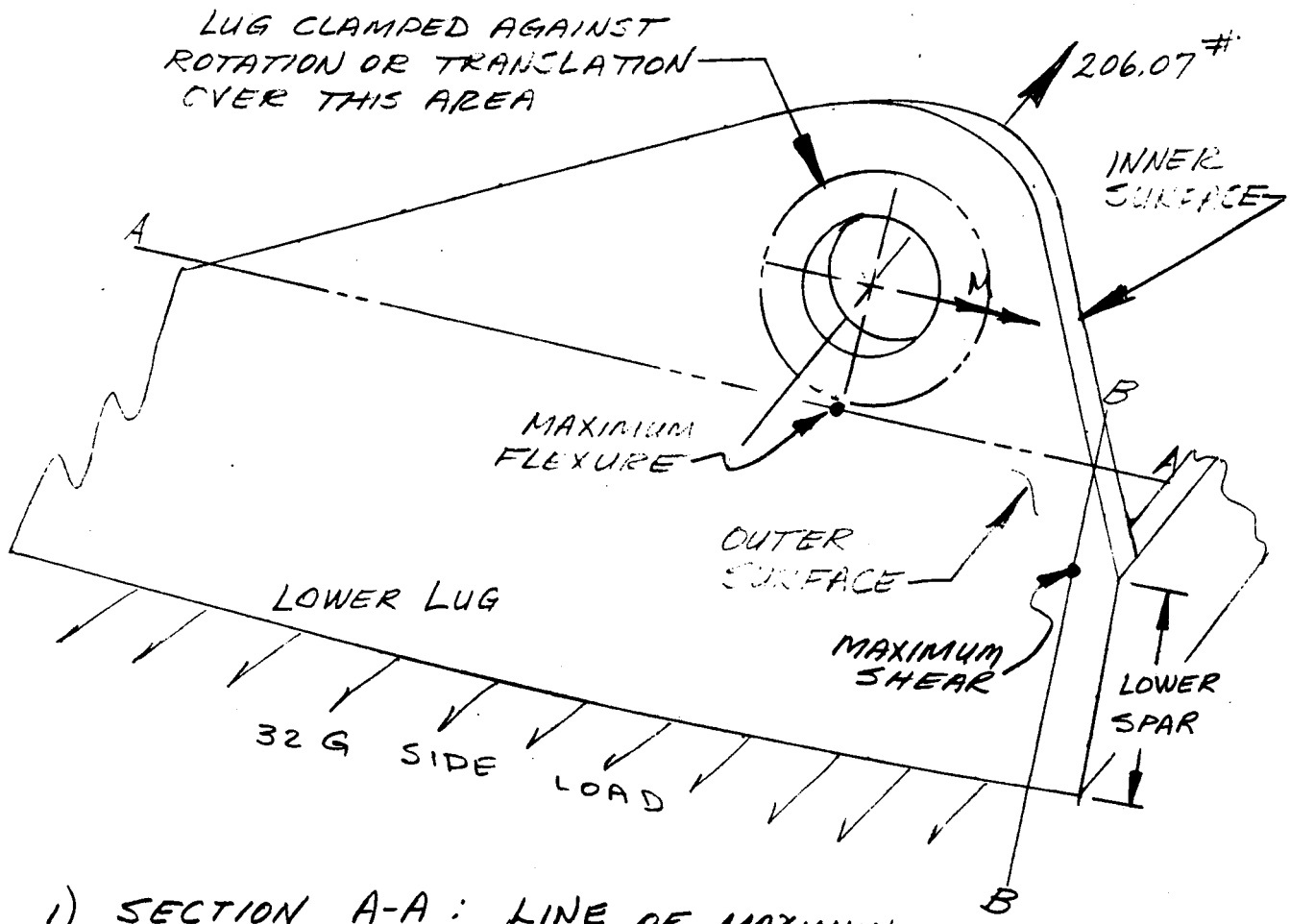

1) SECTION A-A : LINE OF MAXIMUM FLEXURE STRESSES (REF. FIG. 19)

2) SECTION B-B : LINE OF MAXIMUM SHEAR STRESS (REF. FIG. 10)

3) IN-PLANE LUG LOADS LOWER THAN FOR BOOST PHASE (REF. PGS. 27, 28, 32)

FIGURE 9 LOWER LUG STRESSES – 32 G SIDE LOAD

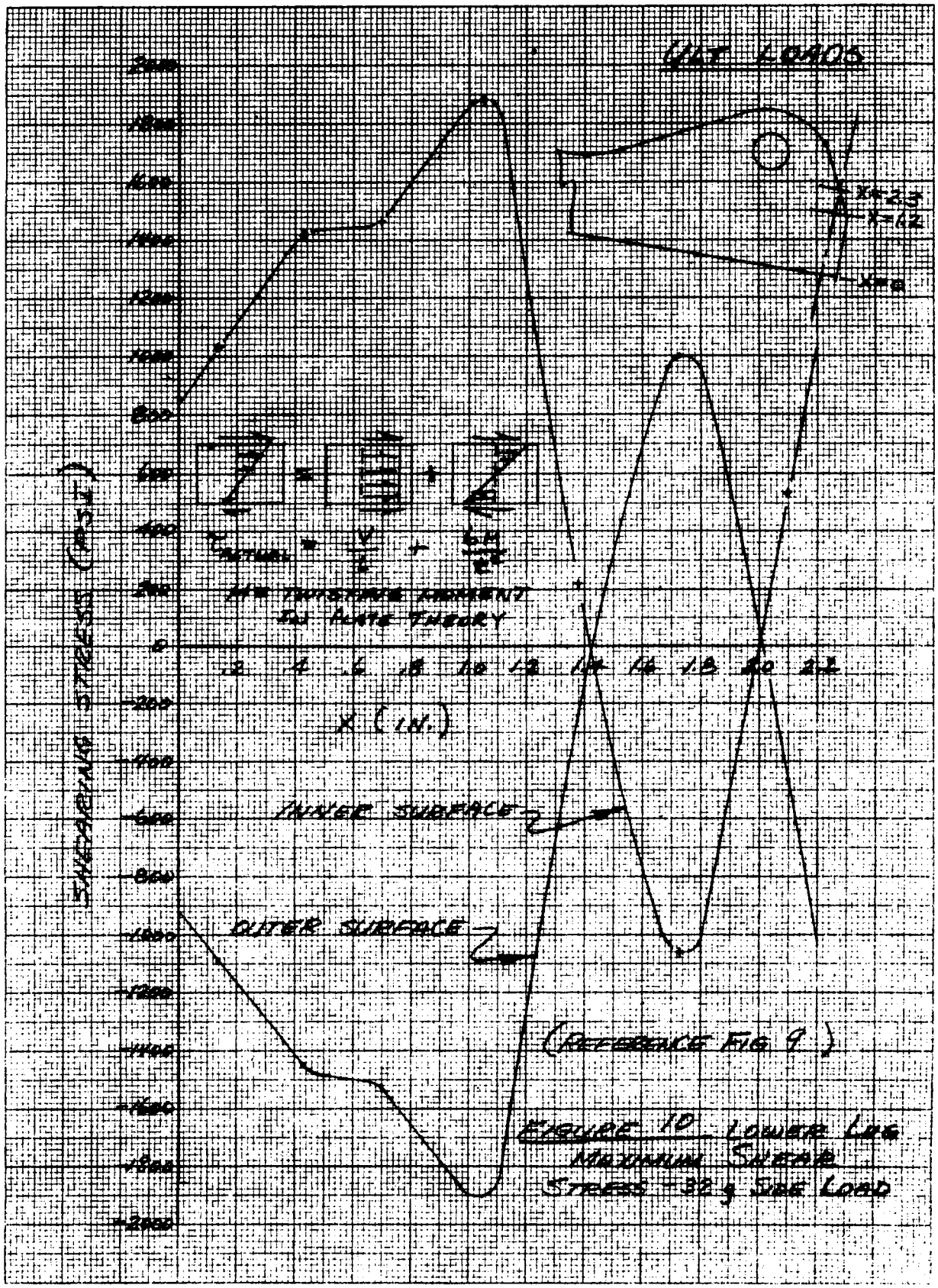

FIGURE 10 LOWER LEG MAXIMUM SHEAR STRESS - 32 g SIDE LOAD

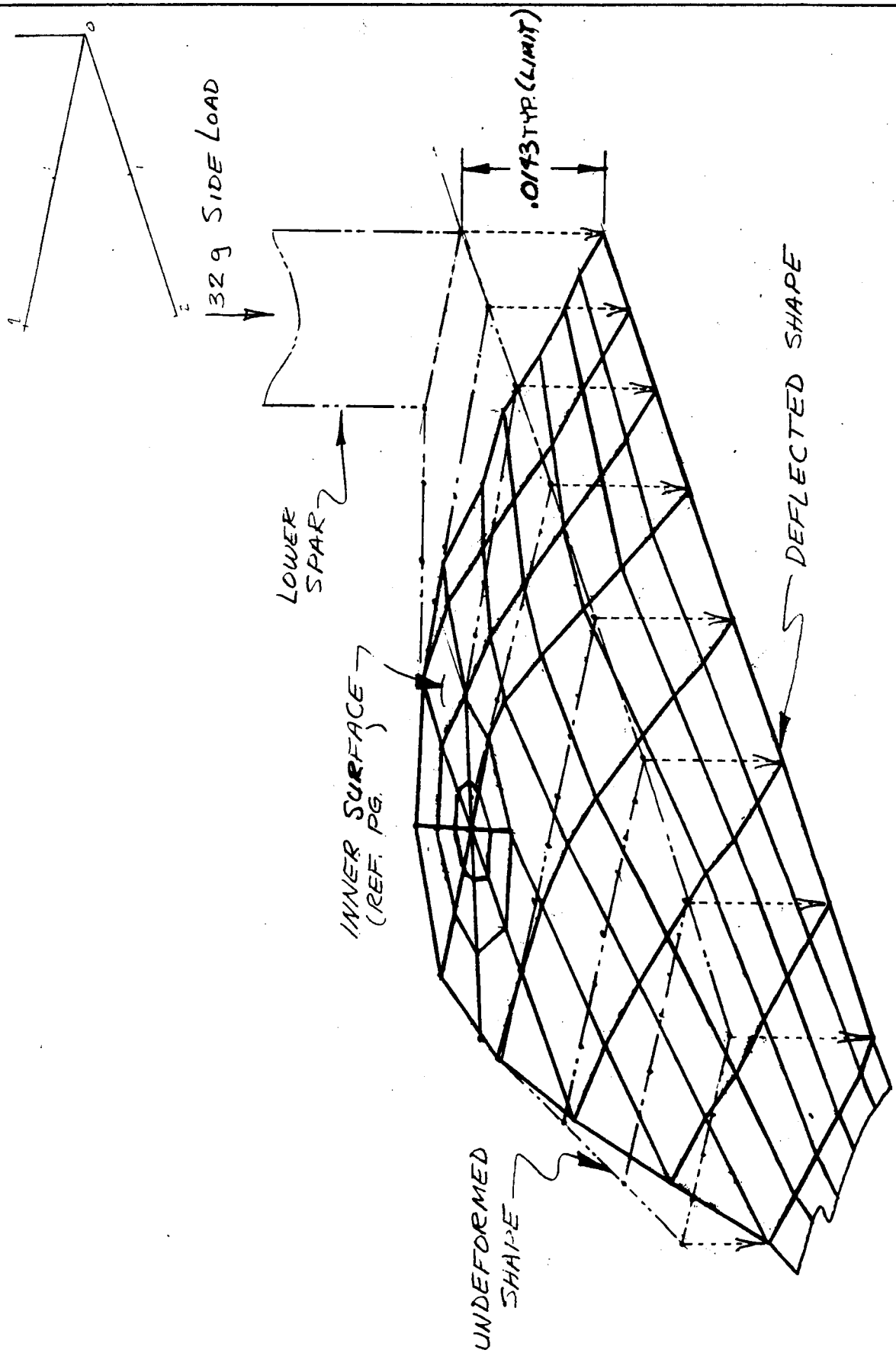

FIGURE 11 LUG DEFLECTION DUE TO 32 "g" SIDE LOAD

The following margins of safety are summarized for the 8 ply "oxidized" panel.

LOCATION	M.S.	BASED ON	
Rib	High	Tension	
Upper Spar	High	Compression	(Ref Page 13)
Lower Spar	+ 4.13	Tension	
Skin	High	Tension	
Skin	High	Flexure	
Skin	+ 1.50	Shear	
Skin	+ 2.43	Buckling	(Ref Page 7)

The maximum panel deflection occurs at the panel centerline near the lower spar. Maximum deflection at that point is .050" (limit). The panel is deflection critical which accounts for the high margins of safety in all areas.

DISCUSSION OF RESULTS:

Static Analysis - Based on design criteria, Reference (C), the external surface of the panel is assumed to be without the aid of the oxidation protective coating, leaving the panel free to ablate. Using predicted heating rates, the amount of thickness lost due to ablation was determined including a 20% tolerance, Reference (D). The panel was then sized such that a uniform 10 ply skin would remain. Of the ten (10) remaining plies, two (2) were assumed to be internal coating and consequently ineffective for load carrying capability. Therefore, this analysis considered the effective leading edge skin as 8 ply bare RPP-3. The rib remained 12 ply, coated RPP-3 and the upper and lower spars remained 20 ply, coated RPP-3. From Reference (A), the following material properties were used:

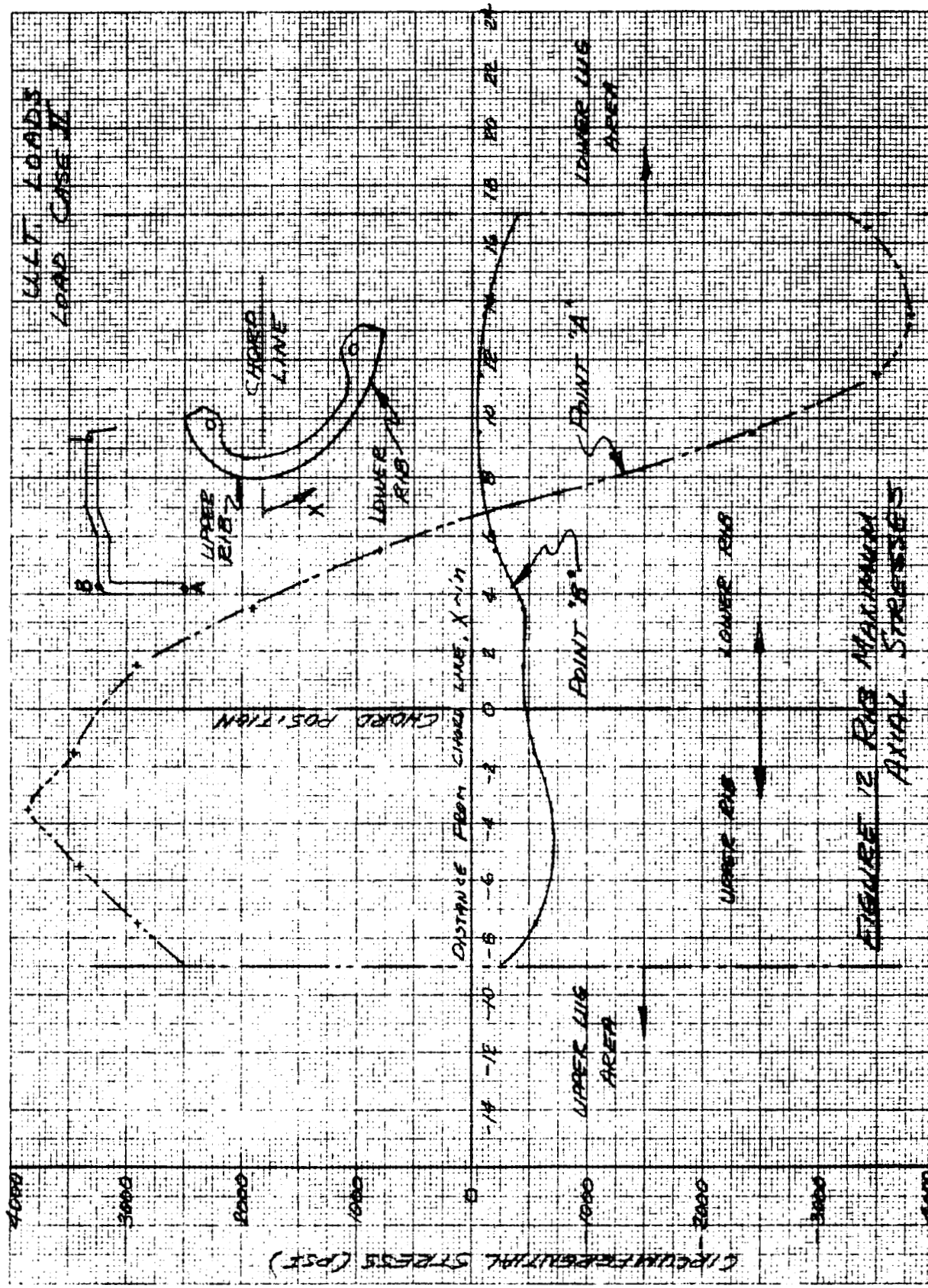

FIGURE 12 RIB MAXIMUM AXIAL STRESSES

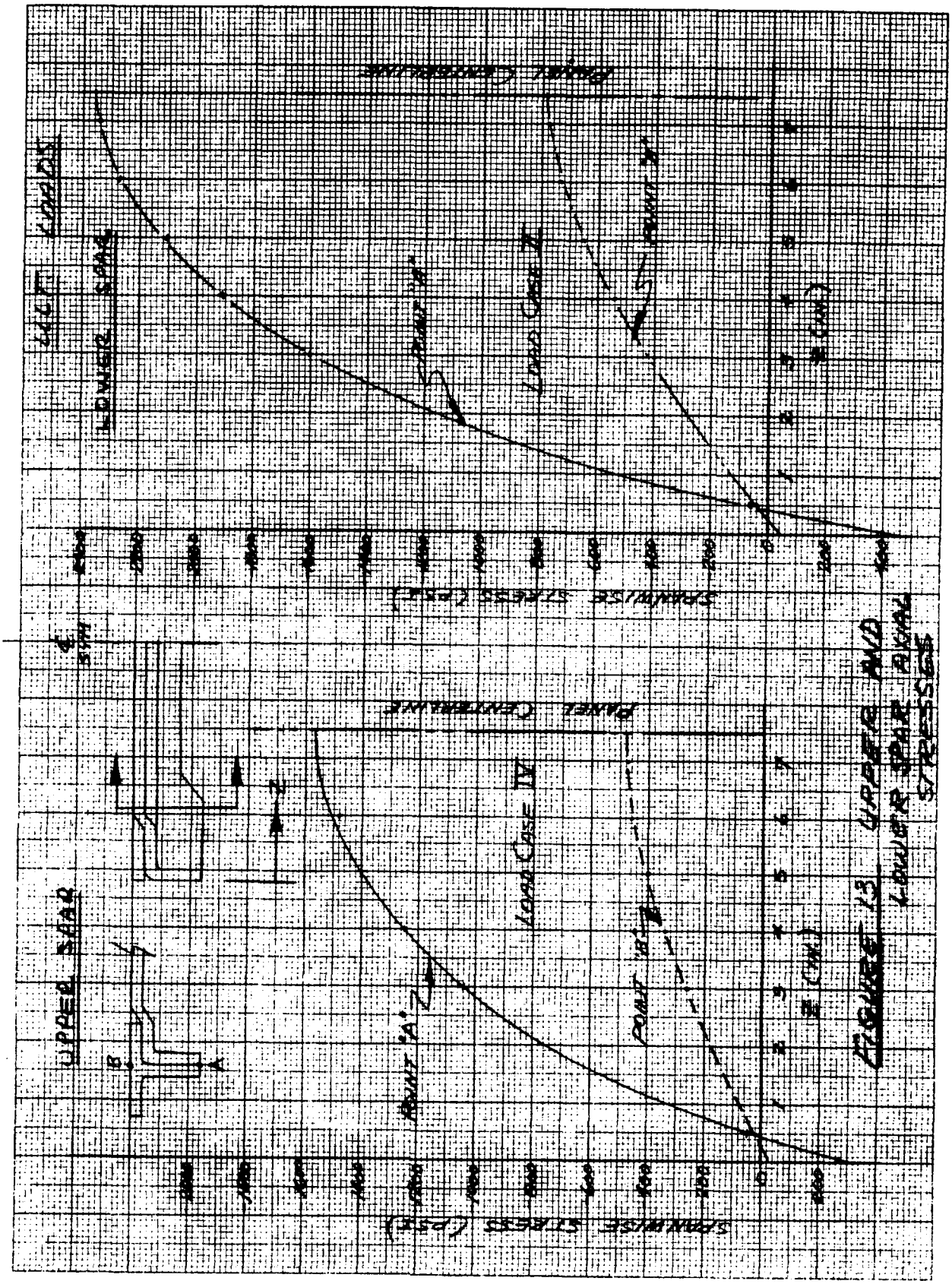

FIGURE 13 UPPER AND LOWER SPAR AXIAL STRESSES

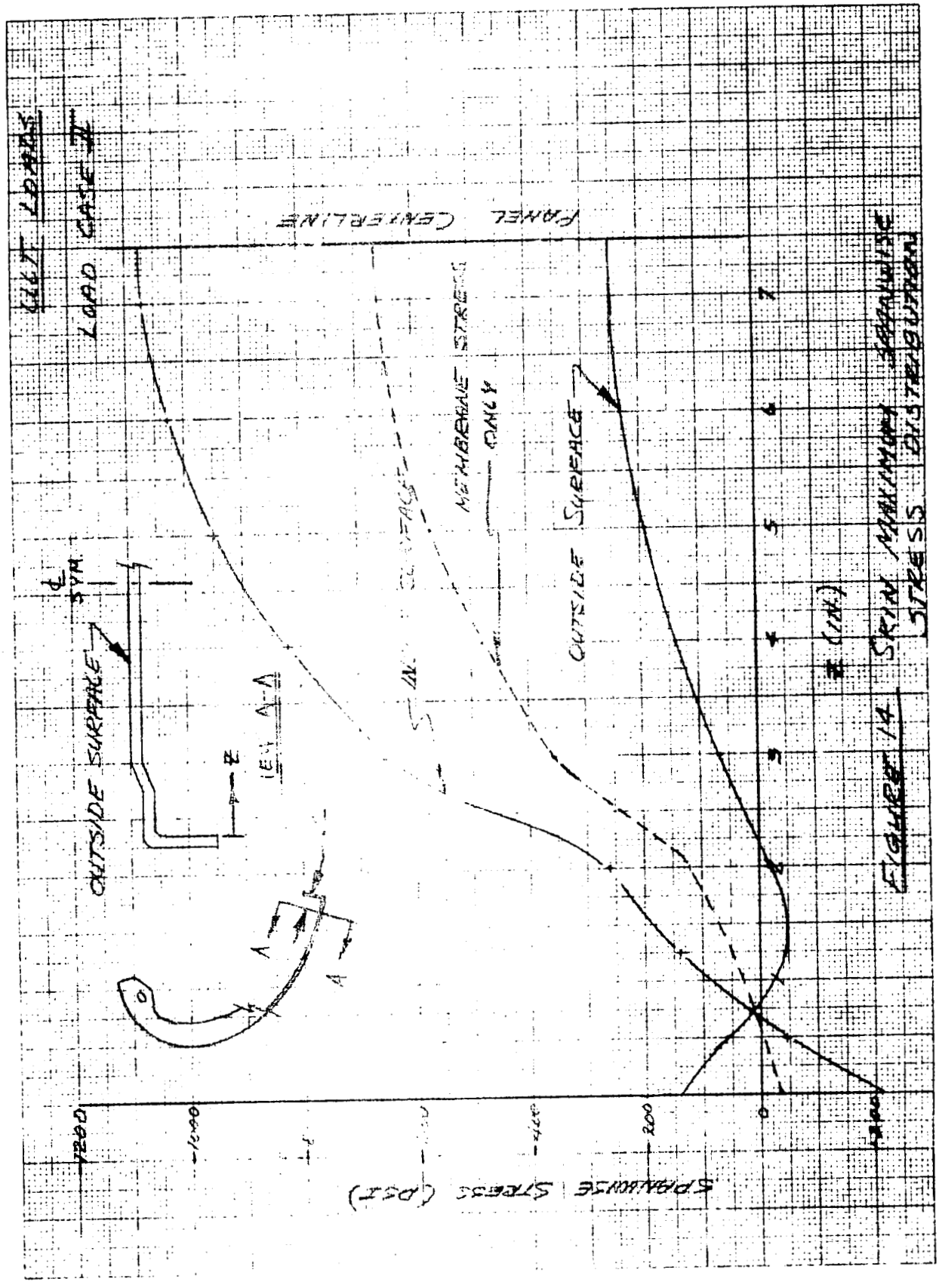

PRINTED IN U.S.A. ON CLEARPRINT TECHNICAL PAPER NO. 1015
CLEARPRINT CHARTS
CLEARPRINT PAPER

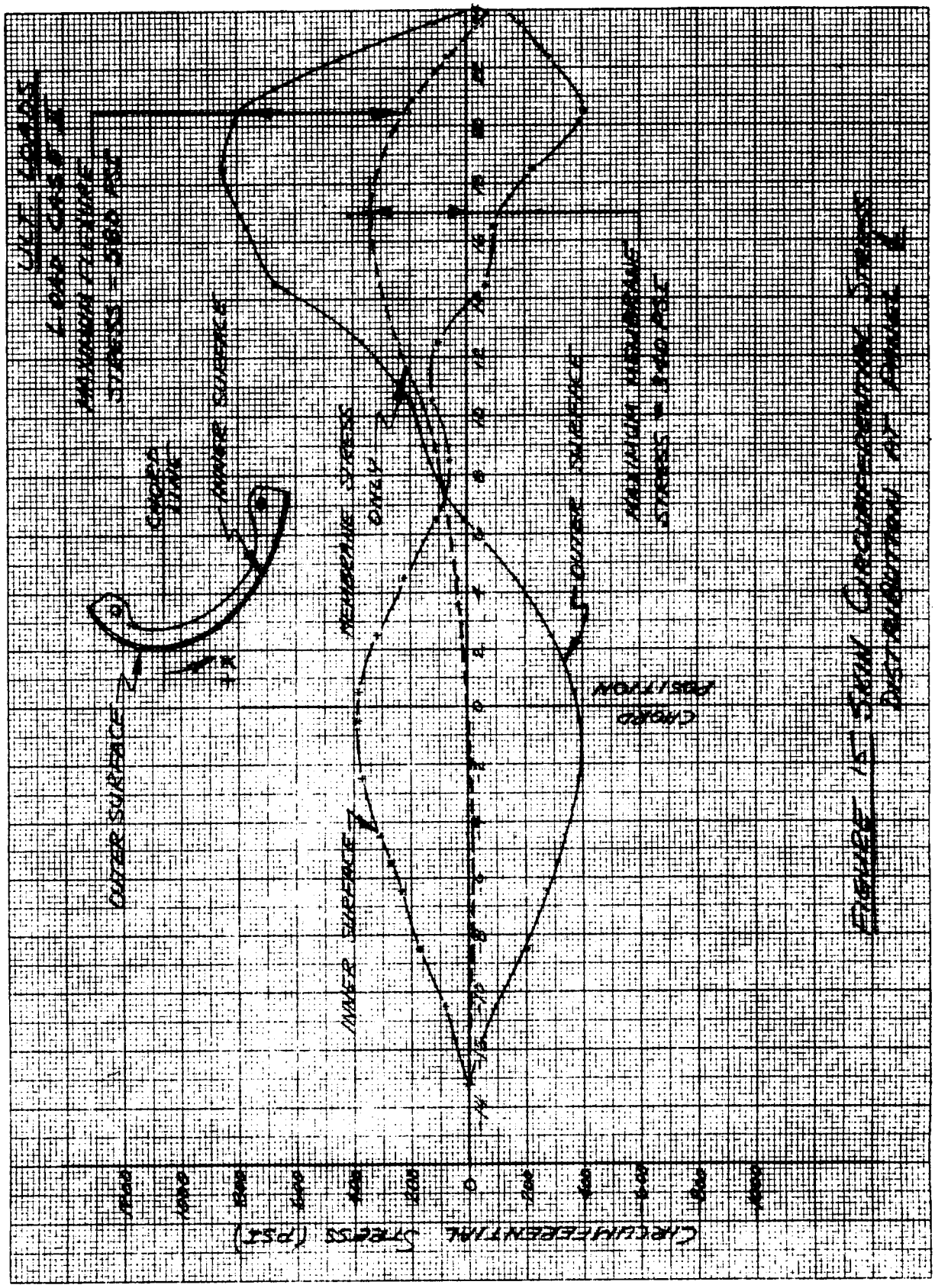

FIGURE 15 SKIN CIRCUMFERENTIAL STRESS DISTRIBUTION AT PANEL 2

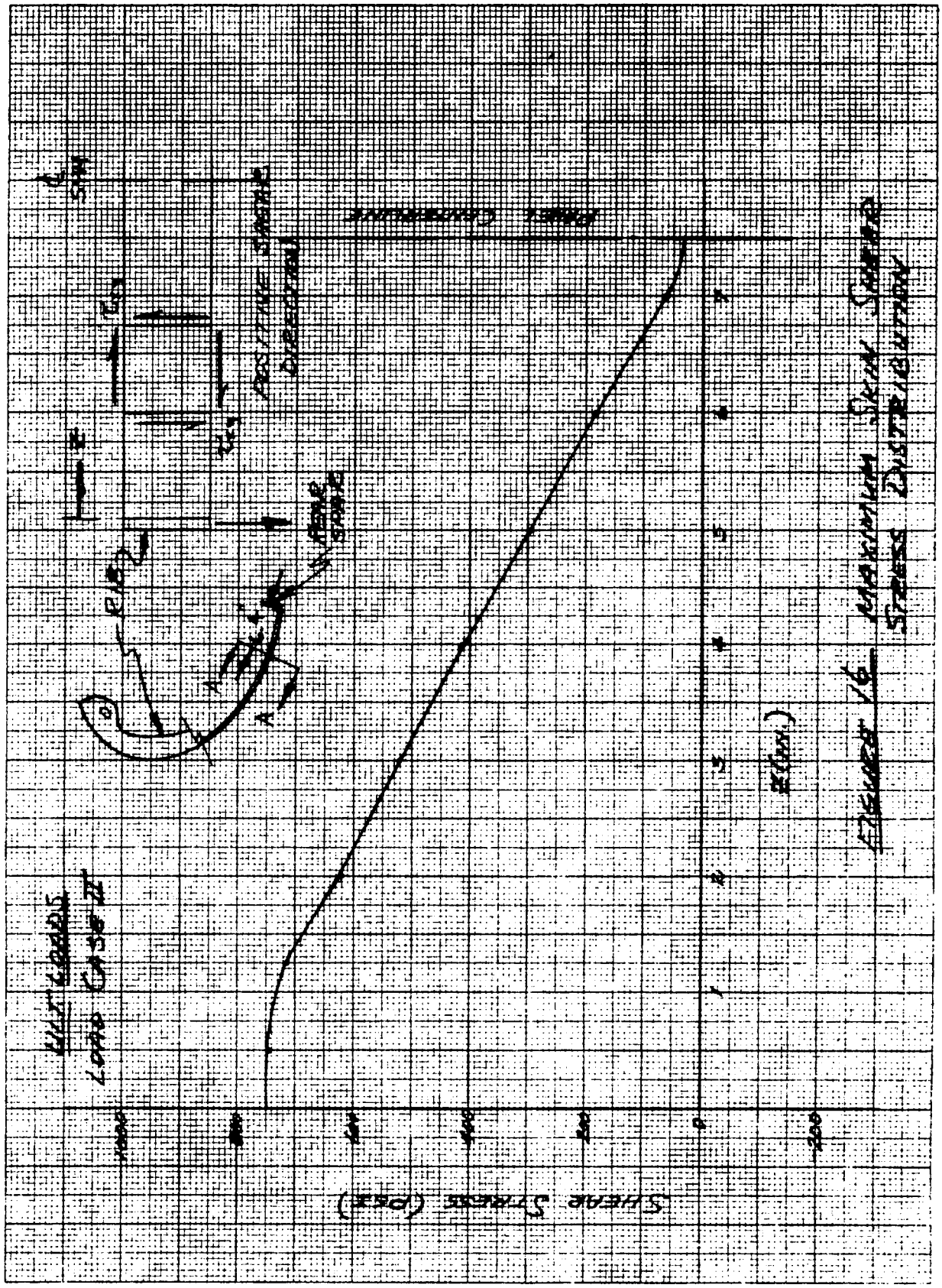

FIGURE 16 MAXIMUM SKIN SHEAR STRESS DISTRIBUTION

ULT LOADS

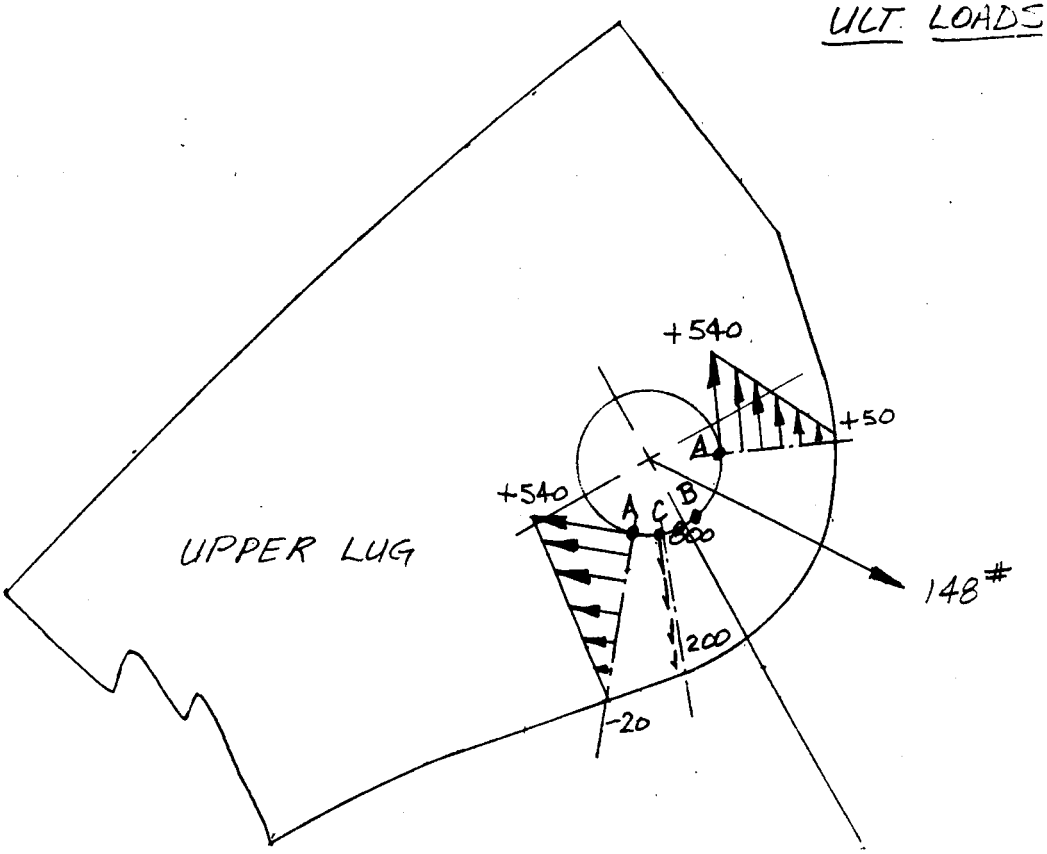

LOAD CASE III (REF. PG. 12)

LOCATION	TYPE OF STRESS	MATERIAL SPEC.	MAXIMUM STRESS	ALLOWABLE STRESS (REF. (A))	M.S. (ULT)
A	TENSION	23 PLY, COATED	540	6200	+10.5
B	COMPRESSION	23 PLY, COATED	-489*	-5600	+16.7
C	SHEAR	23 PLY, COATED	800	2500	+2.12

* COMPRESSION STRESS WAS NOT PLOTTED BUT WAS TAKEN DIRECTLY FROM THE NASTRAN RUN

FIGURE 17. UPPER LUG LOADS FOR LOAD CASE III

ULT. LOADS

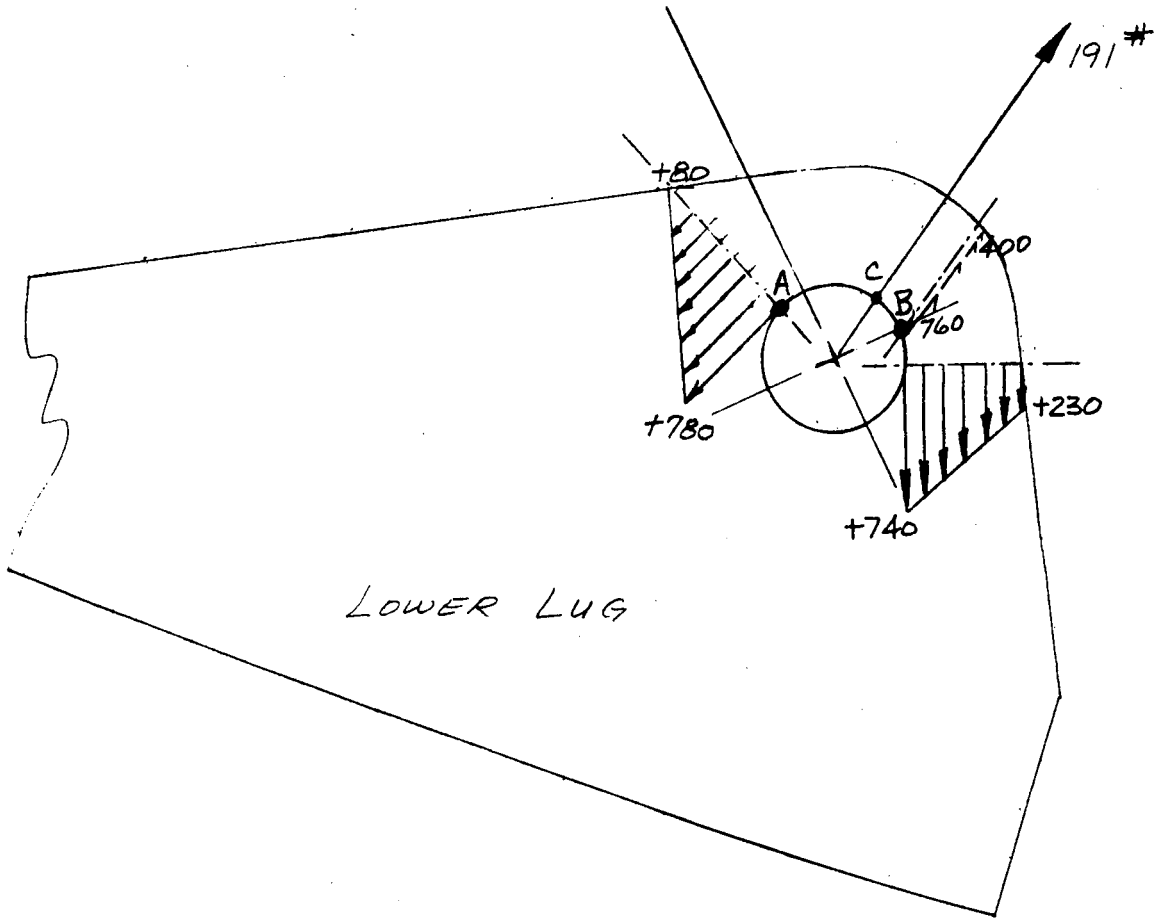

LOAD CASE II (REF. PG 11)

LOCATION	TYPE OF STRESS	MATERIAL SPECS.	MAXIMUM STRESS	ALLOW. STRESS (REF (A))	M.S. (ULT.)
A	TENSION	23 PLY, COATED	780	6200	+6.95
B	SHEAR	23 PLY COATED	760	2500	+2.29
C	COMPRESSION	23 PLY COATED	-600*	-8600	+13.3

* COMPRESSION STRESS WAS NOT PLOTTED BUT WAS TAKEN DIRECTLY FROM THE NASTRAN RUN

FIGURE 18. LOWER LUG LOADS FOR LOAD CASE II

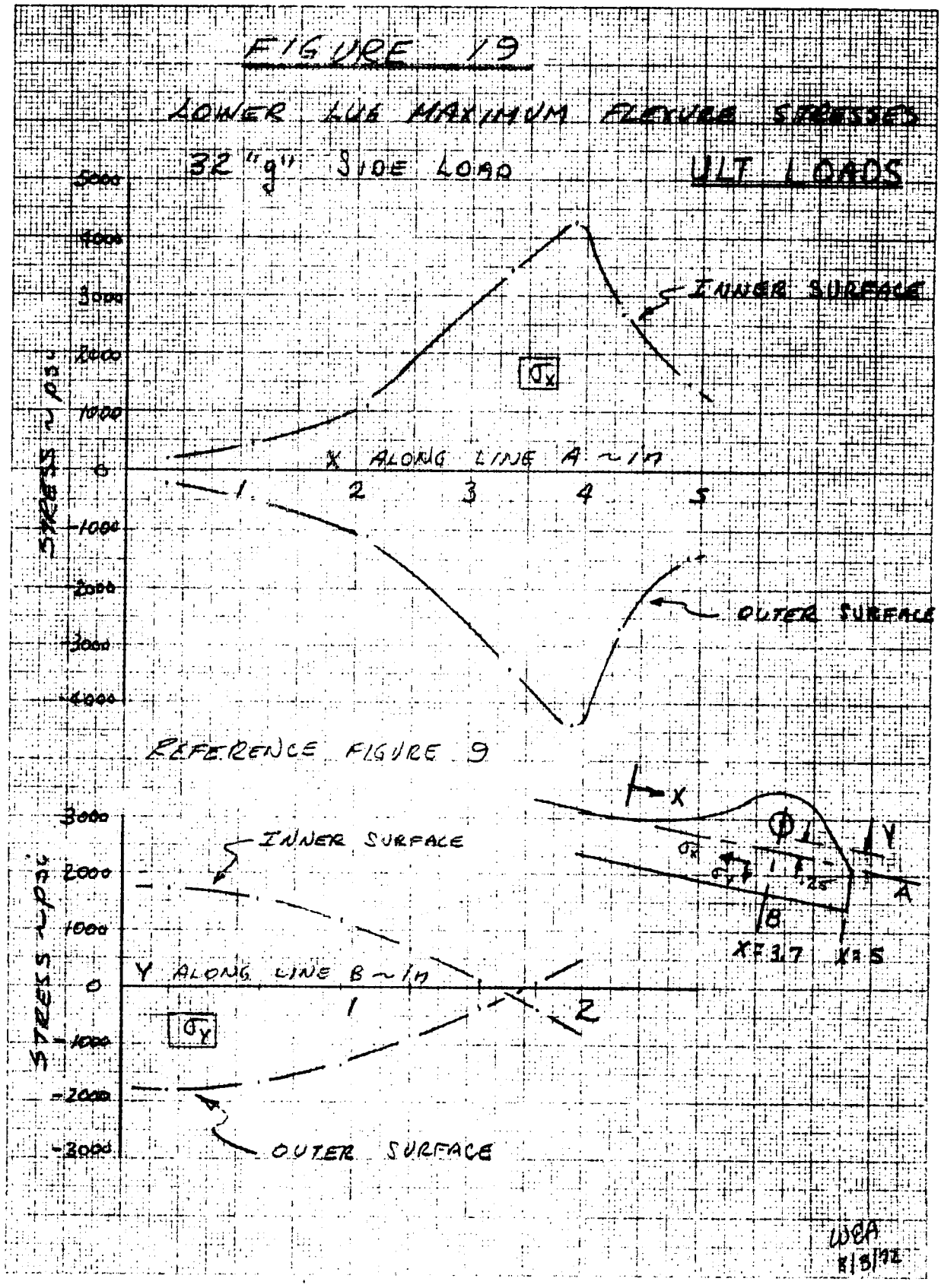
FIGURE 19
LOWER LUG MAXIMUM FLEXURE STRESSES
32 "g" SIDE LOAD
ULT LOADS
INNER SURFACE
OUTER SURFACE
X ALONG LINE A ~ in
STRESS ~ psi
REFERENCE FIGURE 9
INNER SURFACE
OUTER SURFACE
Y ALONG LINE B ~ in
STRESS ~ psi
X = 3.7
X = 5
WEA
8/3/72

CLEARPRINT PAPER CO. NO. 1015 MILLIMETERS BOTH WAYS 150 X 220 DIVISIONS PRINTED IN U.S.A. ON CLEARPRINT TECHNICAL PAPER NO. 1015
CLEARPRINT CHARTS

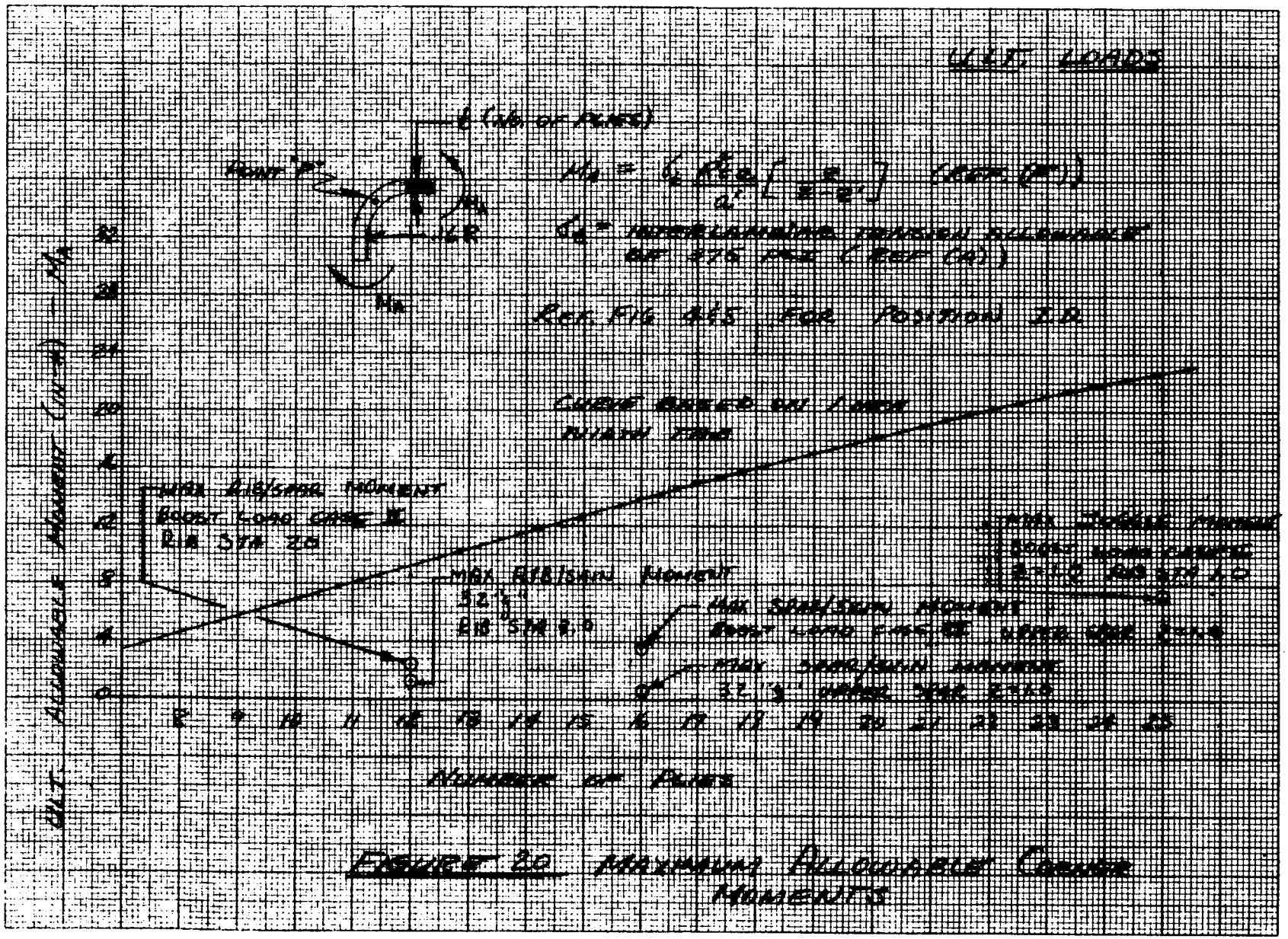

Figure 20 Maximum Allowable Cover Moments

EXTERNAL BALANCE

TABLE II

FAILSAFE LEADING EDGE/STATIC ANALYSIS/BOOST LOAD CASE II

α = -5.8°, venting lag

TYPE	FF (lbs)	FU (lbs)	FO (lbs)	MF (in-lbs)	MU (in-lbs)	MO (in-lbs)
1	0.165E 03	0.120E 01	0.576E 00	0.125E 04	0.639E 03	0.101E 04
1	-0.243E 02	-0.316E 03	-0.741E 01	-0.495E 01	-0.979E 02	-0.144E 03
2	0.0	0.316E 03	0.804E 03	0.782E 04	0.375E 04	0.103E 04
2	-0.141E 03	0.0	-0.797E 03	-0.903E 04	-0.430E 04	-0.190E 04
3				0.0	0.0	0.0
3				0.0	0.0	0.0
4				0.712E 01	0.225E 02	0.0
4				-0.516E 02	-0.160E 02	0.0
TOTALS	-0.184E 00	0.158E 01	-0.419E-03	-0.102E 02	-0.139E 01	-0.112E 02

TYPE 1= BALANCE FROM APPLIED POINT LOADS
2= BALANCE FROM CONSTRAINT POINT LOADS
3= BALANCE FROM APPLIED MOMENTS
4= BALANCE FROM CONSTRAINT MOMENTS

NOTE- WHEN ONLY THERMAL LOADING IS PRESENT, TYPES 1 AND 3 ARE NOT CONSIDERED IN THE BALANCE

FF, MF - FORCE AND MOMENT FORWARD
FU, MU - FORCE AND MOMENT UP
FO, MO - FORCE AND MOMENT OUTBOARD

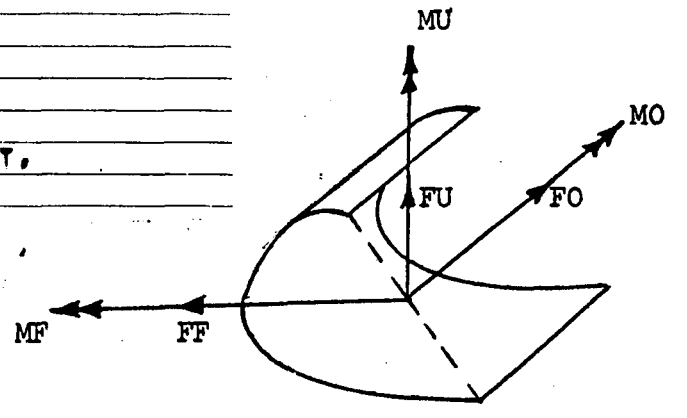

SIGN CONVENTION

ULT LOADS

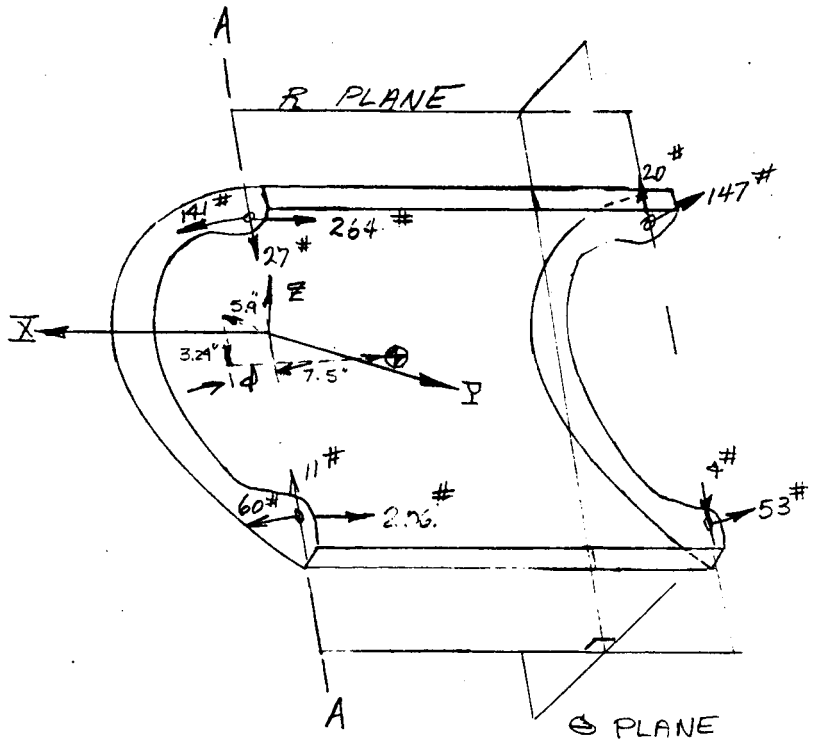

$N_x = 49.5$ g's
WT: 10.48 lbs

$\Sigma F_{R\,PLANE} = 27 + 4 - 11 - 20$

$\boxed{\Sigma F_R = 0}$

$\Sigma F_x = -2.76 - 264 + (10.48)(44.8)$

$\boxed{\Sigma F_x = -0.5\#}$

$\Sigma F_{\theta\,PLANE} = 141 + 60 - 147 - 53$

$\boxed{\Sigma F_\theta = 1}$

$\Sigma M_{A-A} = 10.48(-44.8)(d) + (147+53)15$

d = ⊥ DISTANCE FROM CG OF PANEL TO LINE A-A
d = .674"
10.48# = WEIGHT OF PANEL UNDER 1g
44.8 = ACCELERATION OF PANEL IN g's

$\Sigma M_{A-A} = -3140 + 3015$

$\boxed{\Sigma M_{A-A} = -125 \text{ in-\#}}$

FIGURE 21 SIDE LOAD REACTIONS & EQUILIBRIUM

Entry Thermoelastic Analysis - During normal operation, the "fail safe" leading edge passes through the entry phase with protection of the oxidation inhibiting coating. As a result of entry heating, thermal gradients are produced in the thick laminate skin as well as the ribs and the spars. One design condition, therefore, is to insure that the entry heating will not produce excessive thermoelastic stresses. For this analysis, three times were chosen representing the worst thermal loading conditions encountered. These times are 260, 300, and 400 seconds after initiation of the entry profile. The time 260 seconds represents the maximum temperature gradient across the rib, and is referred to as thermal load case I. The time 300 seconds represents the maximum gradient through the skin, and is referred to as thermal load case II. The time 400 seconds represents the maximum gradient in the circumferential direction around the leading edge, and is referred to as thermal load case III. The skin surface temperatures for the three thermal load cases are shown in Figure 22 and are from Reference (E). The rib temperatures at the maximum heating location are presented in Figure 23 for the three thermal load cases. These data are from Reference (E), which also contains similar information at different rib stations. The spectrum of rib temperatures was determined by interpolating between rib stations.

The thermoelastic problem was modeled and run using the NASTRAN computer routine. The model is identical to the one used for the static boost loads and is shown in Figures 4 and 5. The rib and spars use the same elements as were used for the static loads model. However, the skin was modeled using thermoelastic elements which allow temperature gradients to be specified through the element thickness. Appendix A contains a closed form solution using this element in a thermoelastic analysis. NASTRAN handles thermoelastic problems by averaging the temperatures at the grid points defining each element, and then assumes that the temperature is constant over the whole element. Thermal elements allow the average temperature to vary through the thickness only. Free thermal

strains are computed based on the input reference temperature, the element geometry and the element coefficient of thermal expansion. Then, using the input material properties, the forces necessary to return the element to its original size and shape are computed. These "equivalent static loads" are then divided equally and applied at the grid points defining the element. The anisotropic nature of the elements is retained and warp and fill properties were used. In addition, all element properties were made temperature dependent. Different from the static analysis, the compression modulus was used for the membrane element in all thermoelastic analyses, which is conservative for tensile stresses.

Figure 24 shows the maximum skin deflection of .055" (limit) which occurs at t = 400 seconds. Figures 25, 26, and 27 are plots of the spanwise deformation due to thermal expansion. The maximum deflection occurs at 400 seconds and is .052" (limit).

Table II presents a summary of thermoelastic margins of safety at entry. Figures 28, 29 and 30 are plots of the circumferential (hoop) stress for 260, 300 and 400 seconds. All are plotted for stresses occurring 2" from the rib, just inboard of the joggle and represent maximum developed tensile stresses. The largest stress occurs at 400 seconds at rib station -10.0, Reference Figure 5, and is +1790 psi. The element at that point is at 1960°F, giving a tension allowable of 6300 psi, Reference (A).

$$M.S. = \frac{6300}{1790} - 1 \qquad M.S. = +2.52 \text{ ULT}$$

The maximum flexure stress of 1050 psi occurs at 400 seconds at rib station +2.0, Reference Figure 5. The element is at 2420°F which yields a flexure strength of 15,250 psi, Reference (A).

$$M.S. = \frac{15,250}{1,050} - 1 \qquad M.S. = +13.5 \text{ ULT}$$

Figure 31 is another circumferential cut taken along the joggle at 1.25" from the rib. The plot is for 400 seconds which gives the greatest skin compression stress of -2900 psi at rib station -13.5 The temperature at that point of 1560°F gives the material a compression strength of -10,400 psi, Reference (A).

$$M.S. = \frac{10,400}{2,900} - 1 \qquad M.S. = +2.59 \text{ ULT}$$

The maximum skin shear stress for each thermal load case is shown in Figures 32, 33, and 34. The maximum shear stress of 1070 psi occurs 1.25" from the rib at 400 seconds. The local temperature at 400 seconds is 1560°F which gives a shear strength of 2500 psi, Reference (A).

$$M.S. = \frac{2500}{1070} - 1 \qquad M.S. = +1.34 \text{ ULT}$$

Maximum stresses for the upper spar is developed at 400 seconds and is shown in Figure 35. The stress is tensile and has a value of 1400 psi. At the local temperature of 805°F, the tension strength is 5600 psi.

$$M.S. = \frac{5600}{1400} - 1 \qquad M.S. = +3.00 \text{ ULT}$$

Maximum stress for the lower spar, shown in Figure 36, is compressive and occurs at 260 seconds. The stress of -1000 psi, with an allowable at 920°F of 9000 psi, Reference (A), gives a margin of safety of:

$$M.S. = \frac{9000}{1000} - 1 \qquad M.S. = +8.00 \text{ ULT}$$

Rib stress distributions at rib stations corresponding to local maximum stresses are shown in Figures 37, 38, and 39. The maximum rib tensile stress of +2050 psi occurs for t = 300 seconds at rib station 9.5, Reference

Figure 5. The local tensile strength is 5600 psi at 1410°F, from Reference (A).

$$M.S. = \frac{5600}{2050} - 1 \qquad M.S. = +1.74 \text{ ULT}$$

Note that the maximum rib stress (t = 300 seconds) does not occur at the time of maximum rib temperature gradient (t = 260 seconds); however, the stresses at both times are within about 200 psi of each other. The leading edge has three variables that influence the thermoelastic stresses; namely, temperatures, temperature gradients, and temperature dependent material properties, and therefore critical conditions are not always easily predicted.

The stress distribution around the perimeter of the rib is shown in Figure 40 for tension and Figure 41 for compression. Each plot is taken at a constant rib height that passes through the point of maximum stress.

The spanwise stress distribution at the panel centerline is presented in Figure 42. The majority of the upper surface is either tension or compression membrane stresses, while the lower panel is primarily flexure. The minimum margin of safety is at rib station -11.0 where the stress is 1030 psi tension. The temperature is 620°F and the 16 ply tension fill allowable is 3600 psi.

$$M.S. = \frac{3600}{1030} - 1 \qquad M.S. = +2.5 \text{ ULT}$$

The reactions developed as a result of the thermal loads are shown in Figure 43. These reactions correlate with the rib stresses, i.e., tension at 260 and 300 seconds and compression at 400 seconds. External equilibrium for the thermoelastic analyses has been verified by an independent routine that utilizes model geometry and constraint point loads (reactions). The equilibrium data is presented in Tables IV through VI for the three thermal load cases and shows good balance. The summation of moments (MO) about the "O" axis shows a maximum imbalance of 103 in-lbs. This imbalance results from a solution involving many

large internal loads (equivalent static loads on page 34), and is the difference between two large numbers, estimated to be approximately 500,000 in-lbs. The internal loads do not figure in external equilibrium; so, the loads that generated the moment were not included in the equilibrium check. The percent error of 103 in-lbs out of 500,000 in-lbs is about 0.02%.

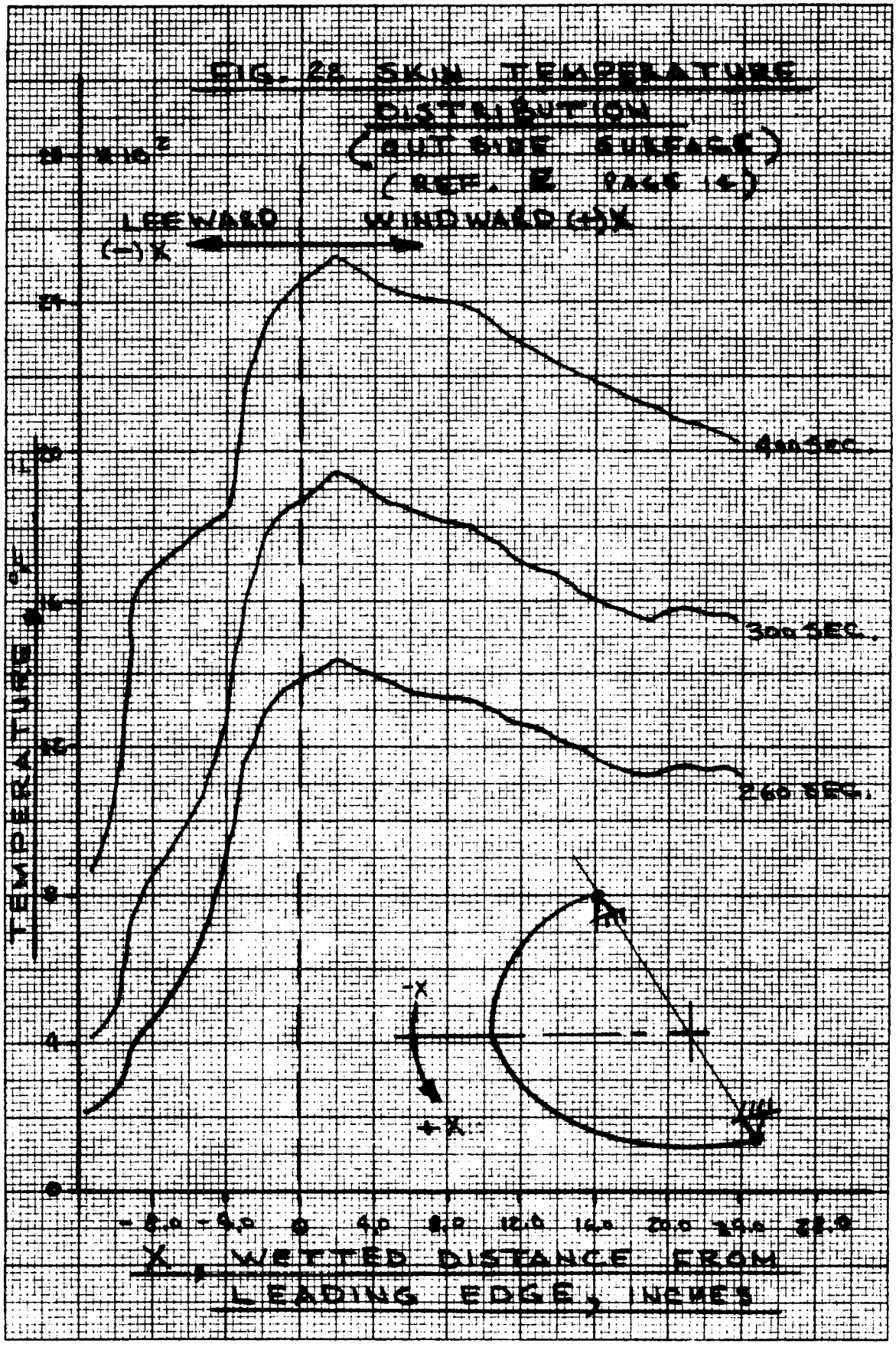

FIG. 28 SKIN TEMPERATURE DISTRIBUTION (OUTSIDE SURFACE) (REF. E PAGE 14)

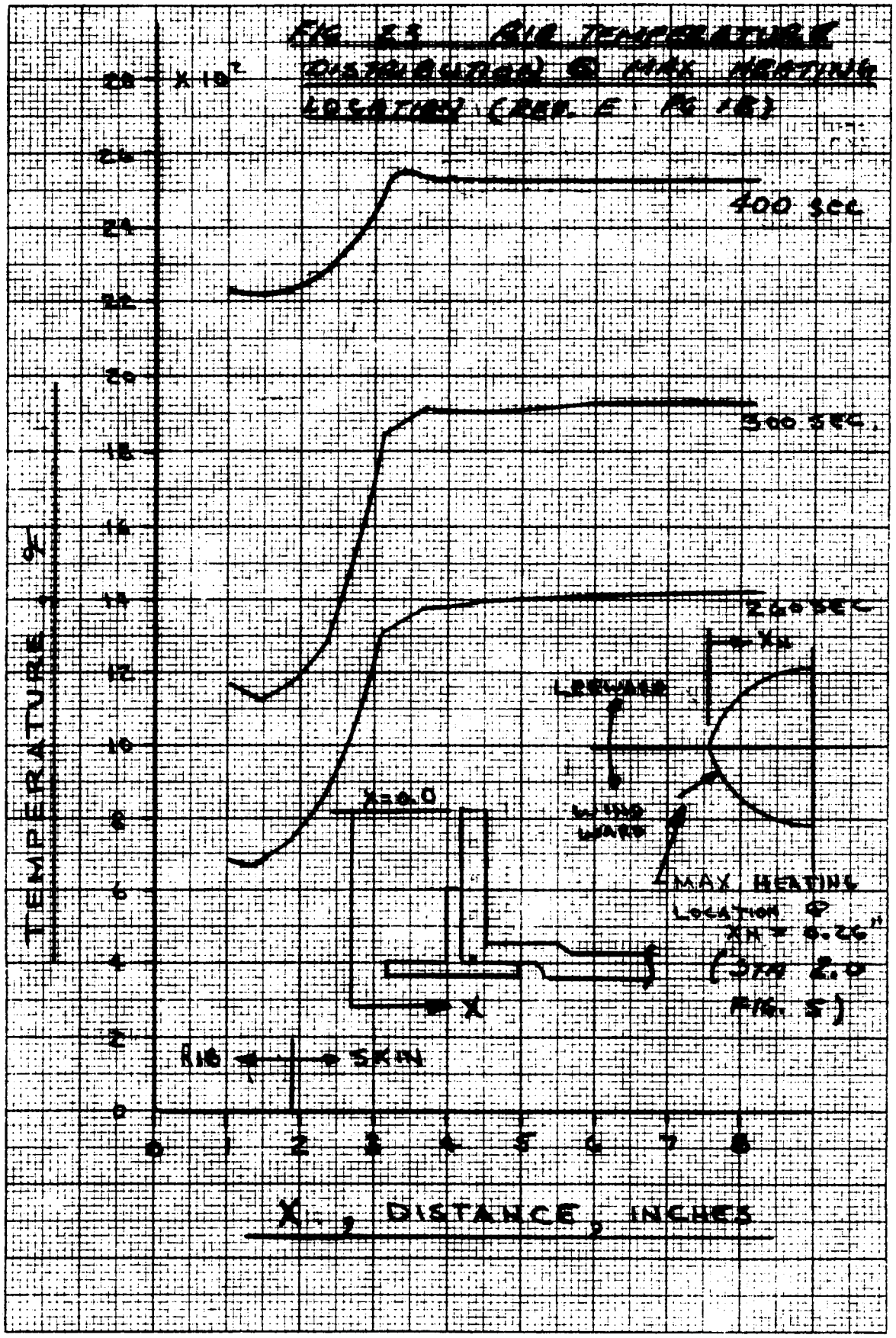
FIG 23 RIB TEMPERATURE DISTRIBUTION @ MAX HEATING LOCATION (REF. E FIG 18)
X 10²
400 SEC
300 SEC
260 SEC
TEMPERATURE, °F
X=0.0
X
LEEWARD
WIND WARD
MAX HEATING LOCATION @ XH = 0.26" (STA 2.0 FIG. 5)
RIB
SKIN
X, DISTANCE, INCHES

LIMIT LOADS

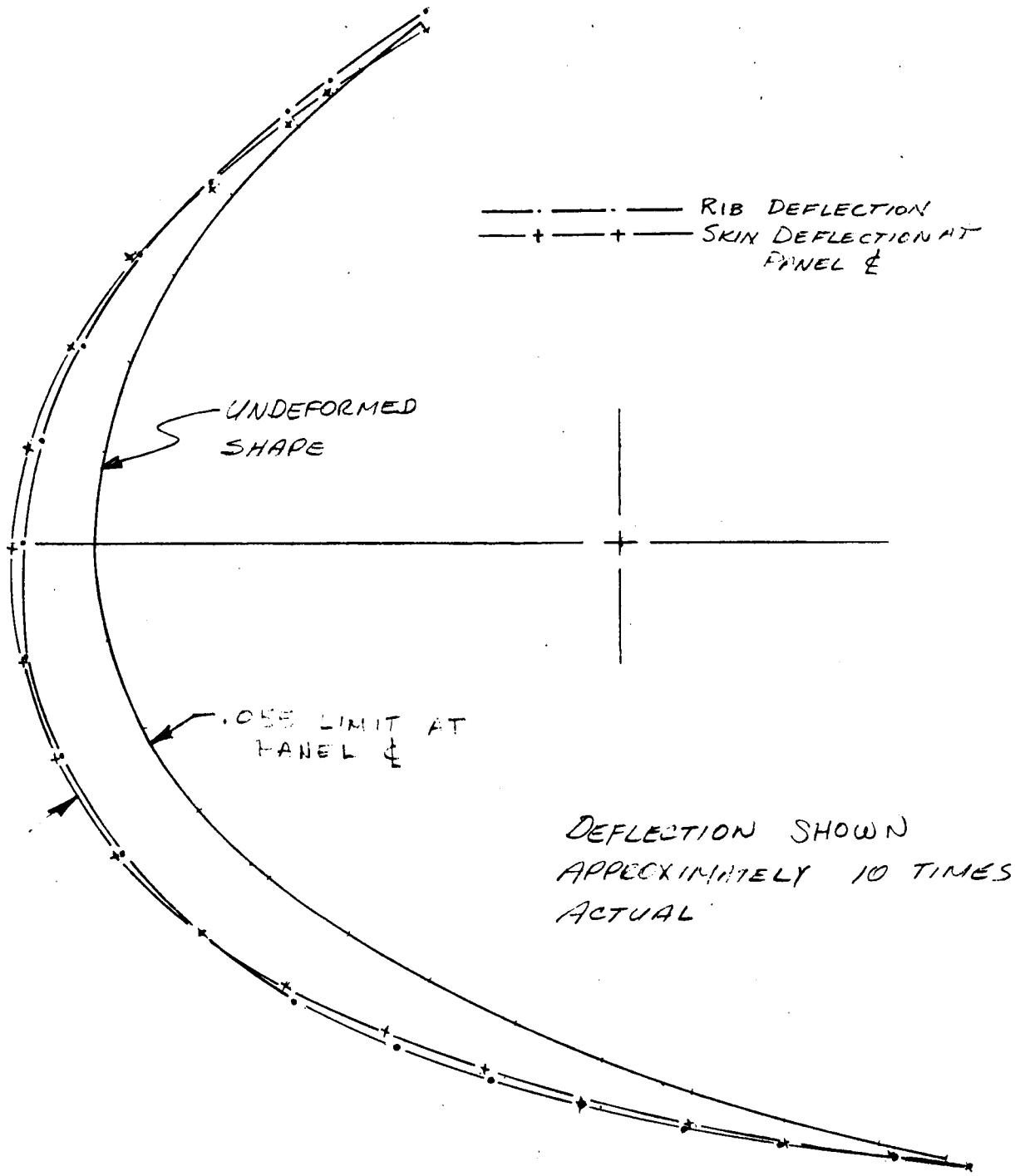

FIGURE 24 MAXIMUM PANEL DEFLECTION; t = 400 SEC

ULT LOADS

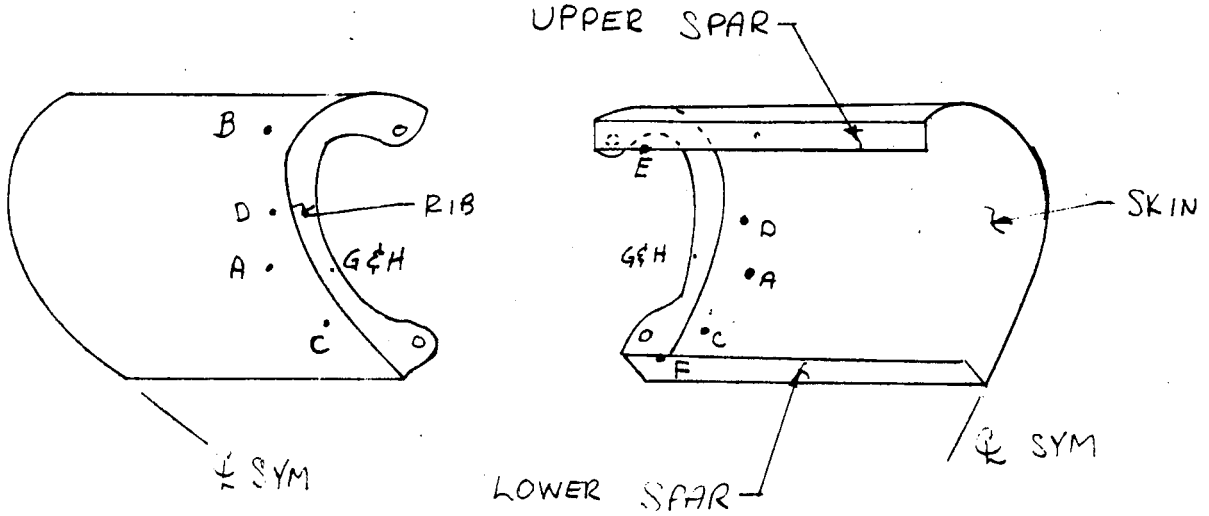

TABLE II - MARGIN of SAFETY SUMMARY ~ ENTRY

POSI-TION	STRUCT-URE	MATERIAL SPEC	TYPE of STRESS	MAXIMUM STRESS	ALLOW* STRESS	M.S.	SEC FROM ENTRY	REF. FIG.
A	SKIN	24 PLY COATED 1960°F	TENSION	1790	6300	+2.52	400	30
B	SKIN	34 PLY COATED 2420°F	FLEXURE	1050	15,250	HIGH	400	30
C	SKIN JOGGLE	25 PLY COATED 1560°F	COMPRESSION	-2900	-10,400	+2.59	400	31
D	SKIN	29 PLY COATED 1560°F	SHEAR	1070	2500	+1.34	400	34
E	UPPER SPAR	20 PLY COATED 805°F	TENSION	1400	5600	+3.00	400	35
F	LOWER SPAR	20 PLY COATED 920°F	COMPRESSION	-1000	-9000	HIGH	260	36
G	RIB	12 PLY COATED 1410°F	TENSION	2050	5600	+1.74	300	38
H	RIB	12 PLY COATED 2180°F	COMPRESSION	-1560	-12000	HIGH	400	39
J	SKIN	16 PLY COATED 670°F	TENSION	1030	3600	+2.5	400	42

* FROM REF (A)

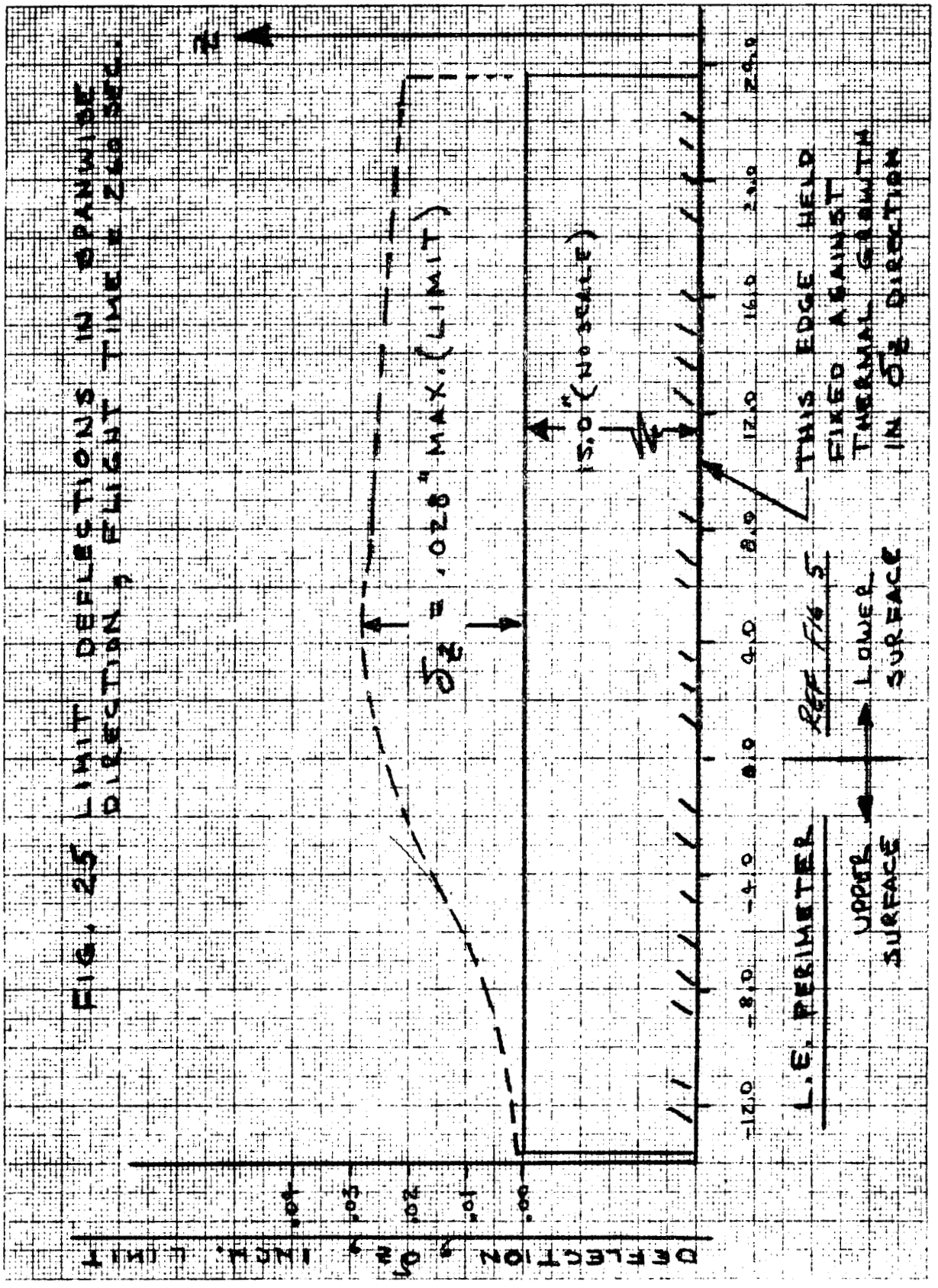
FIG. 25 LIMIT DEFLECTIONS IN SPANWISE DIRECTION, FLIGHT TIME = 240 SEC.
Z
δ_Z = .028" MAX. (LIMIT)
15.0" (NO SCALE)
THIS EDGE HELD FIXED AGAINST THERMAL GROWTH IN δ_Z DIRECTION
L.E. PERIMETER
Ref Fig 5
UPPER SURFACE
LOWER SURFACE
-12.0
-8.0
-4.0
0.0
4.0
8.0
12.0
16.0
20.0
24.0
DEFLECTION, δ_Z, INCH, LIMIT
.04
.03
.02
.01
.00

CLEARPRINT PAPER CO. NO. C35 MILLIMETERS BOTH WAYS 160 X 220 DIVISIONS
PRINTED IN U.S.A. ON CLEARPRINT TECHNICAL PAPER NO. 1015
CLEARPRINT CHARTS

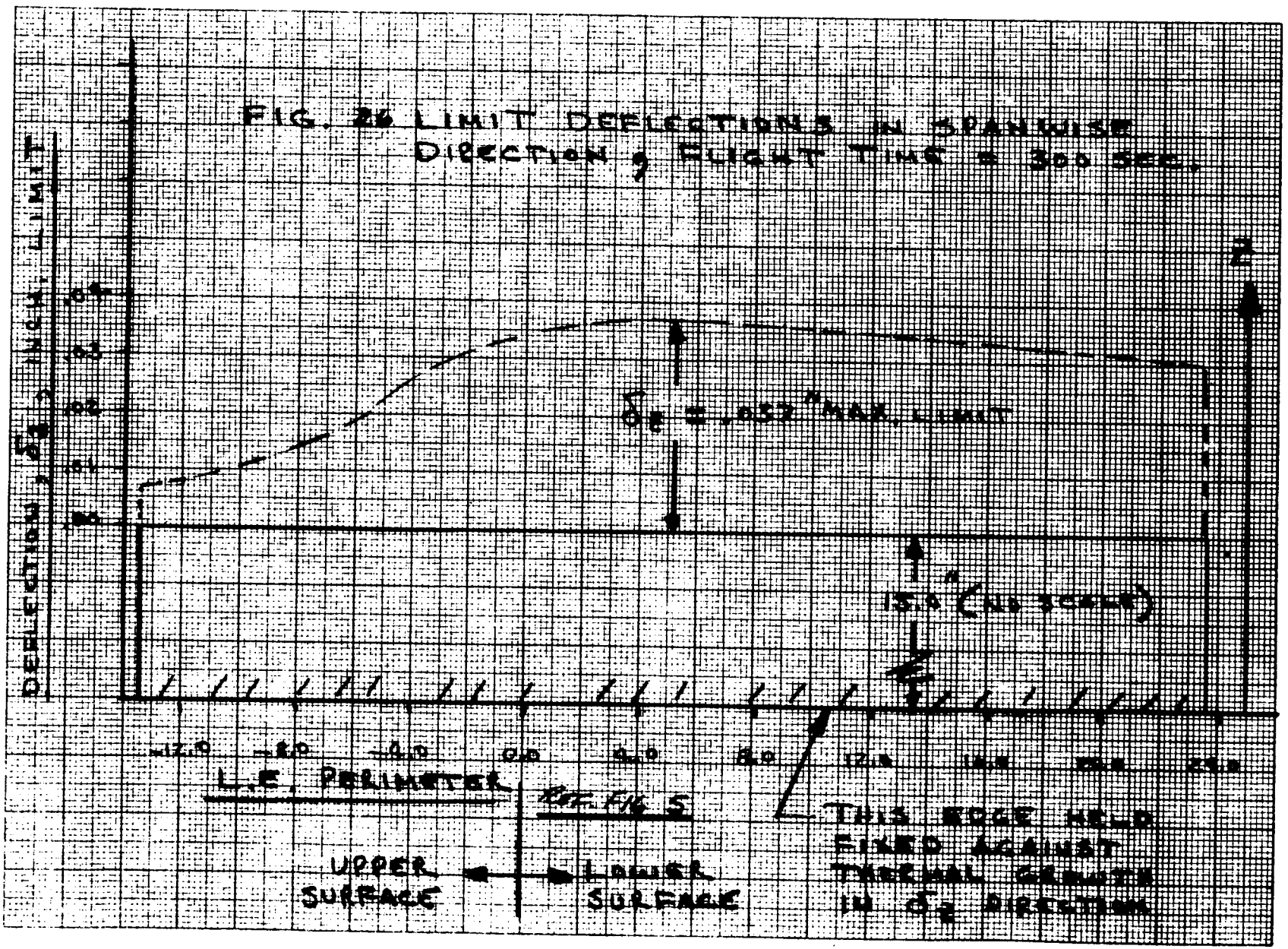

FIG. 26 LIMIT DEFLECTIONS IN SPANWISE DIRECTION, FLIGHT TIME = 300 SEC.

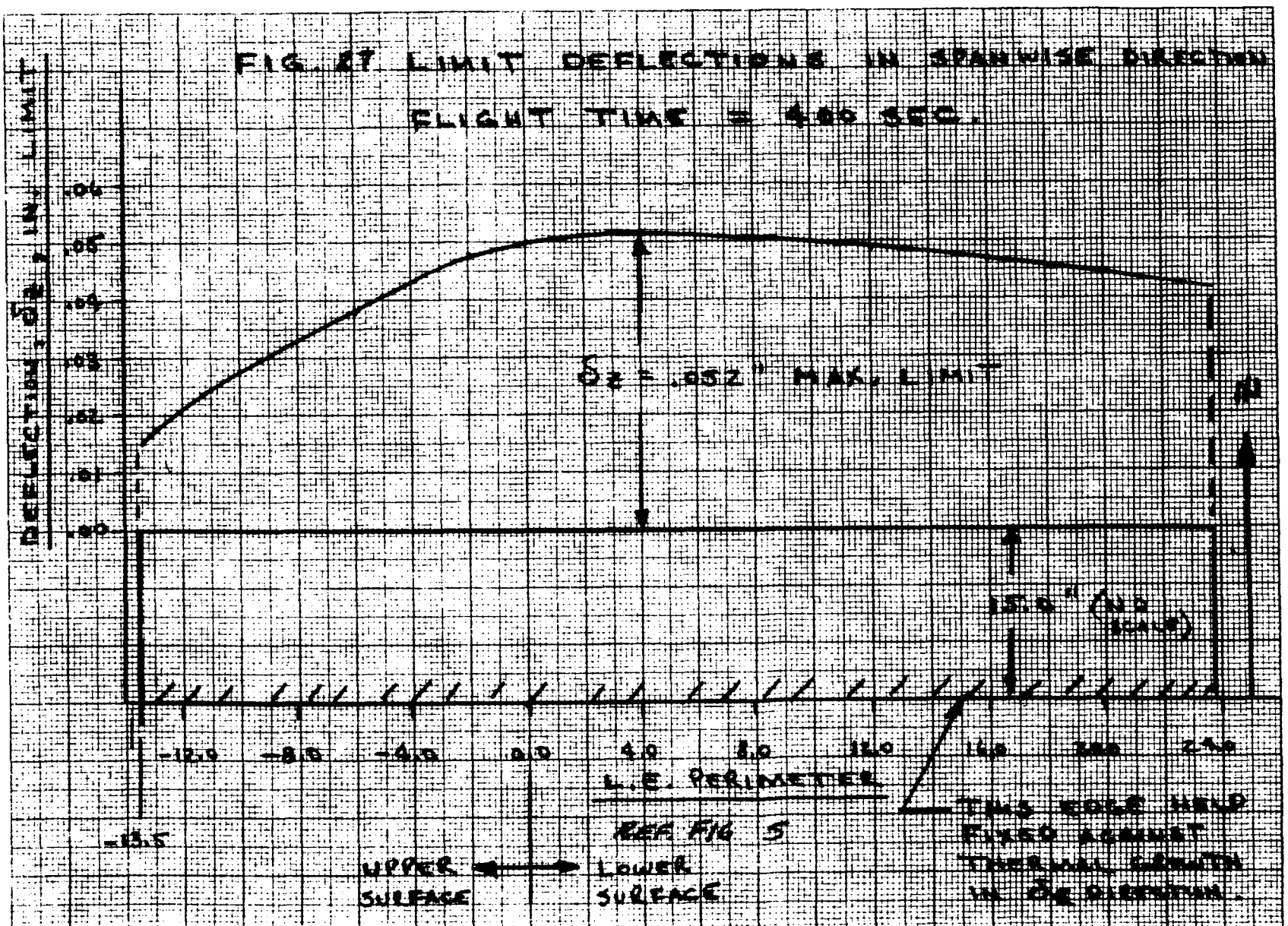
FIG. 27 LIMIT DEFLECTIONS IN SPANWISE DIRECTION
FLIGHT TIME = 400 SEC.
DEFLECTION, δz, IN. LIMIT
.06
.05
.04
.03
.02
.01
.00
δz = .052" MAX. LIMIT
15.0" (NO SCALE)
-12.0
-8.0
-4.0
0.0
4.0
8.0
12.0
16.0
20.0
24.0
L.E. PERIMETER
REF FIG 5
-13.5
UPPER SURFACE
LOWER SURFACE
THIS EDGE HELD FIXED AGAINST THERMAL GROWTH IN δz DIRECTION.

CLEARPRINT PAPER CO NO C39 MILLIMETERS BOTH WAYS 160 x 220 DIVISIONS
PRINTED IN U.S.A. ON CLEARPRINT TECHNICAL PAPER NO. 1015

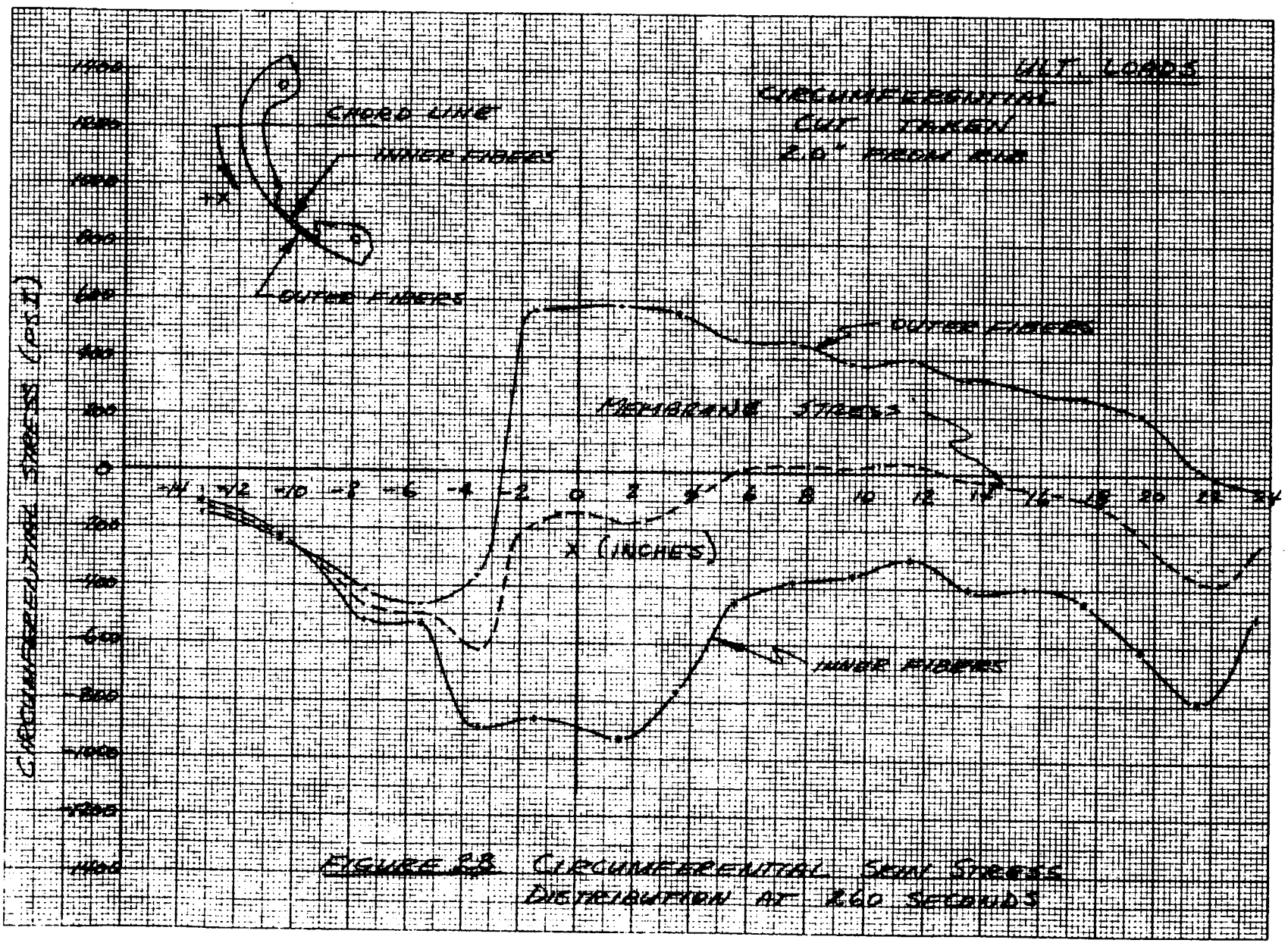

FIGURE 28 CIRCUMFERENTIAL SKIN STRESS DISTRIBUTION AT 260 SECONDS

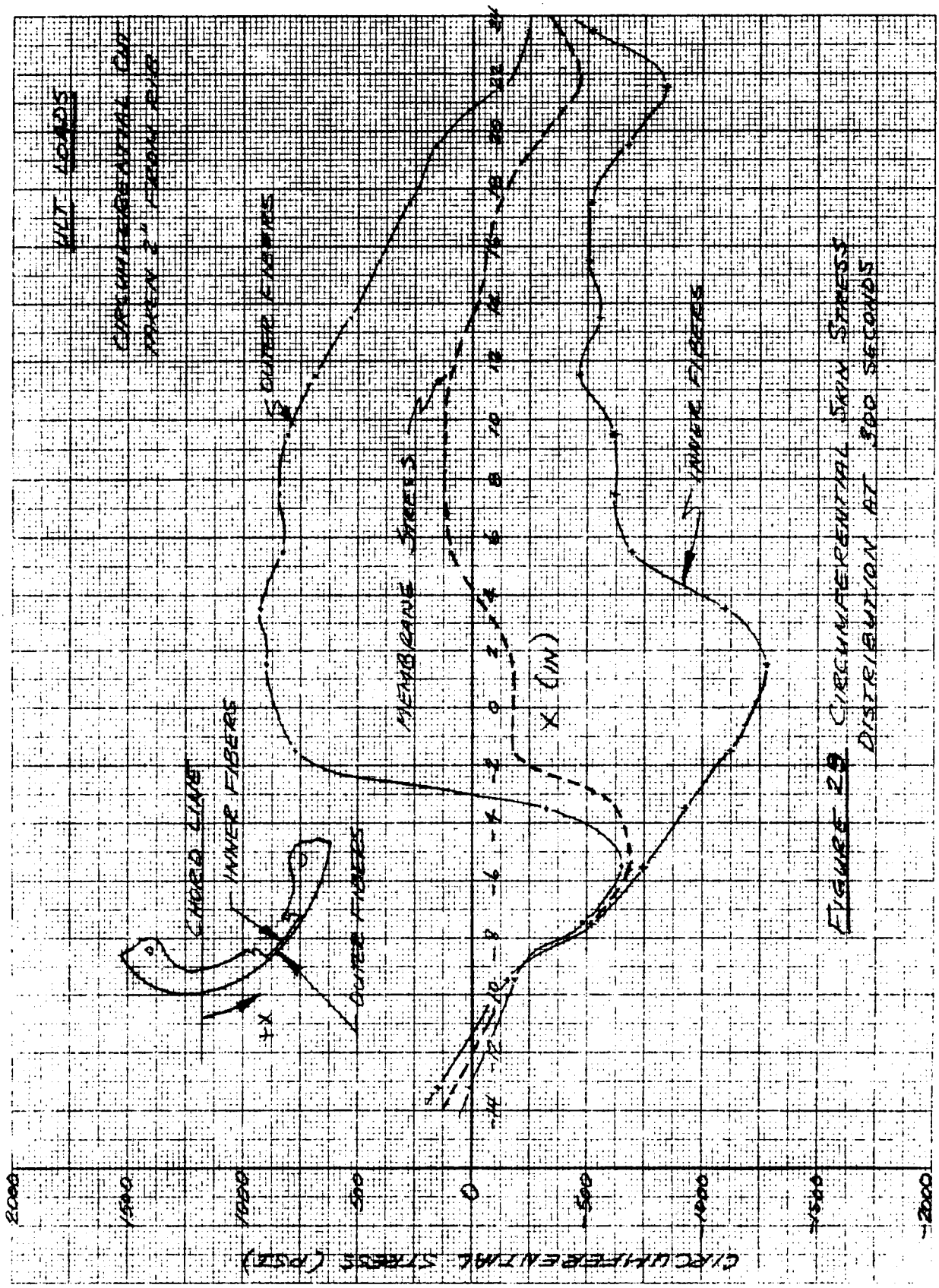

FIGURE 29 CIRCUMFERENTIAL SKIN STRESS DISTRIBUTION AT 800 SECONDS

CLEARPRINT PAPER CO. No. 139 MILLIMETERS BOTH WAYS 150 F. 20 DIVISIONS PRINTED IN U.S.A. ON CLEARPRINT TECHNICAL PAPER NO. 1015
CLEARPRINT CHARTS

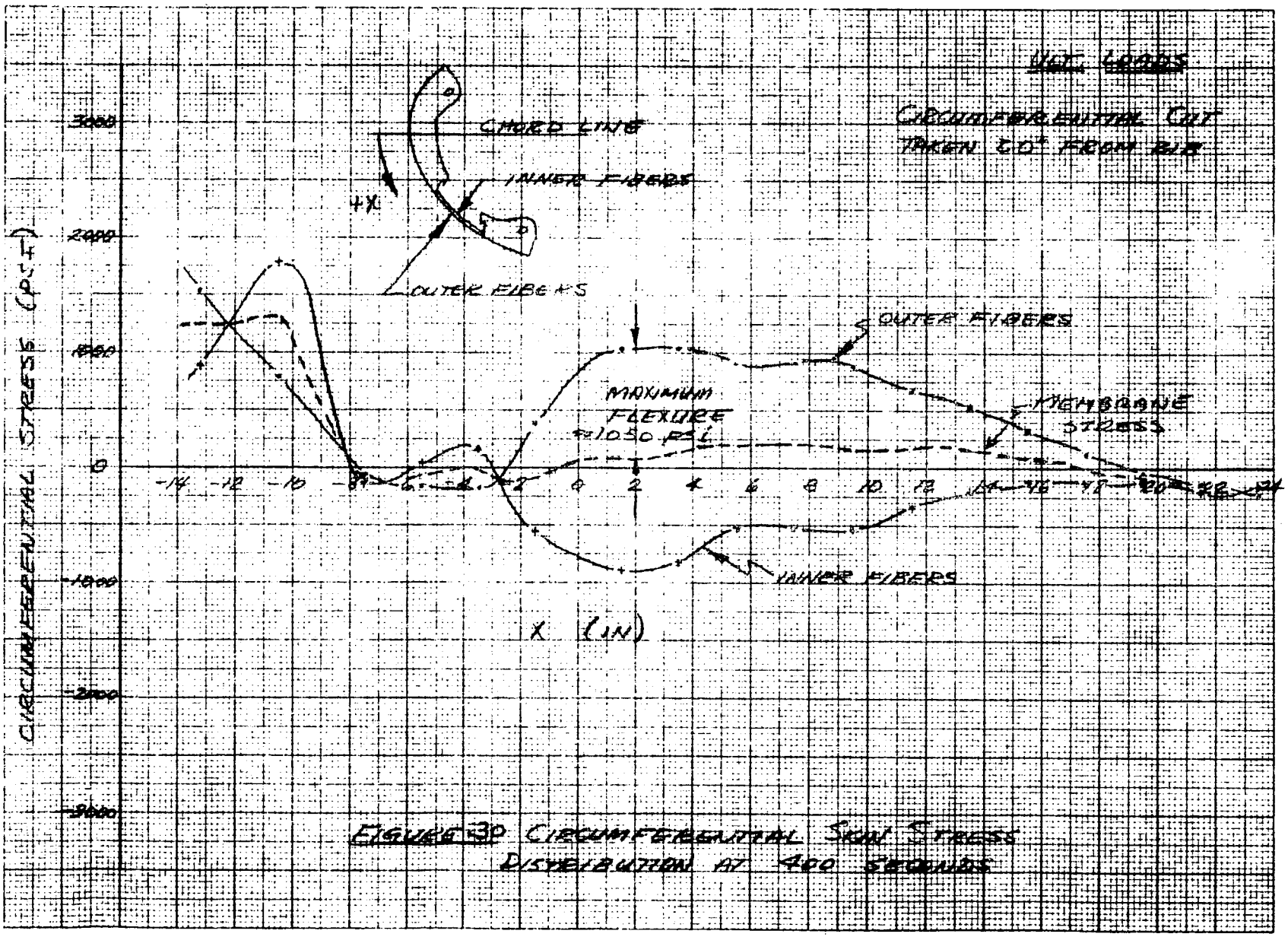

FIGURE 3P CIRCUMFERENTIAL SKIN STRESS DISTRIBUTION AT 400 SECONDS

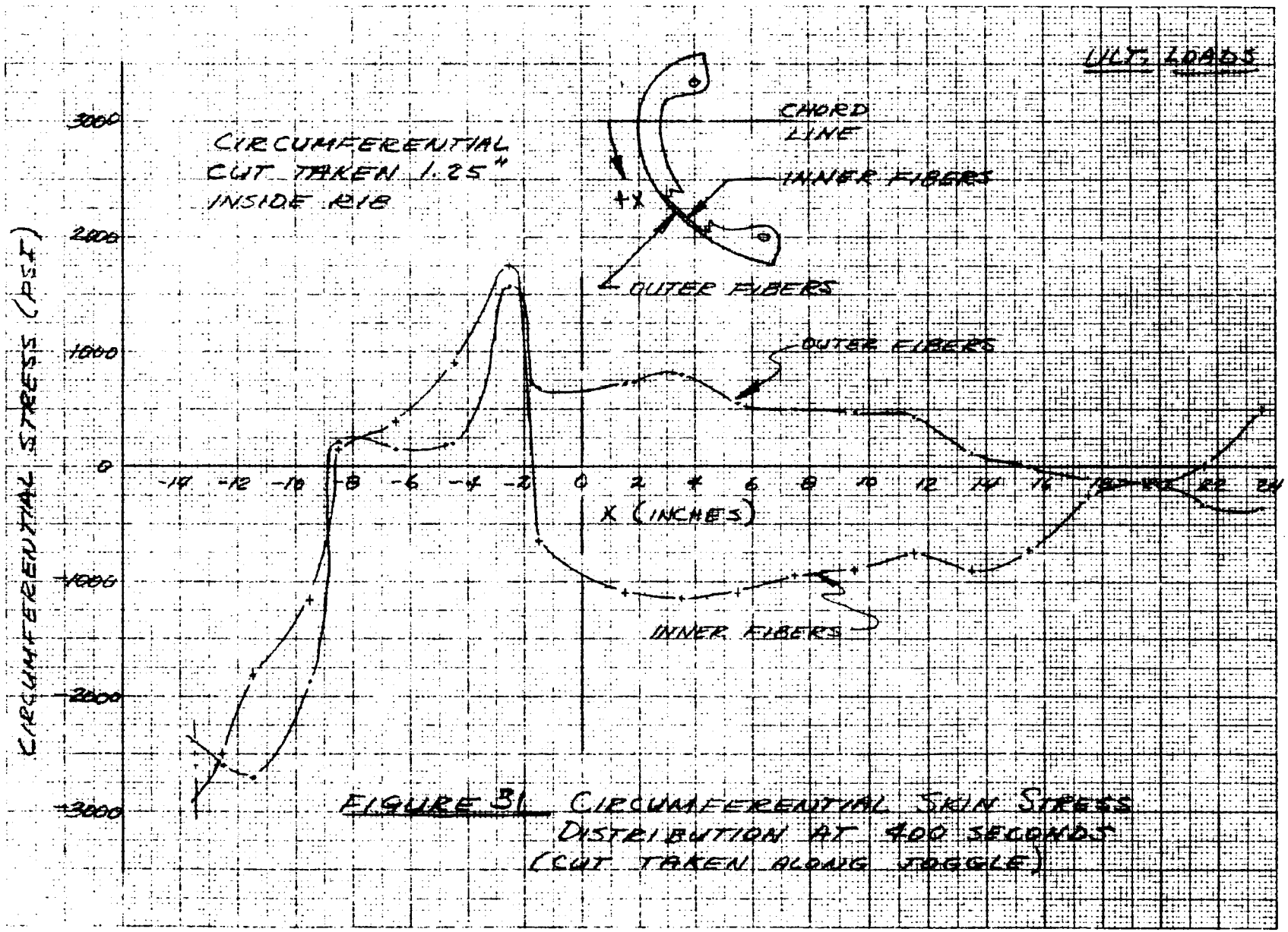

FIGURE 31 CIRCUMFERENTIAL SKIN STRESS DISTRIBUTION AT 400 SECONDS (CUT TAKEN ALONG JOGGLE)

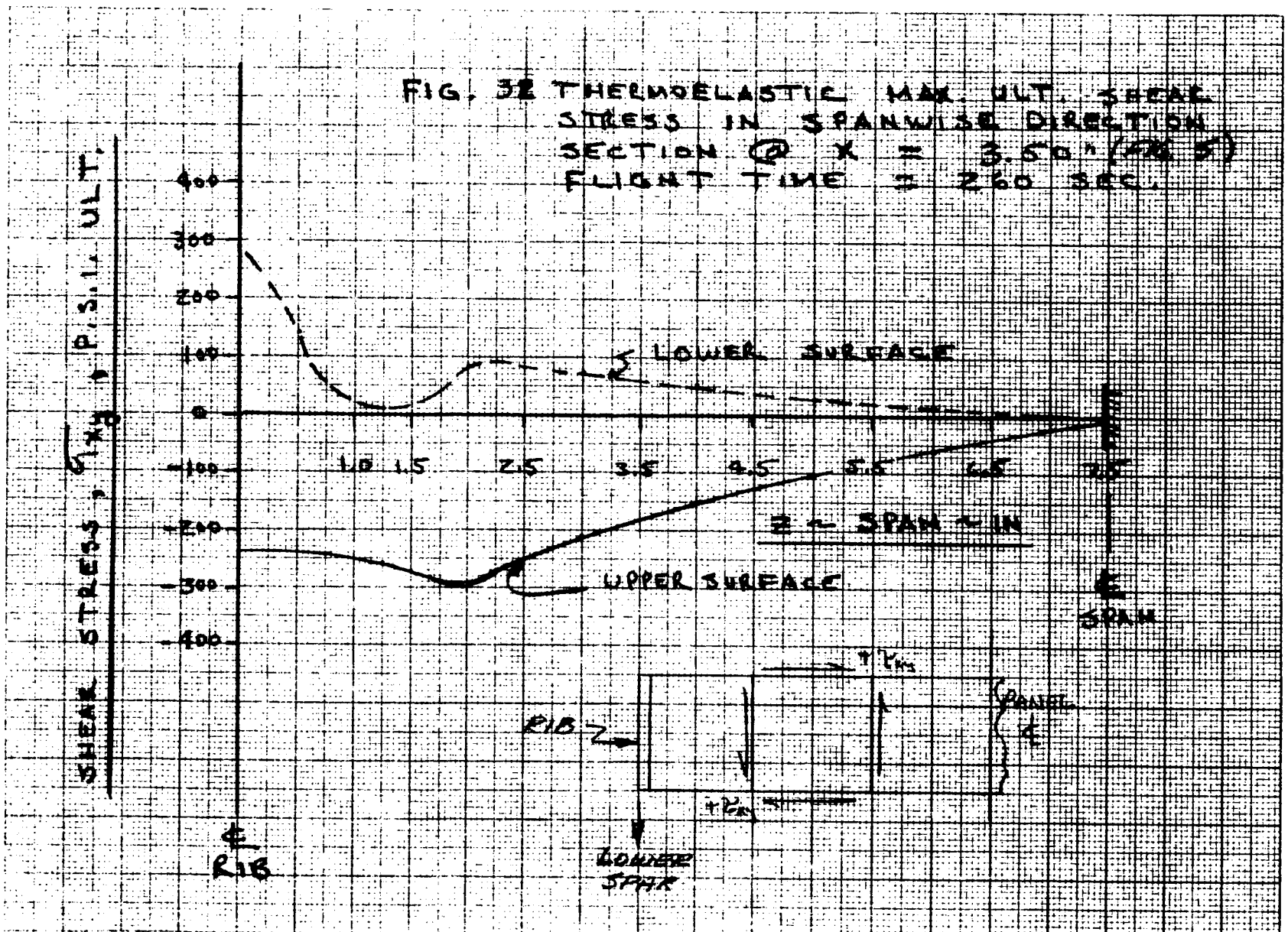

FIG. 32 THERMOELASTIC MAX. ULT. SHEAR STRESS IN SPANWISE DIRECTION SECTION @ X = 3.50" (FIG 5) FLIGHT TIME = 2.60 SEC.

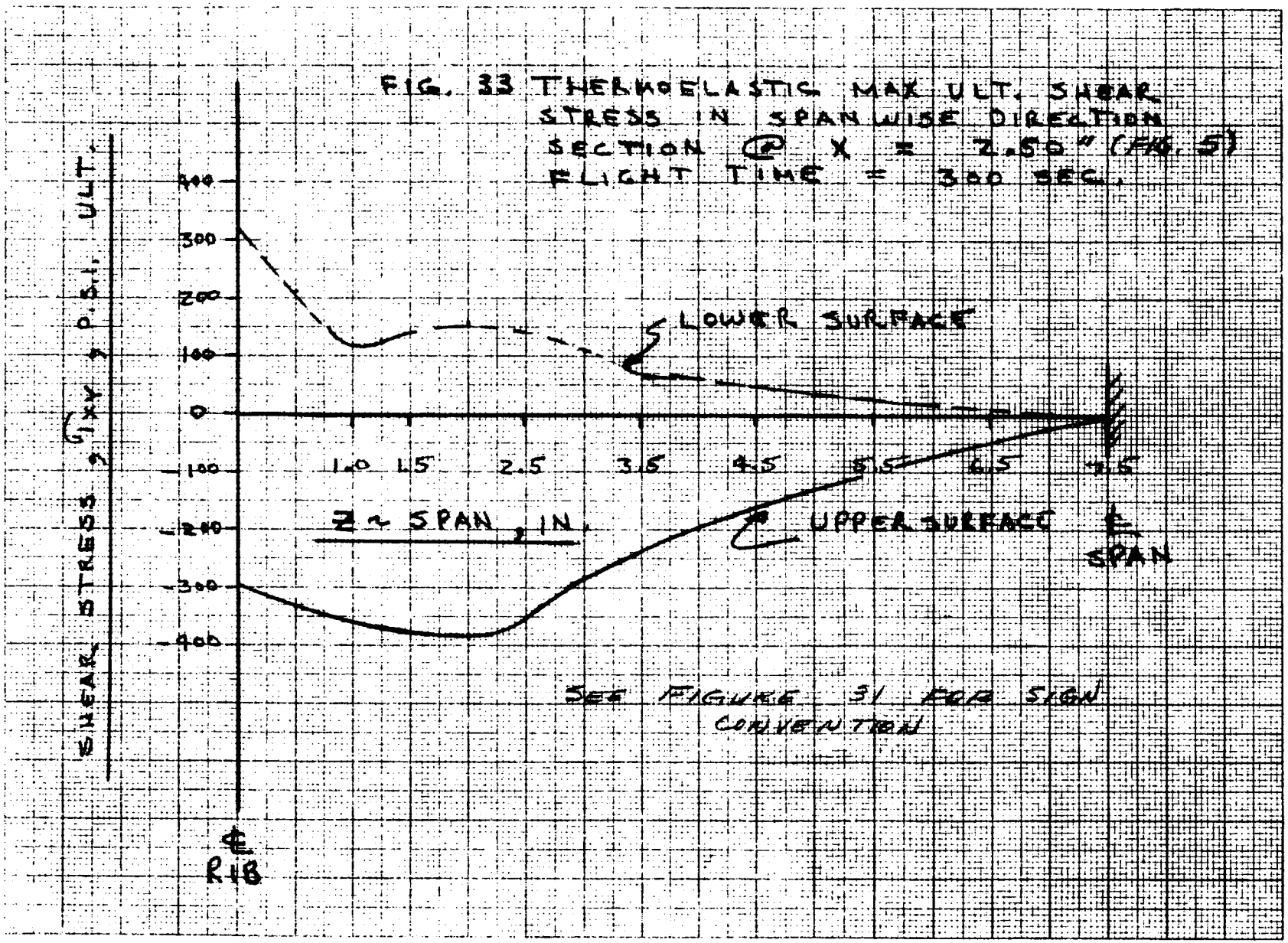

FIG. 33 THERMOELASTIC MAX ULT. SHEAR STRESS IN SPANWISE DIRECTION
SECTION ② X = 2.50" (FIG. 5)
FLIGHT TIME = 300 SEC.

PRINTED IN U.S.A. ON CLEARPRINT TECHNICAL PAPER NO. 1015
CLEARPRINT CHARTS

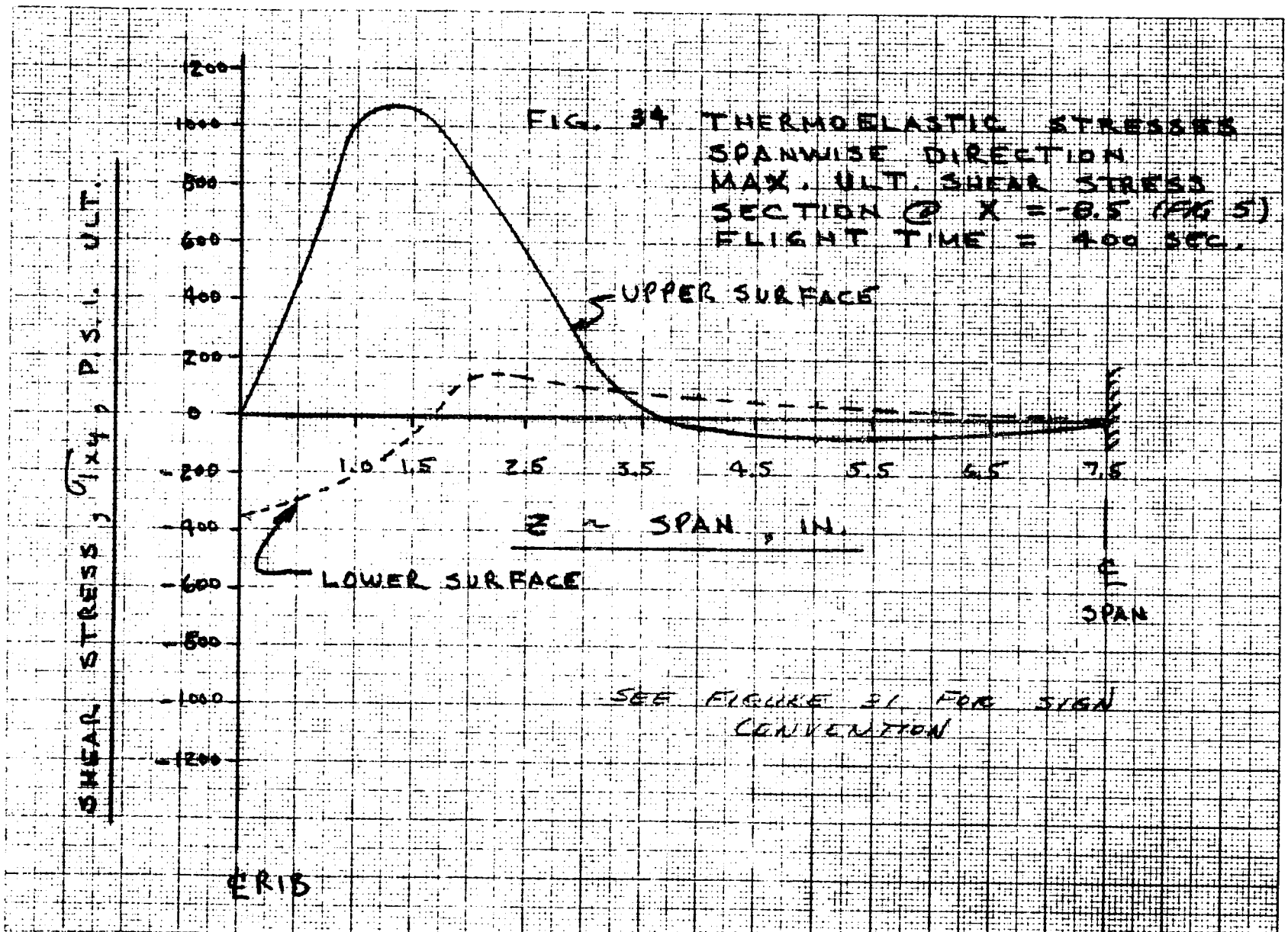

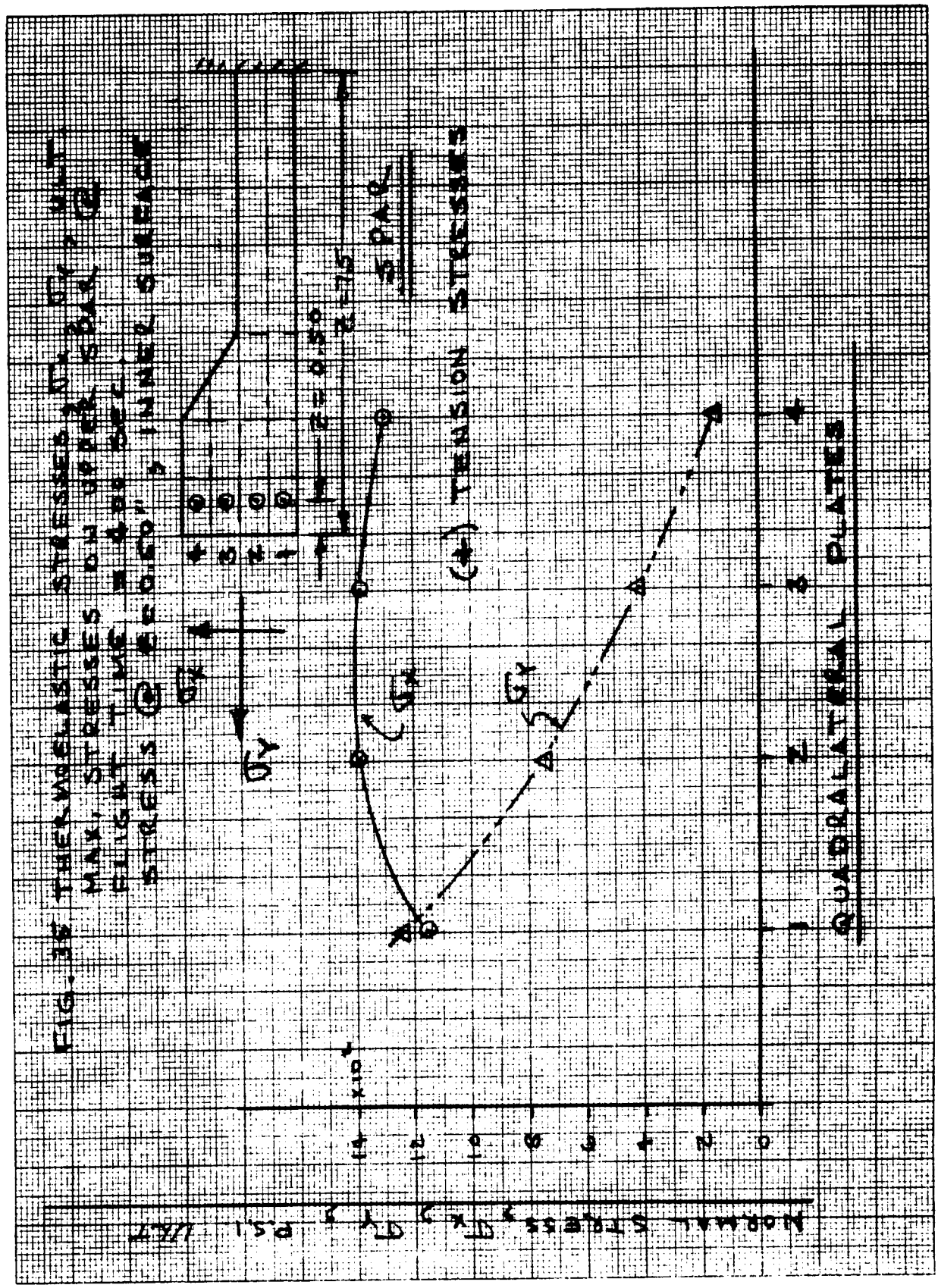

CLEARPRINT PAPER CO. NO. C39 MILLIMETERS POTH WAYS 160 X 220 DIVISIONS
PRINTED IN U.S.A. ON CLEARPRINT TECHNICAL PAPER NO. 1015

CLEARPRINT PAPER CO. NO. 1050 MILLIMETERS BOTH WAYS 160 X 220 DIVISIONS
PRINTED IN U.S.A. ON CLEARPRINT TECHNICAL PAPER NO. 1015
CLEARPRINT CHARTS

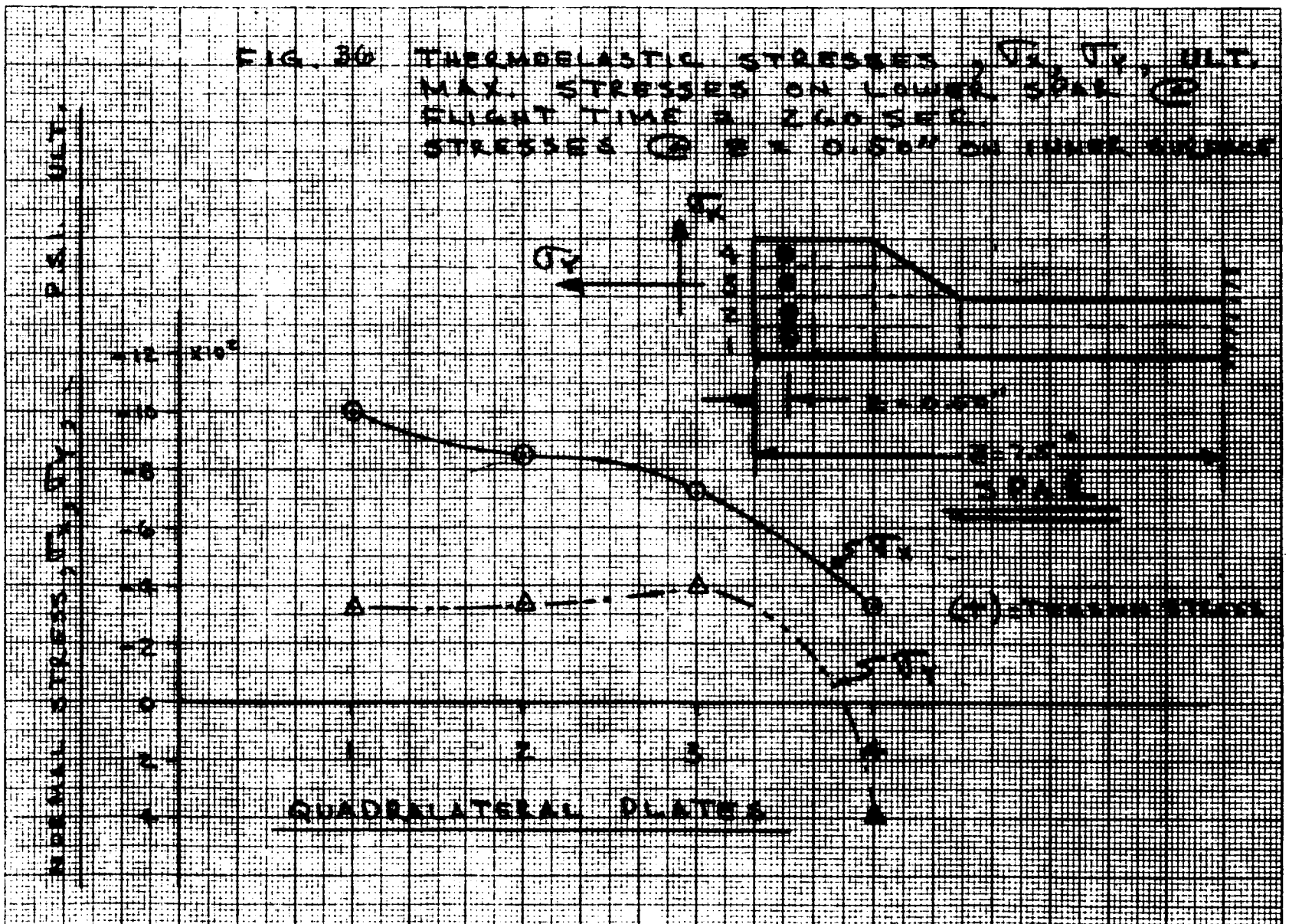

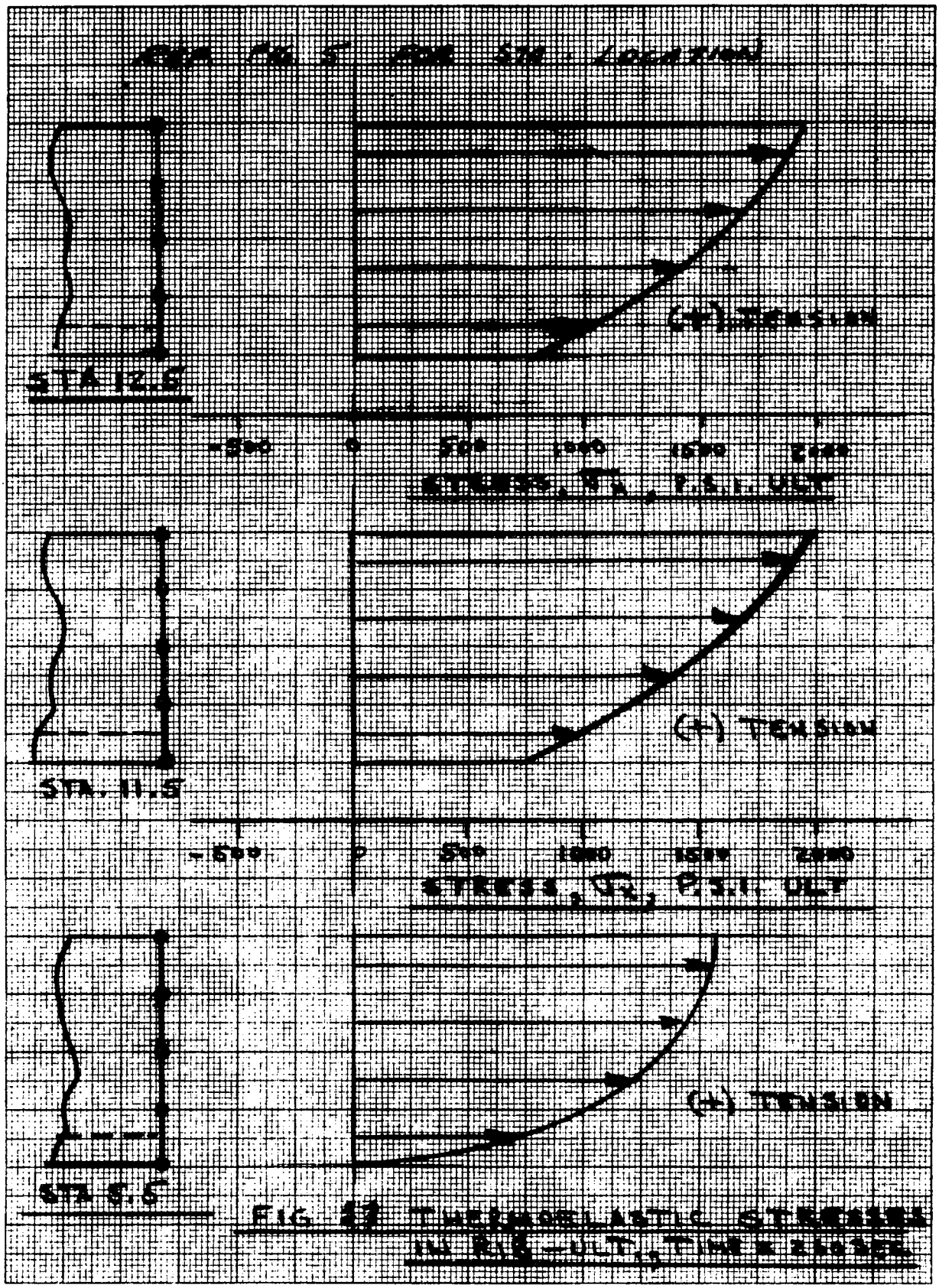

FIG. 47 THERMOELASTIC STRESSES IN RIB - ULT., TIME = 260 SEC.

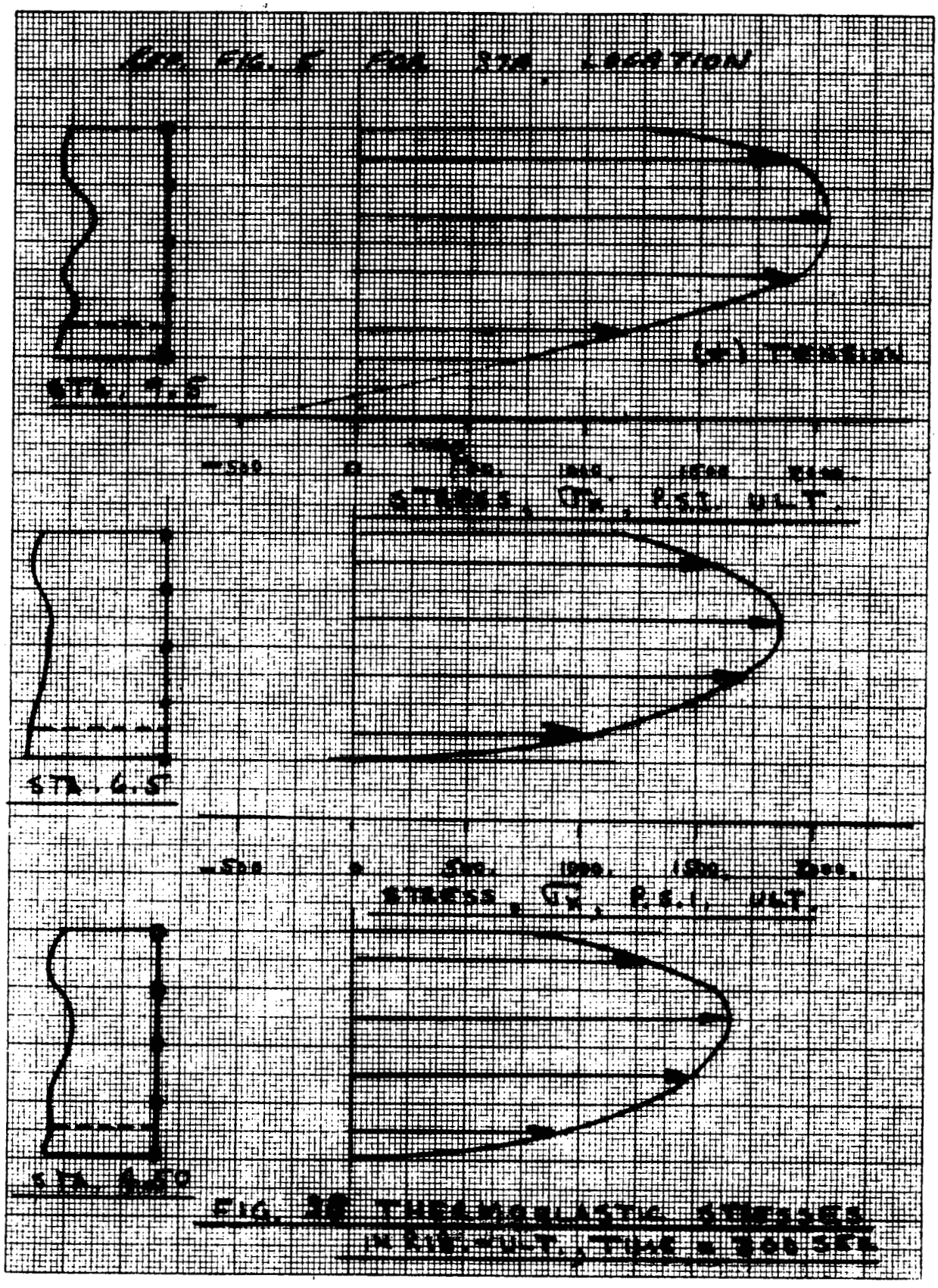

FIG. 38 THERMOELASTIC STRESSES IN RIB-ULT., TIME = 300 SEC.

CLEARPRINT PAPER CO. NO. C39. MILLIMETERS BOTH WAYS 160 X 220 DIVISIONS.
PRINTED IN U.S.A. ON CLEARPRINT TECHNICAL PAPER NO. 1015

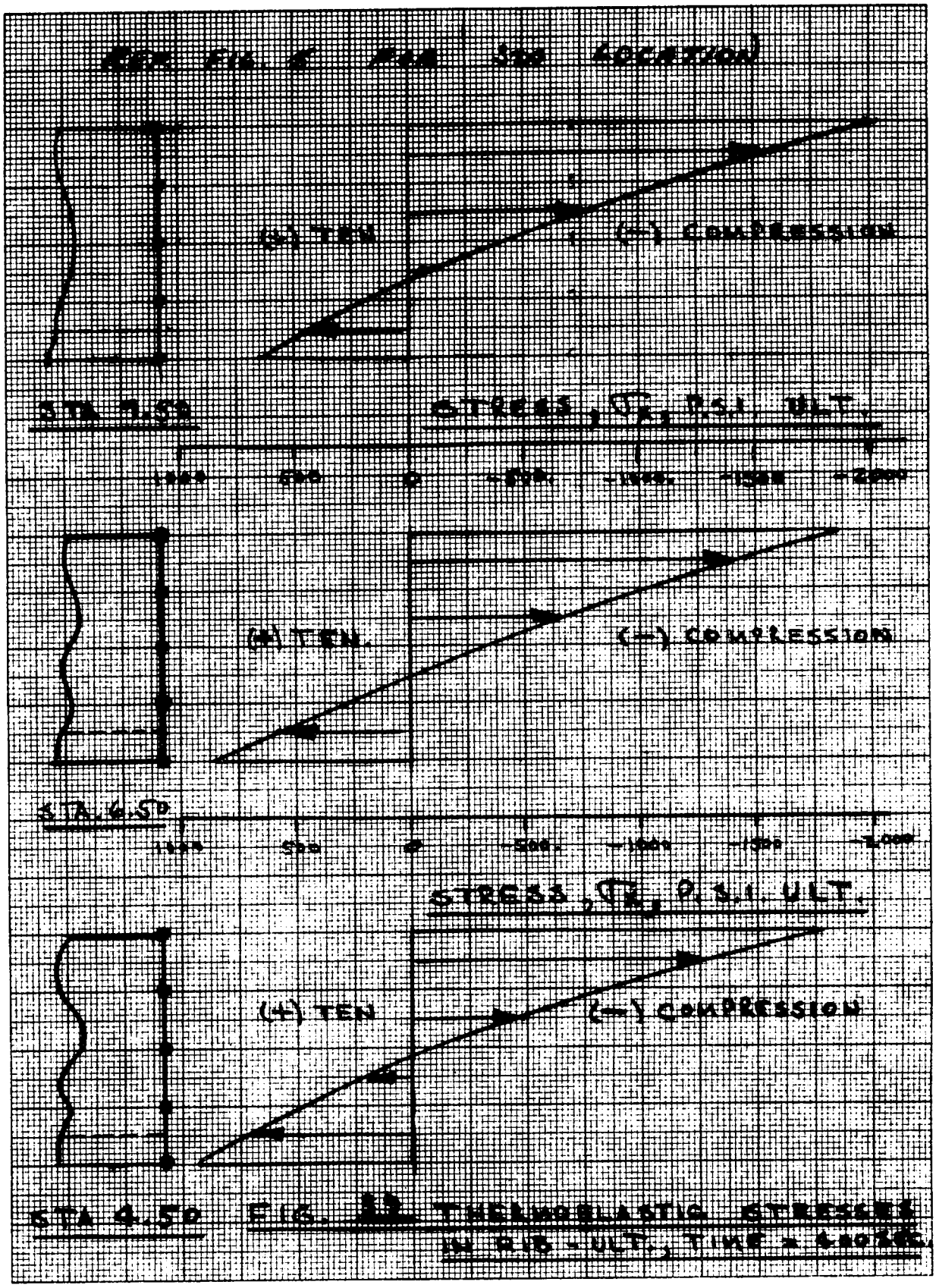

FIG. 22 THERMOELASTIC STRESSES IN R.S. - ULT., TIME = 480 SEC.

PRINTED IN U.S.A. ON CLEARPRINT TECHNICAL PAPER NO. 1015
CLEARPRINT PAPER CO. NO. C39. MILLIMETERS BOTH WAYS. 160 X 220 DIVISIONS.

CLEARPRINT PAPER CO. NO C32 MILLIMETERS BOTH WAYS 160 X 220 DIVISIONS: PRINTED IN U.S.A. ON CLEARPRINT TECHNICAL PAPER NO. 1015

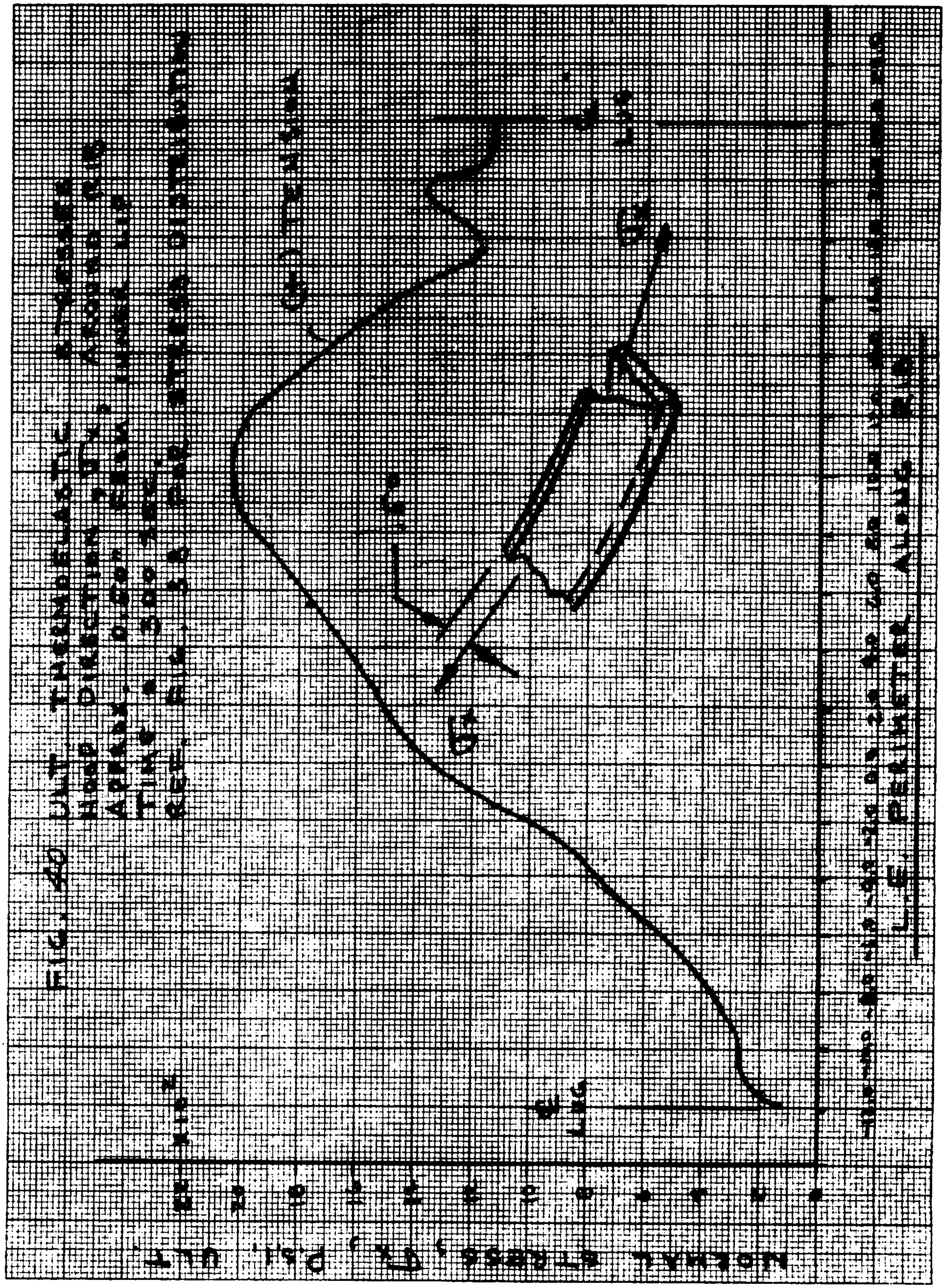

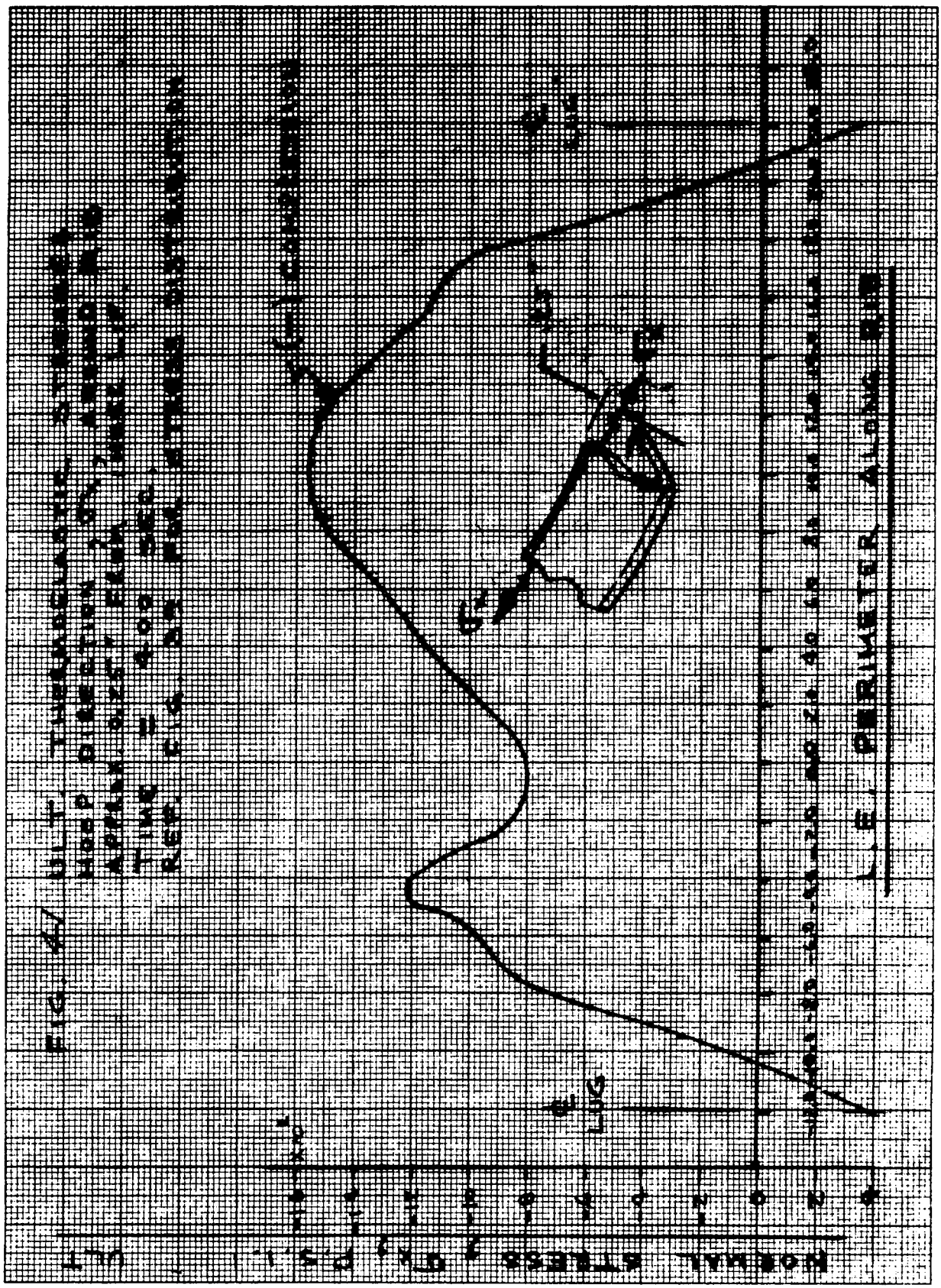
FIG. 41 ULT. THERMOELASTIC STRESSES
HOOP DIRECTION
TIME = 400 SEC.
REF. FIG. 39 FOR STRESS DISTRIBUTION
(-) COMPRESSION
℄ LUG
℄ LUG
L.E. PERIMETER ALONG RIB
NORMAL STRESS, σx, P.S.I.
ULT

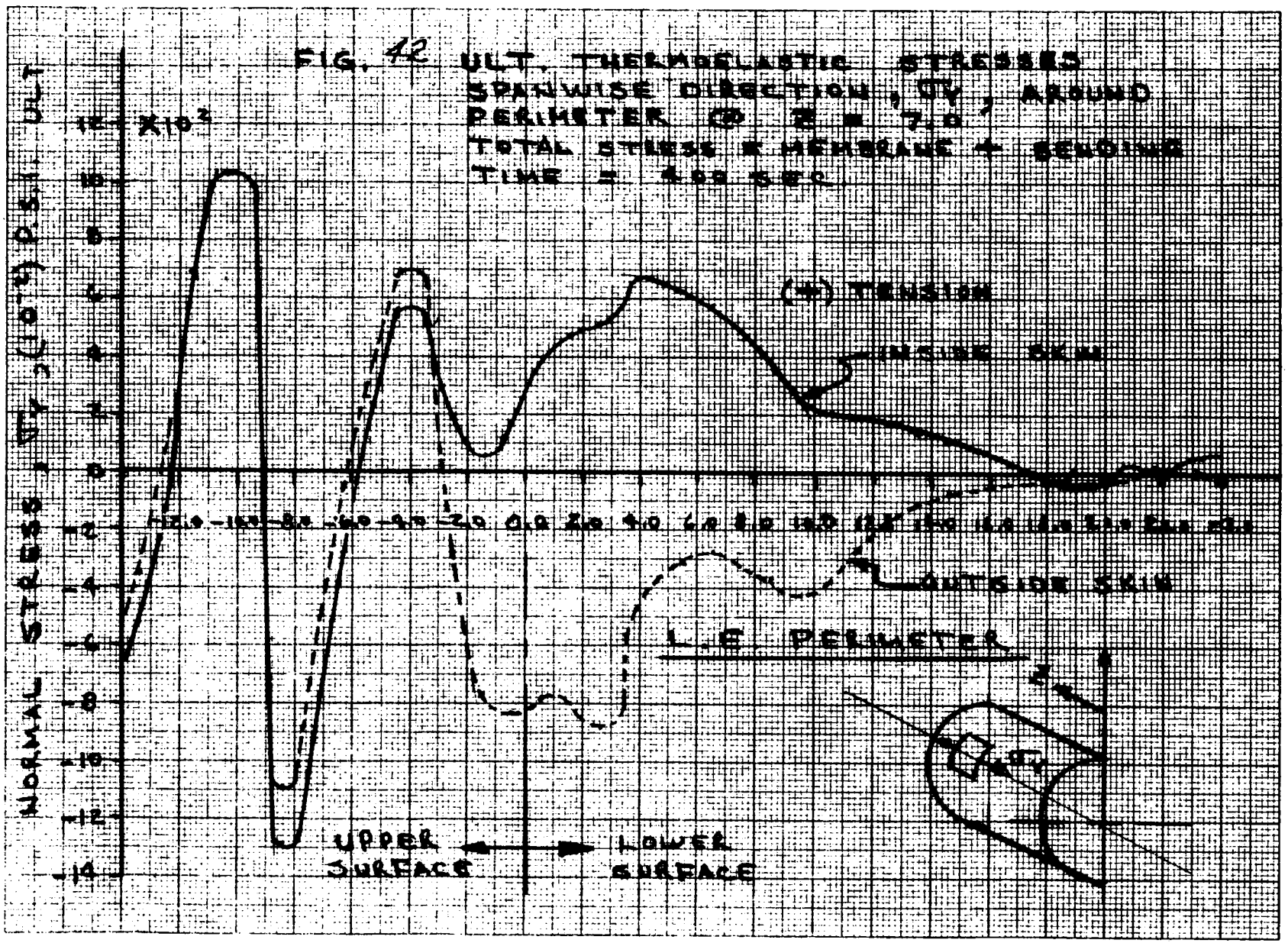

FIG. 42 ULT. THERMOELASTIC STRESSES SPANWISE DIRECTION, σ_y, AROUND PERIMETER @ Z = 7.0, TOTAL STRESS = MEMBRANE + BENDING TIME = 4.99 SEC.

ULT LOADS

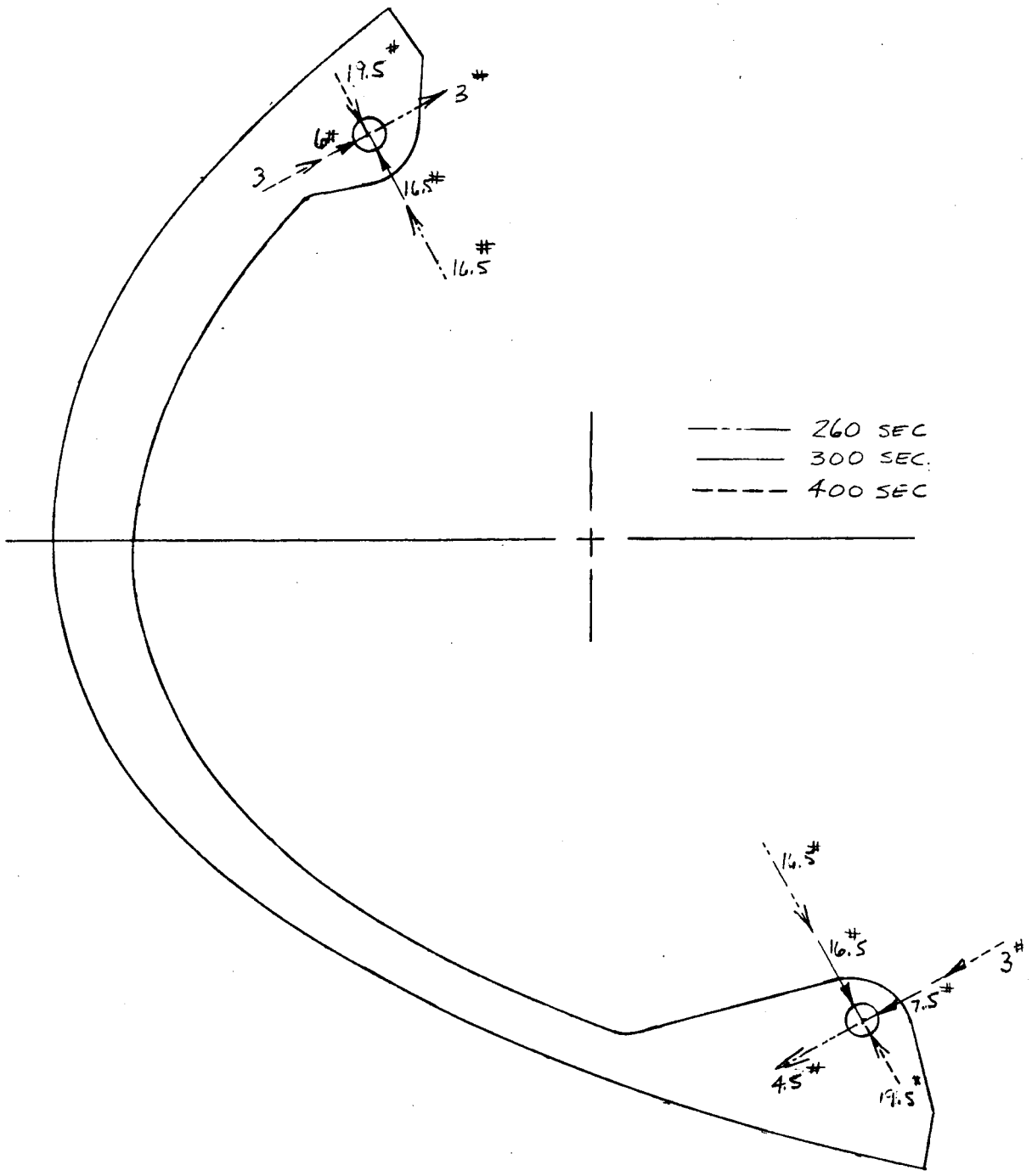

FIGURE 43 THERMAL LOAD LUG REACTIONS (ULT) FOR 260, 300, AND 400 SECONDS

0.	0.0	0.0	0.0
	0.0	0.0	0.0

EXTERNAL BALANCE

TABLE IV

RPP LEADING EDGE THERMOELASTIC ANALYSIS AT TIME = 260 SECONDS

TYPE	FF(lbs)	FU(lbs)	FO(lbs)	MF(in-lbs)	MU(in-lbs)	MO(
1	0.0	0.0	0.0	0.0	0.0	0.0
1	0.0	0.0	0.0	0.0	0.0	0.0
2	0.314E 01	0.111E 02	0.451E 03	0.236E 04	0.397E 04	0.601E
2	-0.267E 01	-0.118E 02	-0.451E 03	-0.241E 04	-0.404E 04	0.0
3				0.0	0.0	0.0
3				0.0	0.0	0.0
4				0.520E 02	0.659E 02	0.0
4				-0.312E 01	-0.117E 01	0.0
TOTALS	0.469E 00	-0.674E 00	-0.270E-01	0.186E 00	0.972E-01	0.601E

TYPE 1= BALANCE FROM APPLIED POINT LOADS
2= BALANCE FROM CONSTRAINT POINT LOADS
3= BALANCE FROM APPLIED MOMENTS
4= BALANCE FROM CONSTRAINT MOMENTS

NOTE- WHEN ONLY THERMAL LOADING IS PRESENT, TYPES 1 AND 3 ARE NOT CONSIDERED IN THE BALANCE

FF,MF = FORCE AND MOMENT FORWARD
FU,MU = FORCE AND MOMENT UP
FO,MO = FORCE AND MOMENT OUTBOARD

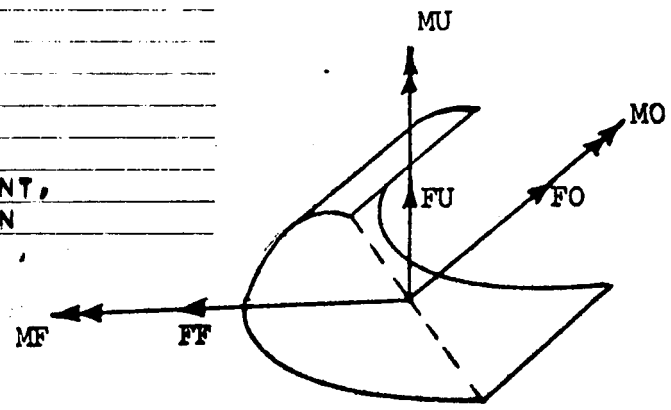

SIGN CONVENTION

EXTERNAL BALANCE

TABLE V

RPP LEADING EDGE THERMOELASTIC ANALYSIS AT TIME = 300 SECONDS

TYPE	FF(lbs)	FU (lbs)	FO(lbs)	MF(in-lbs)	MU(in-lbs)	MO
1	0.0	0.0	0.0	0.0	0.0	0.0
1	0.0	0.0	0.0	0.0	0.0	0.0
2	0.162E 01	0.116E 02	0.565E 03	0.321E 04	0.481E 04	0.103
2	0.0	-0.120E 02	-0.565E 03	-0.329E 04	-0.491E 04	0.0
3				0.0	0.0	0.0
3				0.0	0.0	0.0
4				0.775E 02	0.102E 03	0.0
4				-0.351E 01	-0.227E 01	0.0
TOTALS	0.162E 01	-0.366E 00	-0.419E-01	0.402E 00	0.212E 00	0.103

TYPE 1= BALANCE FROM APPLIED POINT LOADS
2= BALANCE FROM CONSTRAINT POINT LOADS
3= BALANCE FROM APPLIED MOMENTS
4= BALANCE FROM CONSTRAINT MOMENTS

NOTE- WHEN ONLY THERMAL LOADING IS PRESENT, TYPES 1 AND 3 ARE NOT CONSIDERED IN THE BALANCE

FF,MF - FORCE AND MOMENT FORWARD
FU,MU - FORCE AND MOMENT UP
FO,MO - FORCE AND MOMENT OUTBOARD

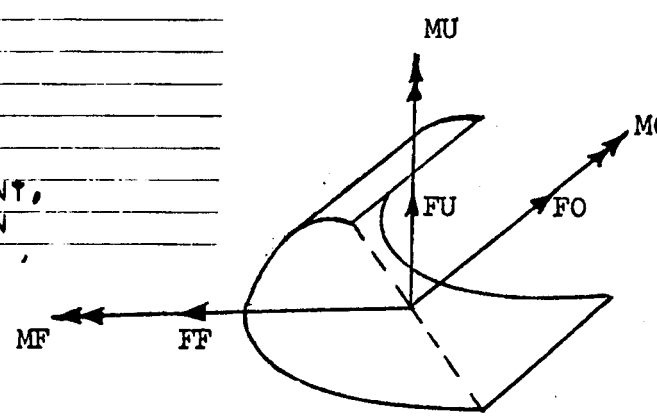

SIGN CONVENTION

EXTERNAL BALANCE

TABLE VI

RPP LEADING EDGE THERMOELASTIC ANALYSIS AT TIME = 400 SECONDS

TYPE	FF(lbs)	FU(lbs)	FO(lbs)	MF(in-lbs)	MU(in-lbs)	MO(in
1	0.0	0.0	0.0	0.0	0.0	0.0
1	0.0	0.0	0.0	0.0	0.0	0.0
2	0.853E 01	0.102E 02	0.747E 03	0.462E 04	0.638E 04	0.538E 0
2	-0.816E 01	-0.104E 02	-0.747E 03	-0.466E 04	-0.642E 04	0.0
3				0.0	0.0	0.0
3				0.0	0.0	0.0
4				0.419E 02	0.550E 02	0.0
4				-0.106E 01	-0.144E 02	0.0
TOTALS	0.376E 00	-0.200E 00	0.179E-01	0.117E 01	-0.508E 00	0.538E 0

TYPE 1= BALANCE FROM APPLIED POINT LOADS
2= BALANCE FROM CONSTRAINT POINT LOADS
3= BALANCE FROM APPLIED MOMENTS
4= BALANCE FROM CONSTRAINT MOMENTS

NOTE- WHEN ONLY THERMAL LOADING IS PRESENT, TYPES 1 AND 3 ARE NOT CONSIDERED IN THE BALANCE

FF,MF = FORCE AND MOMENT FORWARD
FU,MU = FORCE AND MOMENT UP
FO,MO = FORCE AND MOMENT OUTBOARD

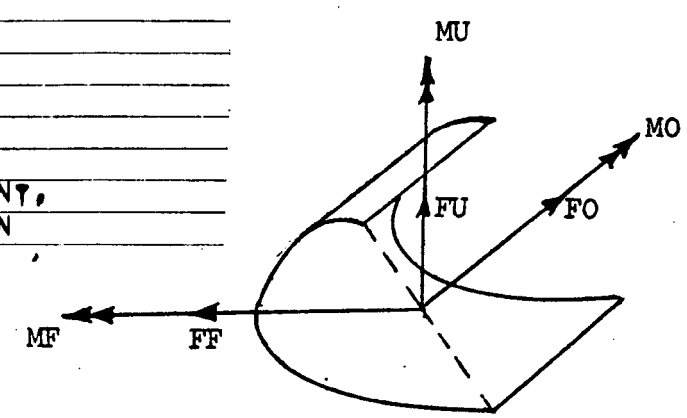

SIGN CONVENTION

APPENDIX A

The purpose of Appendix A is to show the correlation obtained between NASTRAN and thick plate theory for thermoelastic stresses.

The leading edge thermoelastic model contains two different thermal elements. The rib is thermally thin and uses nodal temperature inputs as explained on page 33. The thick laminate skin has thermal gradients which are specified through the model element thickness.

A sample plate problem 9" x 9" x 1" was evaluated for fully restrained and unrestrained edges using the following properties:

Young's Modulus	E	$= 30 \times 10^6$ psi
Shear Modulus	G	$= 11 \times 10^6$ psi
Coefficient of Thermal Expansion	α	$= 5 \times 10^{-6}$ in/in/°F
Poisson's Ratio	V	$= 0.36$

A linear temperature gradient of -1000°F to +1000°F was specified from the lower to upper surface. Nominally, linear gradients exist in the leading edge thick laminate skin.

Theoretical thermoelastic stresses were calculated from Reference (G).

$$\sigma_{x_{max}} = \sigma_{y_{max}} = \frac{-\alpha E\, T(z)}{1-V} + \frac{1}{2(t/2)(1-V)} \int_{-t/2}^{t/2} \alpha E\, T(z)\, dz + \frac{3z}{2(t/2)^3(1-V)} \int_{-t/2}^{t/2} \alpha E\, T(z)\, z\, dz$$

Comparison of the maximum stresses are shown below and the results compare favorably.

METHOD	FULLY RESTRAINED	UNRESTRAINED
NASTRAN	$\sigma_{max} = \pm 234{,}374$ psi	$\sigma_{max} = 6$ psi
THICK PLATE THEORY	$\sigma_{max} = \pm 234{,}375$ psi	$\sigma_{max} = 0$ psi

DESIGN INFORMATION ~~REQUEST~~ - RELEASE

9-7-

MODEL (S) AND EFF.	DIR. NO.	REV.
ULTIMATE STATIC LOADS DISTRIBUTION AND PRELIMINARY	T143-DIR-2-12	

	DATE	PAGE	OF
CANTED H/S PANEL ANALYSIS - LEADING EDGE SUPPORT	8/30/72	1	22

	SYSTEM	REF. G. O. NUMBER
STRUCTURE	PHASE III LEADING EDGE	3357 AA 1160

Fill in block below for Information Request

TO _____ GROUP _____

REQ. BY _____ GROUP _____

REASON _____

LTV ONLY ☐ BWR ☐ BUWEPS ☐ ☐ _____

Fill in block below for Information Release

IN REPLY TO DIR. NUMBER —

REL. TO D. M. While GROUP 3-52000

PREPARED BY	DATE	CHECKED BY	DATE
W. E. Agan WEA T. K. Henry TKH	9/5/72 9/5/72	W E Agan	9/5/72
GROUP APP.	**DATE**	**PROJ OFFICE**	**DATE**
H. E. Brougham	9/5/72	While	9/6/72

CC

E. C. Matza, F. D. Tarsia, R. B. Bost, H. I. Knight, G. B. Whisenhunt, B.A. Forcht

DESIGN INFORMATION:

REFERENCES:

(A) Phase III "Fail Safe" Leading Edge Structural Analysis, T143-DIR-2-09, dated 28 July 1972.

(B) Space Shuttle Wing Leading Edge Design Criteria, Phase III, T143-5R00060, dated 25 June 1971.

(C) Vought Aeronautics Division, LTV Aerospace Corp., Dallas, Texas, Designing for Acoustic Fatigue, Report No. 2053 424/SDM-153, dated December 1969.

(D) Air Force Flight Dynamics Lab, Wright Patterson Air Force Base, Ohio, Refinement of Sonic Fatigue Structural Design Criteria, AD-831118, dated January 1968.

(E) Trevarno Co., Livermore, Calif., Data Bulletin #86a, Structural Heat Resistant Polyimide Impregnating Resin System.

(F) Heatshield Thermal Analysis, T143-DIR-2-13, dated 15 August 1972.

PURPOSE:

The purpose of this DIR is to release the ultimate static loads and the internal load distributions to be used in the design of the leading edge support structure. The lug loads are from Reference (A) and the upper panel pressure is specified in Reference (B). A preliminary stiffness analysis of the canted heatshield panel is also presented.

DISCUSSION:

A general schematic and lug load coordinate system is shown in Figure 1. The lug rib truss, upper panel, and support lugs provide the primary load paths. The heat-shield canted panel is mounted with oversized holes to preclude carrying primary loads

Support structure geometry and upper panel load identification are presented in Figure 2.

The upper panel reactions are computed on pages 5 and 6 and are summarized on page 7. The leading edge and upper panel reactions are summarized on pages 8 and 9

The assumptions dealing with the rib truss analysis are listed on page 10 while equilibrium and member loads are shown in Figure 3. The support lug reaction equation and the equilibrium check are presented on pages 12 and 13. A summary of support lug reactions is shown in Table 1.

The 32 "g" RMS side load equilibrium is shown on page 18 for both the lower and upper lug. In the case of the upper lug, the loads are distributed through the upper access panel to the support lug.

The canted heatshield panel is designed such that its natural frequency is greate than 120 hz which is estimated to be stiff enough to prevent heatshield failure in the Shuttle acoustic and vibration environments. This is a preliminary analysis and is used as initial sizing only. Detailed analysis of the panel will be accomplished late The preliminary analysis and additional discussion is presented on pages 19 to 21, wit final results being shown in Figure 4.

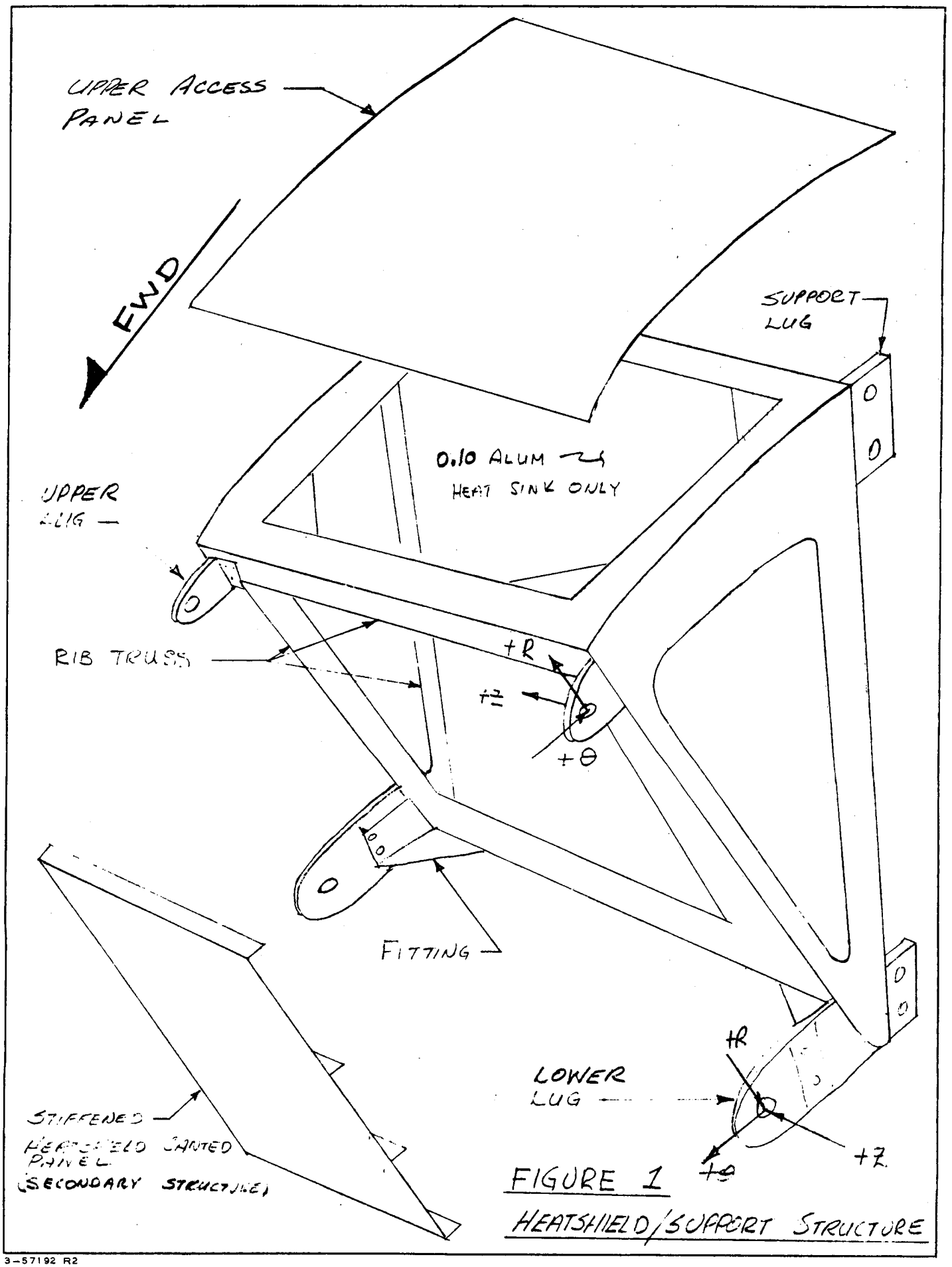

FIGURE 1
HEATSHIELD/SUPPORT STRUCTURE

FIGURE 2. GEOMETRY AND UPPER PANEL LOADS

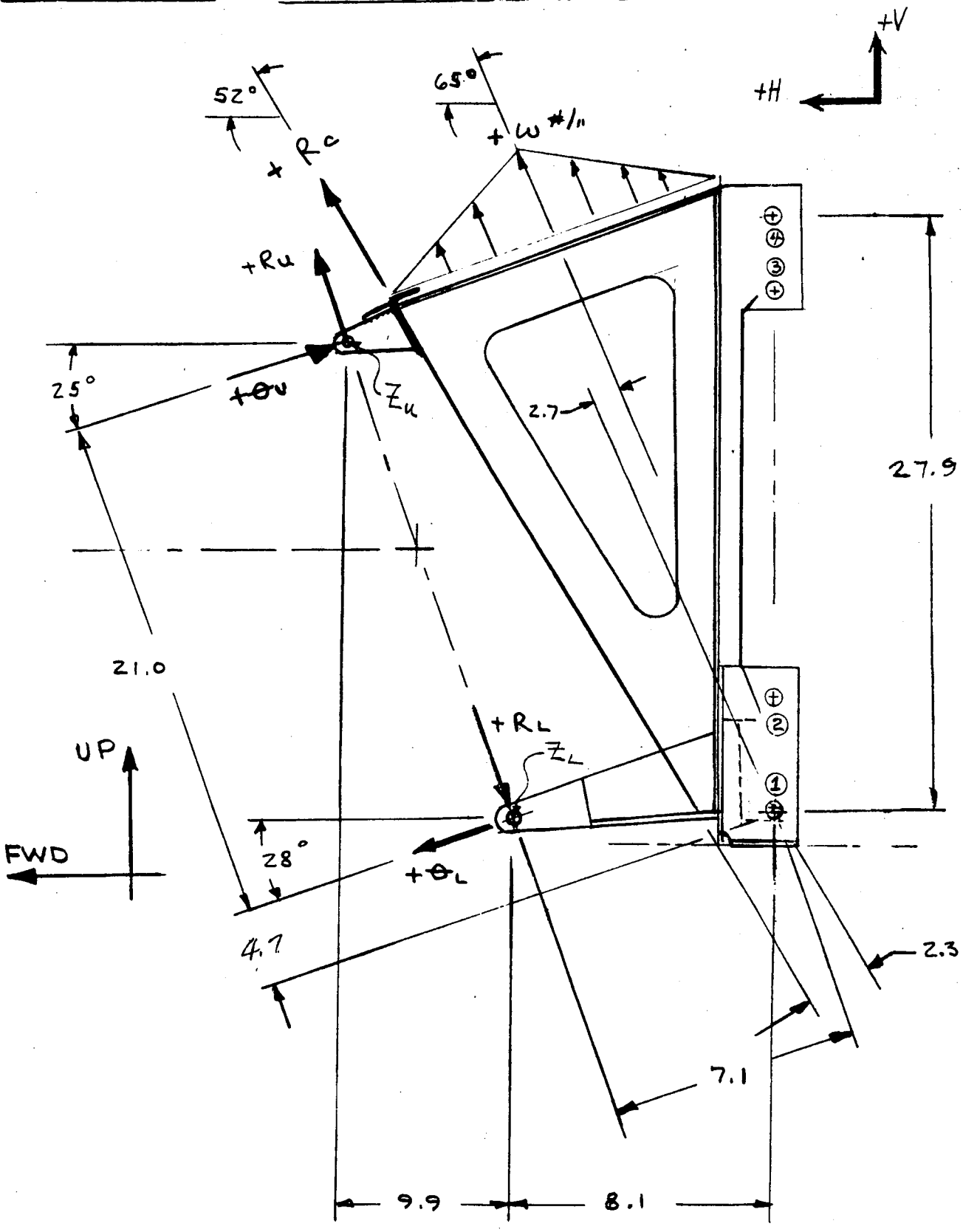

AIR LOAD DISTRIBUTION ON UPPER PANEL

ASSUME TRIANGULAR DISTRIBUTION OF PRESSURE LOADS TO THE STIFF SUPPORT BEAMS.

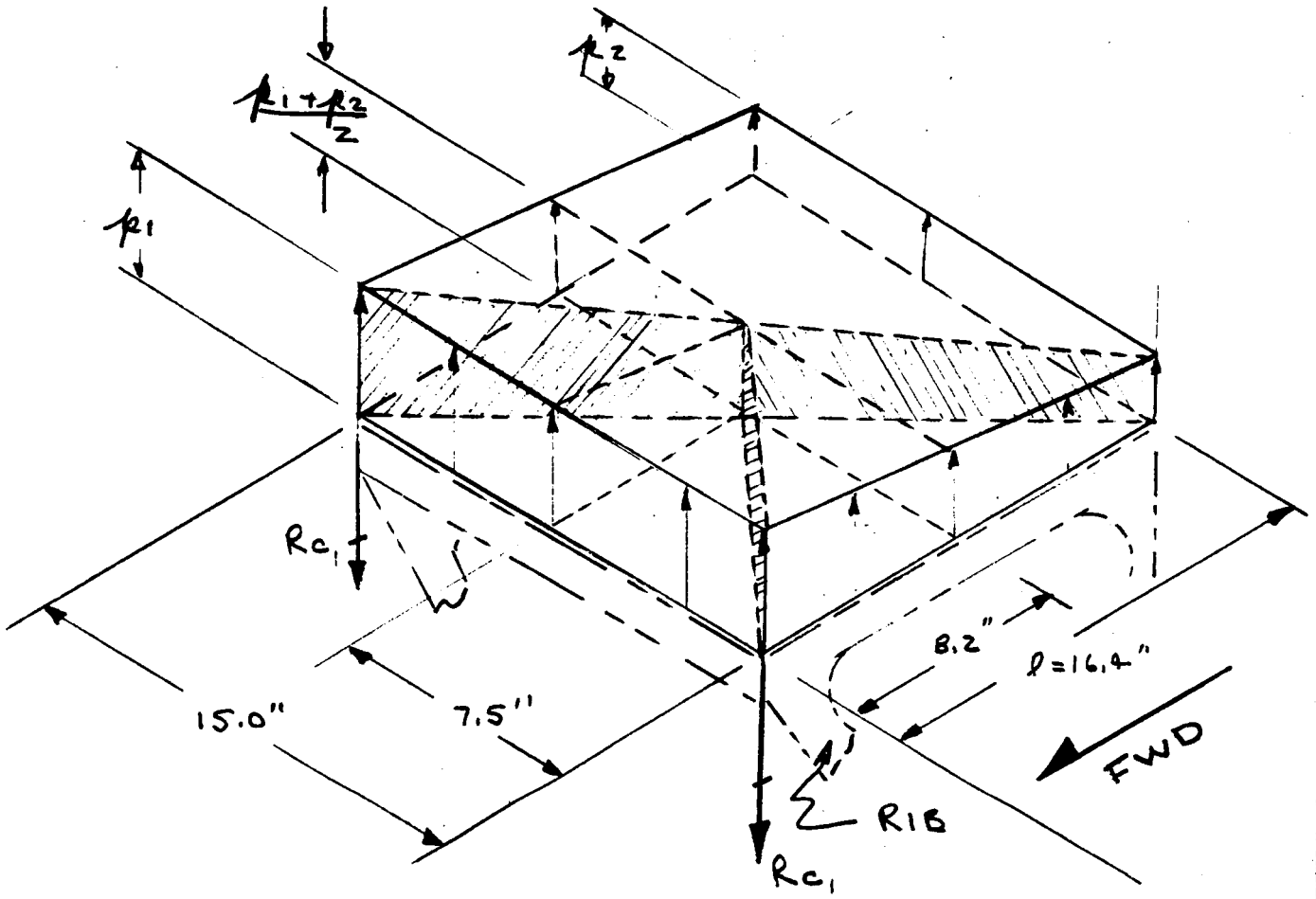

SOLVE FOR R_a

AVE. PRESSURE, (P.S.I.)

$$p_0 = \left\{p_1 + \frac{p_1 + p_2}{2}\right\}\frac{1}{2} = \frac{1}{4}\left[3p_1 + p_2\right]$$

$$w_0 = p_0(8.2) \quad (\text{LB/IN.})$$ w_0 = max running load

$$R_{C_1} = \frac{1}{2}\left[\frac{1}{2}(w_0)15.0\right] = \frac{1}{4}(15.0)\,p_0(8.2)$$

$$R_{C_1} = \frac{1}{4}(15.0)\,8.2\left(\frac{1}{4}\right)\left[3p_1 + p_2\right]$$

$$R_{C_1} = 7.69\left[3p_1 + p_2\right] \quad (\text{LB.})$$

AIRLOAD DIST. (CONT'D)

CHORDWISE LOADING ON RIB

AVE. PRESSURE,

$$\omega = \frac{p_1 + p_2}{2}(7.5)$$

$$\omega = [p_1 + p_2]\,3.75 \ \#/''$$

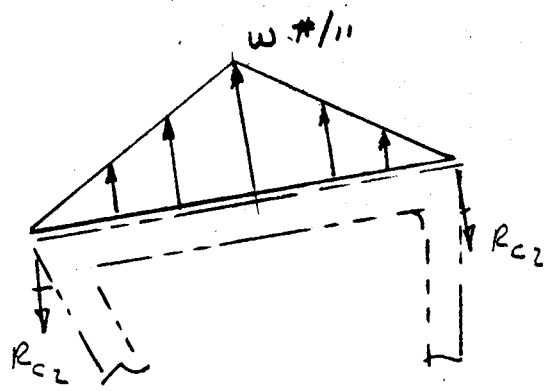

$$R_{c_2} = \tfrac{1}{2}[\omega\,(16.4)(1/2)]$$

$$R_{c_2} = \frac{16.4}{4}[3.75(p_1+p_2)] = 15.4(p_1+p_2)$$

$$R_c = R_{c_1} + R_{c_2} = 7.69[3p_1+p_2] + 15.4[p_1+p_2]$$

R_{c_1} REF. PG. 5

$$R_c = 38.47\,p_1 + 23.09\,p_2$$

ULT LOADS

UPPER PANEL AIRLOAD DISTRB. CONT'D

ω & R_c FOR FOUR BOOST CONDITIONS (REF. B PAGE 20)

CASE 1 TOTAL VENTING, $\alpha = -5.80°$

$\Delta P_1 = .90(1.4) = 1.26$ P.S.I. ULT
$\Delta P_2 = .50(1.4) = .70$ P.S.I. ULT.
$R_c = -64.6$ # ULT.
$\omega = -7.4$ #/" ULT.

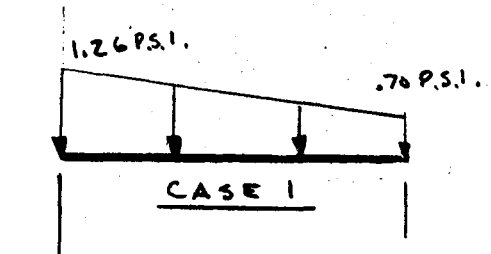

CASE 2 VENTING LAG, $\alpha = -5.80°$

$\Delta P_1 = -.14(1.4) = -.20$ P.S.I. ULT.
$\Delta P_2 = -.60(1.4) = -.84$ P.S.I. ULT.
$R_c = 26.6$ # ULT.
$\omega = 3.9$ #/" ULT.

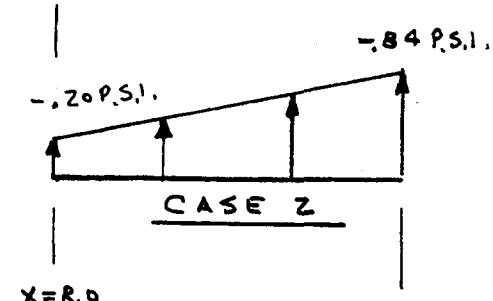

CASE 3 TOTAL VENTING, $\alpha = 4.0°$

$\Delta P_1 = -1.9(1.4) = -2.66$ P.S.I. ULT.
$\Delta P_2 = -1.2(1.4) = -1.68$ P.S.I. ULT.
$R_c = 139.2$ # ULT.
$\omega = 16.3$ #/" ULT.

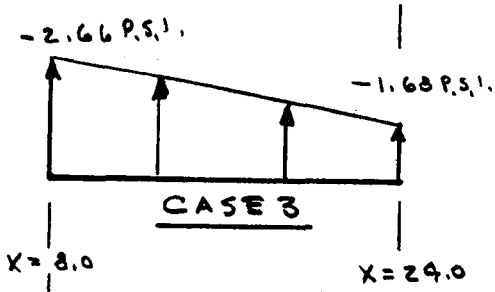

CASE 4 VENTING LAG, $\alpha = 4.0°$

$\Delta P_1 = -2.9(1.4) = -4.06$ P.S.I. ULT.
$\Delta P_2 = -2.2(1.4) = -3.08$ P.S.I. ULT.
$R_c = 2240$ # ULT.
$\omega = 26.8$ #/" ULT.

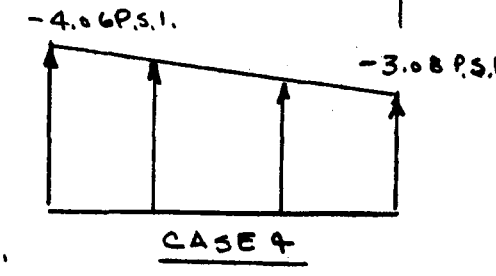

ULT. LOADS

LOADS TO LEADING EDGE LUGS FROM FOUR BOOST CONDITIONS

(REF A PAGES 11 & 12)

LOADS ACT ON ONE SIDE of L.E.

CASE 1

R_u = -131.0#
R_L = 96.0#
θ_u = -12.0#
θ_L = 63.0#
R_c = -64.60#
ω = -7.4#/"

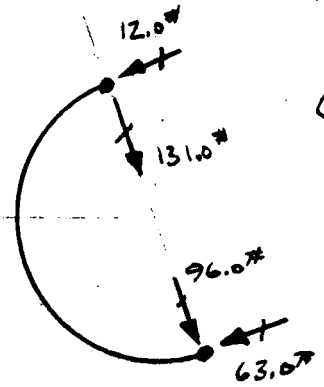

R_c = 64.6#
ω = 7.4#/"
(REF. PG. 7.)

CASE 2

R_u = -119.0#
R_L = 95.0#
θ_u = -108.0#
θ_L = 165.0#
R_c = 26.60#
ω = 3.9#/"

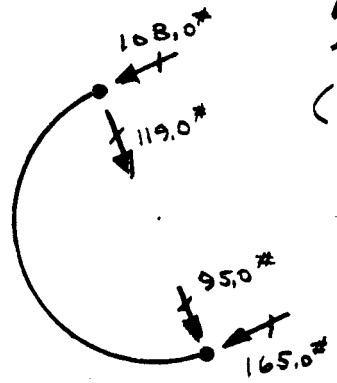

R_c = 26.6#
ω = 3.9#/"
(REF. PG. 7.)

CASE 3 ON PAGE 9

CASE 4

R_u = 139.0#
R_L = 6.0#
θ_u = -16.0#
θ_L = 24.0#
R_c = 224.0#
ω = 26.8#/"

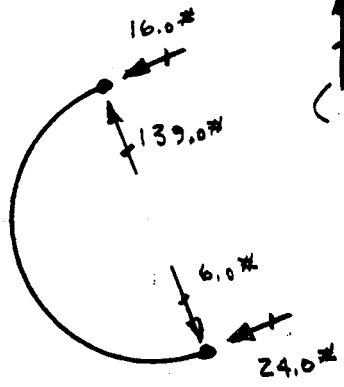

R_c = 224#
ω = 26.8#/"
(REF. PG. 7.)

CONT

CASE 3

$R_u = -121.8^{\#}$
$R_L = -8.2^{\#}$
$\theta_u = 83.1^{\#}$
$\theta_L = 81.9^{\#}$
$R_c = 139.2^{\#}$
$\omega = 16.3\ ^{\#}/in$

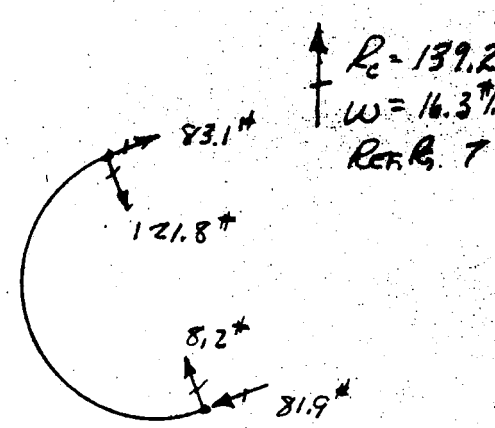

ASSUMPTIONS - RIB TRUSS

REF. FIGURE 3

1. LOWER LUG LOADS ARE REACTED ONLY BY THE LOWER SUPPORT LUG (THE LUG IS NOT ATTACHED TO THE RIB TRUSS).

2. THE UPPER LUG LOADS ARE CARRIED AS AXIAL FORCES IN THE RIB TRUSS (THE LOAD VECTORS AND RIB TRUSS MEMBERS ARE COLINEAR WITHIN 5°).

3. THE INDUCED MOMENT AT THE UPPER LUG IS DISTRIBUTED TO THE RIB TRUSS PER THE ENERGY SOLUTION OF PAGES 16 & 17.

FIGURE 3 EQUILIBRIUM AND MEMBER LOADS RIB TRUSS

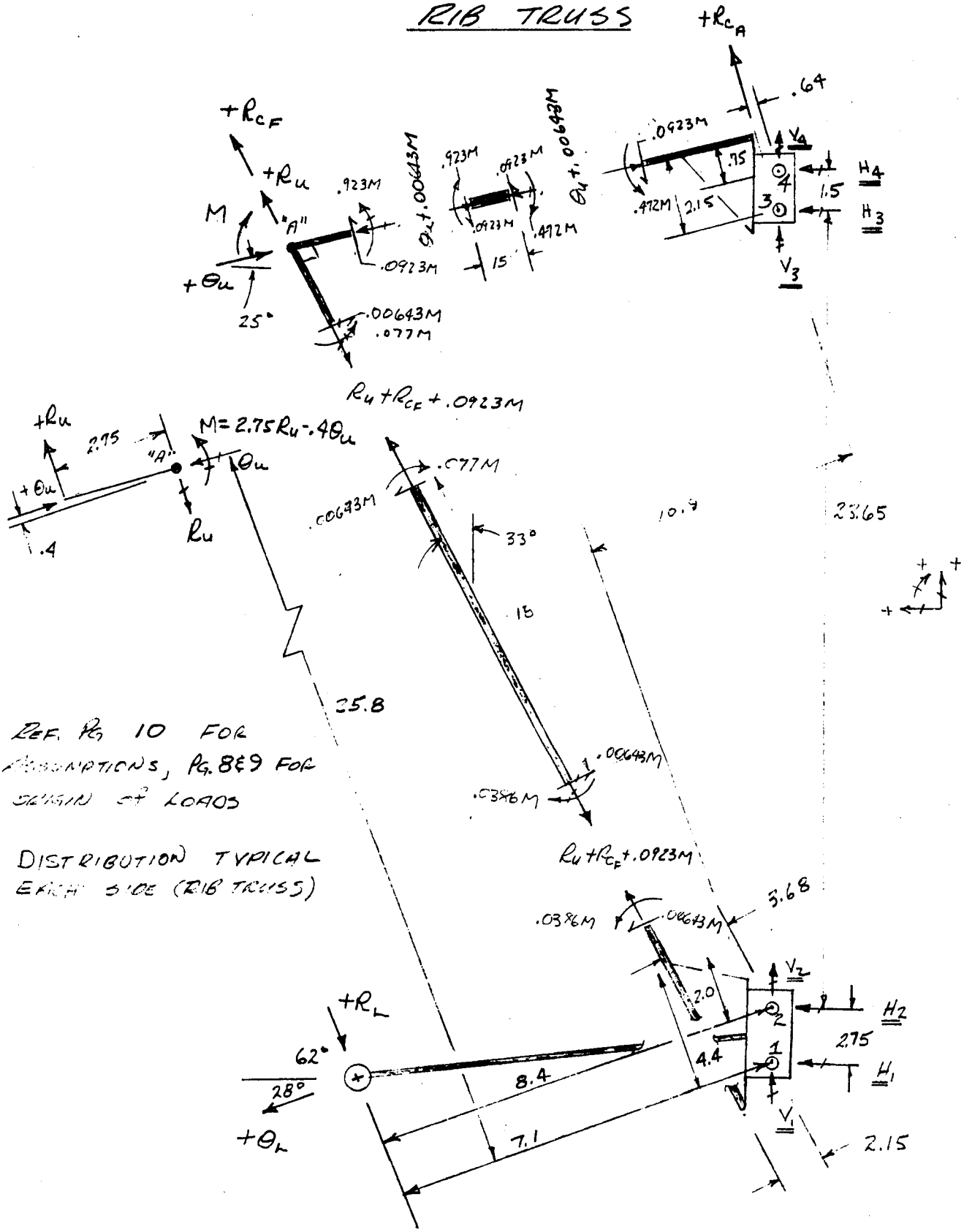

REF. PG 10 FOR ASSUMPTIONS, PG. 8&9 FOR ORIGIN OF LOADS

DISTRIBUTION TYPICAL EACH SIDE (RIB TRUSS)

REF. FIG 11 FOR GEOMETRY & LOAD DIRECTION

1. ASSUME VERTICAL LOAD EQUALLY DIVIDED BETWEEN 1 & 2

$$V_1 = V_2 = \tfrac{1}{2}(R_L \sin 62 + \theta_L \sin 28) - \tfrac{1}{2} R_u \cos 33 - \tfrac{1}{2} R_{c_F} \cos 33 - \tfrac{1}{2}(.0923M)\cos 33$$

$$\boxed{V_1 = V_2 = 0.442 R_L + 0.235 \theta_L - 0.419 R_u - 0.419 R_{c_F} - 0.0387M}$$

2. SUMMATION OF MOMENTS ABOUT 2

$$H_1 = \frac{7.1 R_L + 2\theta_L}{2.75} - \frac{3.68 R_u}{2.75} - \frac{3.68 R_{c_F}}{2.75} + \frac{.0586M}{2.75} - \frac{3.68(.0923M)}{2.75}$$

$$\boxed{H_1 = 3.06 R_L + 0.725 \theta_L - 1.34 R_u - 1.34 R_{c_F} - 0.11M}$$

3. SUMMATION OF MOMENTS ABOUT 1

$$H_2 = \frac{-7.1 R_L - 4.4\theta_L}{2.75} + \frac{2.15 R_u}{2.75} + \frac{2.15 R_{c_F}}{2.75} - \frac{.0586M}{2.75} + \frac{2.15(.0923M)}{2.75}$$

$$\boxed{H_2 = -2.58 R_L - 1.6 \theta_L + 0.782 R_u + 0.782 R_{c_F} + 0.0582M}$$

4. SUMMATION OF VERTICAL FORCES AT 3 & 4

$$V_3 = -\tfrac{1}{2} \theta_u \sin 25 - \tfrac{1}{2}(.00643M)\sin 25 - \tfrac{1}{2} R_{c_A} \cos 25$$

$$\boxed{V_3 = -0.221 \theta_u - 0.00142M - 0.453 R_{c_A}}$$

$$V_4 = -\tfrac{1}{2} \theta_u \sin 25 - \tfrac{1}{2}(.00643M)\sin 25 - \tfrac{1}{2} R_{c_A} \cos 25$$

$$\boxed{V_4 = -0.221 \theta_u - 0.00142M - 0.453 R_{c_A}}$$

5. SUMMATION OF MOMENTS ABOUT 4

$$H_3 = \frac{-.75\theta_u}{1.5} + \frac{.472M}{1.5} - \frac{.75(.00643M)}{1.5} - \frac{.64R_{CA}}{1.5}$$

$$\boxed{H_3 = -0.5\theta_u + 0.31M - 0.442R_{CA}}$$

6. SUMMATION OF MOMENTS ABOUT 3

$$H_4 = \frac{2.15\theta_u}{1.5} - \frac{.472M}{1.5} + \frac{2.15(.00643M)}{1.5}$$

$$\boxed{H_4 = 1.435\theta_u - 0.305M}$$

7. CHECK EQUILIBRIUM REF. PGS. 11

$$\Sigma M_1 = -95(7.1) - 165(4.4) - 119(2.75+2.15) - 108(25.8) + 26.6(3.15)$$

$$-26.6(10.9) + 617.8(2.75) + 45.9(2.75+23.65) + 68(2.75+23.65) = 0$$

$$\Sigma M_1 = -674.5 - 726 - 345 - 2786 + 57.2 - 289.9 + 1699 + 1212 + 1870 = 0$$

$$\Sigma M_1 = -4821 + 4838 = \underline{\underline{0 = +17 \text{ in-lbs}}}$$

$$\Sigma F_V = +130.4 + 130.4 + 12.3 + 12.3 - 95\sin 62 - 165\sin 28$$

$$-108\sin 25 - 119\cos 25 + 26.6\cos 25 + 26.6\cos 25 = 0$$

$$\Sigma F_V = 285.3 - 74 - 77.5 - 44.7 - 108 + 24.1 + 24.1 = \underline{\underline{0 = 333.5 - 327.2 = +19.3}}\ \#$$

$$\Sigma F_H = +566.1 - 617.8 - 45.9 - 68 - 95\cos 62 + 165\cos 28 - 119\cos 25$$

$$+108\cos 25 + 26.6\sin 25 + 26.6\sin 25 = 0$$

$$= +566.1 - 731.7 - 44.6 + 146 - 50.3 + 98 + 11.2 + 11.2 = 0$$

$$= +832.5 - 826.6 = \underline{\underline{0 = +5.9}}\ \#$$

TABLE 1 SUMMARY of REACTIONS

			H_1	V_1	H_2	V_2	H_3	V_3	H_4	V_4
CASE 1 - REF. Pg 8	R_u	-131	175.5	54.8	-102.5	54.8	-	-	-	-
	θ_u	-12	-	-	-	-	6	3	-17.2	3
	R_L	96	294	42.5	-248	42.5	-	-	-	-
	θ_L	63	45.8	14.8	-101	14.8	-	-	-	-
	M	-355	39.1	13.7	-20.6	13.7	-110	.5	107.5	.5
	R_{C_F}	-64.6	86.6	27.1	-50.6	27.1	-	-	-	-
	R_{C_A}	-64.6	-	-	-	-	27.1	29.4	-	29.4
	Σ		641.0	152.9	-522.7	152.9	-76.9	32.9	19.3	32.9
CASE 2 - REF. Pg 8	R_u	-119	159.5	49.8	-93	49.8	-	-	-	-
	θ_u	-108	-	-	-	-	54	23.9	-155	23.9
	R_L	95	291	42	-265	42	-	-	-	-
	θ_L	165	120	38.8	-264	38.8	-	-	-	-
	M	-284.8	31.3	11	-16.6	11	-88.3	0.4	87	0.4
	R_{C_F}	26.6	-35.7	-11.2	20.8	-11.2	-	-	-	-
	R_{C_A}	26.6	-	-	-	-	-11.6	-12.0	-	-12.0
	Σ		566.1	130.4	-617.8	130.4	-45.9	12.3	-68	12.3

CONT

TABLE 1 (CONT) SUMMARY of REACTIONS

			H_1	V_1	H_2	V_2	H_3	V_3	H_4	V_4
CASE 3 - REF. FIG. 9	R_u	-121.8	163	51	95	51	-	-	-	-
	θ_u	83.1	-	-	-	-	-41.6	-20.8	119	-20.8
	R_L	-8.2	-25.1	-4	21.2	-4	-	-	-	-
	θ_L	81.9	59.7	19.2	-131	19.2	-	-	-	-
	M	-368	40.5	14.2	-21.4	14.2	-114	.5	111	.5
	R_{C_F}	139.2	-187	-58.5	109	-58.5	-	-	-	-
	R_{C_A}	139.2	-	-	-	-	-58.5	-63.5	-	-63.5
	Σ		51.1	21.9	72.8	21.9	-214	-163.8	230	-83.8
CASE 4 - REF. FIG. 8	R_u	139	-186	-58.2	109	-58.2	-	-	-	-
	θ_u	-16	-	-	-	-	8	4	-22.9	4
	R_L	6	19.4	3	-15.5	3	-	-	-	-
	θ_L	24	17.5	5.6	-38.4	5.6	-	-	-	-
	M	386	-42.5	-14.9	22.4	-14.9	120	-.5	-117	-.5
	R_{C_F}	224	-300	-93.5	175	-93.5	-	-	-	-
	R_{C_A}	224	-	-	-	-	-93.5	-102	-	-102
	Σ		-492.6	-158	252.5	-158	34.5	-98.5	-139.9	-98.5

DETERMINE DISTRIBUTION INTO TWO LEGS FROM ECCENTRIC MOMENT

THE UPPER LEG HAS 10 TIMES STIFFNESS OF DIAGONAL LEG.

SOLVE FOR SUPPORTS

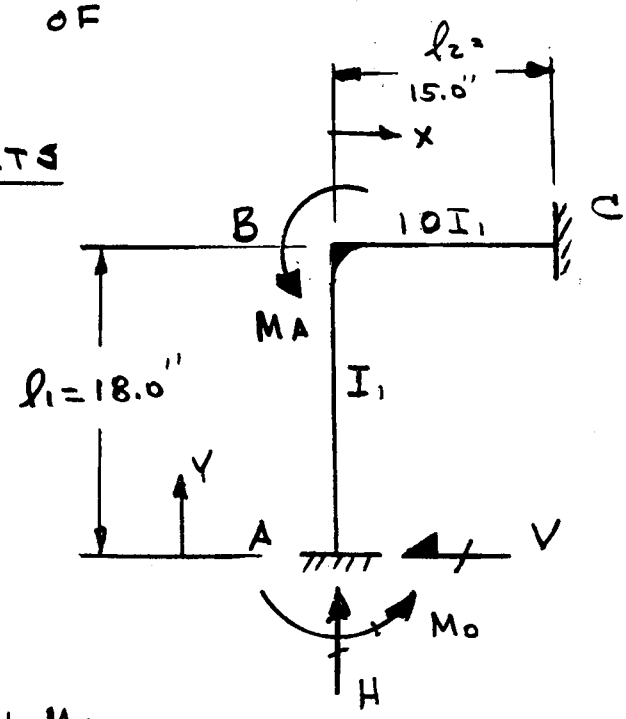

$$M\Big]_A^B = M_o - Vy$$

$$\frac{\partial M}{\partial M_o} = 1.0$$

$$\frac{\partial M}{\partial V} = -y$$

$$M\Big]_B^C = M_o - Vl_1 - HX + M_A$$

$$\frac{\partial M}{\partial M_o} = 1.0 \quad , \quad \frac{\partial M}{\partial H} = -X$$

$$\frac{\partial M}{\partial V} = -l_1$$

$$① \frac{\partial U}{\partial M} = 0 = \int_0^{l_1} (M_o - Vy)\frac{dy}{EI_1} + \int_0^{l_2} (M_o - Vl_1 - HX + M_a)\frac{dx}{10EI_1}$$

$$② \frac{\partial U}{\partial V} = 0 = \int_0^{l_1} (-M_o y + Vy^2)\frac{dy}{EI_1} + \int_0^{l_2} (-M_o l_1 + Vl_1^2 + HXl_1 - M_a l_1)\frac{dx}{3EI}$$

$$③ \frac{\partial U}{\partial H} = 0 = \int_0^{l_2} (-M_o X + Vl_1 X + HX^2 - M_a X)\frac{dx}{10EI_1}$$

MOMENT DISTRB. (CONT'D)

INTEGRATING EQUATIONS 1, 2, 3

$$M_A = -M_o(13.0) + V(126.0) + H(7.5)$$

$$M_A = -M_o(7.00) + V(90.0) + H(7.5)$$

$$M_A = -M_o + V(18.0) + H(10.0)$$

SOLVING ABOVE

$$V = M_a(.00643)$$

$$H = M_a(.0923)$$

$$M_o = M_a(.0386)$$

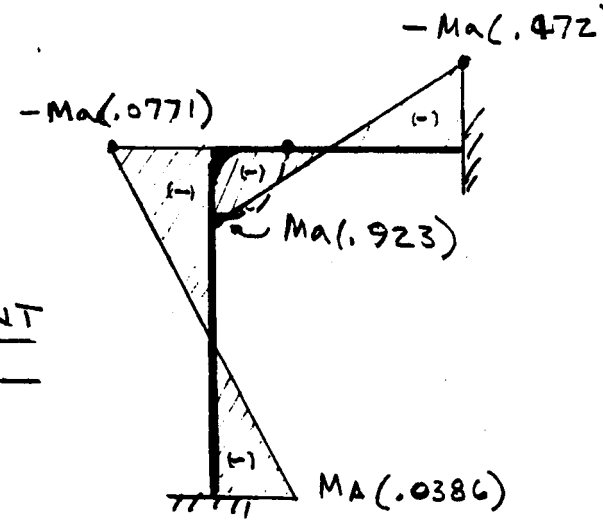

MOMENT CURVE

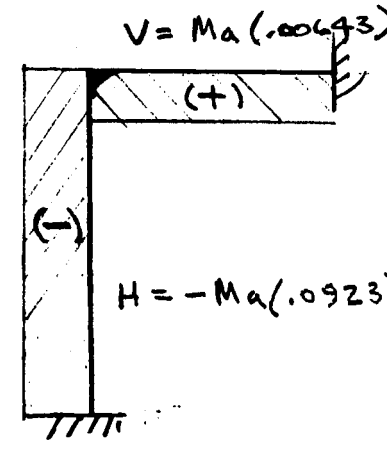

AXIAL & SHEAR LOADS

ULT LOADS

32 "g" RMS SIDE LOAD REF. A

LOWER LUG

$Z_L = \pm 206$ lbs
$R_L = \pm 11$ lbs
$\theta_L = \pm 60$ lbs

UPPER LUG

$Z_u = \pm 264$ lbs
$R_u = \mp 27$ lbs
$\theta_u = \mp 141$ lbs

THE R & θ LOADS ARE REACTED AT THE SUPPORTS SIMILAR TO THE R & θ LOAD ON PAGES 10-15. THE R & θ SIDE LOAD COMPONENTS ARE NOT SHOWN. EQUILIBRIUM FOR THE SIDE LOAD (Z) IS SHOWN BELOW.

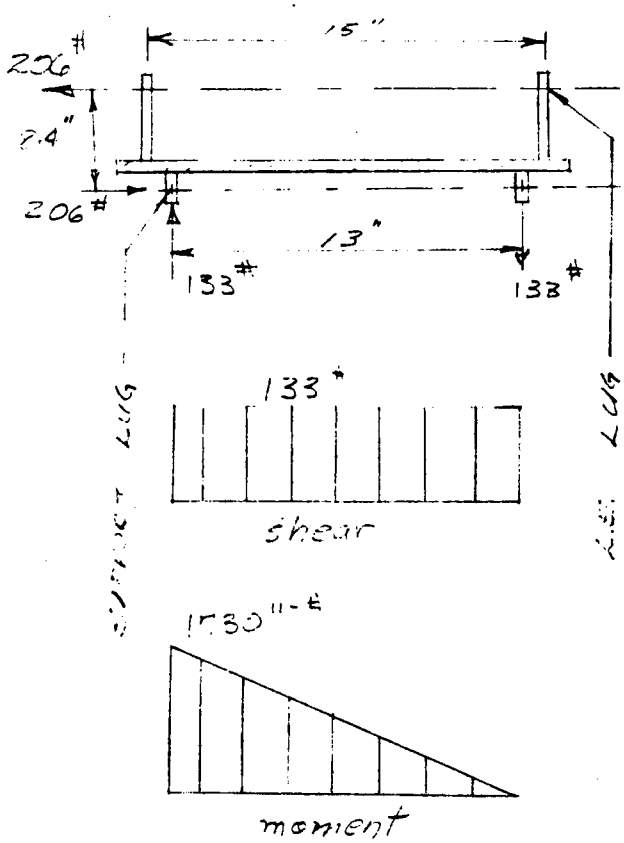

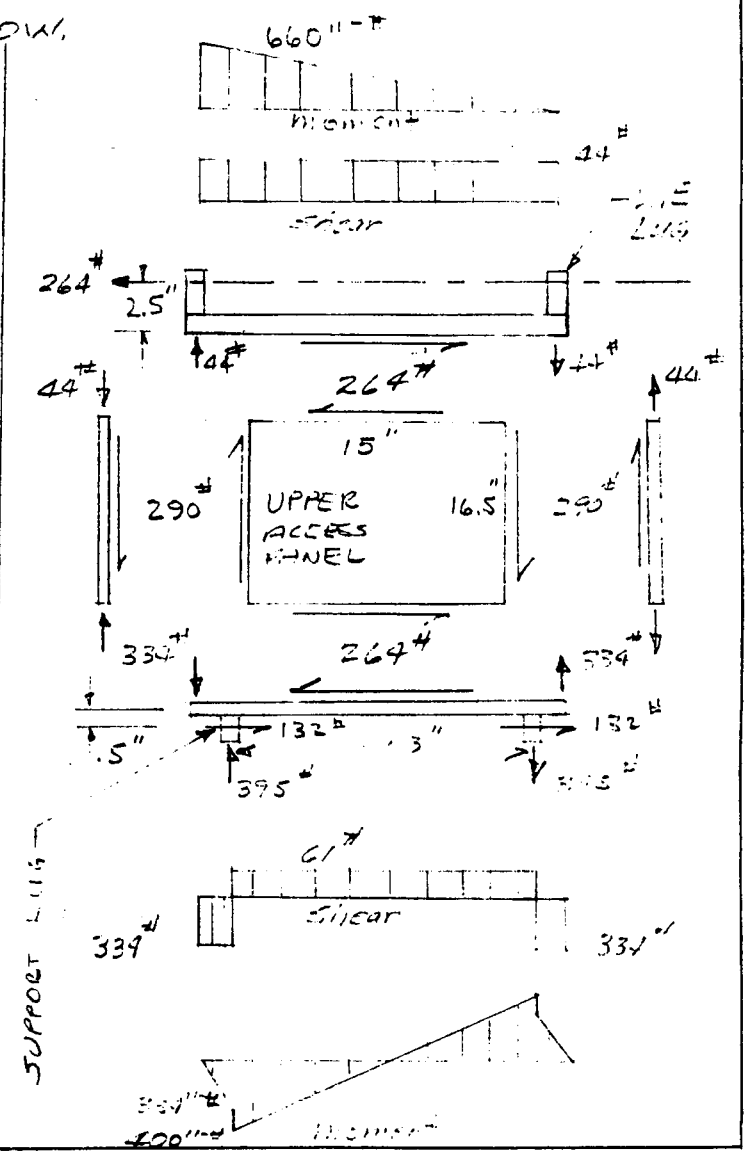

HEATSHIELD CANTED PANEL

THE HEATSHIELD PANEL IS A POLYIMIDE OR TITANIUM CONSTRUCTION WITH RSI BONDED TO THE FORWARD SIDE AND DYNAQUARTZ ATTACHED TO THE AFT SIDE. THE VIBRATION AND ACOUSTIC ENVIRONMENTS ARE CRITICAL STRUCTURALLY FOR THE INSULATION MATERIALS. THE PANEL IS SIZED SUCH THAT ITS NATURAL FREQUENCY IS GREATER THAN 120 hz IN ORDER TO PRECLUDE FAILURE DUE TO VIBRATION AND ACOUSTIC LOADS. DETAIL ACOUSTIC ANALYSIS WILL BE CONDUCTED LATER.

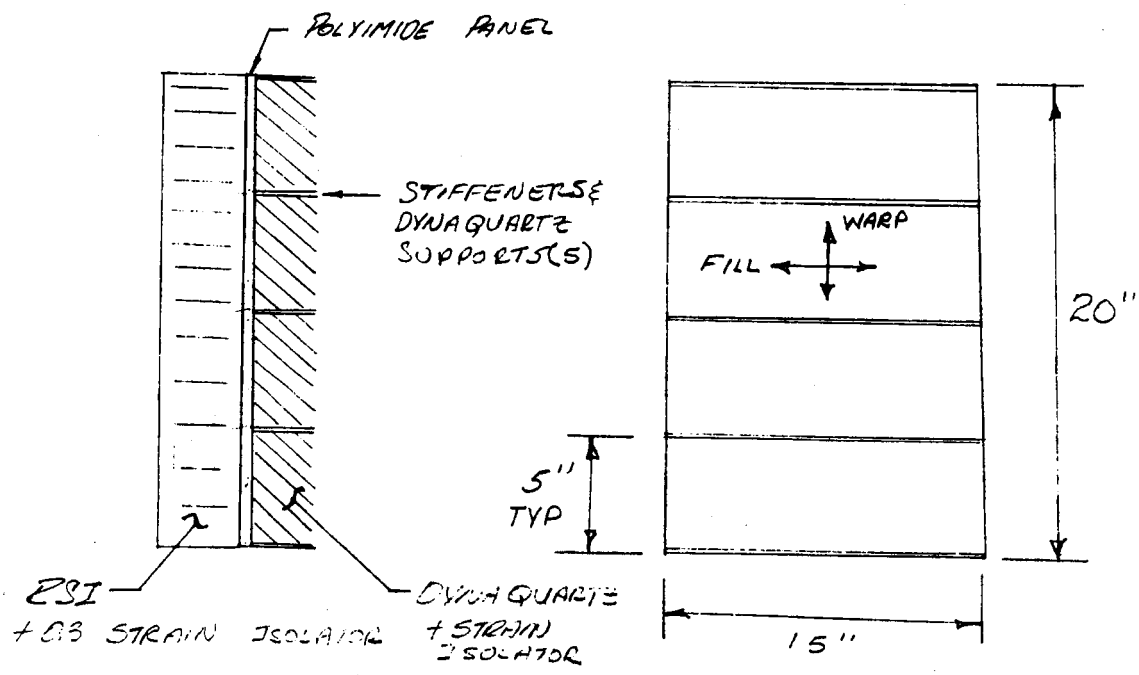

TOTAL WEIGHT = 5.09 LB/FT² REF. E

THE FREQUENCY of SHEET/STRINGER PANELS IS GIVEN IN REFS. (C) & (D) THIS IS EMPIRICAL DATA WHICH ACCOUNTS FOR END FIXITY NORMALLY ACHIEVED IN THIS TYPE of CONSTRUCTION.

$$f_o = K_r \frac{t}{a^2} (X)$$

a = short side
$K_r \propto b/a$ (ALUM)
t = thickness

(X) FOR SINGLE DEGREE of FREEDOM

$$f_o = \sqrt{\frac{K_o}{M_o}}$$

$K \propto E$
$M \propto \rho$

THE K_r IN REF (C) IS FOR ALUMINUM, CONVERTING TO ANOTHER MATERIAL

$$\frac{f}{\sqrt{\frac{E}{\rho}}} = \frac{f_o}{\sqrt{\frac{E_o}{\rho_o}}}$$

$$f = f_o \left(\frac{E \rho_o}{E_o \rho}\right)^{1/2} \qquad X = \left(\frac{E \rho_o}{E_o \rho}\right)^{1/2}$$

where $E_o = 10.5 \times 10^6$ psi ALUM
$\rho_o = 0.10$ lb/in^3 ALUM

E = modulus of polyimide
$\rho = W/t$
W = total weight, polyimide plus insulation = 5.09 lb/ft^2
REF. FIG. 19

FOR 5"X15" PANEL

$b/a = 3.0$ $\quad K_r = 1.55 \times 10^5$ REF. PG. 20

$a^2 = (5)^2 = 25$

for $t = .08$ $\quad \rho = \frac{5.09}{144}\left(\frac{1}{.08}\right) = .442 \ \frac{lb}{in^3}$

REF. PG. 20

$E = 2.5 \times 10^6$ REF. (E)

$$f = 1.55 \times 10^5 \ \frac{(.08)}{(25)} \left(\frac{2.5 \times 10^6 \ (.10)}{10.5 \times 10^6 \ (.442)}\right)^{1/2}$$

$$f = 1.55 \times 10^5 (.0032)(.232) = 115 \ hz$$

FIGURE 4 PRESENTS PANEL FREQUENCY VERSUS PANEL THICKNESS. MODULUS SENSITIVITY IS ALSO SHOWN.

SUMMARY

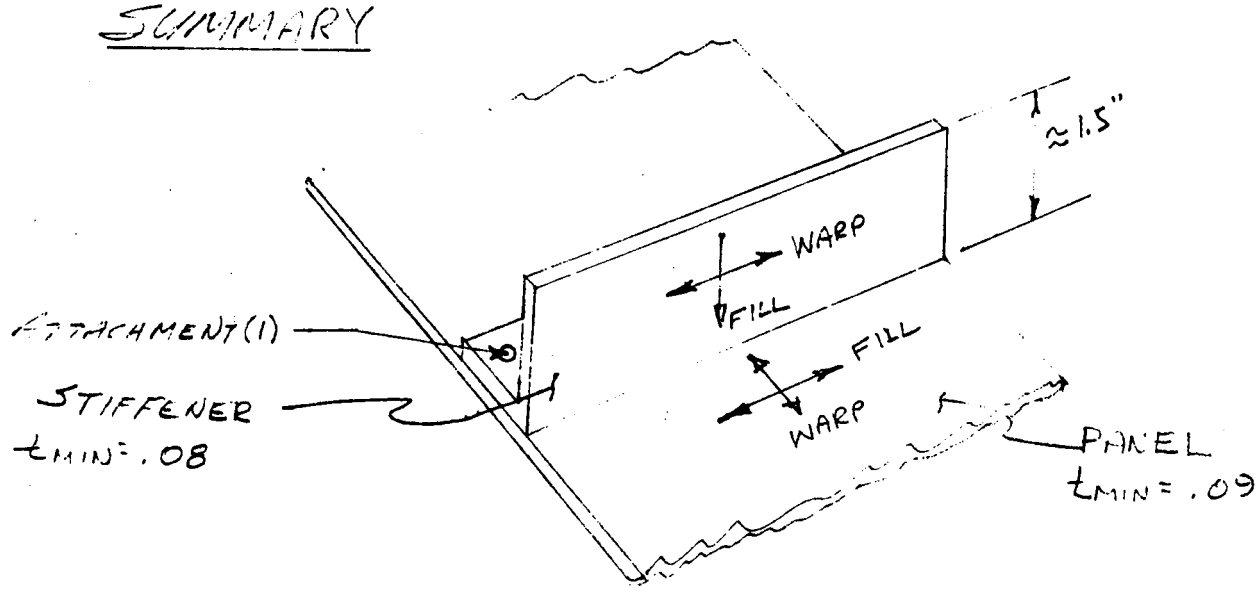

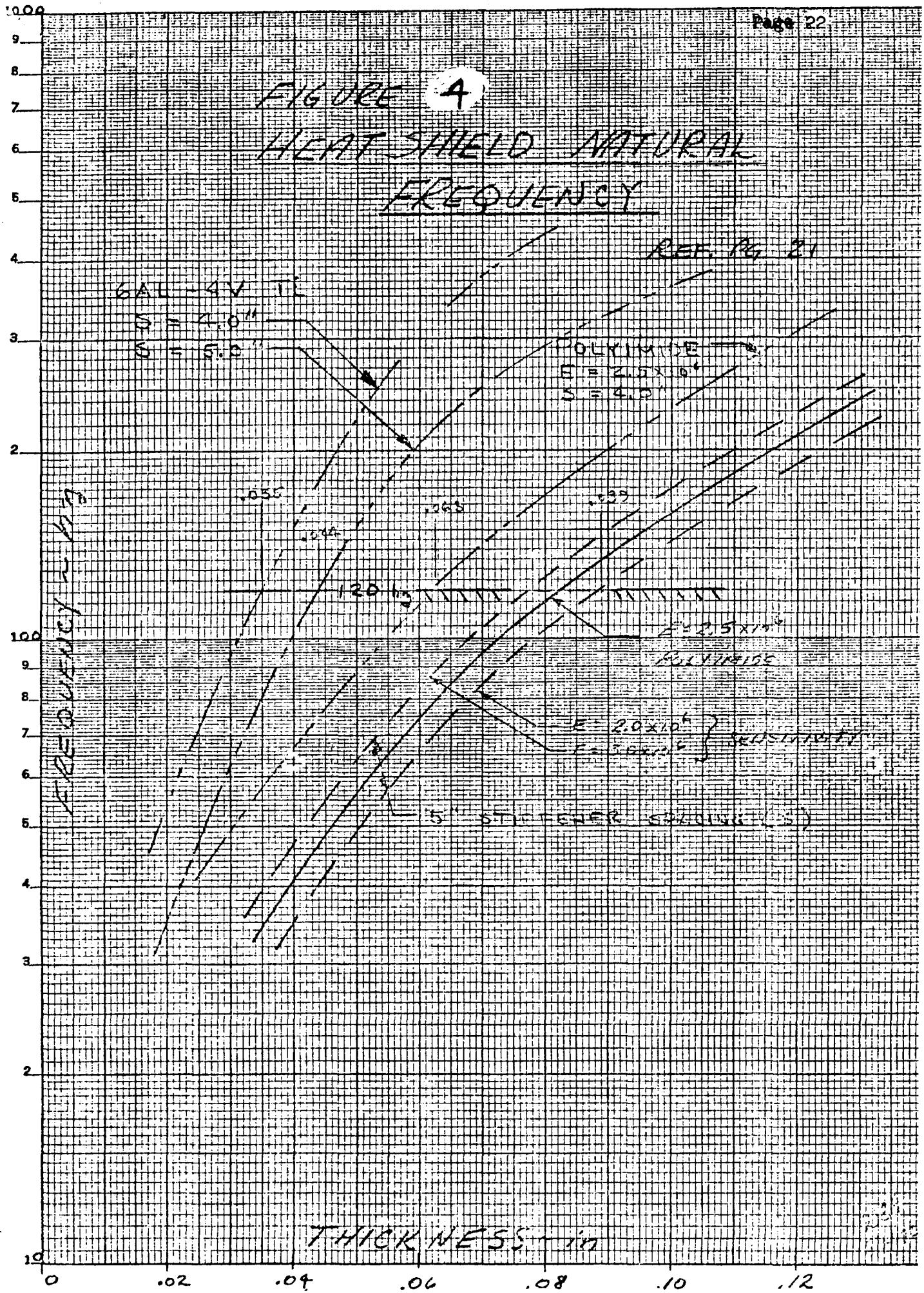

K+E SEMI-LOGARITHMIC 46 5133
2 CYCLES X 140 DIVISIONS MADE IN U.S.A.
KEUFFEL & ESSER CO.

DESIGN INFORMATION ~~REQUEST~~ RELEASE

10-3-72

MODEL (S) AND EFF.	DIR. NO.	REV.
LEADING EDGE SUPPORT STRUCTURE STRUCTURAL ANALYSIS	T143-DIR-2-17	
	DATE 9/29/72	PAGE 1 OF 41
SYSTEM Phase III Leading Edge	REF. G. O. NUMBER 3357 AA 1160	

Fill in block below for Information Request	Fill in block below for Information Release
TO _____ GROUP _____	IN REPLY TO DIR. NUMBER _____
REQ. BY _____ GROUP _____	REL. TO D. M. While GROUP 3-52000
REASON	PREPARED BY W.F. Agan WEA DATE 9/29/72 — CHECKED BY WE Agan DATE 9/29/72
LTV ONLY ☐ BWR ☐ BUWEPS ☐ ☐ _____	GROUP APP. H.E. Brougham DATE 10/2/72 — PROJ OFFICE While DATE 10/2/72

CC

E.C.Matza, F.D.Tarsia, R.B.Bost, J.E.Medford, I.E.Harder, H.I.Knight, G.B.Whisenhunt, B.A. Farch

DESIGN INFORMATION:

REFERENCES:

(A) Ultimate Static Loads Distribution and Preliminary Canted H/S Panel Analysis - Leading Edge Support. T143-DIR-2-12, dated 30 August 1972.

(B) E. L. Bruhn, Analysis and Design of Flight Vehicle Structures, copyright 1965, Tri-State Offset Company, Cincinnati, Ohio.

(C) Structural Design Data, Vought Aeronautics Division, LTV Aerospace Corp., Dallas, Texas.

(D) MIL-HDBK-5B, 1 September, 1971, Metallic Materials and Elements for Aerospace Vehicle Structures, Volume I.

(E) Phase III "Fail Safe" Leading Edge Structural Analysis, T143-DIR-2-09, dated 28 July 1972.

(F) Space Shuttle Wing Leading Edge Design Criteria, Phase III, T143-5R00060, dated 25 June 1971.

(G) Trevarno Co., Livermore Calif., Data Bulletin #86a, Structural Heat Resistant Polyimide Impregnating Resin System.

(H) Vought Aeronautics Division, LTV Aerospace Corp., Dallas, Texas, Designing for Acoustic Fatigue, Report No. 2-53 424/SDM-153, dated December 1969.

(I) Dynamic Response of Space Shuttle Orbiter Leading Edge Section, T143-DIR-1-07, dated 2 December 1971

(J) Shell Analysis Manual, NASA CR-9R, National Aeronautics and Space Administration, dated April 1968.

PURPOSE

The purpose of this DIR is to release the structural analysis of the Phase III Leading Edge Support Structure.

SUMMARY

A general schematic of the support structure is shown in Figure 1, including part identification and drawing callouts.

A summary of margins of safety is presented in Table 1. The critical load conditions are identified as are the pages containing the analyses. The minimum margin of safety for the structure is +0.19 and occurs in the rib truss diagonal from thermal expansion during entry. Most of the other margins are greater than +1.00 at ultimate because of fatigue considerations for acoustic and vibration loads. Fatigue life is computed and presented in the text for the applicable parts.

DISCUSSION AND RESULTS

The leading edge support structure provides continuity between the RPP leading edge and the wing box. It reacts the loads from the leading edge plus those acting on its own surface. The wing box is simulated by the support lug and beam which will be mounted to a rigid test fixture. The design assumption is that deflection and rotation at the support lug is precluded by the test fixture. This rationale is used because the wing box should be very stiff for the relatively small loads and dimensions of the leading edge.

TABLE I SUMMARY OF MARGINS OF SAFETY

Item	Material	Critical Condition	M.S.	Mode	Ref. Pg.
Upper Access Panel	.064 6AL-4V TI	Boost	+1.81	Buckling	10
Rib Truss					
- Fwd Beam	.064-.072 6AL-4V TI	Boost	+1.02	Crippling	16
- Side Beam	.04-.072 6AL-4V TI	Boost	+1.00	Crippling	17
- Diagonal	.04 6AL-4V TI	Boost	+1.31	Crippling	22
		Entry-Thermal Expansion	+0.19	Crippling	27
- Vertical	.04 6AL-4V TI	Entry-Thermal Expansion	+1.90	Crippling	29
Upper Lug	.156 Inconel 718	Side Load Vibration	+1.21	Bending	31
Back-up bracket	.156 321 Stainless Steel	Side Load Vibration	+0.66	Bending	33
Lower Lug	.078 Inconel 718	Side Load Vibration	+0.51	Crippling	36
- Splice	.25 Polyimide	Side Load Vibration	High	Compression	37
- Attach angles	.125 2024-T4 Alum	Side Load Vibration	+0.83	Bending	38
Lug Bolt	Inconel 718	Boost Entry	High High	Bending Bending	39
Support Lug & Beam	1/2" AISI 1025 Steel	Side Load Vibration	High	Bending	41

The .064 titanium upper access panel is a constant radius curved section and is analyzed for acoustic fatigue and for buckling as a cylinder subjected to an external radial pressure. An 0.05 in. thick panel was good for buckling but not acoustic fatigue which required going to the next stock thickness of 0.064 in. The frame supporting the panel is examined for deflections to determine if the panel radius changes significantly under load. The radius did not change so adequate stiffness is provided validating the analogy of cylindrical buckling. All spanwise shear introduced at the upper lugs is carried by the panel.

The rib truss, Figure 1, is comprised of the frame (fwd and side beams supporting the access panel), diagonal, and vertical members. The forward and side beams are built up of .04 and .072 titanium sheet. They support the access panel and react upper lug loads. They are both critical in crippling during boost; however, the minimum margin of safety is +1.00. The diagonal and vertical members are 0.04 in.titanium sheet. The diagonal also supports the access panel and reacts upper lug loads but the critical design condition is thermal expansion during entry where the margin of safety is +0.19. The vertical member does not carry loads from the leading edge or access panel because of the restraint offered by the support lugs and test fixture. Its only loading condition is thermal expansion and the margin of safety is +1.90.

The upper lug is an Inconel 718 welded bracket with gussets and end plate. A stainless steel back up fitting is nested in the corner of the sheet metal aft of the lug and is used to distribute the upper lug loads into the sheet metal rib truss. The upper lug is designed against fatigue failure for the vibratory side loads.

The lower lug is comprised of three parts, (a) an Inconel angle/lug, (b) a polyimide insulator shear clip, and (c) aluminum attach angles. The lower lug is tied directly into the support lug and therefore its loads are not reacted by the rib truss. The vibratory side load is the critical condition and the joint minimum margin of safety is +0.51.

The lug bolt is made of Inconel 718 and is hollowed out to reduce the heat conduction path. The margin of safety in bending is HIGH for both the boost (maximum load = 191#) and entry (maximum temperature = 1330°F, Maximum load = 19.7#) conditions.

The support lug and beam are made of commercial AISI 1025 steel. Its purpose is to provide a stiff support and to interface with the test fixture. Margins of safety are HIGH.

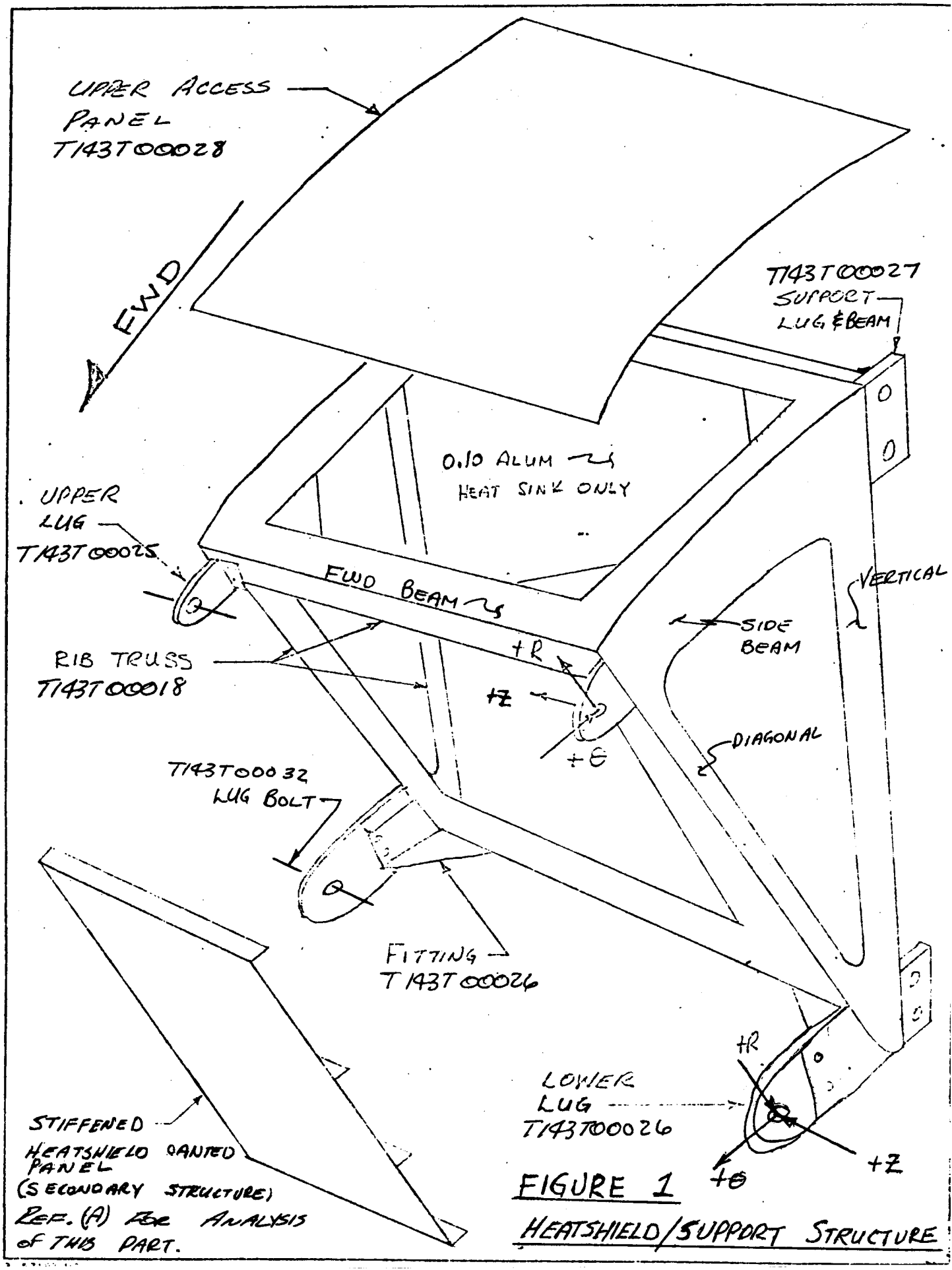

FIGURE 1

HEATSHIELD/SUPPORT STRUCTURE

UPPER ACCESS PANEL

DWG T143T00028

THE UPPER ACCESS PANEL IS ANALYZED FOR TWO CRITICAL CONDITIONS:

a) acoustic fatigue.

b) boost static pressure.

FAILURE FOR ACOUSTIC FATIGUE IS EVALUATED BY THE NOMOGRAPHS of REF. (H) WHICH PREDICTS PANEL LIFE RATHER THAN A MARGIN of SAFETY.

A MARGIN of SAFETY IS COMPUTED FOR BUCKLING DURING THE BOOST STATIC PRESSURE CONDITION.

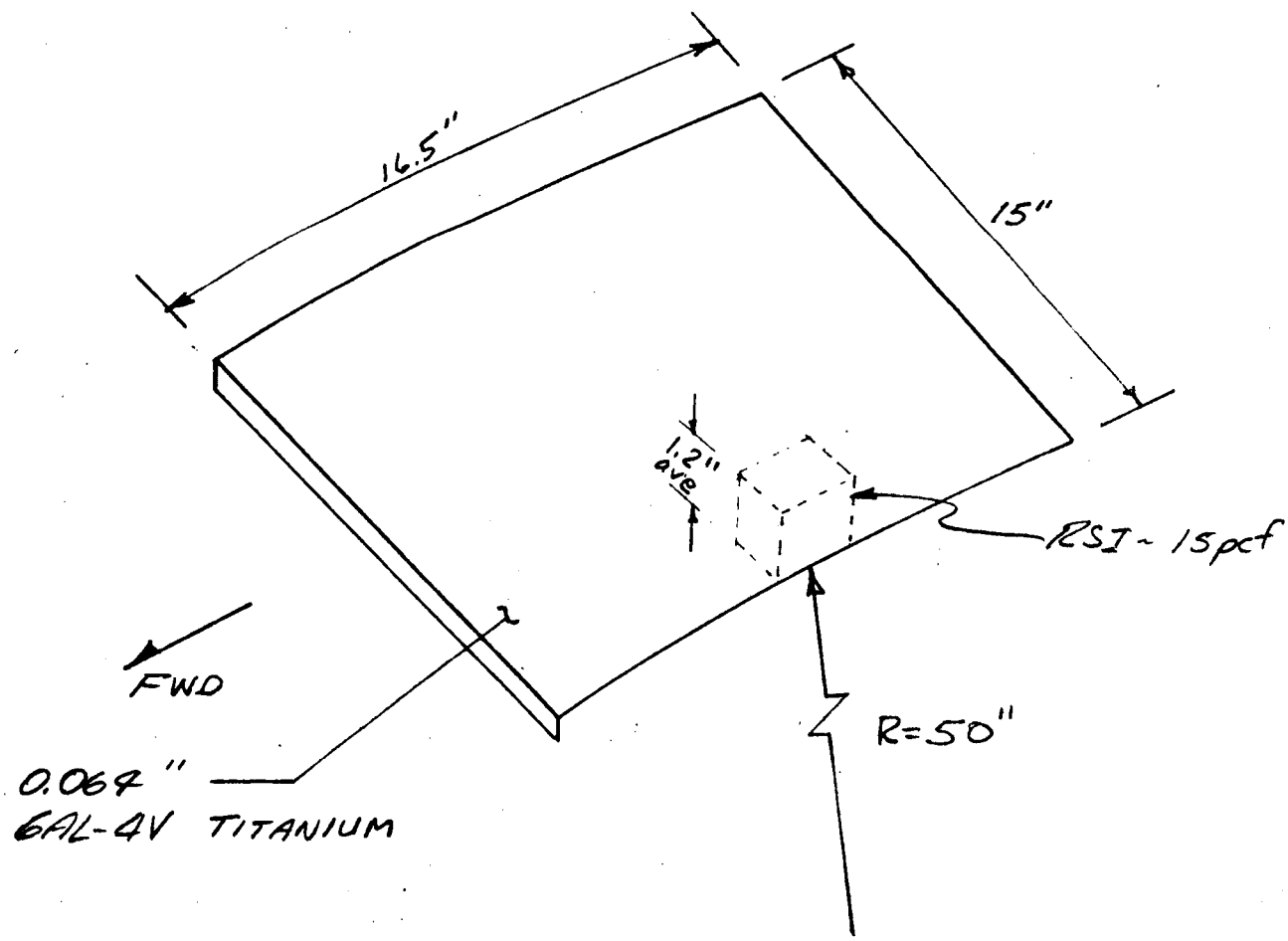

ACOUSTIC FATIGUE

1. FIND NATURAL FREQUENCY (f_o) of PANEL
(CONSIDER AS FLAT PANEL)

density (ρ) panel = .161 #/in³ Ti

Weight RSI = $\frac{15 \times 1.2}{1728}$ = .0104 #/in²

REF. PG. 7

BOND = .002 #/in² EST.

$$\rho = .161 + \frac{.0104 + .002}{.064} = 0.355 \ \#/in^3$$

$$f_o = K_r \frac{t}{a^2}(X) \quad \text{REF. (H)} \quad \text{FOR ALUM SHEET}$$

$a/b = 16.5/15 = 1.1$ $\quad K_r = 2.5 \times 10^5$

WHERE $X = \left(\frac{E \rho_o}{E_o \rho}\right)^{1/2}$ FACTOR TO CONVERT FROM ALUM TO TITANIUM AND TO ACCOUNT FOR THE RSI MASS

$E_o = 10.5 \times 10^6$, $\rho_o = 0.10$ } ALUM REF. (D)

$E = 16.4 \times 10^6$ TITANIUM
$\rho = 0.355$

$$X = \left[\frac{16.4 \times 10^6 (.1)}{10.5 \times 10^6 (.355)}\right]^{1/2} = 2.1$$

$$f_o = 2.5 \times 10^5 \frac{0.064}{(16.5)^2}(2.1) = 124 \text{ hz} \longleftarrow$$

2. FIND SPECTRUM LEVEL
FOR $f_o = 124$ hz

OCTIVE BAND LEVEL (O.B.L.) = 150.5 db
REF. (F)

SPECTRUM LEVEL (S.L) = O.B.L. $- 10 \log_{10} \Delta f$

$\Delta f = 0.2275 f_c$ FOR 1/3 OCTIVE BAND LEVEL

$f_c = f_o = 124$ hz

$\Delta f = .2275 (124) = 28.2$ hz

S.L. = $150.5 - 10 \log_{10} (28.2) = 136$ db ←

3. DETERMINE CYCLE ENVIRONMENT (n)

TOTAL TIME = 50 MIN × 60 sec/MIN = 3000 sec
REF (F)

$n = f_o(t) = 124 (3000) = 372{,}000$

USE SCATTER FACTOR of 3 (JUDGEMENT)

$n = 372{,}000 \times 3 = 1.1 \times 10^6$ cycles ←

4. DETERMINE PANEL LIFE (N)

REF. (H) FIGURE 3.6

PANEL WIDTH = 15.0 SKIN THICKNESS = 0.064
DAMPING RATIO = 0.012
SPECTRUM LEVEL = 136 db
ASPECT RATIO = 1.1
CYCLES TO FAILURE (N) = 6.5×10^6 6AL-4V TI ANN

$\frac{n}{N} < 1.0$ $\frac{1.1 \times 10^6}{6.5 \times 10^6} = 0.169 < 1.0$ ←

STATIC BOOST PRESSURE

ULT LOADS

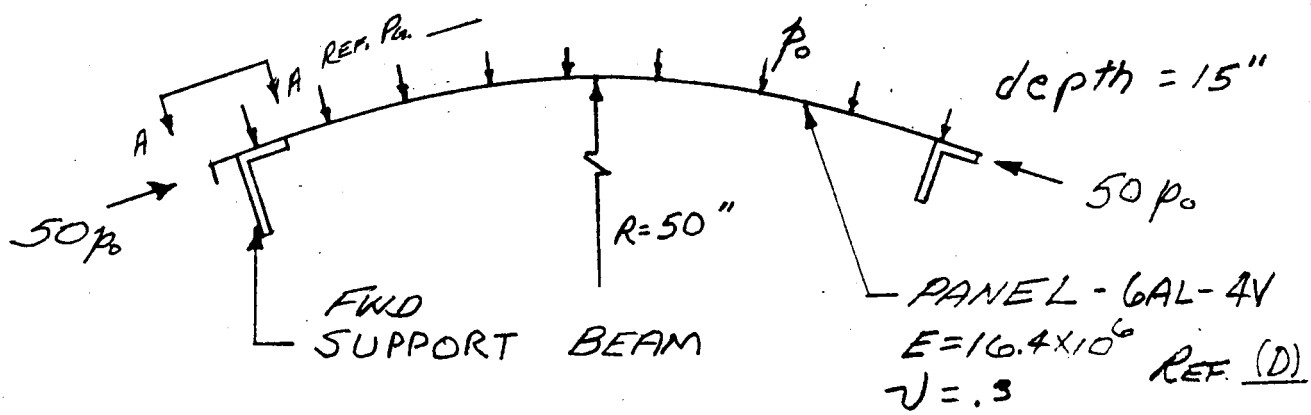

THE PANEL IS EVALUATED AS A CYLINDER SUBJECTED TO RADIAL PRESSURE. IT IS THEN SHOWN THAT THE SUPPORT BEAMS PROVIDE ADEQUATE BOUNDARY SUPPORT FOR THE PANEL i.e. SUPPORT DEFLECTIONS DO NOT CHANGE PANEL GEOMETRY. THE SUPPORT BEAMS ARE THEN EVALUATED FOR THEIR CRITICAL LOAD CONDITION.

1. BUCKLING

MAX COLLAPSE COND CASE I

$p_o = 1/2(1.26 + .70) = 0.98$ psi REF. (A) PG. 7

$$\sigma = \frac{p_o R}{t} = \frac{0.98(50)}{.064} = 765 \text{ psi}$$

ALLOWABLE REF. (I)

$$Z = \frac{L^2}{Rt}(1-\nu^2)^{1/2} = \frac{(15)^2}{50(.064)}(1-.3^2)^{1/2} = 67$$

$$K_p = 8$$

$$F_{c_{cr}} = K_p \frac{\pi^2 E}{12(1-\nu^2)}\left(\frac{t}{L}\right)^2 = \frac{8\pi^2(16.4\times10^6)}{12(1-.3^2)}\left(\frac{.064}{15}\right)^2 = 2150 \text{ psi}$$

$$MS = \frac{2150}{765} - 1 = \boxed{+1.81 \text{ ULT}}$$

SHEAR BUCKLING

ULT LOADS

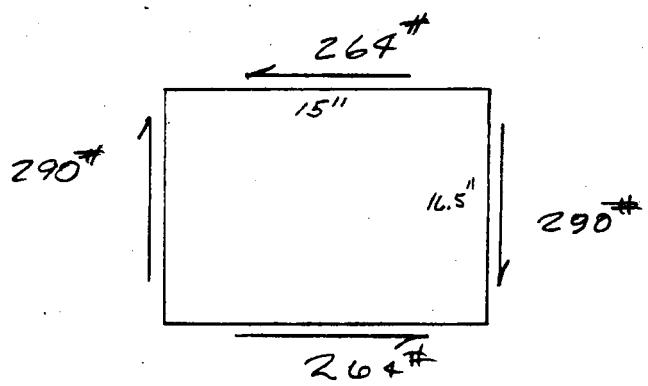

REF. (A) PG. 18

$$\tau = \frac{V}{lt} = \frac{264}{15(.064)} = 275 \text{ psi}$$

ALLOWABLE FOR CURVED SHEET
REF. (C)

$$\frac{b^2}{rt} = \frac{(15)^2}{50(.064)} = 70.4$$

$$\sqrt{K_s} = 4.8$$

$$\frac{b}{t\sqrt{K_s}} = \frac{15}{.064(4.8)} = 48.8$$

$$F_{s_{cr}} = 6200 \text{ psi}$$

$$M.S. = \frac{6200}{275} - 1 = \boxed{\text{HIGH - ULT}}$$

2. SUPPORT BEAM — ULT LOADS

FWD BEAM ~ DEFLECTION
DWG T143T00018
VIEW A-A
REF. PG. 10

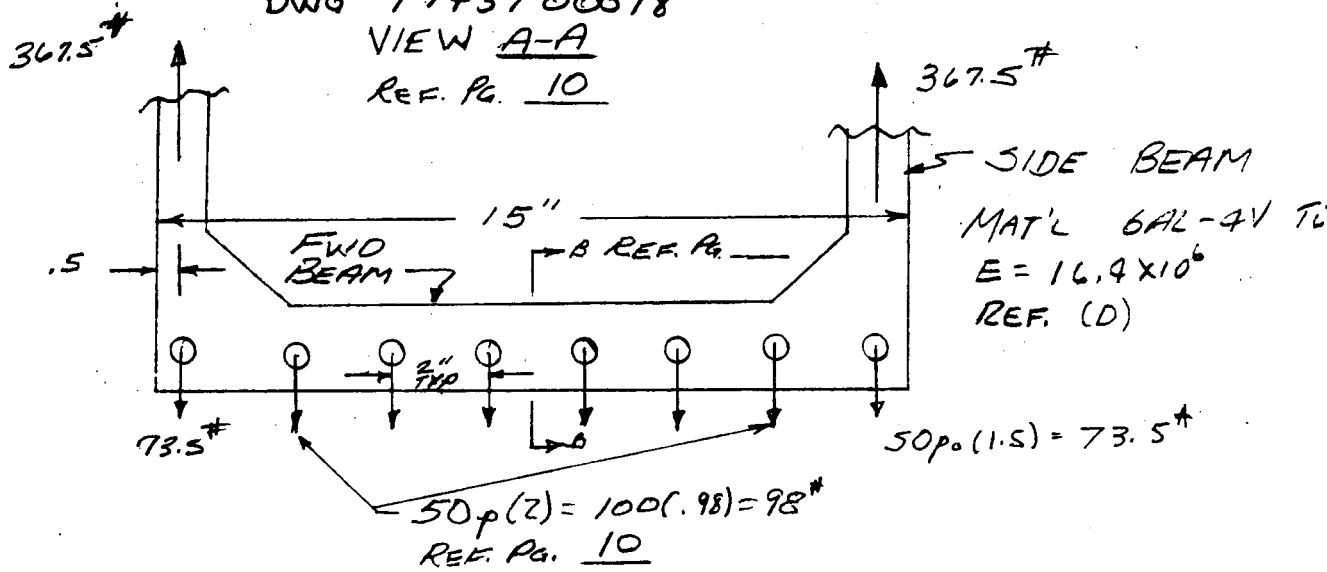

COMPUTE DEFLECTION AS SIMPLE SUPPORTED BEAM. REF. ENERGY ANALYSIS of SUPPORT FRAME ON PG. 13-15 FOR SIMPLE SUPPORT ASSUMPTION. END FIXITY WAS FOUND TO BE VERY SMALL.

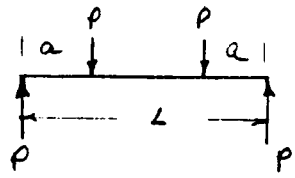

FOR SYM CONCENTRATED LOADS

$$\Delta = \frac{Pa(3L^2 - 4a^2)}{24EI} \quad \text{REF. (C)}$$

SUMMING THE 3 SETS of SYM LOADS

$$\Delta = \frac{P}{24EI} \sum_1^4 a[3L^2 - 4a^2]$$

$I = .124 \text{ in}^4$
REF. PG. 13

$L = 14 \quad 3L^2 = 588$

$a_1 = 2 \quad a_2 = 4 \quad a_3 = 6$

$$\Delta = \frac{98}{24(16.4\times10^6)(.124)}\left[2(588 - 4\cdot2^2) + 4(588 - 4\cdot4^2) + 6(588 - 4\cdot6^2)\right]$$

$\Delta = 0.00985 \text{ in} \sim \text{ULT}$ AN 0.01" TANGENTIAL MOVEMENT of THE SUPPORT CHANGES THE RADIUS FROM 50" to 50.1". ∴ THE BEAM IS STIFF ENOUGH TO SUPPORT THE PANEL AS A SHELL.

RIB TRUSS - SUPPORT BEAMS

ULT LOADS

DWG
T143T00018

FRAME ANALYSIS
MAX BURST LOADS CASE IV REF. (A) PG. 7

$p_o = \frac{1}{2}(4.06 + 3.08) = 3.57$

$F = 2(50 p_o)$ PG. 10

$F = 357$ lbs

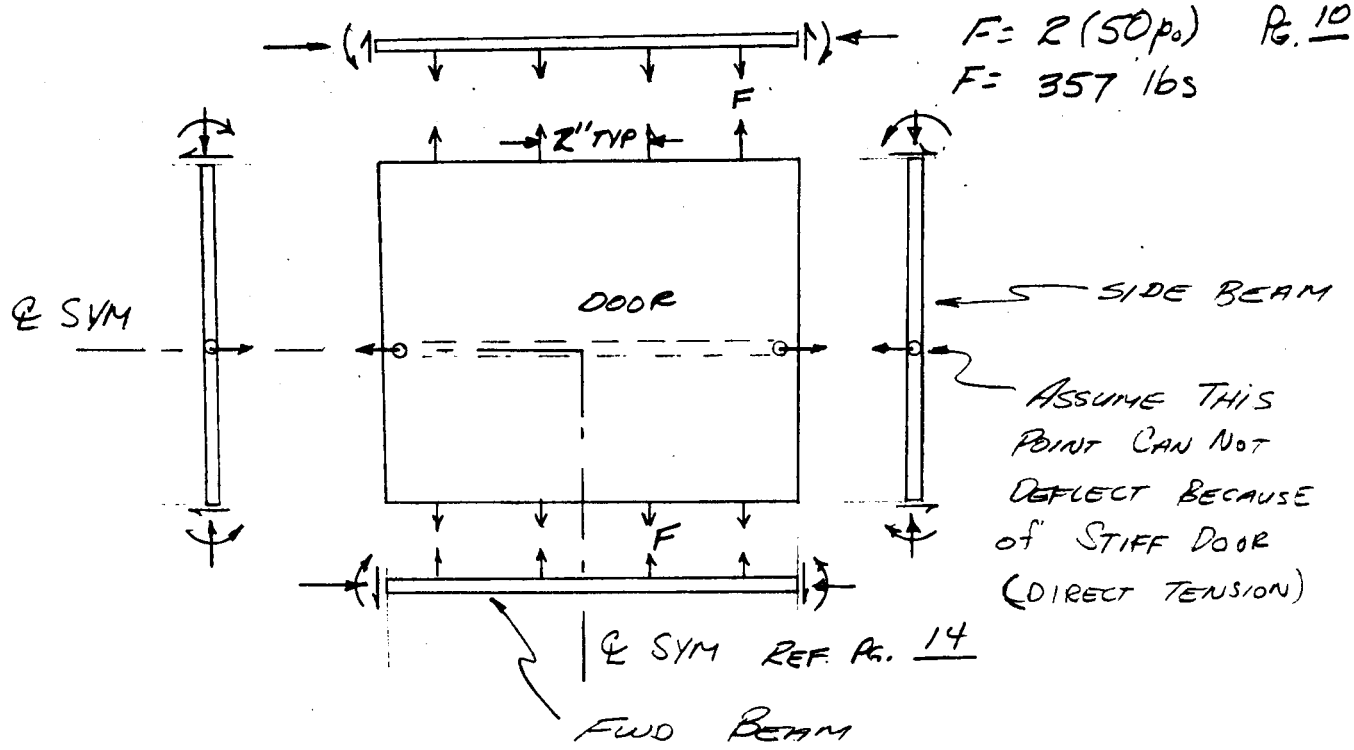

FWD BEAM

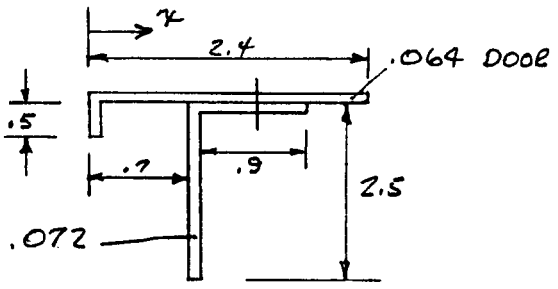

SIDE BEAM

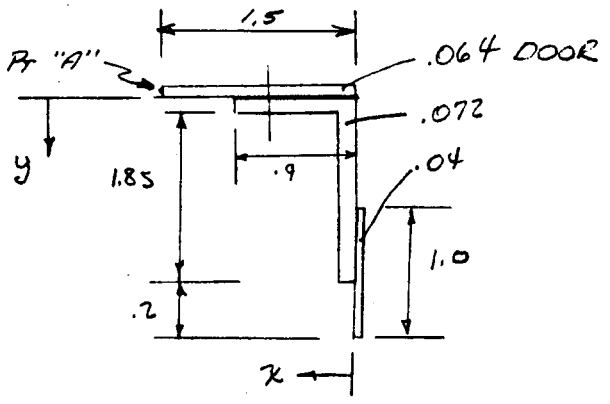

AREA = .4298 in²

$\bar{x} = 1.02$ in

$I_y = 0.124$ in⁴

AREA = .3338 in²

$\bar{x} = 0.316$ in

$I_y = 0.0559$ in⁴

$\bar{y} = 0.563$

$I_x = 0.1448$ in⁴

ULT LOADS

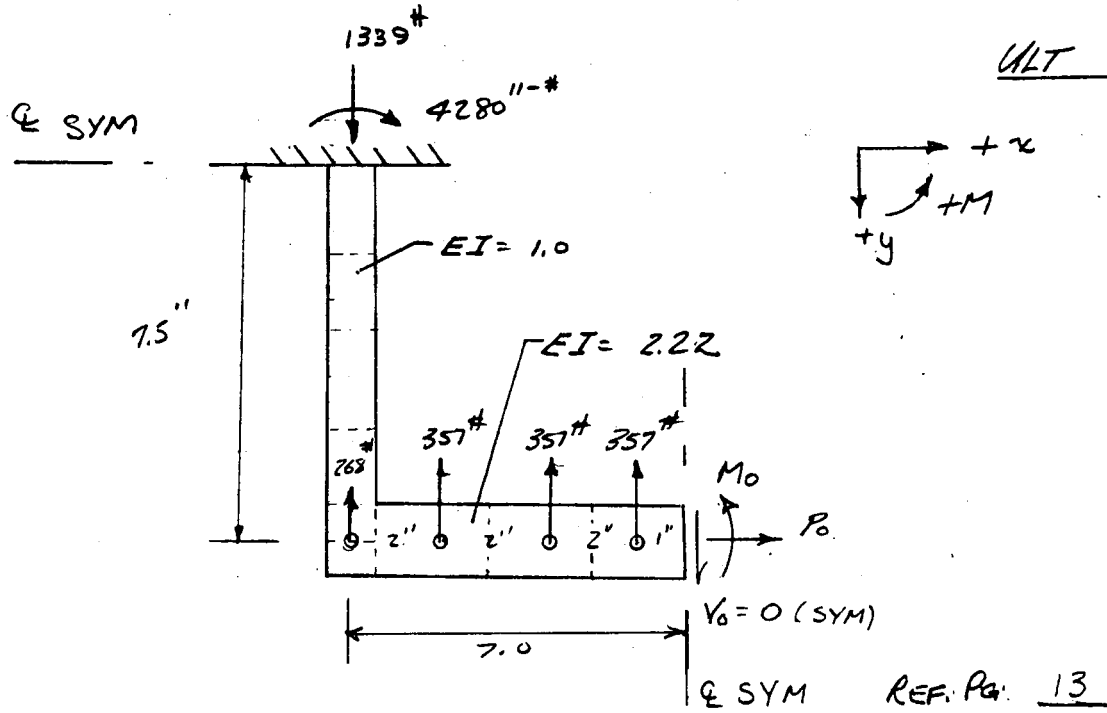

REF. PG. 13

BY VIRTUAL WORK

$$-\Delta X^F = -P_o(\delta_x^{P=1}) + M_o(\delta_x^{M=1})$$

$$\theta^F = -P_o(\delta_\theta^{P=1}) - M_o(\delta_\theta^{M=1})$$

where

$$\Delta X^F = \int \frac{M_s(y)\,ds}{EI} = 248,640$$

$$\theta^F = \int \frac{M_s\,ds}{EI} = 36,637$$

$$\delta_x^{P=1} = \int \frac{y^2 ds}{EI} = 315.9$$

$$\delta_x^{M=1} = \delta_\theta^{P=1} = \int \frac{y\,ds}{EI} = 51.7$$

$$\delta_\theta^{M=1} = \int \frac{ds}{EI} = 10.65$$

VALUES OBTAINED BY NUMERICAL INTEGRATION

ULT LOADS

$$-248{,}640 = -315.7P_o + 51.7M_o$$

$$36{,}637 = -51.7P_o - 10.65M_o$$

$$M_o = -4050 \text{ in-lbs}$$

$$P_o = +106 \text{ lbs}$$

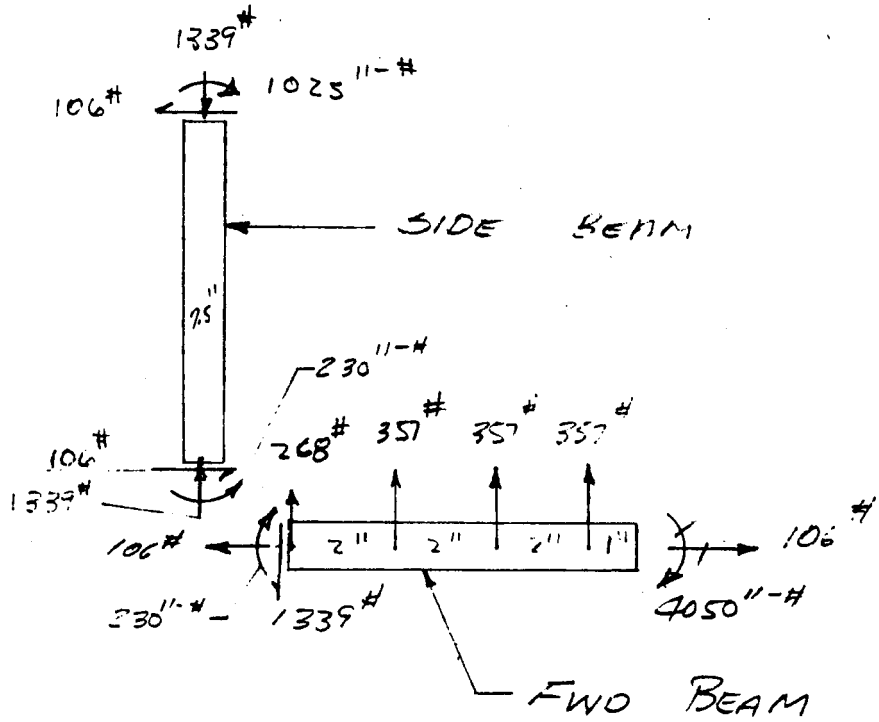

FINAL SHEARS & MOMENTS

ULT LOADS

FWD BEAM

$$f = \frac{P}{A} + \frac{Mc}{I}$$

LOADS ~ PG. 15
A & I ~ PG. 13

$$f = +\frac{106}{.4298} \pm \frac{4050\,(1.02)}{.124}$$

$$f = +33{,}547 \text{ psi} \; ; \; -33{,}053 \text{ psi}$$

ALLOWABLE REF. (C)

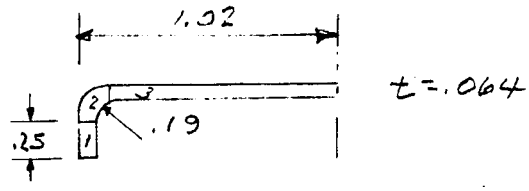

ELEMENT	b/t	AREA	EDGES FREE	F_{cc} (KSI)	P_{cc}
1	4	.016	1	65	1040
2	3	.020	0	70	1400
3	12	.049	0	66	3230
		.085			5670

$$F_{cc_{ave}} = \frac{5670}{.085} = 66{,}700 \text{ psi}$$

$$M.S. = \frac{66{,}700}{33{,}053} - 1 = \boxed{+1.02 - ULT}$$

ATTACHMENTS

FASTENER 3/16" 160 KSI SHEAR ALL. = 2690 #
SHEAR = 357 # REF. PG. 13 REF. (C)

$$M.S. = \frac{2690}{357} - 1 = \boxed{HIGH - ULT}$$

ULT LOADS

SIDE BEAM

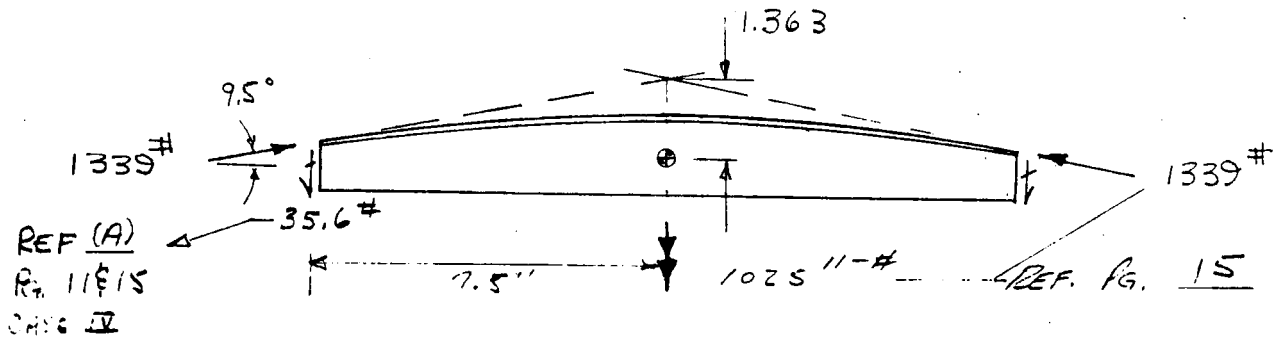

$M_{\mathbb{C}}^{1} = 1339(1.363) - 35.6(7.5) = 1547$ in-lbs

$M_{\mathbb{C}}^{2} = 89$ in-lbs REF. PG. 18

$M_x = 1547 + 89 = 1636$ in-lbs

$M_y = 1025$ in-lb $P = 1339 \cos 7.5 = 1320$ lbs

PT PT "A" REF. PG. 13

$$f_A = \frac{P}{A} \pm \frac{M_x c}{I_x} \pm \frac{M_y c}{I_y}$$ REF. PG. 13

I_x, I_y, A

$$f_A = \frac{-1320}{.3338} - \frac{1636(.563)}{.1448} - \frac{1025(1.5 - .316)}{.0559}$$

$f_A = -3960 - 6370 - 21,700 = -32,030$ psi

ALLOWABLE REF. (C)

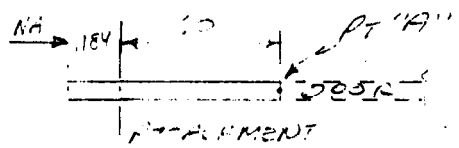

$b/t = \frac{1.0}{.064} = 15.6$ NO EDGE FREE

$F_{cc} = 64,000$ psi

$$M.S. = \frac{64,000}{32,030} - 1 = \boxed{+1.00 \text{ ULT}}$$

ULT. LOADS

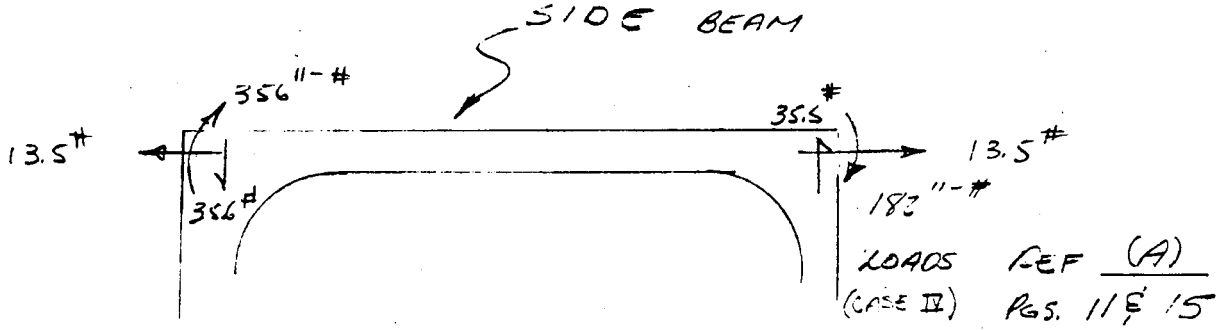

LOADS IN SIDE BEAM ARE APPLIED BY THE LEADING EDGE LUG AND FOR CASE IV ARE SUPERIMPOSED WITH LOADS FROM THE UPPER ACCESS PANEL

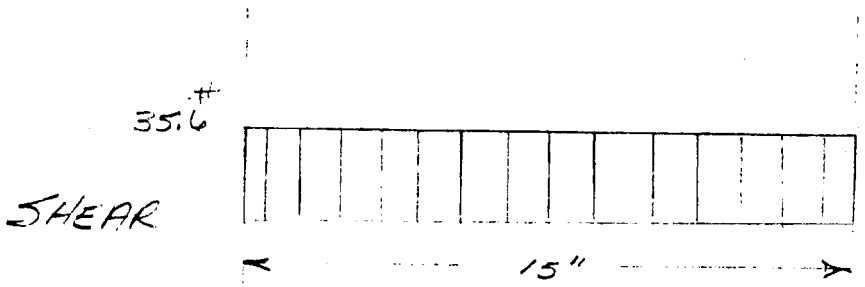

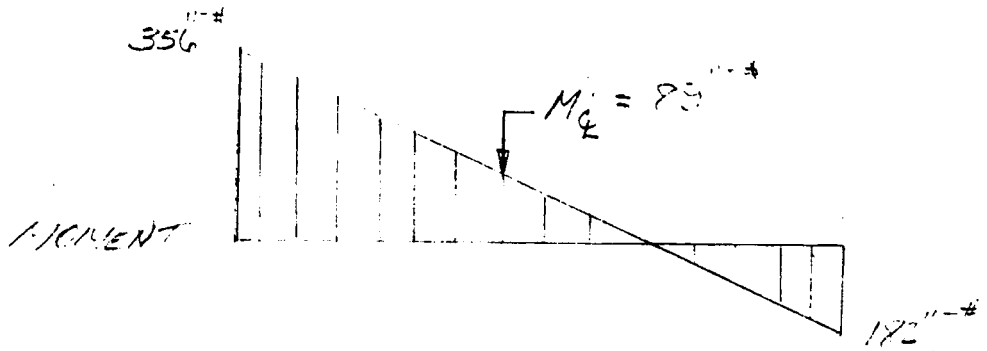

ULT LOADS

SIDE BEAM LOAD CASE III
CHECK BOTTOM of BEAM (PT. 2) FOR COMP. STRESS

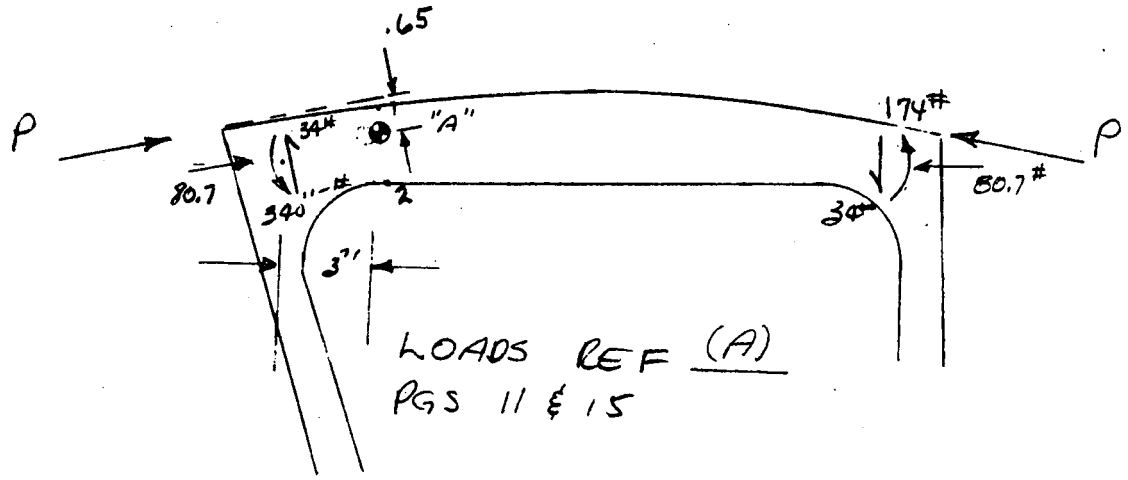

$P = 1339^{\#}$ FOR CASE II REF. PG. 15

$p_o = 3.57$ psi REF PG. 13

$p_o = \frac{1}{2}(2.66 + 1.68) = 2.17$ psi REF. (A) PG. 7

FOR LOAD CASE III

$$P = 1339\left(\frac{2.17}{3.57}\right) = 815^{\#}$$

MOMENT AT PT "A"

$$M_A = 340 - 34(3) - 815(.65) = 292 \text{ in-lbs}$$

$$P_A = 815 + 80.7 = 895.7^{\#}$$

$$f = -\frac{P}{A} \pm \frac{Mc}{I}$$ REF. PG. 13 FOR SIDE BEAM PROP.

$$f_1 = \frac{-895.7}{.3338} - \frac{292(.563)}{.1448} = -3830 \text{ psi}$$

$$f_2 = -\frac{895.7}{.3338} + \frac{292(2.12-.563)}{.1448} = +450 \text{ psi}$$

ULT LOADS

ALLOWABLE COMPRESSION STRESS

F_{cc} = 64,000 psi REF. PG. 17

$$M.S. = \frac{64000}{3830} - 1 =$$

HIGH - ULT

ULT LOADS

RIB TRUSS - DIAGONAL

DWG T143T00018

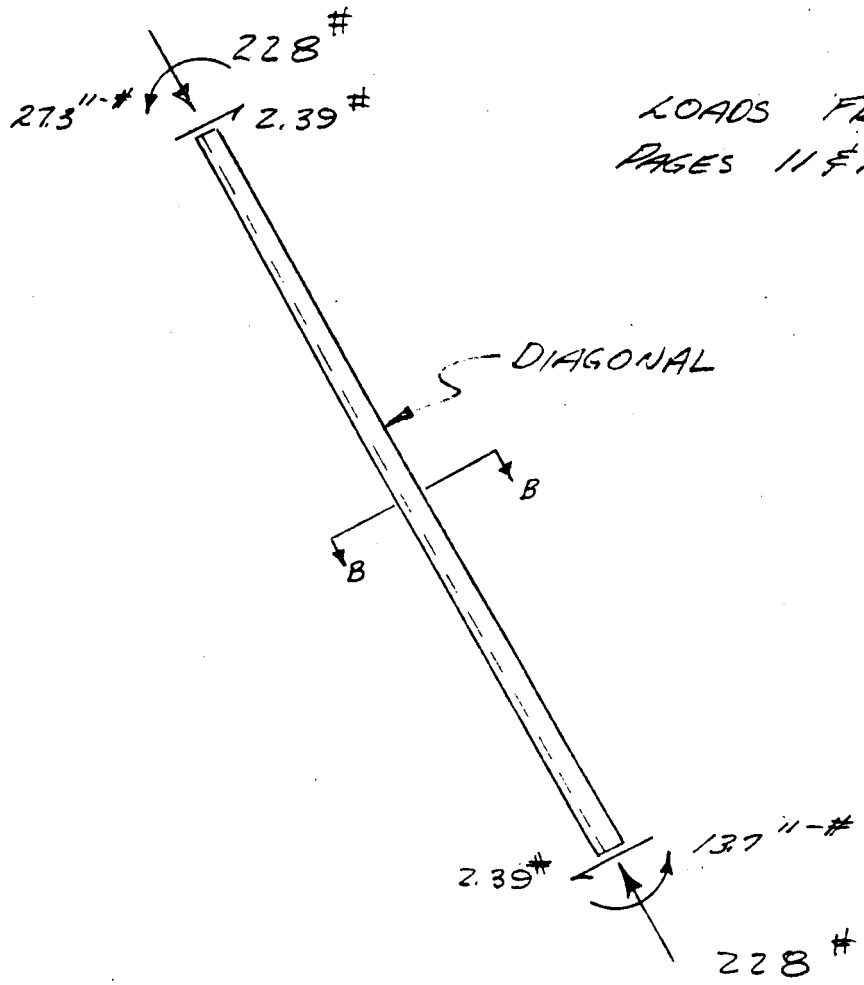

LOADS FROM REF (A)
PAGES 11 & 14, CASE I

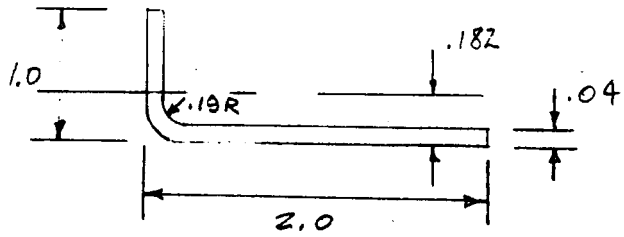

$A = 0.1184 \text{ in}^2$

$\bar{y} = 0.182 \text{ in}$

$I = 0.00943 \text{ in}^4$

ULT LOADS

$$f = \frac{P}{A} + \frac{Mc}{I}$$

$$f = \frac{-228}{.1184} - \frac{27.3(.182)}{.00943} = -1930 - 527$$

$$f = -2457 \text{ psi}$$

ALLOWABLE

MAT'L 6AL-4V Ti ANN

$E = 16.4 \times 10^6$ REF. (D)

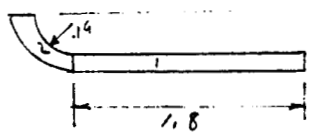

① $F_{cc} = \frac{\pi^2 K_c E}{12(1-\nu^2)} \left(\frac{t}{b}\right)^2$ REF. (B) $a/b = \infty$ $K_c = .4$

$F_{cc} = \frac{\pi^2(.4)(16.4\times10^6)}{12(1-.3^2)} \left(\frac{.04}{1.8}\right)^2 = 2920$ psi

$A = .04(1.8) = \times .072 \text{ in}^2$

$P_{cc} = 210$ #

② $r/t = .19/.04 = 47.5$ $F_{cc} = 24000$ REF. (C)

$A = .012$

$P_{cc} = 288$ #

$$F_{cc_{ave}} = \frac{210 + 288}{.072 + .012} = 5940 \text{ psi}$$

$$MS = \frac{5940}{2457} - 1 = \boxed{+1.31 \text{ ULT}}$$

THE DIAGONAL IS NOT CRITICAL AS A BEAM COLUMN SINCE A BEAM COLUMN ANALYSIS SHOWS THAT THE END MOMENT (27.3 "-#) IS NOT EXCEEDED BY THE INTERMEDIATE MOMENTS.

LIMIT LOADS

THERMAL EXPANSION
RIB TRUSS
DWG T143T00018

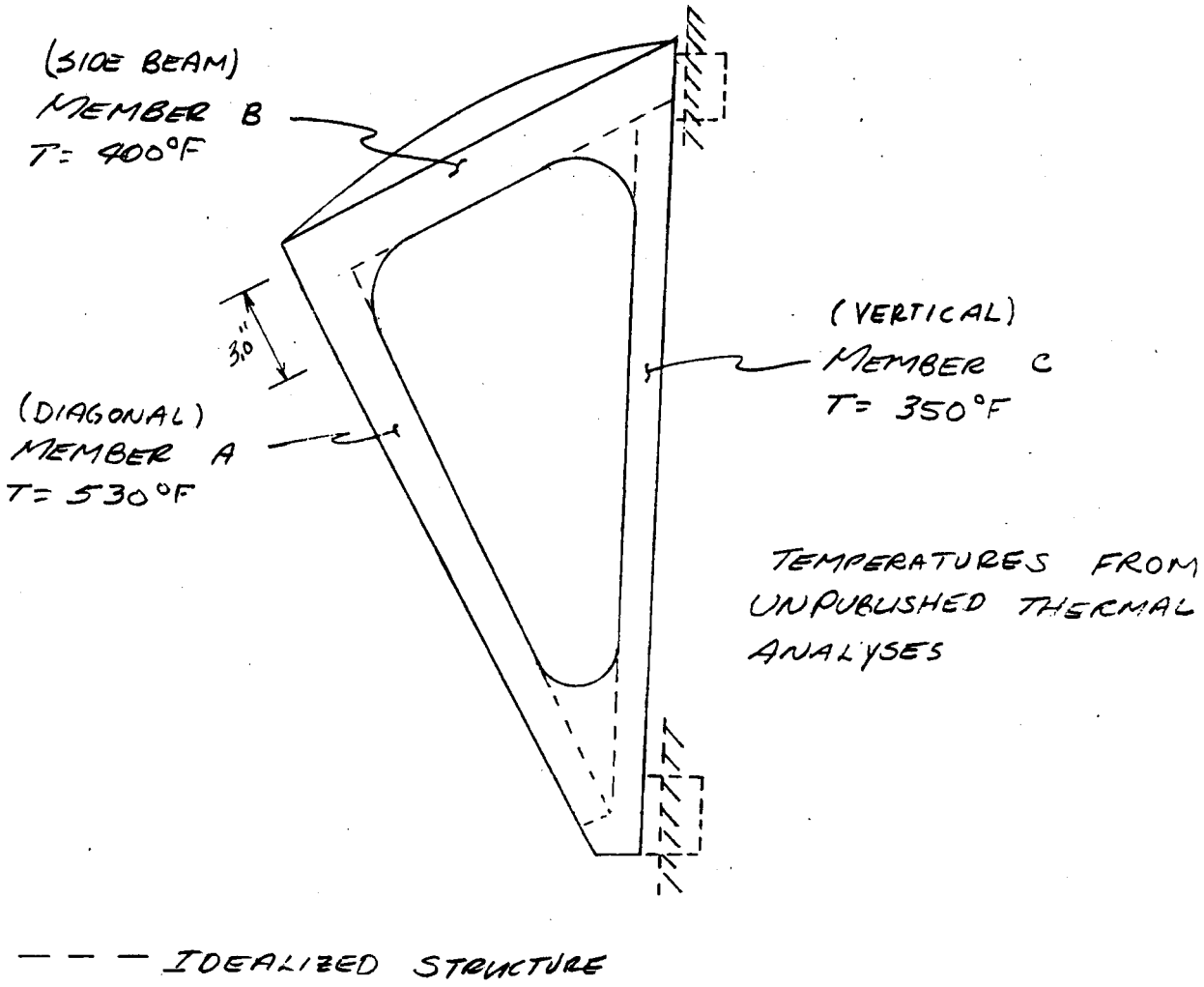

MEMBERS A & B ARE ANALYZED AS A FRAME ON PGS. 24-27. MEMBER C IS HELD RIGID BETWEEN THE TEST SUPPORT FITTINGS AND IS ANALYZED ON PGS. 28-29.

LIMIT LOADS

MEMBERS A & B

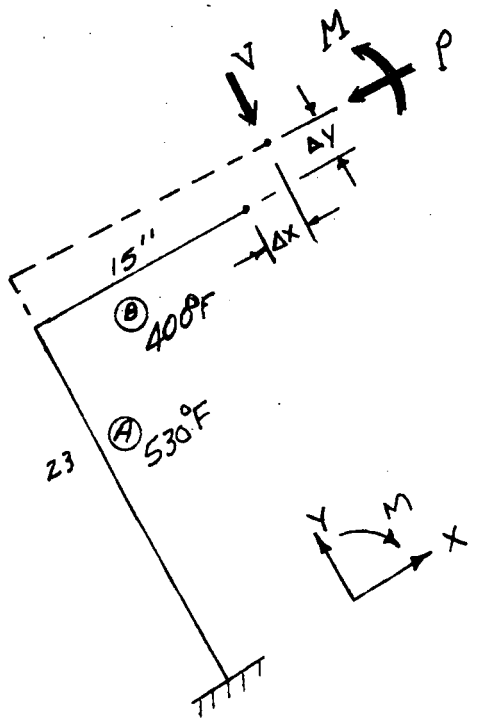

MAT'L: 6AL-4V

$E = 16.4 \times 10^6$

$E_{530} = 13.8 \times 10^6$

$E_{400} = 14.6 \times 10^6$

$\alpha = 5.8 \times 10^{-6}$ in/in/°F

REF. (D)

$I_{(A)} = .00943 \text{ in}^4$

REF. PG. 21

$I_{(B)} = 0.1448 \text{ in}^4$

REF. PG. 13

$\theta = 0$

$\Delta y = \alpha L \Delta T = 5.8 \times 10^{-6}(23)(530-70) = .0614$

$\Delta X = \alpha L \Delta T = 5.8 \times 10^{-6}(15)(400-70) = .0287$

$EI_{(A)} = 13.8 \times 10^6 (.00943) = .13 \times 10^6$

$EI_{(B)} = 14.6 \times 10^6 (.1448) = 2.11 \times 10^6$

EQUATIONS

$$\Delta X = P(\delta_x^{P=1}) - V(\delta_x^{V=1}) + M(\delta_x^{M=1})$$

$$\Delta y = -P(\delta_y^{P=1}) + V(\delta_y^{V=1}) - M(\delta_y^{M=1})$$

$$\theta = P(\delta_\theta^{P=1}) - V(\delta_\theta^{V=1}) + M(\delta_\theta^{M=1})$$

LIMIT LOADS

WHERE

$$\delta_x^{P=1} = \int_0^x \frac{(0)(0)\,dx}{EI_{(B)}} + \int_0^{23} \frac{(y)(y)\,dy}{EI_{(A)}} = \frac{4050}{EI_{(A)}}$$

$$\delta_x^{V=1} = \delta_y^{P=1} = \int_0^{15} \frac{(x)(0)\,dx}{EI_{(B)}} + \int_0^{23} \frac{15y\,dy}{EI_{(A)}} = \frac{3970}{EI_{(A)}}$$

$$\delta_y^{V=1} = \int_0^{15} \frac{(x)(x)\,dx}{EI_{(B)}} + \int_0^{23} \frac{(15)(15)\,dy}{EI_{(A)}} = \frac{75}{EI_{(B)}} + \frac{5175}{EI_{(A)}}$$

$$\delta_x^{M=1} = \delta_\theta^{P=1} = \int_0^{15} \frac{(1)(0)\,dx}{EI_{(B)}} + \int_0^{23} \frac{(1)(y)\,dy}{EI_{(A)}} = \frac{299}{EI_{(A)}}$$

$$\delta_y^{M=1} = \delta_\theta^{V=1} = \int_0^{15} \frac{(1)(x)\,dx}{EI_{(B)}} + \int_0^{23} \frac{(1)(15)\,dy}{EI_{(A)}} = \frac{112.5}{EI_{(B)}} + \frac{345}{EI_{(A)}}$$

$$\delta_\theta^{M=1} = \int_0^{15} \frac{(1)(1)\,dx}{EI_{(B)}} + \int_0^{23} \frac{(1)(1)\,dy}{EI_{(A)}} = \frac{15}{EI_{(B)}} + \frac{23}{EI_{(A)}}$$

(1) $$.0287 = (P)\frac{4050}{.13\times10^6} - (V)\frac{3970}{.13\times10^6} + (M)\frac{299}{.13\times10^6}$$

(2) $$.0614 = -(P)\frac{3970}{.13\times10^6} + (V)\left[\frac{75}{2.11\times10^6} + \frac{5175}{.13\times10^6}\right] - (M)\left[\frac{112.5}{2.11\times10^6} + \frac{345}{.13\times10^6}\right]$$

(3) $$0 = (P)\frac{299}{.13\times10^6} - (V)\left[\frac{112.5}{2.11\times10^6} + \frac{345}{.13\times10^6}\right] - (M)\left[\frac{15}{2.11\times10^6} + \frac{23}{.13\times10^6}\right]$$

LIMIT LOADS

(1) $28{,}700 = 31{,}150\,P - 30{,}550\,V + 2300\,M$

(2) $61{,}400 = -30{,}550\,P + 39{,}836\,V - 2708\,M$

(3) $0 = 2300\,P - 2708\,V - 184\,M$

$M = -5.25$ in-lbs

$V = 8.83$ lbs

$P = 10$ lbs

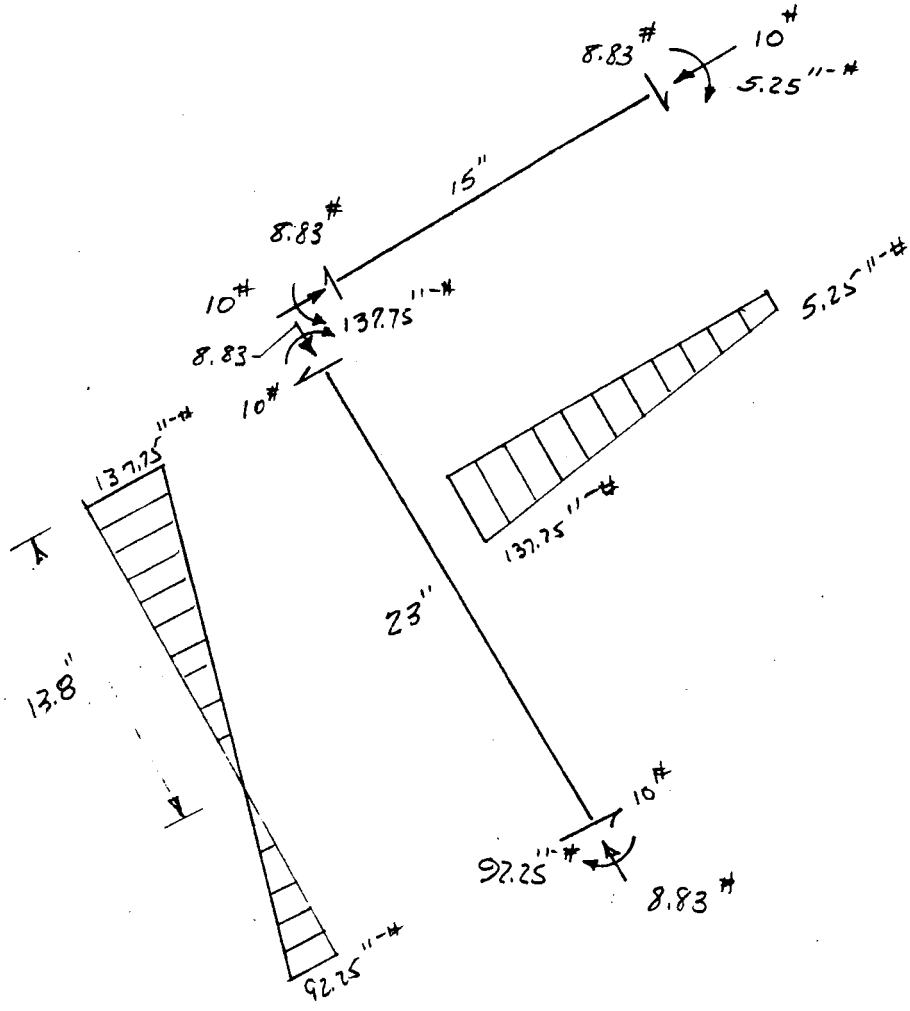

FINAL DISTRIBUTION

LIMIT LOADS

COMPUTING A MARGIN of SAFETY AT THE CORNER TANGENCY ($y = 3.0''$)
REF. PG. 23.

$M = 137.75 - 10^{\#}(3) = 107.75$ in-lbs

$A_{Ⓐ} = 0.1184$ in^2

$I_{Ⓐ} = 0.00943$ in^4 REF. PG. 24

$c = 1.0 - .182 = .818$

$$f_{Ⓐ} = \frac{P}{A} + \frac{Mc}{I} = \frac{-8.83}{.1184} - \frac{107.75(.818)}{.00943}$$

$f_{Ⓐ} = -74.5 - 9350 = -9425$ psi

ULT = 1.5 × LIMIT (THERMOELASTIC) REF. (F)

$f_{Ⓐ} = -9425(1.5) = 14{,}150$ psi ULT

$b/t = .818/.04 = 20.4$ $F_{cc} = 20{,}000$ psi
GAL-4V @ 70°
ONE EDGE FREE
REF. (C)

REDUCE CRIPPLING ALLOW PER $\frac{E_{530°F}}{E_{70°F}}$

$$F_{cc_{530°F}} = 20{,}000\left(\frac{13.8\times10^6}{16.4\times10^6}\right) = 16{,}800 \text{ psi}$$

$$M.S. = \frac{16{,}800}{14{,}150} - 1 = \boxed{+0.19 \text{ ULT}}$$

LIMIT LOADS

MEMBER C (PG. 23)

CHECK MEMBER "C" FOR THERMAL STRESSES BETWEEN RIGID END POINTS AND COMPRISED OF DISSIMILAR MATERIALS.

2024-T3 MATL,
$\alpha = 12.9 \times 10^{-6}$ "/"/°F REF. (D)
$A = 0.30$ IN^2
$E_{350} = 9.85 \times 10^6$

6AL-4V TITANIUM,
$\alpha = 5.8 \times 10^{-6}$ "/"/°F REF. (D)
$A = 0.096$ IN^2
$E_{350} = 14.75 \times 10^6$
$\Delta T = 350 - 70 = 280°F$

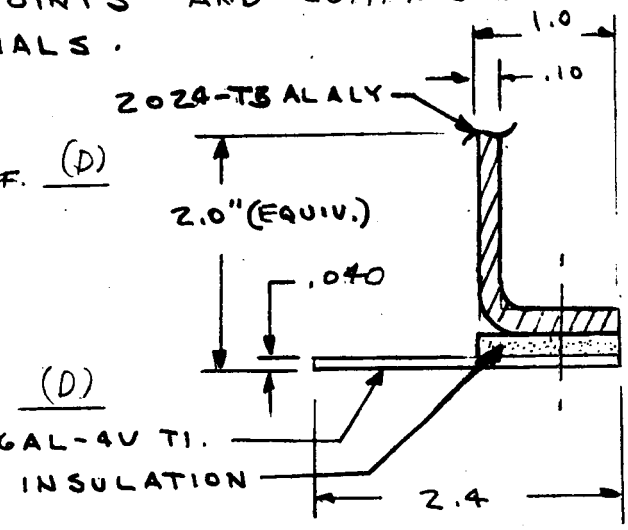

SECTION THRU MEMBER "C"

$$\left[\alpha L \Delta T - \frac{PL}{AE}\right]_{AL} = \left[\alpha L \Delta T + \frac{PL}{AE}\right]_{TI}$$

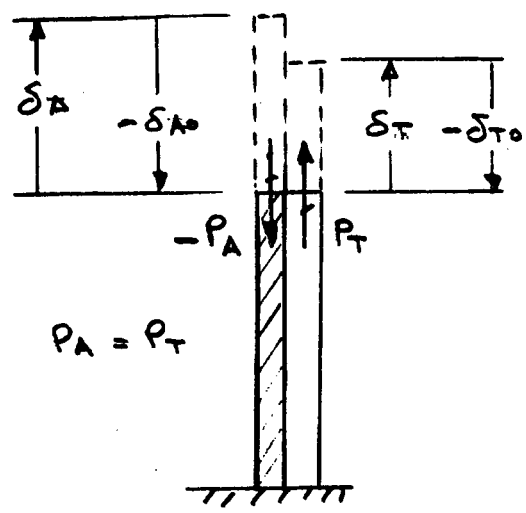

$$P = \frac{\Delta T\left[-\alpha_T + \alpha_{AL}\right]}{\left[\left(\frac{1}{AE}\right)_T + \left(\frac{1}{AE}\right)_{AL}\right]}$$

$$= \frac{280\left[-5.8 + 12.9\right]10^{-6}}{\left[\frac{1}{(.096)(14.75)} + \frac{1}{(.30)(9.85)}\right]\frac{1}{10^6}}$$

$= 1900$ # LIMIT
$= 2850$ # ULT. (COMP. IN AL., TEN. IN TITAN.)

$$f_{cu} = \frac{2850}{.30} = -9500 \text{ P.S.I. ULT (COMP. IN ALUM)}$$

$$f_{cu} = \frac{2850}{.096} = 29{,}700 \text{ P.S.I. ULT. (TEN IN TITAN)}$$

ULT LOADS

CRIPPLING OF ALUM. FLANGE

$\frac{b}{t} = \frac{.65}{.10} = 6.5$

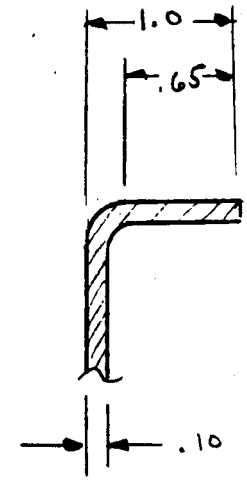

$F_{cc} = 30,000$ P.S.I.

(REF. C, PAGE 61)

REDUCE BY $\frac{E_{350°F}}{E_{70°F}}$

$F_{cc} = 30,000\left(\frac{9.85}{10.7}\right) = 27,600$ psi

$M.S. = \frac{27,600}{9500} - 1 = \boxed{+1.90 \text{ ULT}}$

ALL LOADS ULT.

UPPER LUG

DWG T143T00025

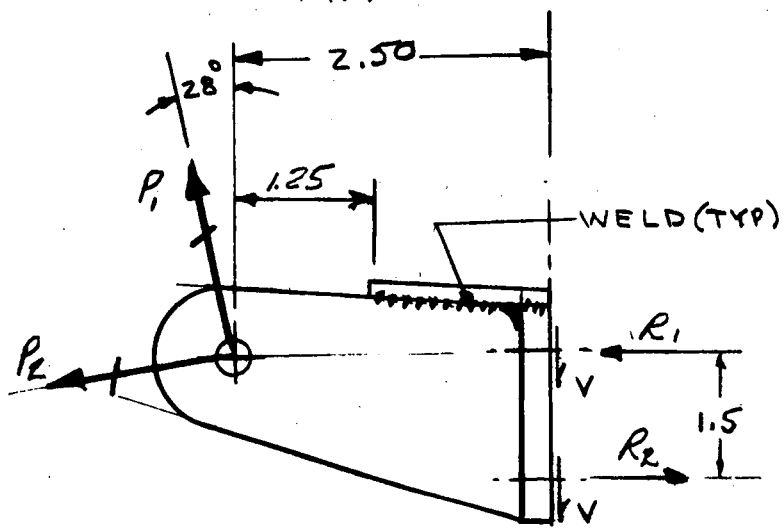

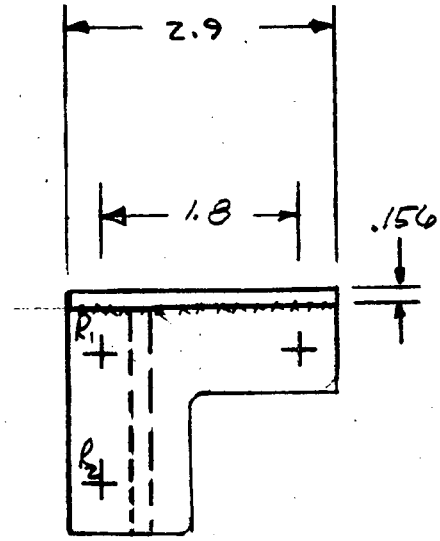

* ① IN-PLANE LOADS

LOADS IN lbs

REF	P_1	P_2	R_1	R_2	V
PG. 8	139↑	16	110	188	57.7↓
PG. 8	119↓	108	259	216	77.8↑

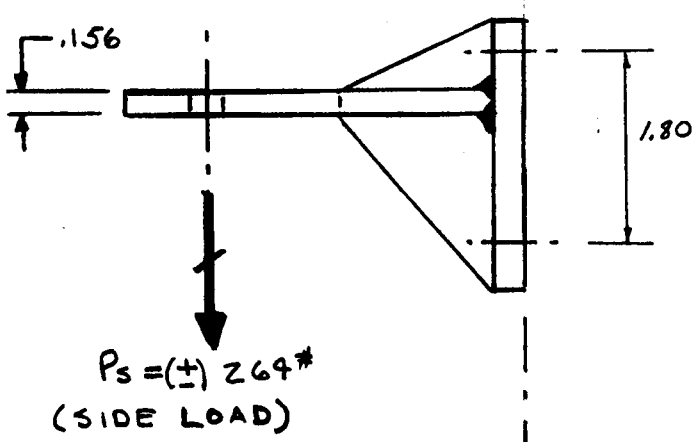

REF PG. 31 FOR EQUILIBRIUM

MATL: INCONEL 718

.156" PLATE (LUG)
.156" PLATE (GUSSET)
ALL PARTS ARE WELDED STRUCTURE.
AMS 5596
F_{tu} = 180K.S.I. (LT)
F_{ty} = 150K.S.I. (LT)
E = 29.6×10^6 P.S.I.
(REF. D, PAGE 6-52)

* ② SIDE LOADING
(REF. (A), PAGE 18)

* NOTE: ABOVE TWO LOADINGS DO NOT COMBINE.

ALL LOADS ULT.

UPPER LUG ~ (CONT'D)

SIDE LOADING

THE SIDE LOAD IS VIBRATORY AND ACTS FOR 50 MIN, REF. (F). THE NATURAL FREQUENCY OF THE LEADING EDGE IS 22 hz, REF. (I).

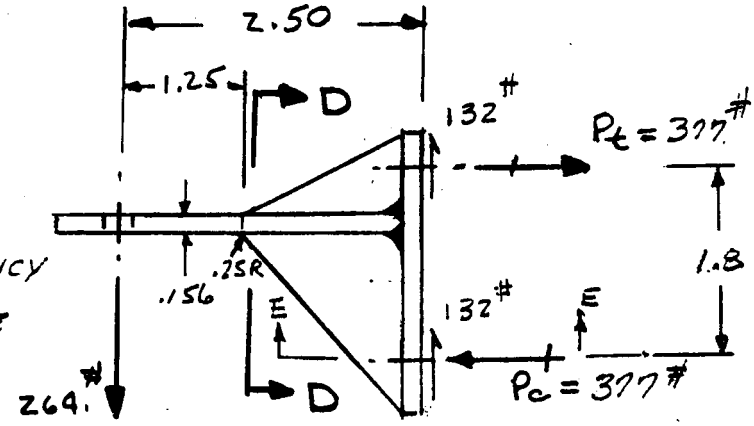

THE CYCLIC ENVIRONMENT IS $N = 22(50 \times 60) = 66{,}000$ cycles

USING A SCATTER FACTOR of 3

$N = 3(66{,}000) = 1.98 \times 10^5$ cycles ←

STRESS AT D-D

$S_{eff} = 1.0$ $\qquad M = 1.25(264) = 330$ in-lbs

$$f = \frac{6M}{Dt^2} = \frac{6(330)}{1.0(.156)^2} = 81{,}500 \text{ psi}$$

$$M.S. = \frac{120{,}000}{81{,}500} - 1 = \boxed{+1.21 \text{ ULT}}$$

$$\text{LIMIT STRESS} = \frac{81{,}500}{1.4} = 58{,}200 \text{ psi}$$

FATIGUE LIFE @ 58,200 psi $\quad K_t = 1.0$

$N = 4.5 \times 10^5$ cycles $\quad$ REF. (D)

$$\frac{N}{N} < 1.0 \qquad \frac{1.98 \times 10^5}{4.5 \times 10^5} = 0.44 < 1.0 \leftarrow$$

ULT LOADS

STRESS AT E-E

THE MAX REACTION FROM THE IN-PLANE AND SIDE LOADS IS 377 lbs, REF. PG. 30-31.

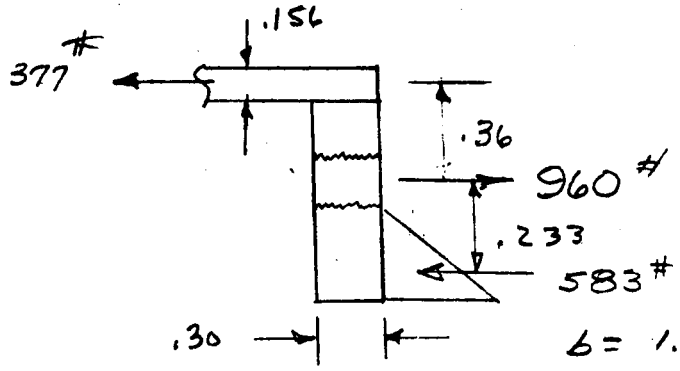

NAS 1303 BOLT

$b = 1.0''$

$M = 377(.36) = 136$ in-lbs

$$f = \frac{6M}{bt^2} = \frac{6(136)}{(1.0)(.3)^2} = 9060 \text{ psi}$$

$$M.S. = \frac{180,000}{9060} - 1 = \boxed{\text{HIGH ULT}}$$

FASTENER

TENSION ALLOWABLE = 2460 REF. (C)

$$M.S. = \frac{2460}{960} - 1 = \boxed{+1.56 \text{ - ULT}}$$

ULT LOADS

UPPER LUG BACK UP FITTING

DWG T143T00025

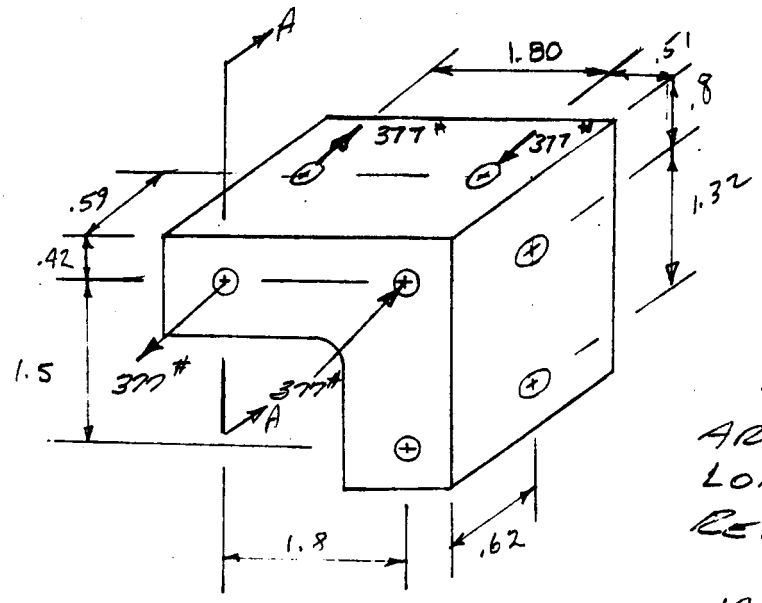

MAXIMUM REACTIONS ARE FROM SIDE LOAD CONDITION REF. PG. 31

MAT'L: 321 S.S.
F_{TU} = 75 KSI
REF. (C)

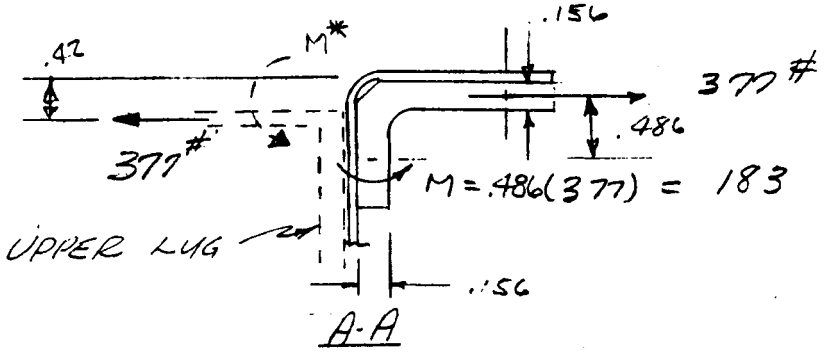

$$f = \frac{6M}{bt^2} = \frac{6(183)}{(1.0)(.156)^2} = 45{,}100 \text{ psi}$$

$$M.S. = \frac{75{,}000}{45{,}100} - 1 = \boxed{+0.66 \text{ ULT}}$$

M* IS BALANCED BY THE ADJACENT BOLT LOADS WHICH ARE EQUAL AND OPPOSITE.

ULT LOADS

LOWER LUG

DWG T143T00026

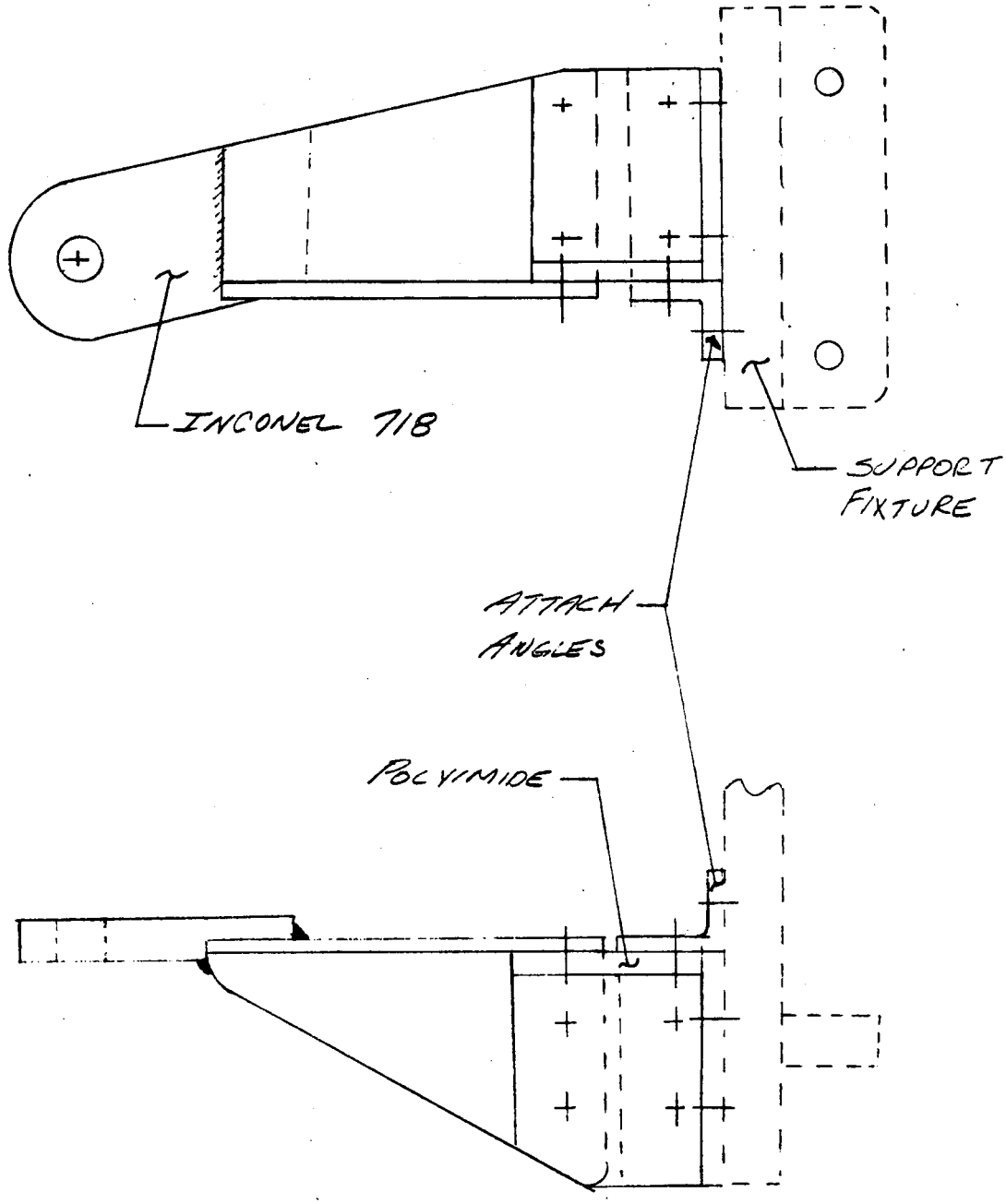

MINIMUM MARGINS of SAFETY FOR THE LOWER LUG OCCUR WITH THE SIDE LOAD.

ULT LOADS

INCONEL PART

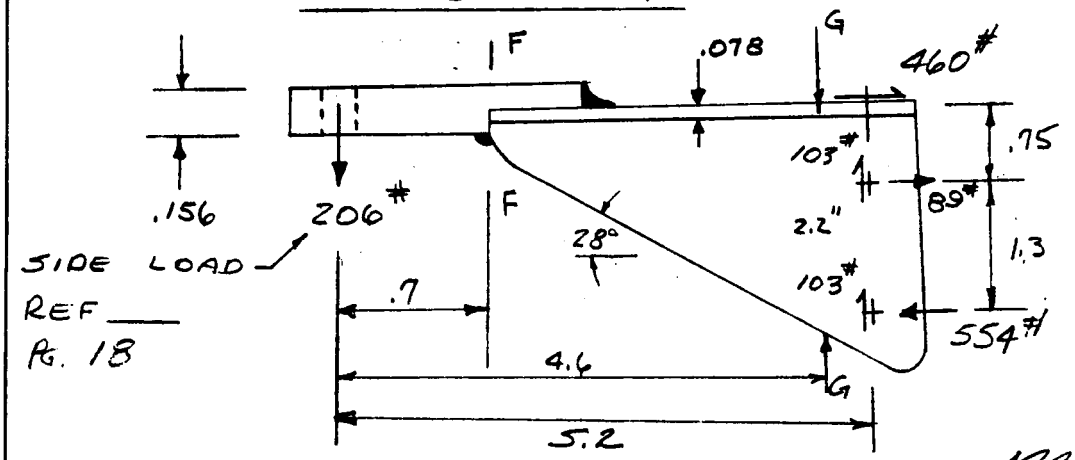

MAT'L :- INCONEL 718
F_{TU} = 180,000 psi
F_{TY} = 150,000 psi
REF. (D)

BENDING @ F-F

$b = .7 \quad M = 206(.7) = 144$

$$f = \frac{6M}{bt^2} = \frac{6(144)}{.7(.156)^2} = 50{,}700 \text{ psi}$$

$$M.S. = \frac{180{,}000}{50{,}700} - 1 = \boxed{+2.55 \text{ ULT}}$$

$f = 50{,}700/1.4 = 36{,}900$ psi LIMIT

$n = 1.98 \times 10^5$ cycles REF. PG. 31

FATIGUE LIFE @ 36,000 psi $K_t = 1.0$

$N = 1 \times 10^7$ cycles REF. (D)

$$\frac{n}{N} < 1.0 \qquad \frac{1.98 \times 10^5}{1 \times 10^7} = 0.0198 << 1.0 \longleftarrow$$

BENDING @ G-G

$$f = \frac{6M}{bt^2 \cos 28°} = \frac{6(206)(4.6)}{.078(2.2)^2 \cos 28°} = 17{,}100 \text{ psi}$$

ULT LOADS

$b/t = 1.0/.078 = 12.8$

$F_{cc} = 25{,}800$ psi REF. (C) (FOR 18-8 1/4 HARD)

$M.S. = \frac{25{,}800}{17{,}100} - 1 = \boxed{+0.51 \text{ ULT}}$

FASTENER

LOAD $R = 103 + 554 = 563^{\#}$

NAS 1003 SHEAR $= 2125^{\#}$ REF. (C)

$M.S. = \frac{2125}{563} - 1 = \boxed{+2.77 \text{ ULT}}$

ULT LOADS

POLYIMIDE PART

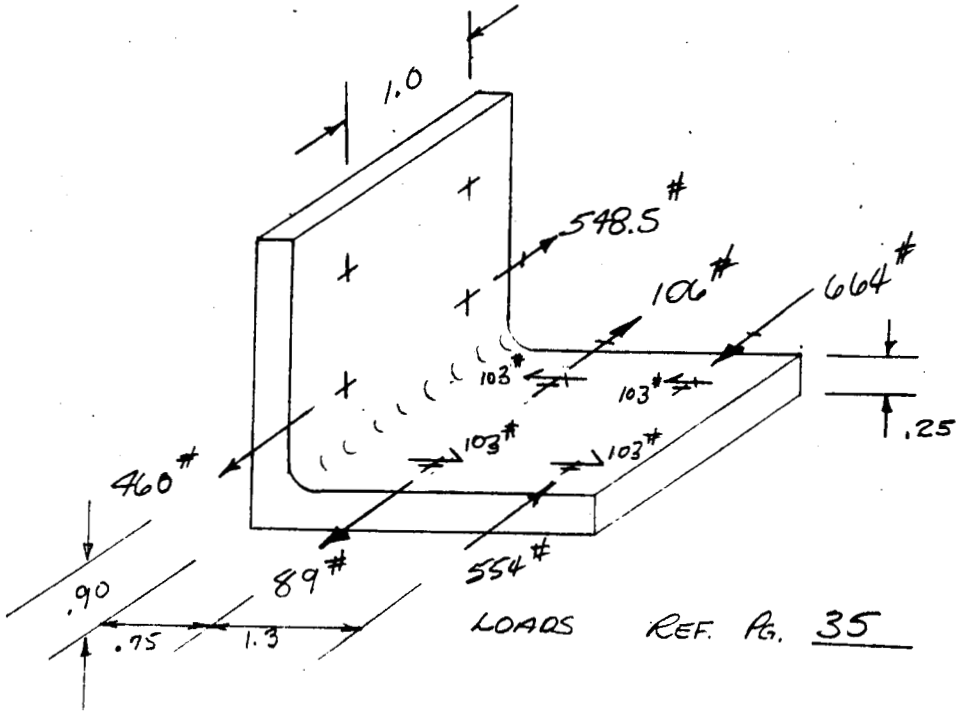

LOADS REF. PG. 35

POLYIMIDE

$F_B = 64{,}000$ psi
$F_C = 45{,}000$ psi
$F_T = 53{,}000$ psi

REF. (G)

$$f_c = \frac{P}{A} = \frac{664}{(1)(.25)} = 2660 \text{ psi}$$

$$M.S. = \frac{45000}{2660} - 1 = \boxed{\text{HIGH - ULT}}$$

THE THICKNESS OF THIS PART IS ESTABLISHED BY THERMAL REQUIREMENTS.

ULT LOADS

ATTACH ANGLES

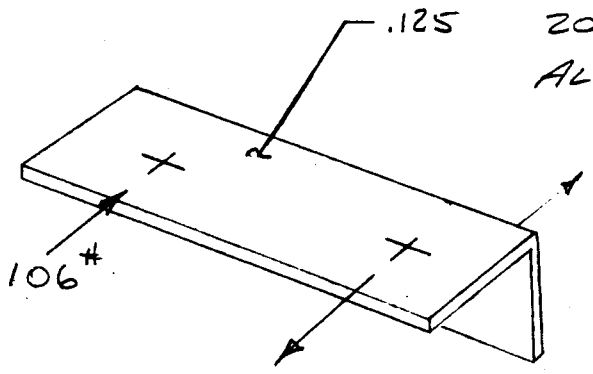

REF. PG. 37 SIDE LOAD IS REVERSIBLE

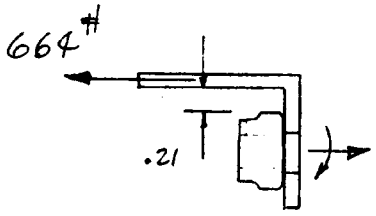

bolt space = 1.0"

ALLOWABLE LOAD REF. (C)

P_{ALL} = 1000 lbs YIELD

ULT = 1.5 X LIMIT
YIELD = 1.15 X LIMIT REF. (F)

$P_{ACT} = 664\left(\frac{1.15}{1.4}\right) = 545$ lbs YIELD

$M.S. = \frac{1000}{545} - 1 =$ **+0.83 YIELD**

ULT LOADS

LUG BOLT

MAXIMUM LOAD OCCURS DURING BOOST - CASE II

$R = 165 + 95 = 191^{\#}$

REF. (A) PG. 8

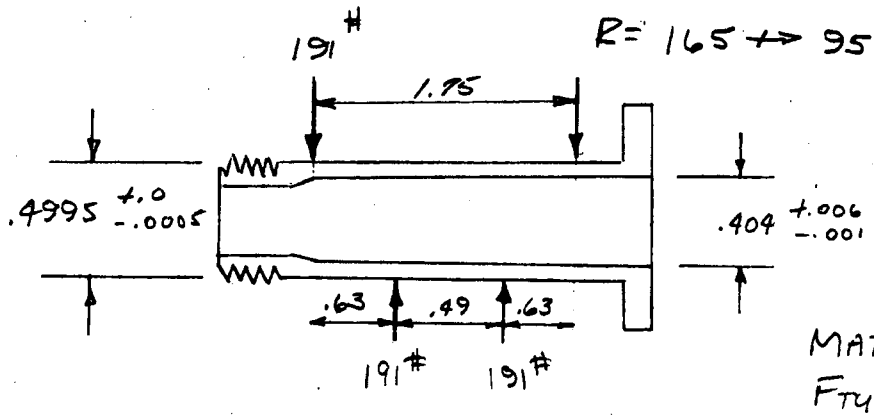

MAT'L: INCONEL 718
$F_{TU} = 180$ ksi
$F_{TY} = 150$ ksi
$F_{SU} = 108$ ksi

shear

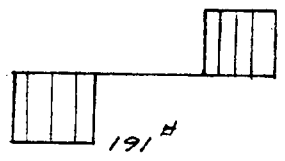

$I_{MIN} = \pi R^3 t$
$= \pi(.227)^3(.0445)$
$= .00163 \text{ in}^4$

moment

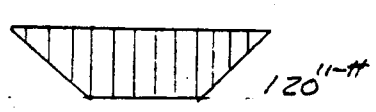

$A_{MIN} = \pi D t$
$= \pi(.4545)(.0445)$
$= .0635 \text{ in}^2$

$$f = \frac{Mc}{I} = \frac{120(.249)}{.00163} = 18{,}350 \text{ psi}$$

$$M.S. = \frac{180{,}000}{18{,}350} - 1 = \boxed{\text{HIGH - ULT}}$$

$$\tau = \frac{VQ}{Ib} = \frac{V\,\pi R t(.6366R)}{\pi R^3 t(2t)} = \frac{2V}{A}$$

$$\tau = \frac{2(191)}{2\pi(.227)(.0445)} = 6030 \text{ psi}$$

$$M.S. = \frac{108{,}000}{6030} - 1 = \boxed{\text{HIGH - ULT}}$$

ULT LOADS

MAXIMUM BOLT TEMPERATURE OCCURS DURING ENTRY AND IS 1330 °F

MAXIMUM LUG LOAD DURING ENTRY OCCURS AT 400sec AND IS 3 → 19.5 = 19.7 #
REF. (E) PG. 60.

$$f_{1330°F} = 18{,}350\left(\frac{19.7}{191}\right) = 1890 \text{ psi}$$

$$F_{TU_{1330°F}} = 121{,}000 \text{ psi} \qquad \text{REF. (D)}$$

$$M.S. = \frac{121{,}000}{1890} - 1 = \boxed{\text{HIGH - ULT}}$$

ULT LOADS

SUPPORT LUG AND BEAM

DWG T143T00027

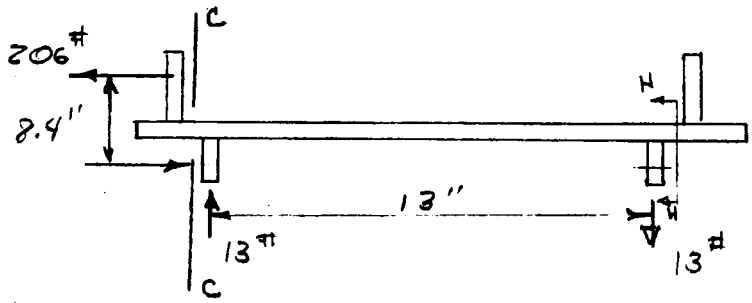

MAT'L:
AISI 1025 STEEL
F_{TU} = 55 ksi
F_{TY} = 36 ksi

REF. (D)

REF. (A) PG. 18

BENDING @ C-C (SIDE LOAD)

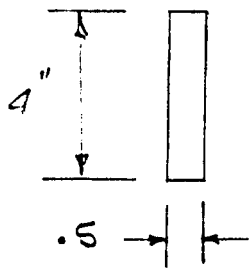

$M = 206(8.4) = 1730$ in-lbs

$f = \frac{6M}{bt^2} = \frac{6(1730)}{4(.5)^2} = 10{,}400$ psi

YIELD IS CRITICAL, REF. PG. 38

$f = 10{,}400\left(\frac{1.15}{1.4}\right) = 8550$ psi YIELD

$M.S. = \frac{36{,}000}{8550} - 1 =$ HIGH-YIELD

IN PLANE LOADS - REF. (A) PG. 11 & 14 CASE I

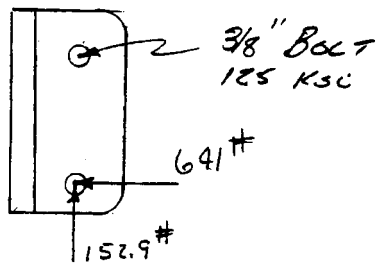

SHEAR ALL. = 8280# REF. (C)

$R = 641 \leftrightarrow 152.9 = 659$#

$M.S. = \frac{8280}{659} - 1 =$ HIGH-ULT

H-H

VOUGHT MISSILES AND SPACE COMPANY

DESIGN INFORMATION REQUEST – RELEASE

1-29-7

MODEL (S) AND EFF.	DIR. NO.	REV.
Dynamic Analyses and Testing of the Shuttle Wing Leading Edge Thermal Insulation System	T-143-DIR-3-1	
	DATE 1-26-73 / PAGE 1	OF 40
SYSTEM Shuttle Leading Edge	REF. G. O. NUMBER 3357 AA 1160	

Fill in block below for Information Request	Fill in block below for Information Release
TO _____ GROUP _____	IN REPLY TO DIR. NUMBER _____
REQ. BY _____ GROUP _____	REL. TO D. M. While GROUP 3-52000
REASON _____	PREPARED BY R. B. Bost DATE 1/25/73 / CHECKED BY RBB DATE
LTV ONLY ☐ BWR ☐ BUWEPS ☐ ☐ _____	GROUP APP. RB Bost DATE 1/26/73 / PROJ OFFICE DMWhile DATE 1/26/73

CC B. A. Forcht, G. B. Whisenhunt, W. E. Agan, E. C. Matza

DESIGN INFORMATION:

REFERENCES: (a) VMSC Drawing No. T143B00005, "Canted Heatshield Assembly," dated 25 August 1972.

(b) VMSC Drawing No. T143B00006, "Canted Frame Heat Shield Assembly," dated 28 August 1972.

(c) VMSC Drawing No. T143B00002, "Removable Heat Shield Assembly, Shuttle Leading Edge Lower Lug," dated 25 August 1972.

1.0 INTRODUCTION

The critical mechanical design environment for the Shuttle Leading Edge Segment thermal insulation system is defined by the severe random vibration and acoustic environments experienced during the boost phase of flight. These environments produce peak stresses in the insulation which are near the ultimate strength of the material and, due to the 100-mission life requirement, are of sufficiently long duration to make fatigue a fundamental design consideration.

The specific environments used in the design are presented in Figures 1 and 2. In the case of the random vibration environment, the curve presented is considered to be a definition of the maximum response expected rather than an input to the component attachment points, in accordance with agreements reached with

NASA/MSC. The acoustic environment is considered to be the environment external to the leading edge segment.

A careful review of the complete leading edge segment design concept indicated that only three components of the insulation system were critical relative to the flight dynamic environments. These three components are referred to as the canted heat shield,the upper access panel and the lower support lug insulation. A discription of the analyses and supporting tests conducted to verify the design of these three components is presented in this report.

2.0 CANTED HEAT SHIELD

2.1 Design Analyses

The canted heat shield is completely enclosed by the basic leading edge structure and hence is isolated from the external acoustic field. On this basis, the internal acoustic levels will be significantly attenuated relative to the external field, typically on the order of 20 to 30 db. These considerations indicate that the critical environment for the heat shield should be the random vibration environment and hence this environment was the only one considered in detail in the design of the heat shield.

The baseline heat shield design configuration is defined in the drawings of References (a) and (b). This configuration was mathematically modeled by the finite element technique as shown schematically in Figure 3. The nodes shown in this figure are located on the basic polyimide fiberglass panel. Twenty additional nodes were located immediately above these nodes at the centerline of the Dynaquartz insulation. This arrangement is shown in Figure 4 along with the basic dimensions used in the analysis.

The polyimide panel and the Dynaquartz insulation was modeled using orthotropic plate bending elements. The stiffeners were represented by general

beam elements to include the effect of the beam elastic axes being offset from the centerline of the polyimide panel. The strain isolator was modeled by a rectangular solid element whose formulation assumes a linear variation in displacement between the eight nodes bounding the element. The material and/or section properties used as inputs to these finite element descriptions are presented in Figure 5.

The random vibration response analysis was conducted using the first ten modes of the heat shield. A summary of the frequencies of these modes and their response participation is presented in Figure 6. Since the first two modes are the primary contributors to the induced stresses, these modes are also shown graphically, in Figures 7 and 8 in terms of the displacements of the basic polyimide panel. In the response analysis, a modal equivalent damping factor of 0.02 was used for each of the modes to insure a conservative estimate of the response.

A large number of variations in the major heat shield design parameters were considered in the response analyses in an attempt to arrive at a viable design. These parameter studies showed that the number of insulation tiles and the thickness of the strain isolator were the controlling variables in defining the critical stress in the insulation weak direction. The influence of these two parameters is shown in Figure 9 for a 4-tile and a 6-tile heat shield configuration. On the basis of these results, the 4 tile configuration with an isolator thickness of 0.20 inches was chosen as the final design configuration.

The calculated distribution of RMS stresses in the insulation weak direction is shown in Figure 10 for the final design configuration. As can be seen, the maximum stress occurs in the center of the panel near the edge of a tile. The stress level at all other points in the tile are significantly below

this level.

A summary of the maximum calculated stresses for all components of the final heat shield design configuration is shown in Figure 11. These calculated 3σ stresses are well below the material allowables for all of the components.

2.2 Random Vibration Tests

In order to gain confidence in the ability of the Dynaquartz insulation material to withstand the flight vibration environment, particularly from the standpoint of fatigue for which no test data is available, random vibration tests were conducted on two test articles which approximated the dynamic characteristics of the actual heat shield. It should be noted, however, that the first natural mode of each of these test articles has a higher natural frequency and greater curvature at the center of the article than is the case for the actual heat shield. The second of these factors should result in greater induced stresses in the insulation material than would occur on the heat shield.

The first of these two test articles is shown in Figure 12. It consisted of a fiberglass panel and stiffeners to which was bonded two 1-3/8" thick tiles of 10 PCF Dynaquartz through a 1/4" thick RL1973 foam strain isolator. This component was configured to represent a full span (14.6 in.) of one of the four bays of the canted heat shield.

The vibration input was normal to the plane of the panel since this axis produces critical loads in the insulation. In accordance with an initial understanding with NASA/MSC, the maximum response was held to approximately a level of 32 GRMS overall. It was anticipated that this peak response would occur at the center of the panel but under actual test conditions the peak of 31 GRMS occurred at one end of the panel. A level of 26 GRMS was measured at the center of the panel with a corresponding level of 17 GRMS at the opposite end. This

result was later determined to be due to local impacting resulting from a gap between two of the rivets which fastened one of the stiffeners to the panel.

Acceleration spectral density (ASD) plots of each of the accelerometer outputs are shown in Figures 13, 14 and 15. These plots show that in the first natural mode of vibration (170 Hertz), the peak response was in the center of the panel with approximately equal responses occurring at the two ends. The high overall vibration level measured at the right end is entirely due to response in the higher frequency regime.

The significant factor to note from these ASD plots is that at the first two resonant frequencies (170 and 500 Hz), the response spectrum peaks at a level of approximately 10 g^2/Hz. This is an order of magnitude greater than the design spectrum level presented in Figure 1.

These levels resulted in failure of one tile at the bondline within two minutes and failure of the second tile in three minutes. This is equivalent to 7 to 10 missions considering the frequencies involved. Failure occurred at the center of the panel in the Dynaquartz adjacent to the bondline. This is exactly where analysis predicts maximum stresses. It appears that these were fatigue failures because minutes of testing were required to produce failure.

In an effort to prove that a feasible design and insulation attachment technique can be accomplished for the leading edge segment, the test component was redesigned using analysis results to define the modifications which would achieve maximum improvements in the insulation fatigue life. The design changes included were as follows:

(1) Tiles were reduced in size.

(2) Strain isolator thickness was doubled

(3) The density (and therefore strength) of the insulation was increased.

(4) The stiffeners were bonded to the panel.

The redesigned test article is shown in Figure 16.

On the basis of the results obtained from the first test article, further discussions on the test environment between VMSC and NASA/MSC resulted in a revision to remove much of the conservatism of the first test. It was agreed to limit the ASD of the response of the article in its first two modes to a level of 2.25 g^2/Hz, which includes a 1.5 factor of safety to account for current unknowns. No requirements were placed on the overall (RMS) levels. Using these new ground rules, the second article was tested.

The component was exposed at two levels. For the first exposure (designated Run #1), the ASD of the response was limited to 1 g^2/Hz in the center of the panel where the maximum response occurred. The corresponding overall level was 18.5 GRMS. At the left and right ends of the panel, the overall levels were 16.7 and 15.8 GRMS, respectively. The ASD plots for these three accelerometers are shown in Figures 17, 18 and 19. The test duration was 36 minutes to simulate 100 missions. This time was arrived at by the ratio of the heat shield resonant frequency to test article resonant frequency and assuming 30 second exposure per flight in the actual flight environment.

The second exposure (designated Run #2) was conducted at a nominal ASD level of 2.25 g^2/Hz at the primary resonant frequencies of 143 and 468 Hertz. A third resonance at 175 Hertz peaked at a level of 1 g^2/Hz. During the 36 minute test run, some variations in spectral levels and frequency distributions occurred. The actual response spectra achieved at the three accelerometer locations are shown in Figures 20, 21 and 22 for the start of the run and in Figures 23, 24 and 25 for the end of the run. As indicated on the figures, the overall vibration level at the point of maximum response varied from a minimum of 25.8 GRMS to a maximum of 29.7 GRMS overall with the average being on the order of 27 GRMS.

No failures were observed at any location on the component after the completion of these two test exposures, even though one of the tiles used in the component had known gross flaws. This suggests that all of the modifications included in the redesigned component were not required. This conclusion is also indicated by the analysis results. At any rate, the test did serve to demonstrate the feasibility of achieving a heat shield design capable of surviving the Shuttle dynamic loads environment.

3.0 UPPER ACCESS PANEL DESIGN ANALYSIS

The upper access panel, Ref. (c), is directly exposed to the external acoustic environment defined in Figure (2). Due to this fact, the acoustic environment for this panel is more critical than the random vibration environment and, hence was the only one considered in the design.

For purposes of analysis, the component was assumed to consist of a 16 x 15 inch titanium panel with a thickness of 0.063 inches and a 0.20 inch thickness of strain isolator supporting four tiles of Dynaquartz insulation varying in thickness from 1.30 inches at the forward edge to 0.70 inches at the aft edge. In addition, 0.063 inch thick titanium stiffeners were considered to support the two edges of the panel. These stiffeners varied in depth from a minimum of 1.0 inches to a maximum of 1.70 inches.

The finite element model of this configuration is shown in Figure 26. As indicated in this figure, the panel was assumed to be symmetric about the centerline and hence only half of the panel was modeled with appropriate symmetry constraints along this centerline. The element types used in the model and the method of representing the strain isolator and insulation tiles were identical to that used in modeling the canted heat shield and, therefore, will not be repeated here.

The acoustic response analysis was conducted using the first ten modes of the access panel. A summary of the frequencies of these modes and their response participation is presented in Figure 27. Again, modal equivalent damping factors of 0.02 were assumed in the analysis.

The calculated distribution of RMS stresses in the insulation weak direction is shown in Figure 28. As can be seen, the maximum stress again occurs in the center of the panel along the edge of a tile.

A summary of the maximum stresses calculated for all components of the upper access panel is presented in Figure 29. These calculated 3σ stresses are well below the material allowables for all of the components.

4.0 LOWER SUPPORT LUG INSULATION

Due to its internal location and small frontal area, the lower support lug and the insulation surrounding it are critical relative to the random vibration environment. On this basis, only this environment was considered in the lug response analysis.

One-half of the lower support lug is shown in Figure 30. The other half is identical. Thermal insulation material is attached between these two halves by means of a 0.10 inch thickness of strain isolator. This results in continuity between the two halves such that any relative motion results in direct loading of the insulation through the strain isolator.

A simple, one-mode analysis was performed to determine the RMS displacement response of the lug to the design random vibration environment. This displacement was then used to calculate the stresses induced in the entrapped insulation through the mechanism of the strain isolator.

The stiffness distribution used for determining the first mode of the lug is shown in Figure 31. As can be seen from this figure, the lug was approximated by a simple, straight beam whose bending rigidity was adjusted

to account for the steps and for the tapered cross sections. The frequency of the first mode was calculated to be 470 Hertz.

Using the criteria of a 32 GRMS peak response in this mode, the resulting deflection was determined to be 0.0014 inches (RMS). This deflection gives a resultant stress level in the insulation material of 0.85 PSI (RMS). The 3σ stress is then 2.55 psi. This is well below the weak direction 4 psi allowable for Dynaquartz.

FIGURE 1
RANDOM VIBRATION ENVIRONMENT
BOOST PHASE

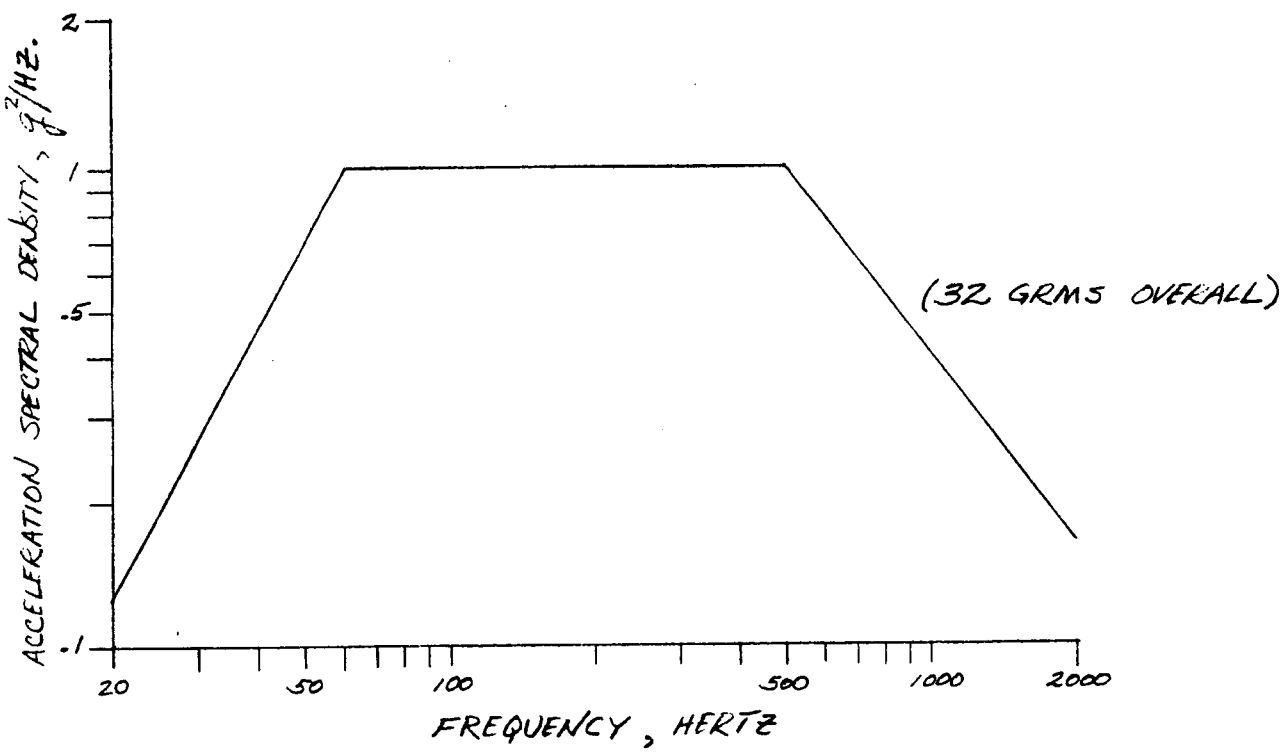

FIGURE 2

ACOUSTIC ENVIRONMENT

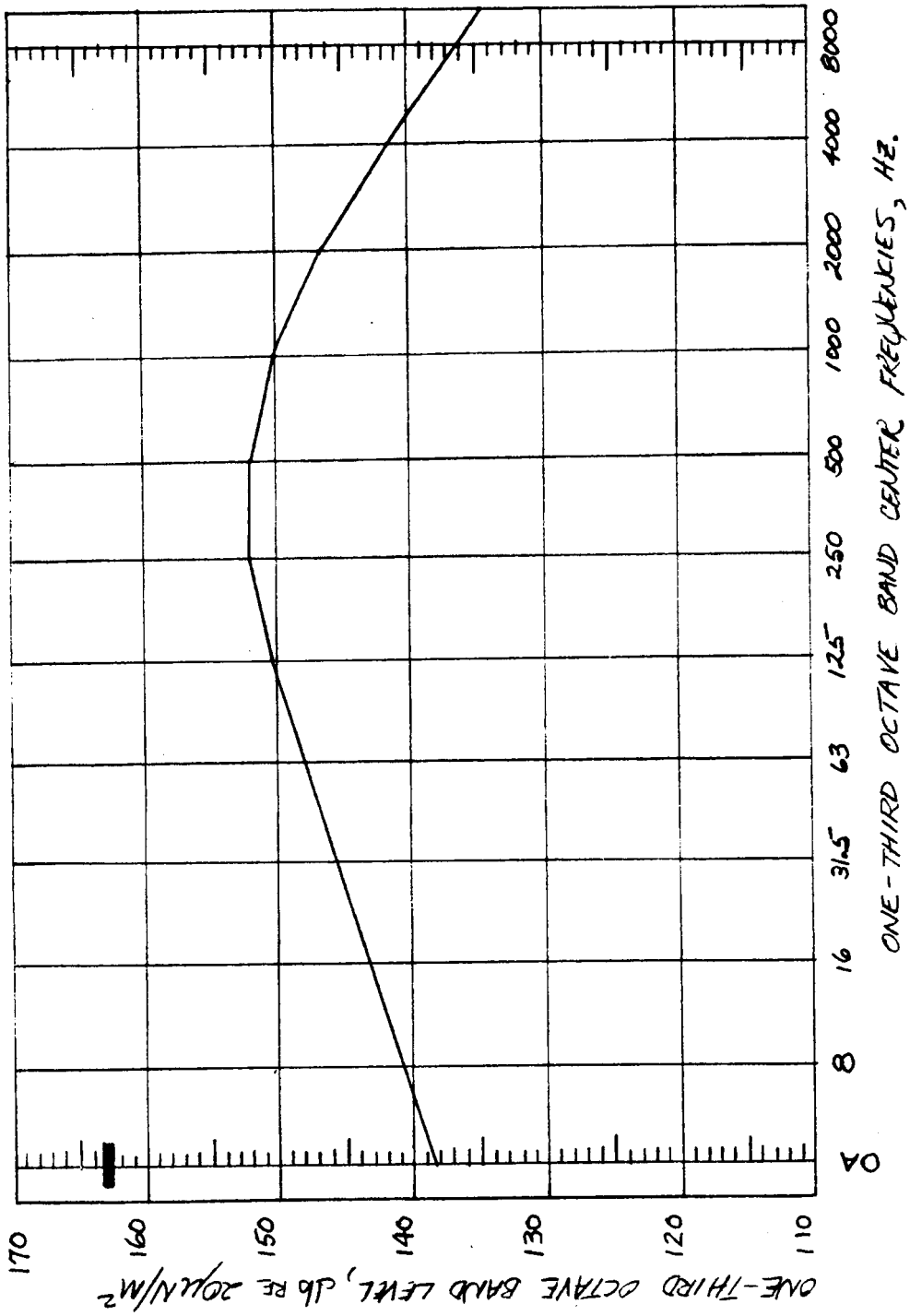

FIGURE 3
FINITE ELEMENT MODEL
OF CANTED HEAT SHIELD

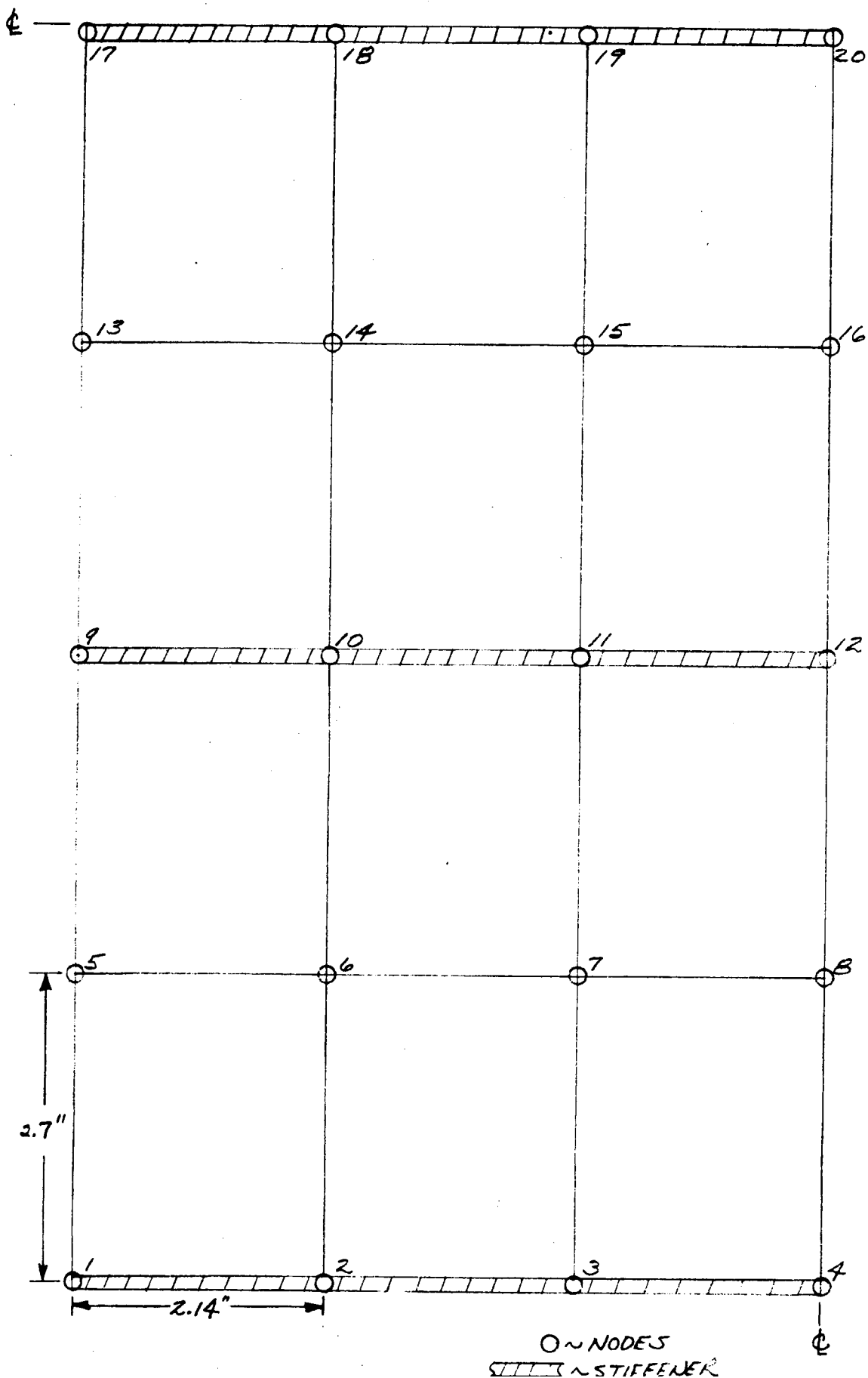

FIGURE 4
CANTED HEAT SHIELD
SECTION THROUGH STIFFENER

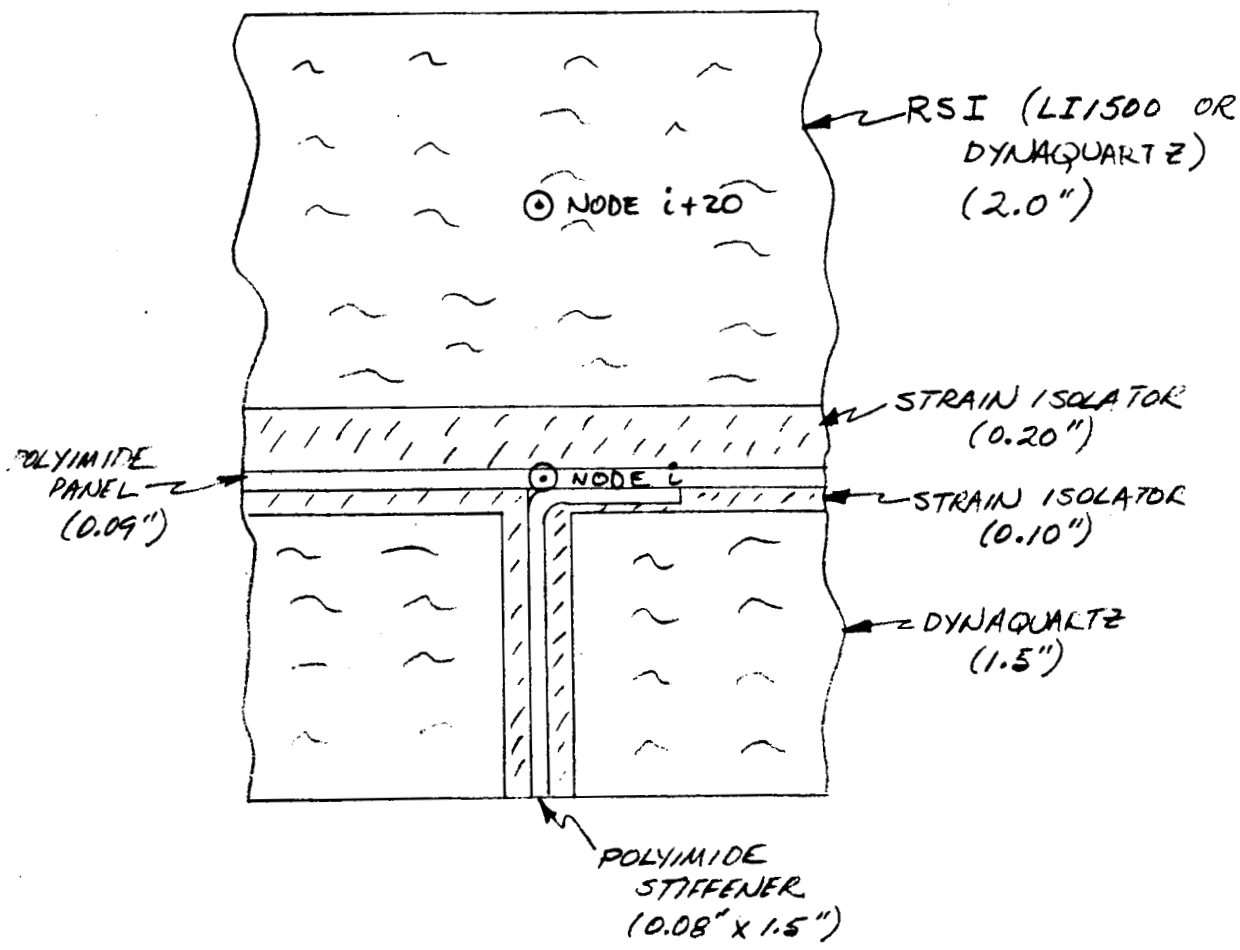

FIGURE 5
CANTED HEAT SHIELD
MATERIAL AND SECTION PROPERTIES

POLYIMIDE	$E = 2.5 \times 10^6$ PSI $\rho = 0.063$ LB/IN.^{3}
RSI (LI1500)	$E = 60{,}000$ PSI $\rho = 0.0087$ LB/IN.^{3}
ISOLATOR	$E = 60$ PSI $\rho = 0.0016$ LB/IN.^{3}
DYNAQUARTZ (10 PCF)	$E = 500$ PSI $\rho = 0.0058$ LB/IN.^{3}
STIFFENERS	$EI = 56{,}200$ LB-IN.^{2} $\rho A = 1.96 \times 10^{-5}$ LB-SEC^2/IN.^{2}
FRAME	$EI = 3.24 \times 10^5$ LB-IN.^{2} $GJ = 692$ LB-IN.^{2} $EA = 3.19 \times 10^6$ LB. $\rho A = 8.3 \times 10^{-3}$ LB-SEC^2/IN.^{2}

FIGURE 6
CANTED HEAT SHIELD
MODAL DATA

MODE NO.	FREQUENCY HERTZ	MODAL PARTICIPATION FACTOR
1	144	5.42
2	290	2.15
3	371	3.46
4	561	0.05
5	597	0.20
6	615	0.79
7	650	0.33
8	706	0.96
9	734	0.45
10	939	2.08

FIGURE 7
FIRST HEATSHIELD MODE SHAPE
f = 144 Hz

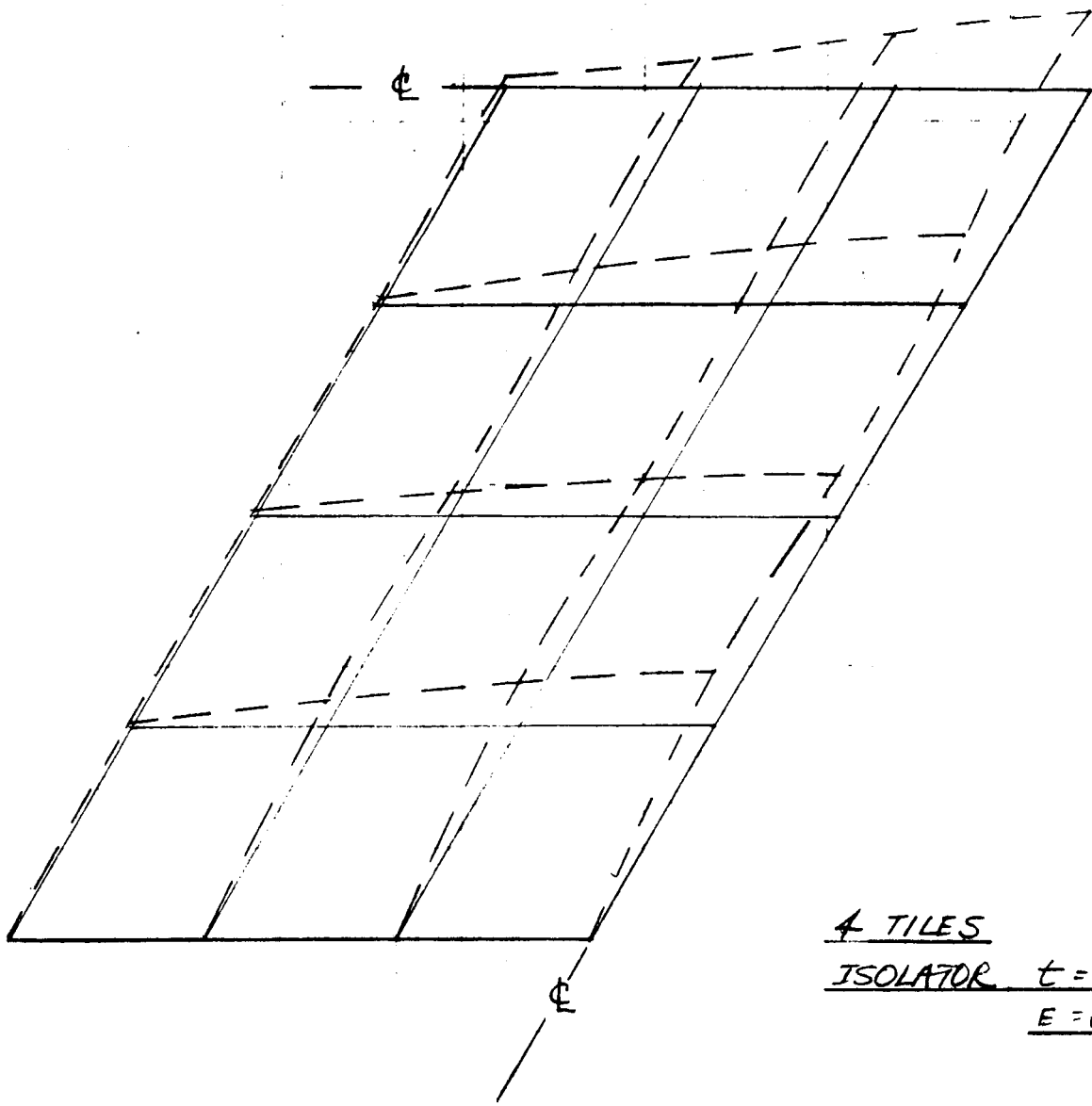

4 TILES
ISOLATOR t = 0.20"
E = 60 PSI

FIGURE 8
SECOND HEAT SHIELD MODE SHAPE
$f = 290$ HZ.

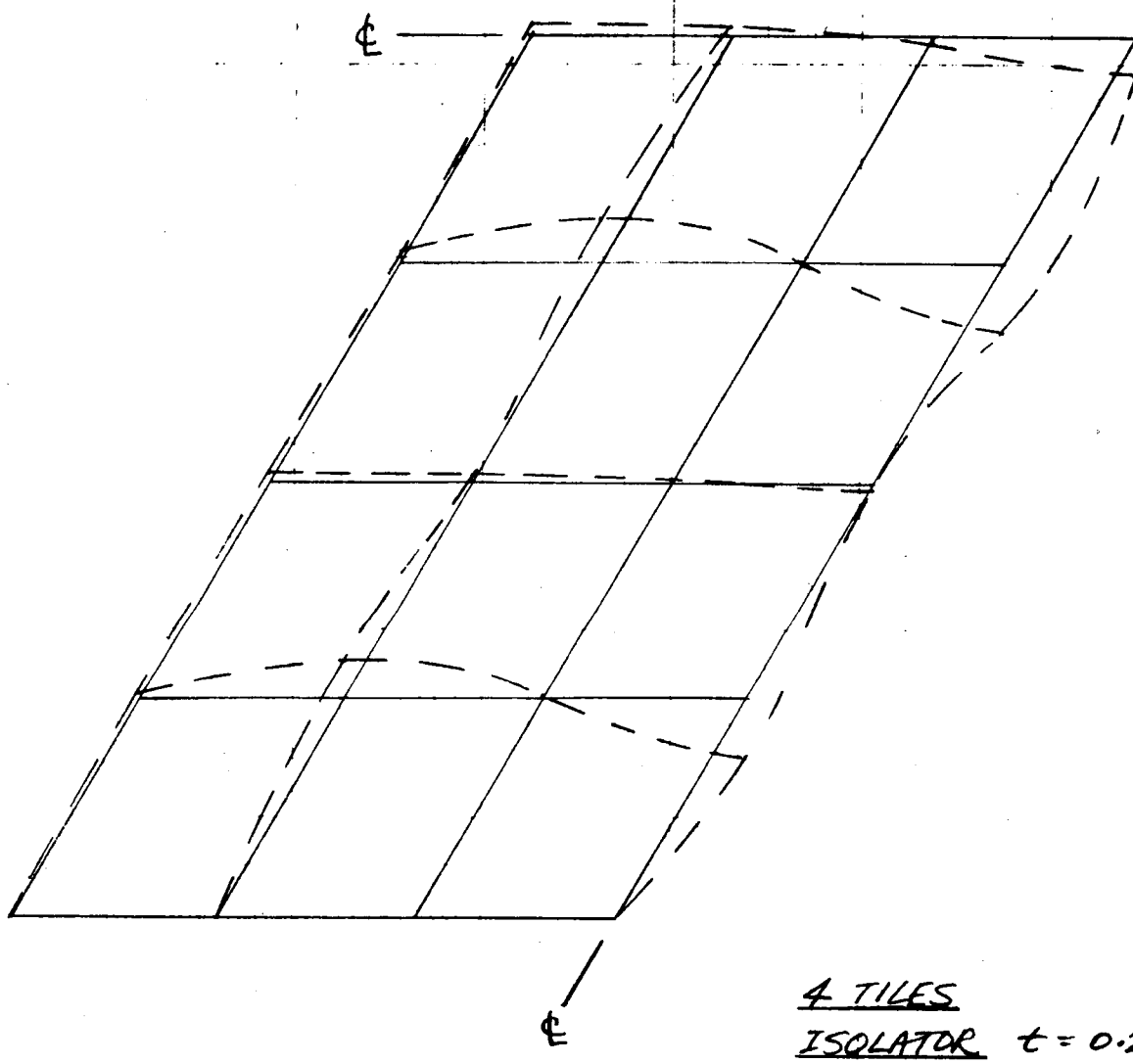

4 TILES
ISOLATOR $t = 0.20''$
$E = 60$ PSi

FIGURE 9
EFFECTS OF ISOLATOR THICKNESS
AND NO. OF TILES ON
RSI PEAK STRESS

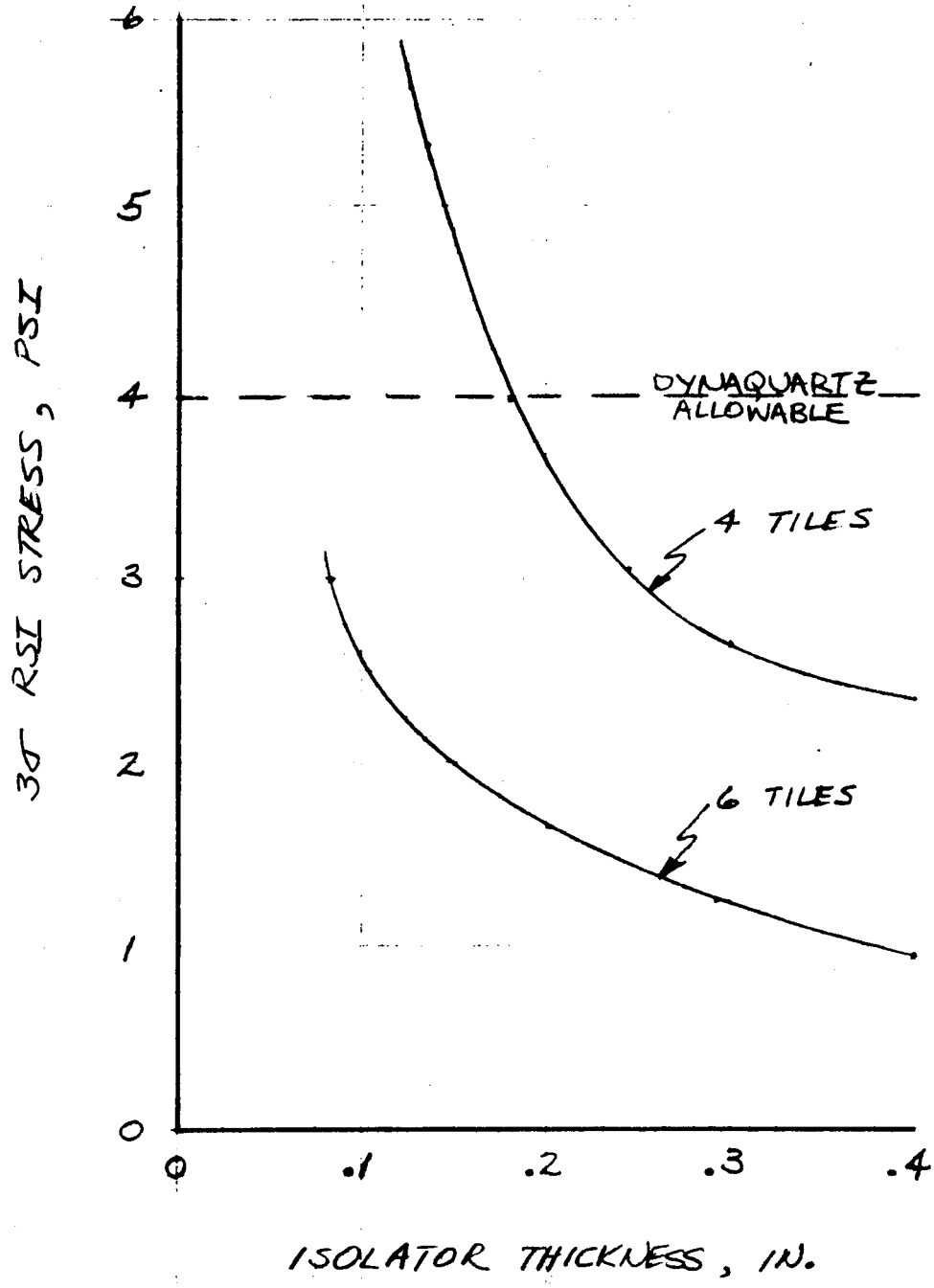

FIGURE 10
RSI STRESS DISTRIBUTION
WEAK DIRECTION.

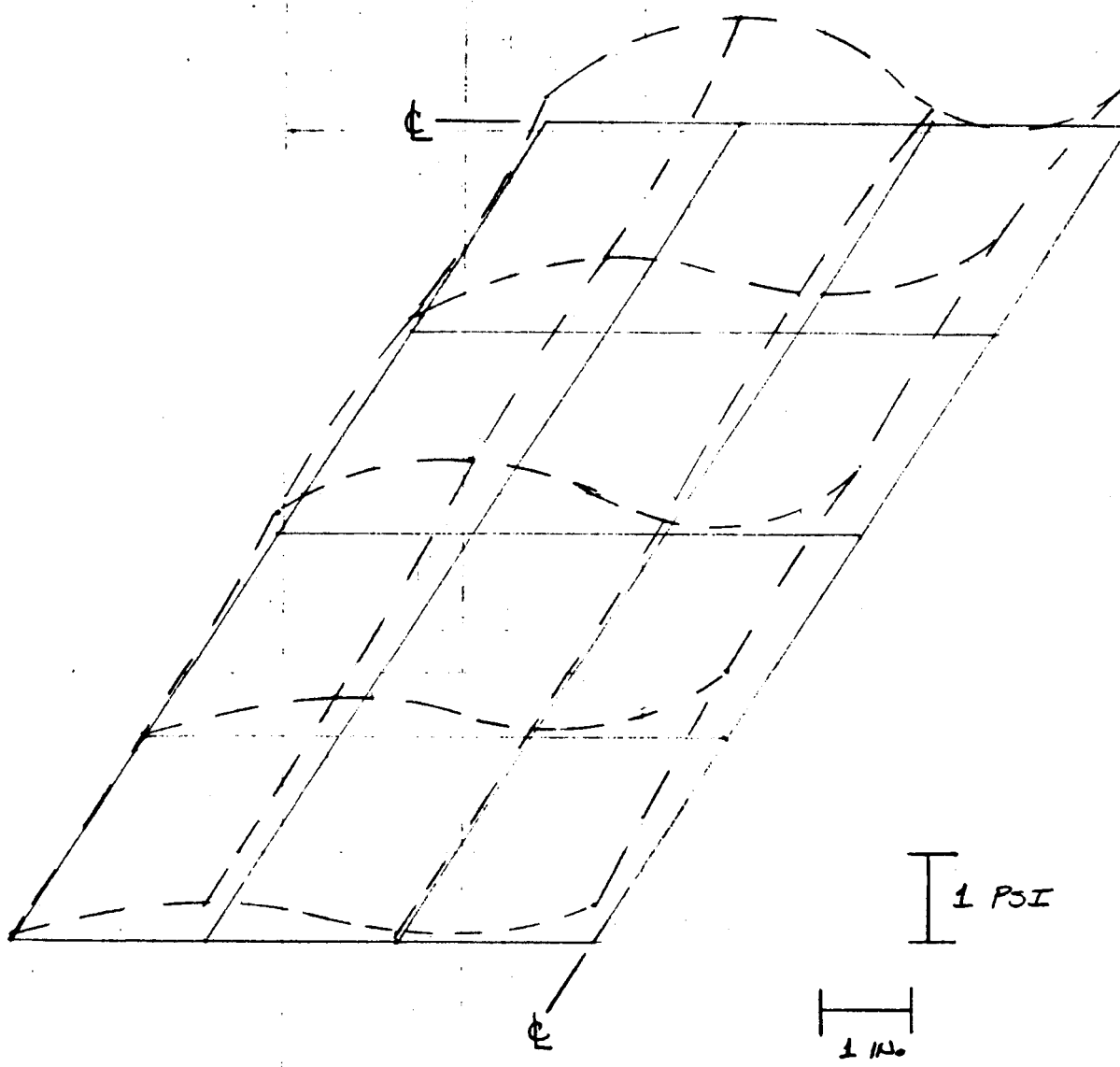

FIGURE 11
SUMMARY OF MAXIMUM STRESSES
CANTED HEAT SHIELD

COMPONENT	RMS STRESS	3σ STRESS
RSI (WEAK DIR.)	1.2 PSI	3.6 PSI
RSI (STRONG DIR.)	1.8	5.4
POLYIMIDE PANEL	62	186
STIFFENER	14,500	43,500

FIGURE 12

RPP HEATSHIELD COMPONENT

VIBRATION TEST ARTICLE #1

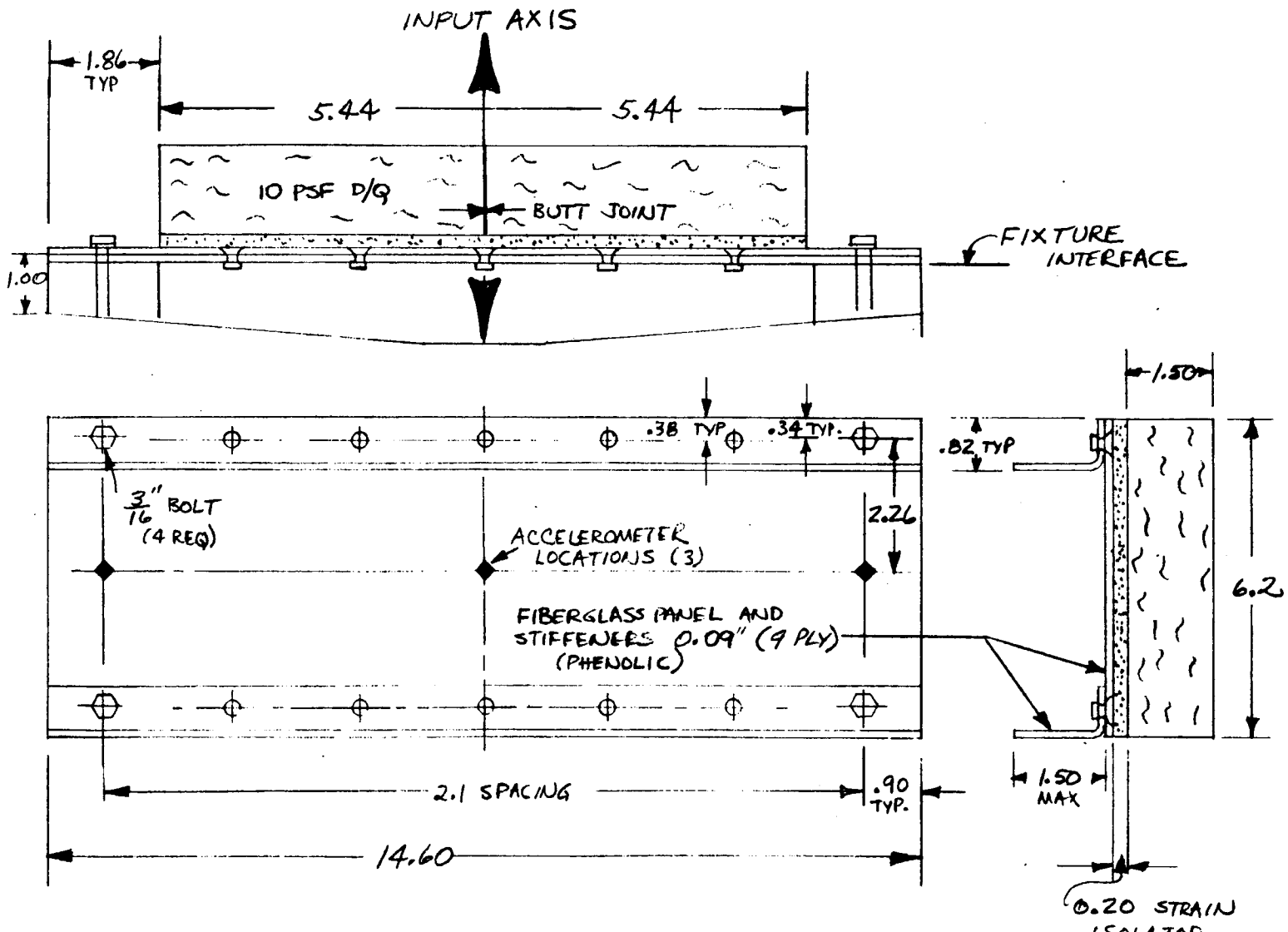

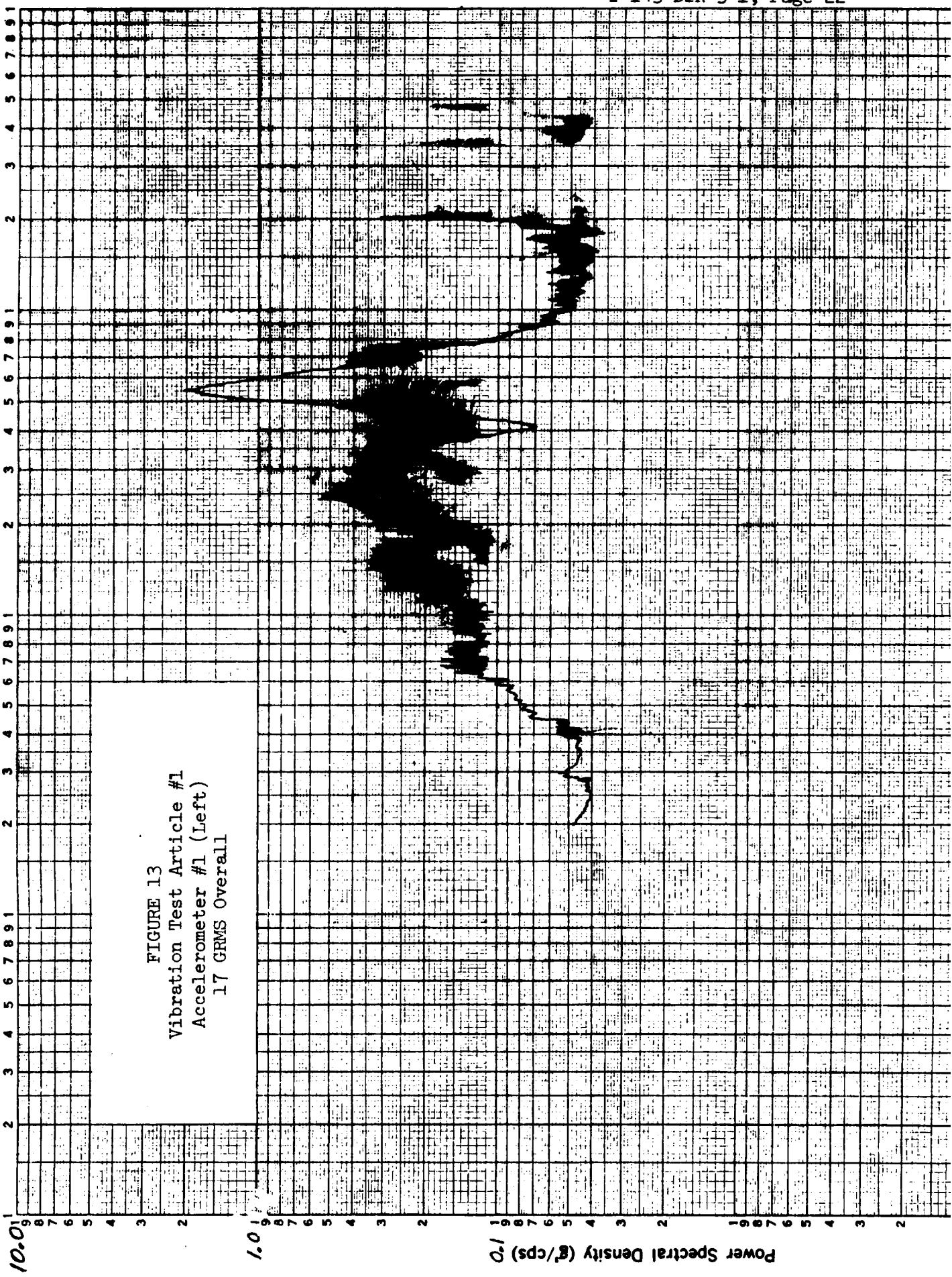

FIGURE 13
Vibration Test Article #1
Accelerometer #1 (Left)
17 GRMS Overall

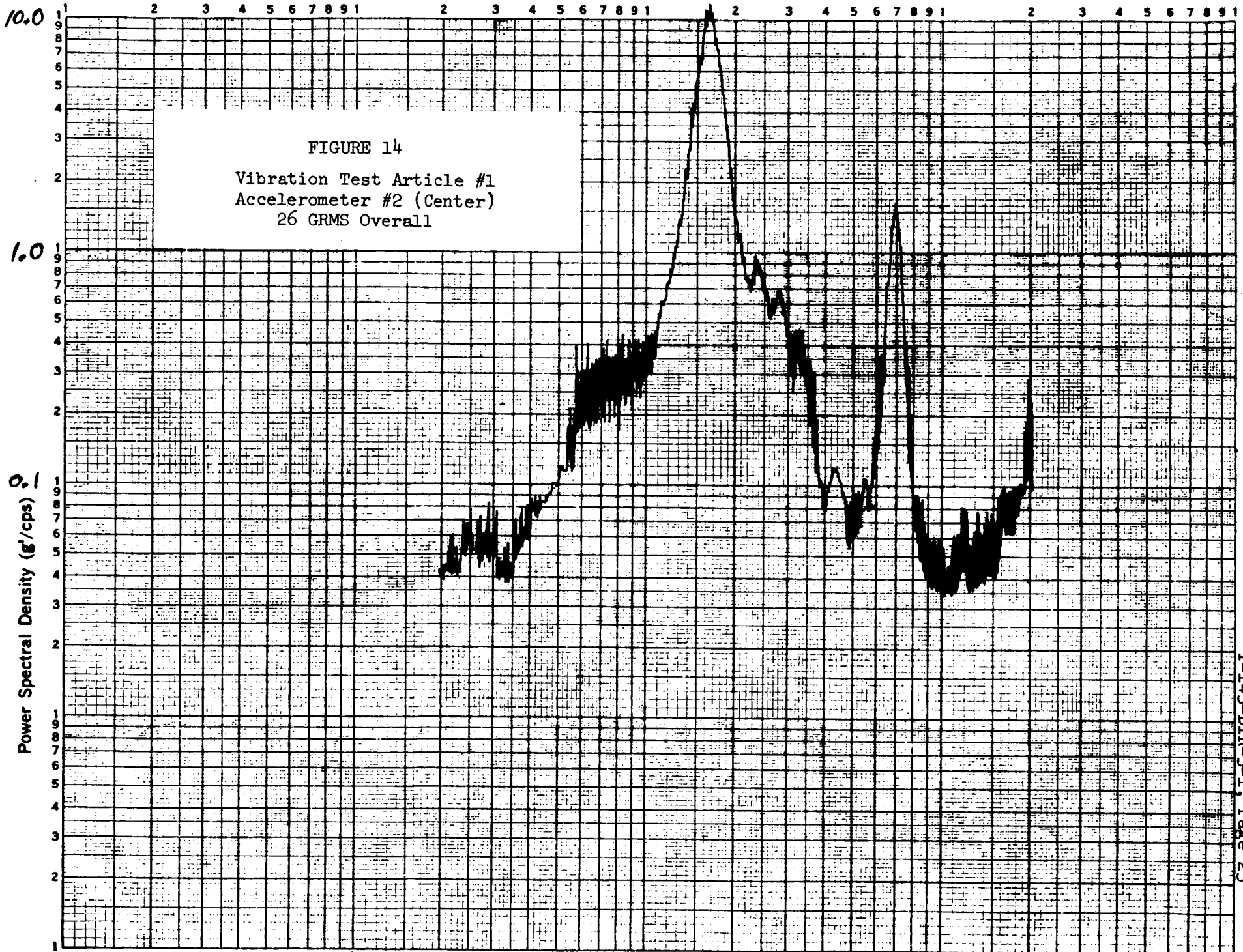

FIGURE 14

Vibration Test Article #1
Accelerometer #2 (Center)
26 GRMS Overall

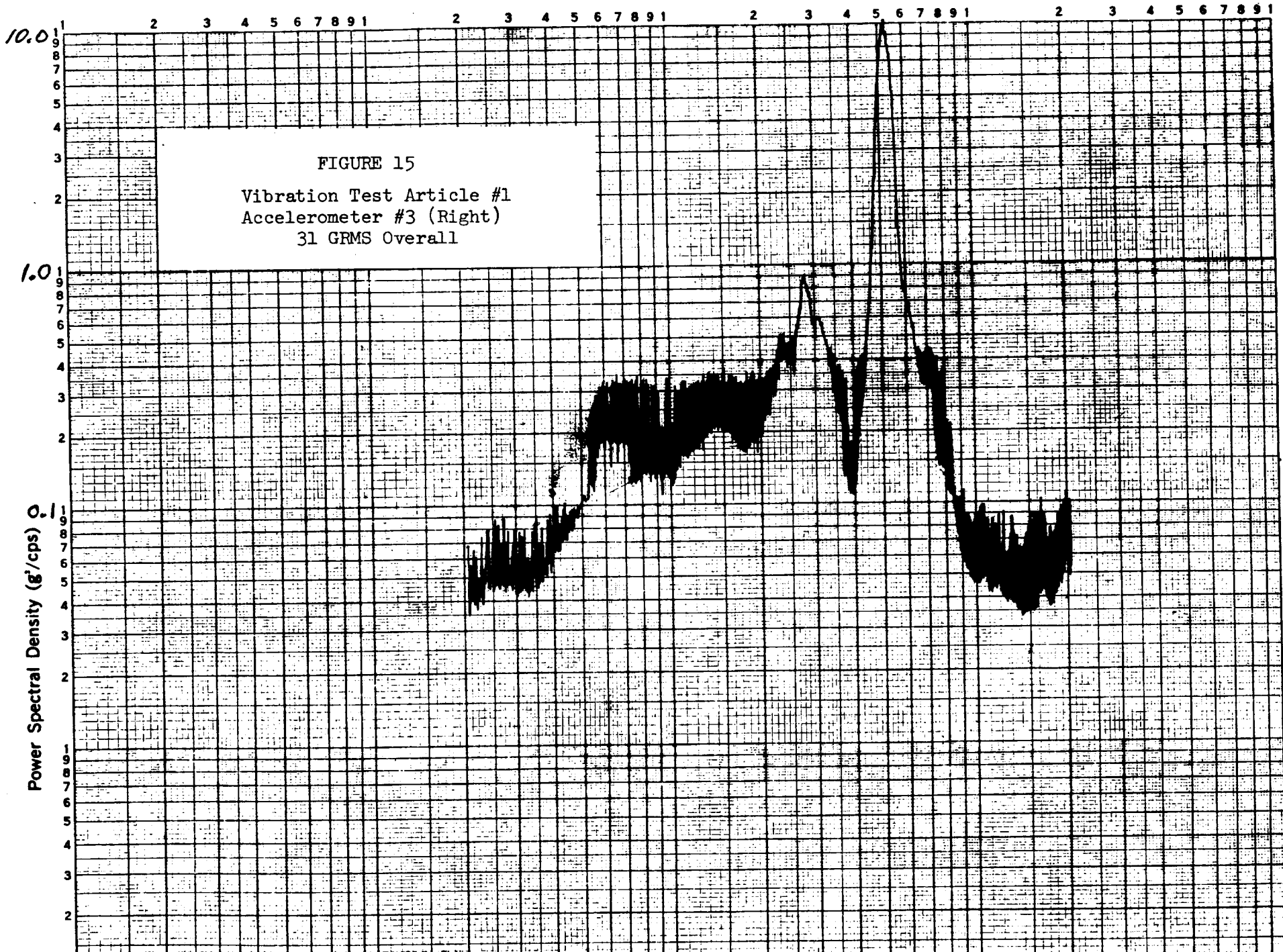

FIGURE 15

Vibration Test Article #1
Accelerometer #3 (Right)
31 GRMS Overall

FIGURE 16

RPP HEATSHIELD COMPONENT

VIBRATION TEST ARTICLE #2

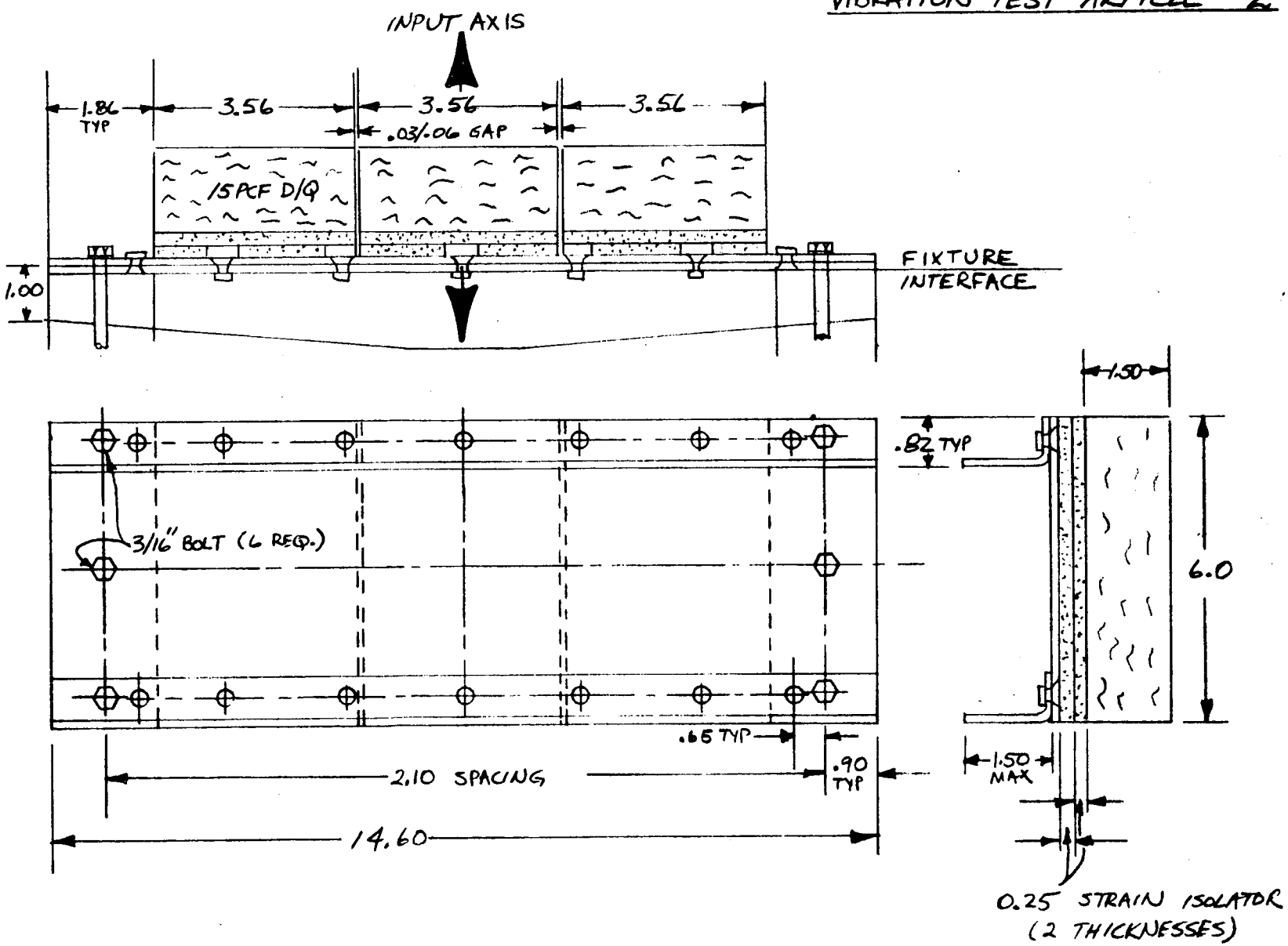

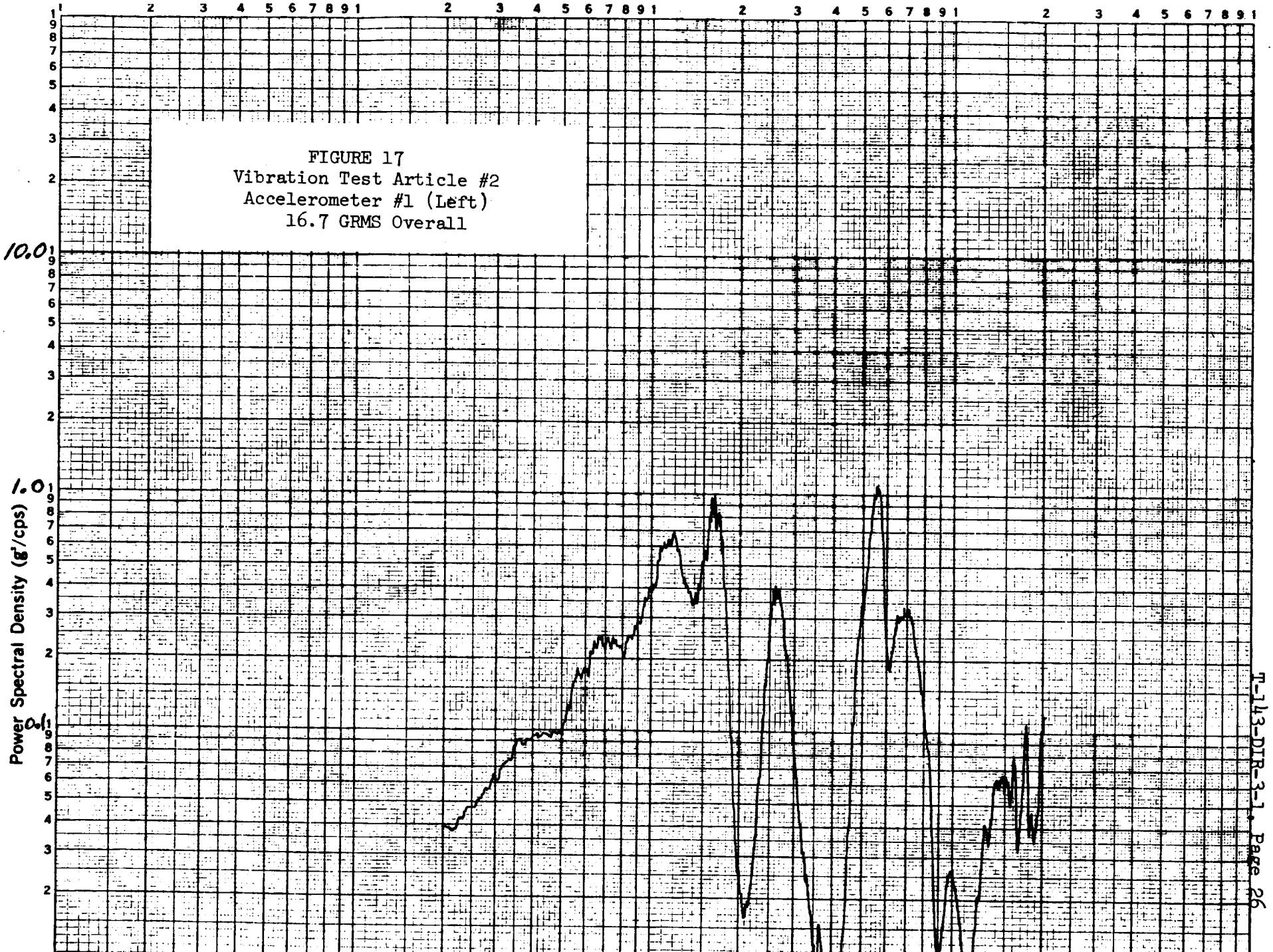

FIGURE 17
Vibration Test Article #2
Accelerometer #1 (Left)
16.7 GRMS Overall

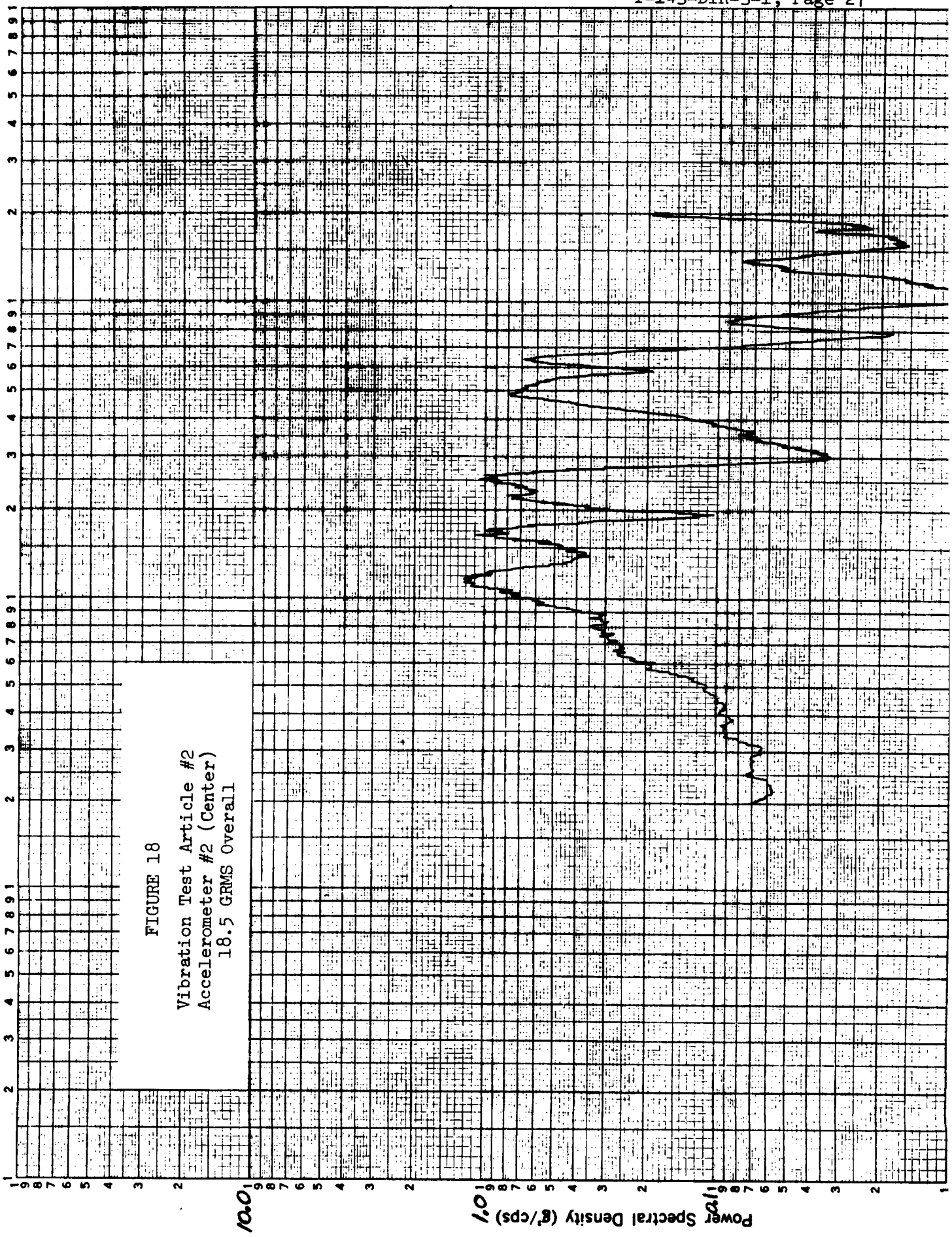

FIGURE 18

Vibration Test Article #2
Accelerometer #2 (Center)
18.5 GRMS Overall

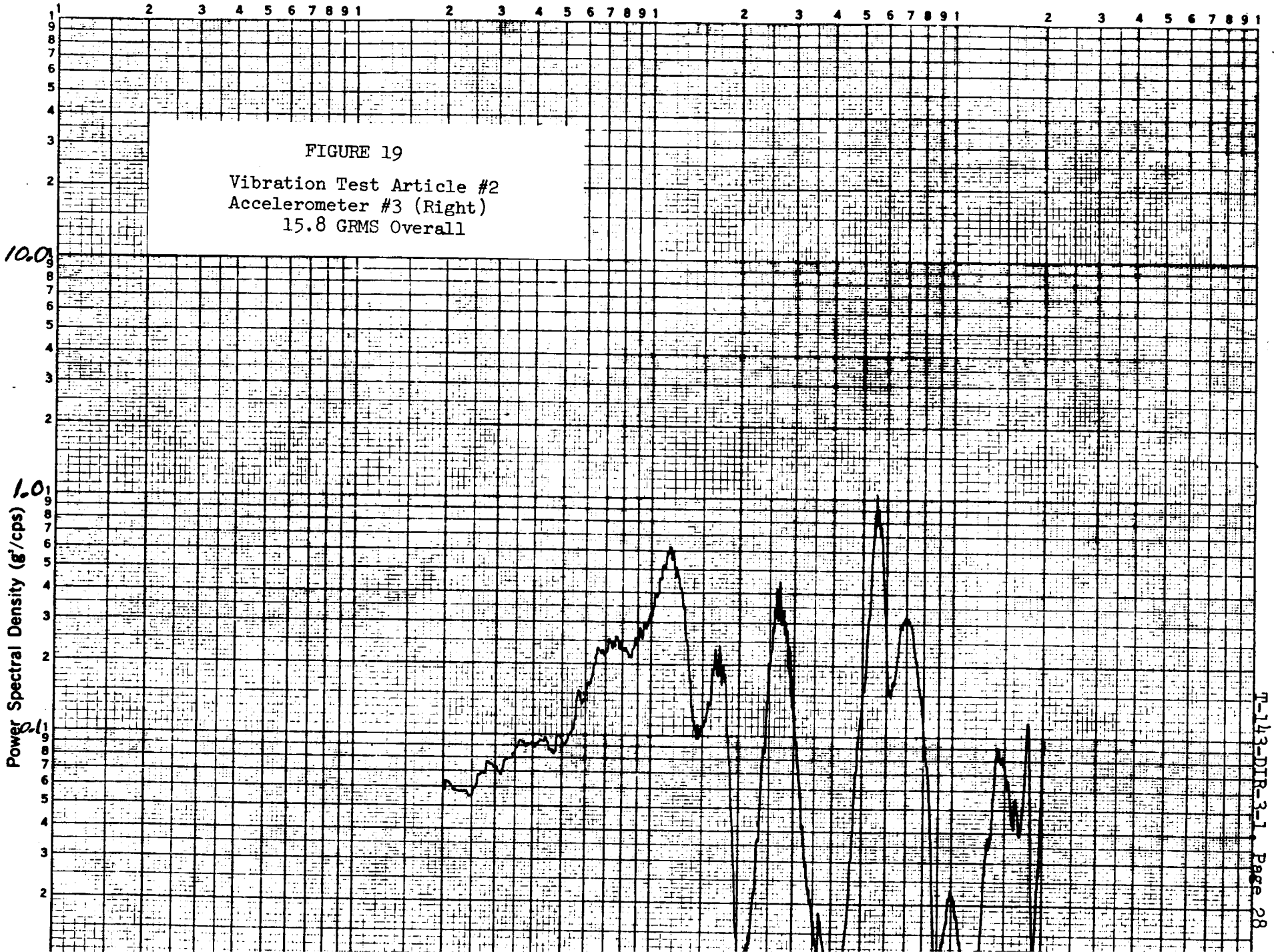

FIGURE 19

Vibration Test Article #2
Accelerometer #3 (Right)
15.8 GRMS Overall

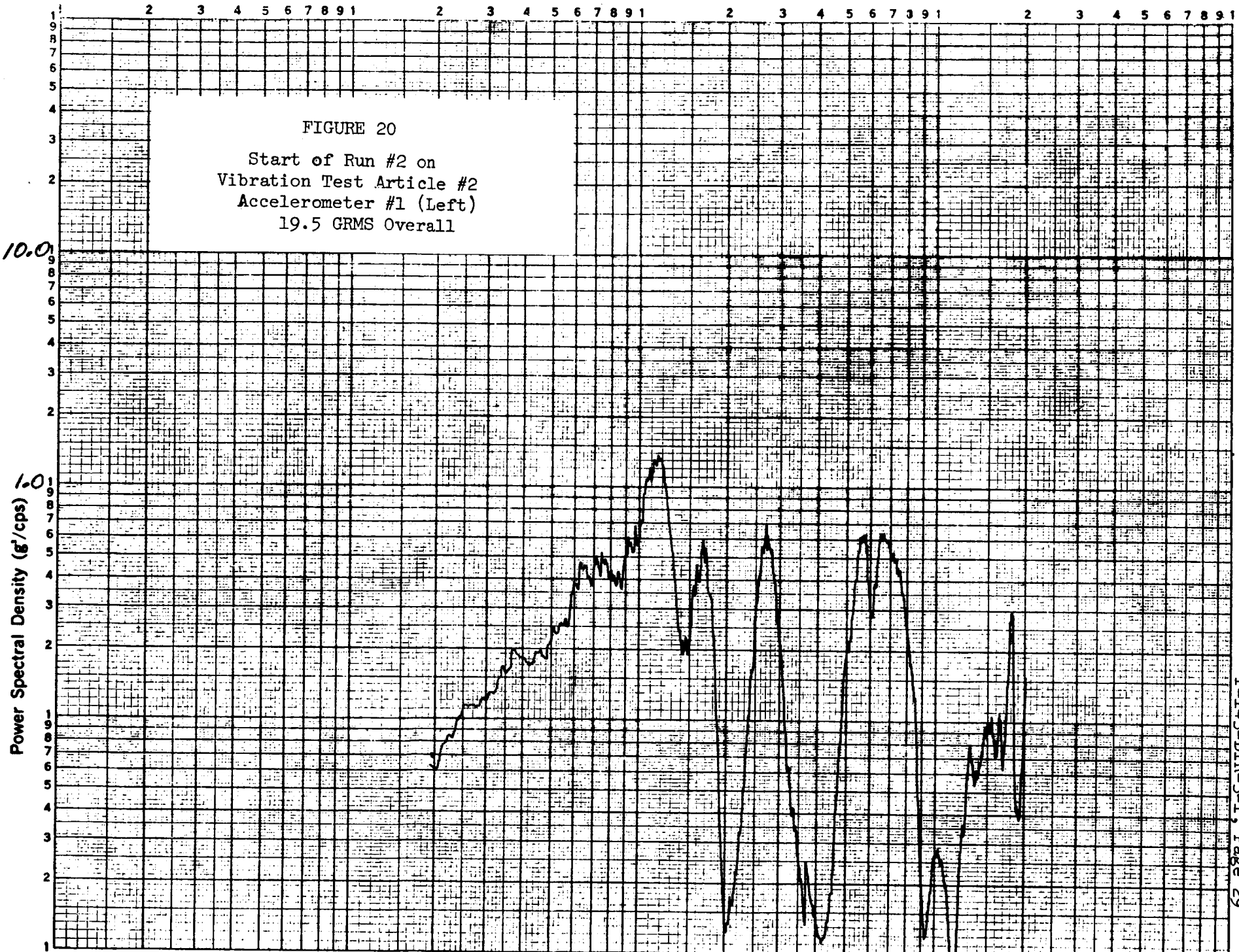

FIGURE 20

Start of Run #2 on
Vibration Test Article #2
Accelerometer #1 (Left)
19.5 GRMS Overall

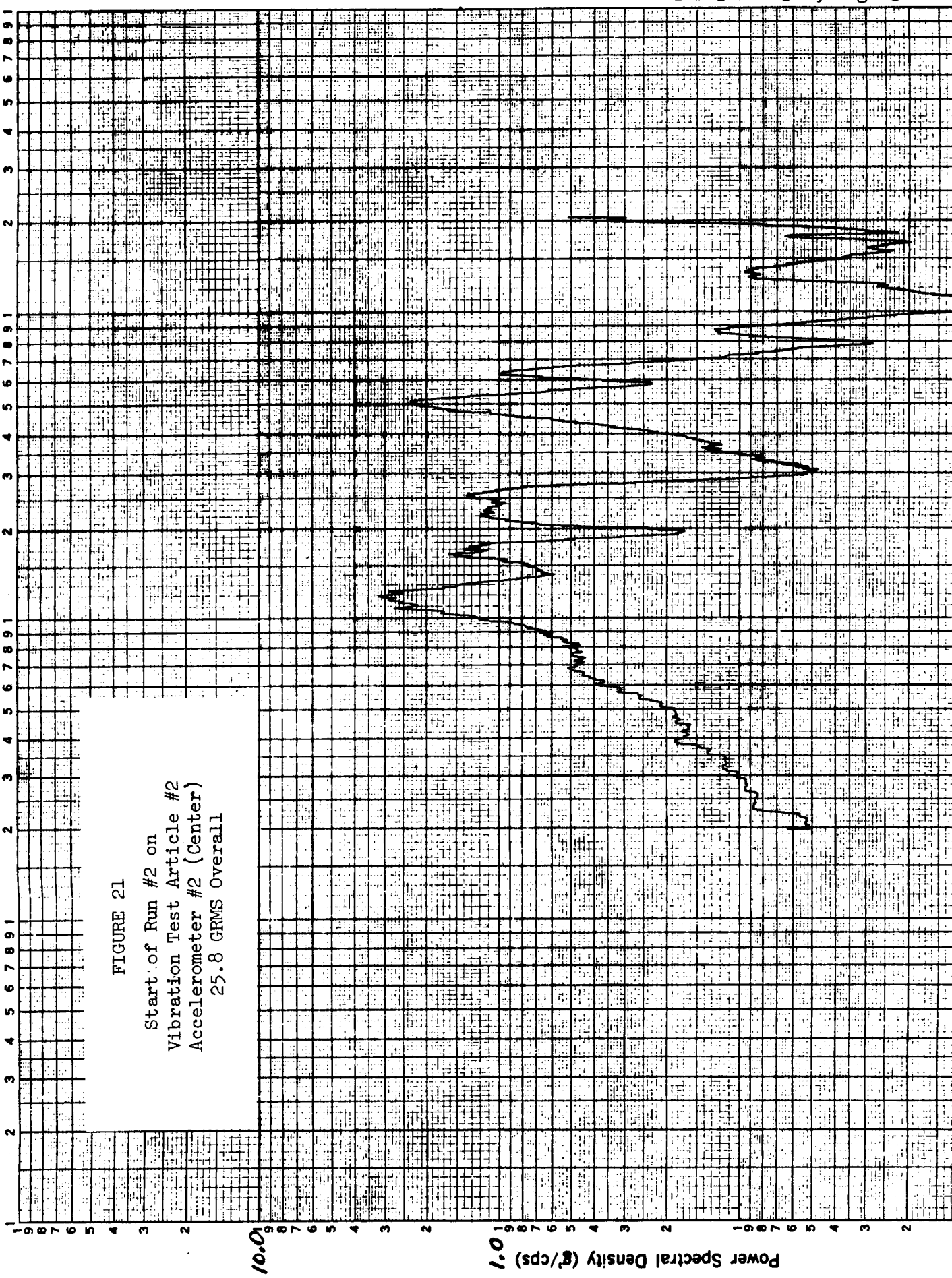

FIGURE 21
Start of Run #2 on
Vibration Test Article #2
Accelerometer #2 (Center)
25.8 GRMS Overall

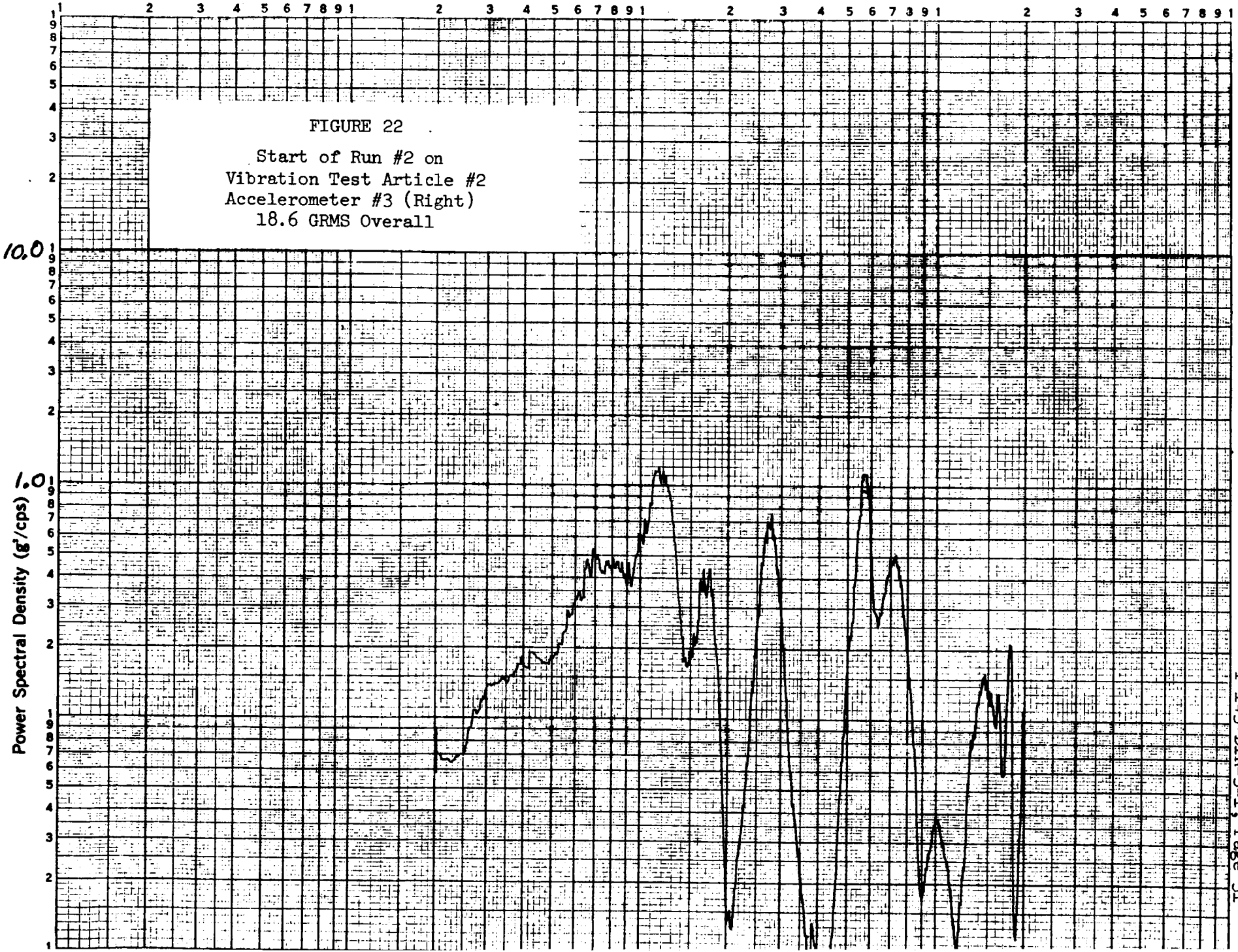

FIGURE 22

Start of Run #2 on
Vibration Test Article #2
Accelerometer #3 (Right)
18.6 GRMS Overall

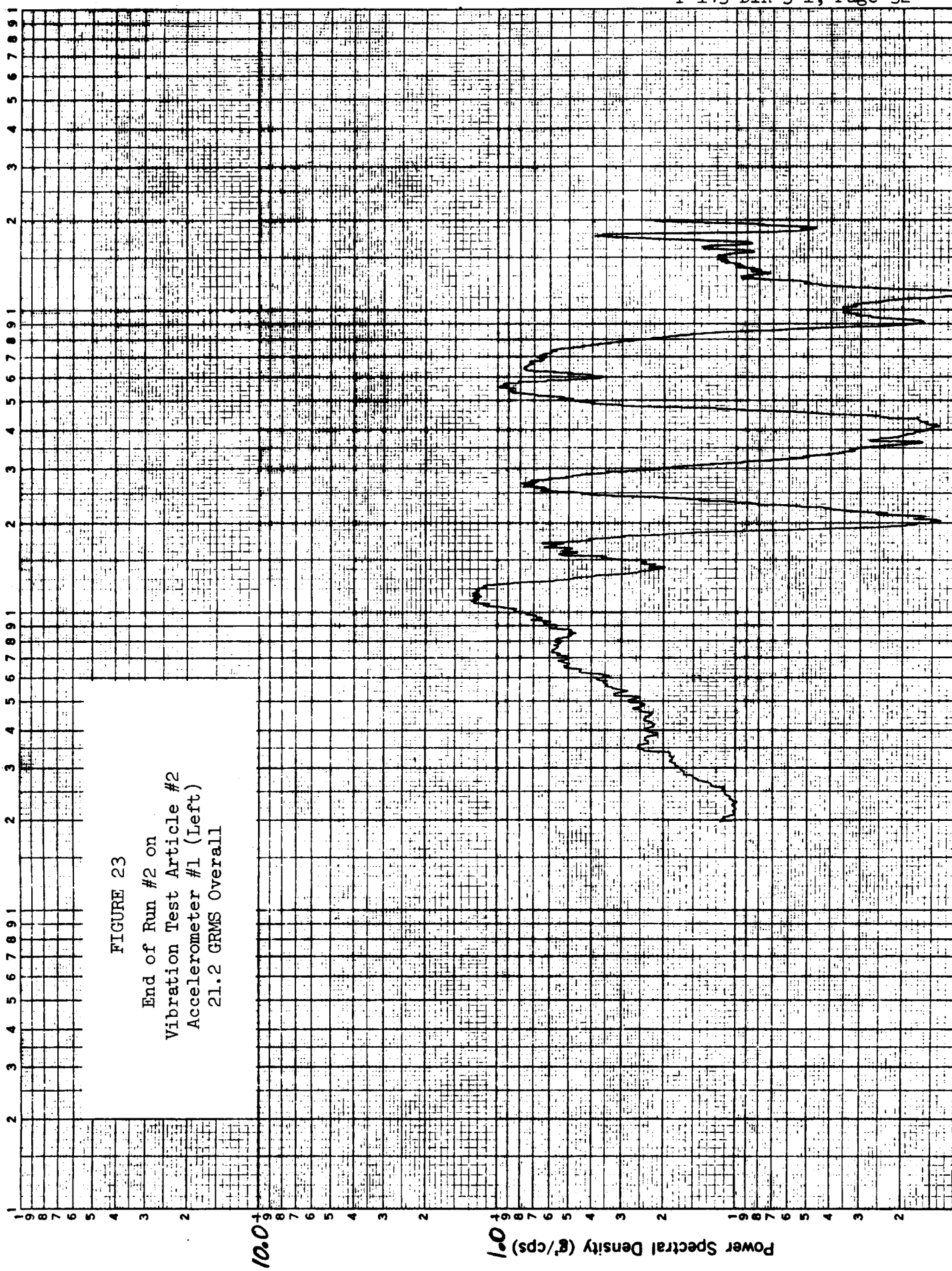

FIGURE 23

End of Run #2 on
Vibration Test Article #2
Accelerometer #1 (Left)
21.2 GRMS Overall

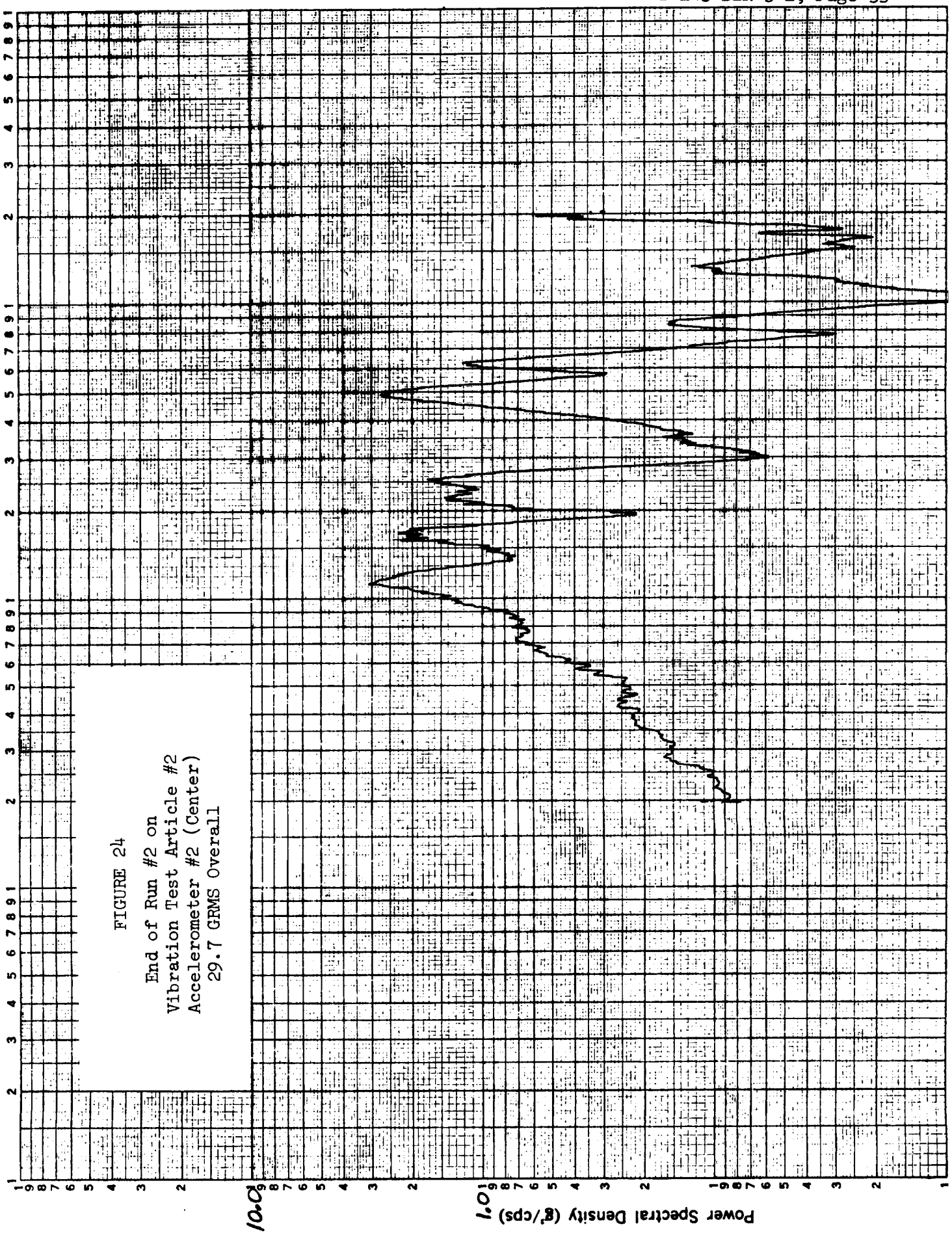

FIGURE 24

End of Run #2 on
Vibration Test Article #2
Accelerometer #2 (Center)
29.7 GRMS Overall

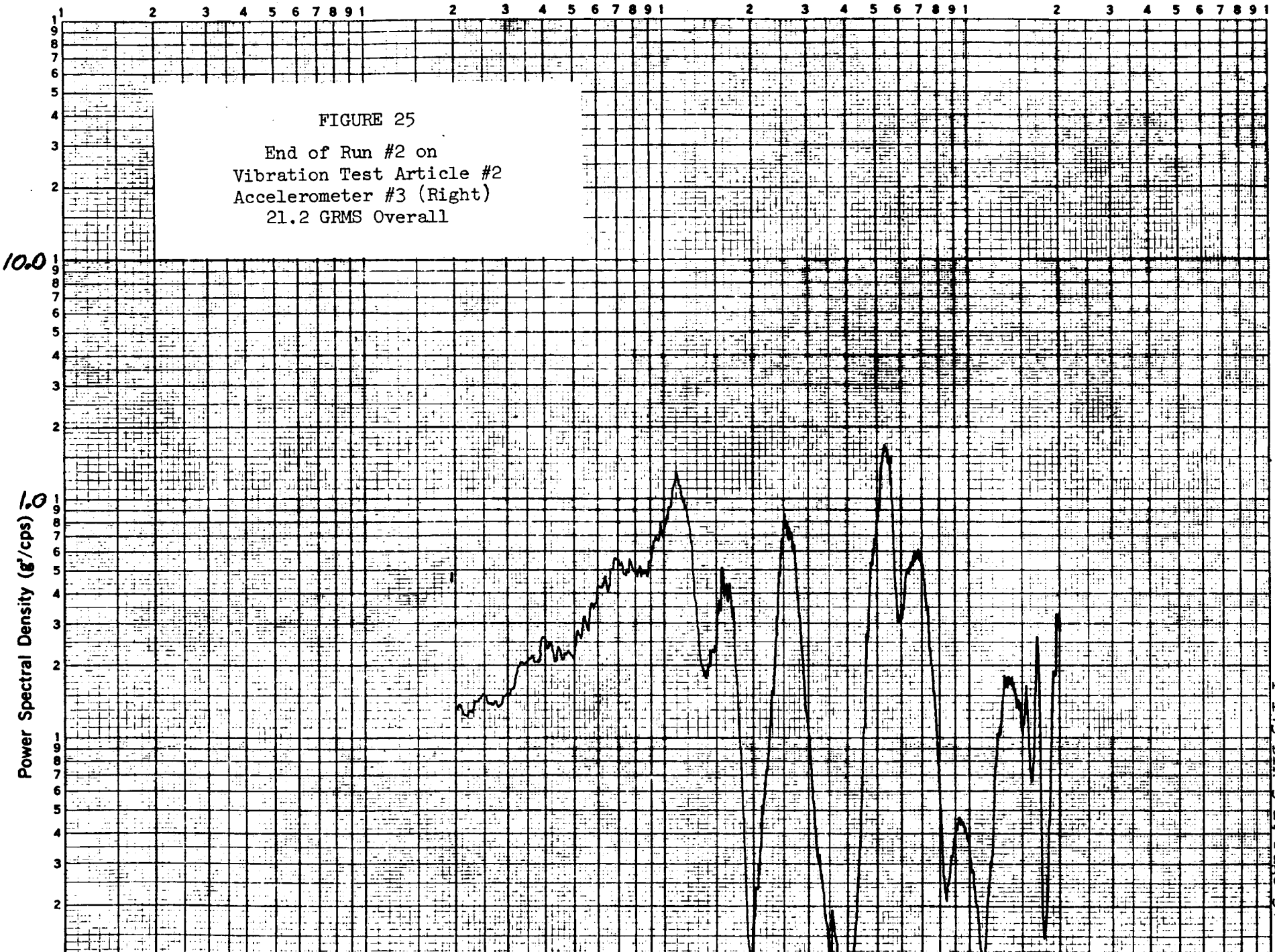

FIGURE 25

End of Run #2 on
Vibration Test Article #2
Accelerometer #3 (Right)
21.2 GRMS Overall

FIGURE 26
FINITE ELEMENT MODEL
OF UPPER ACCESS PANEL

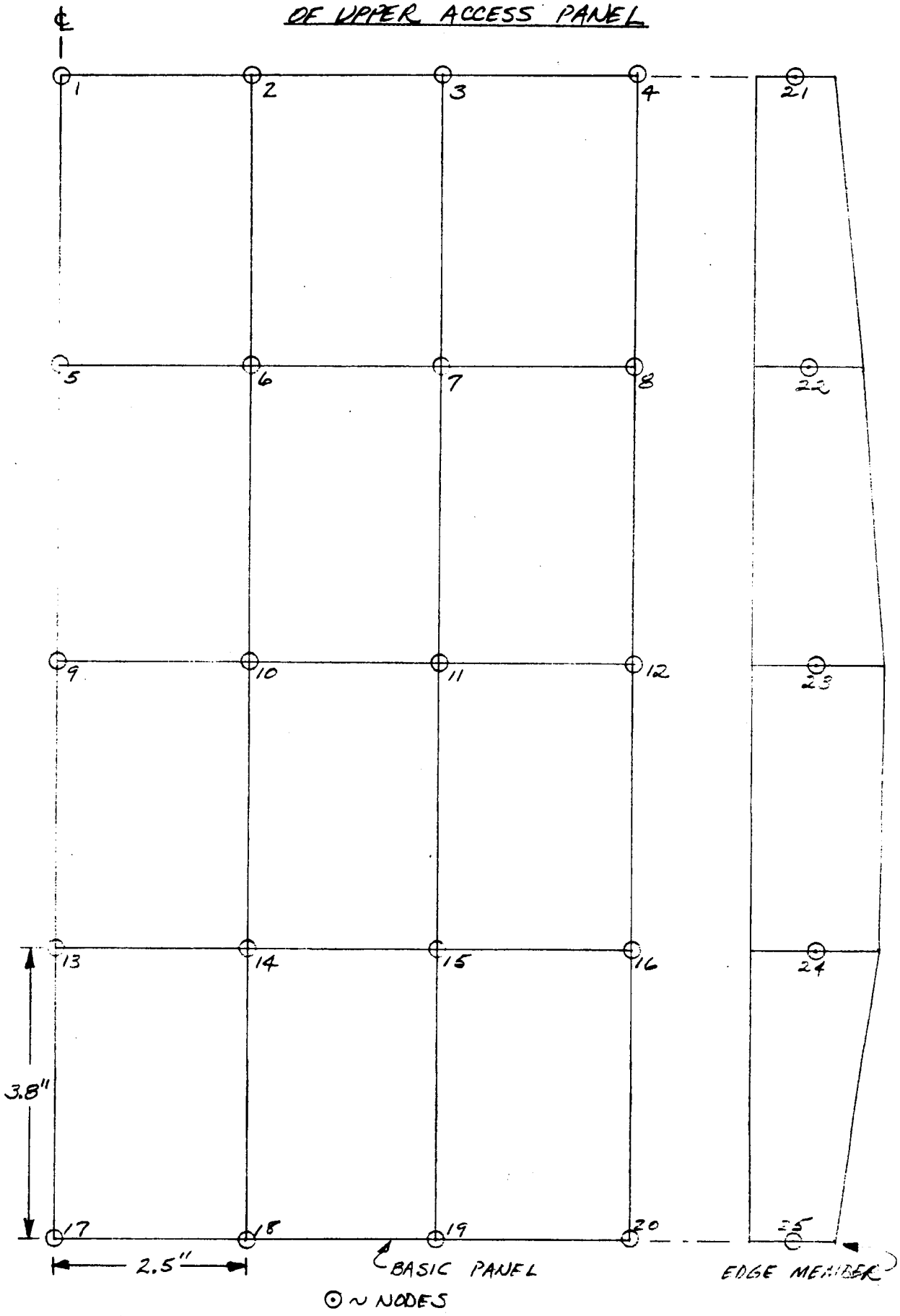

FIGURE 27
UPPER ACCESS PANEL
MODAL DATA

MODE NO.	FREQUENCY HERTZ	MODAL PARTICIPATION FACTOR
1	80	2.52
2	211	0.11
3	292	1.01
4	352	1.89
5	426	0.08
6	594	1.51
7	687	4.92
8	735	0.35
9	756	0.17
10	790	0.02

FIGURE 28

UPPER ACCESS PANEL

DISTRIBUTION OF STRESSES IN DYNAQUARTZ

(WEAK DIRECTION)

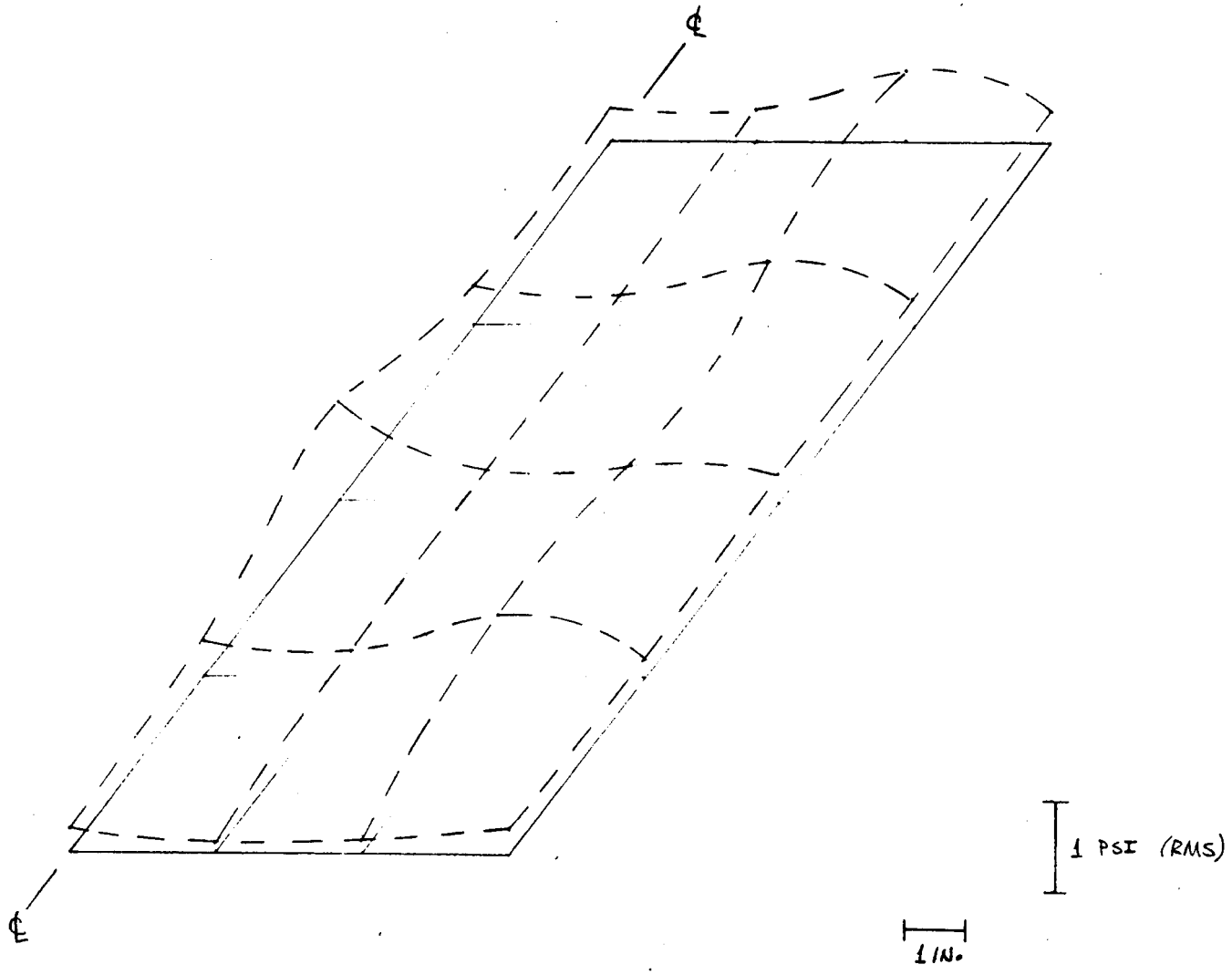

FIGURE 29
SUMMARY OF MAXIMUM STRESSES
UPPER ACCESS PANEL

COMPONENT	RMS STRESS	3σ STRESS
D/Q (WEAK DIR.)	1.15 PSI	3.45 PSI
D/Q (STRONG DIR.)	3.7	11.1
TITANIUM PANEL	2,850	8,550
EDGE MEMBER	4,050	12,150

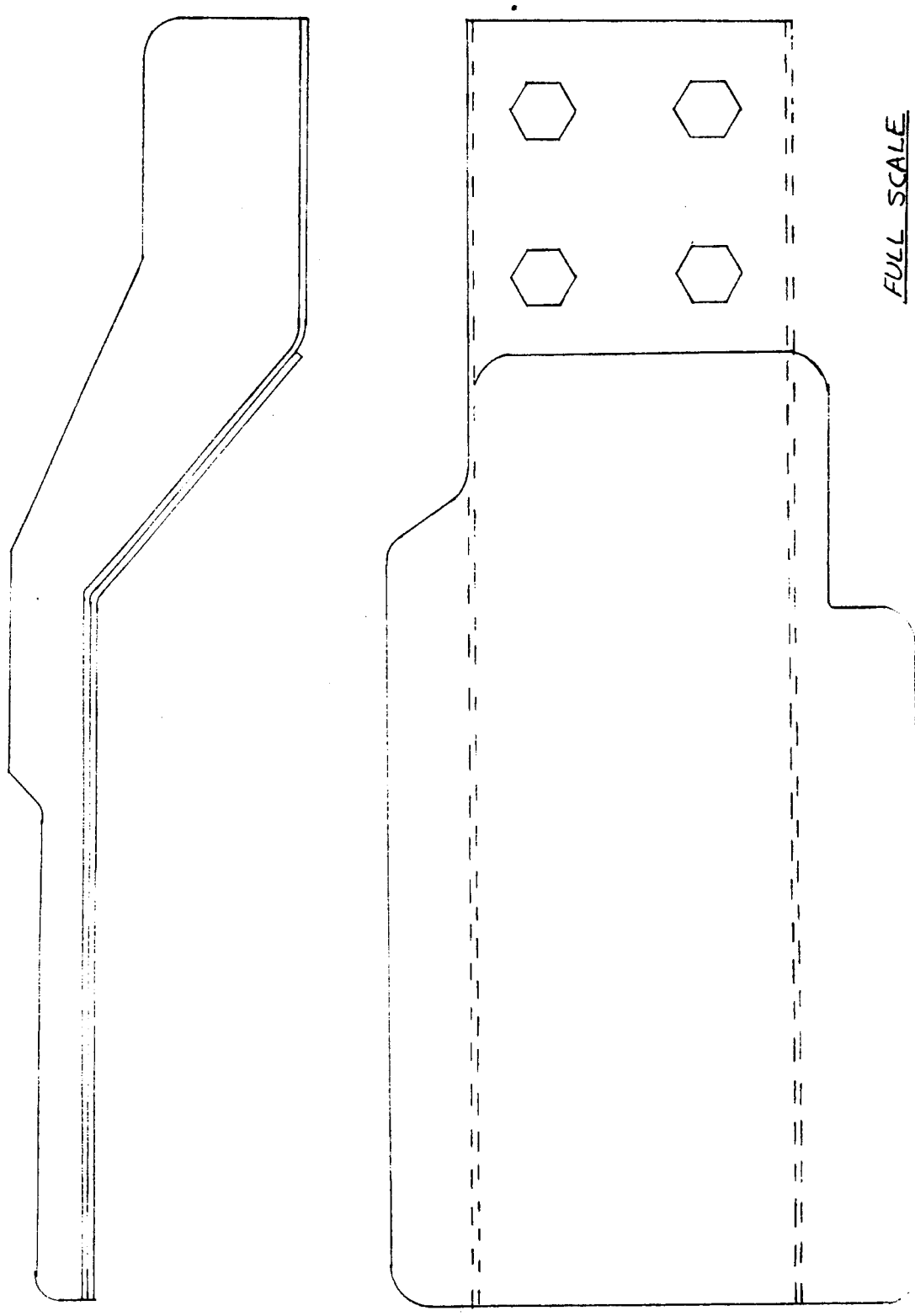

FIGURE 30
LOWER SUPPORT LUG

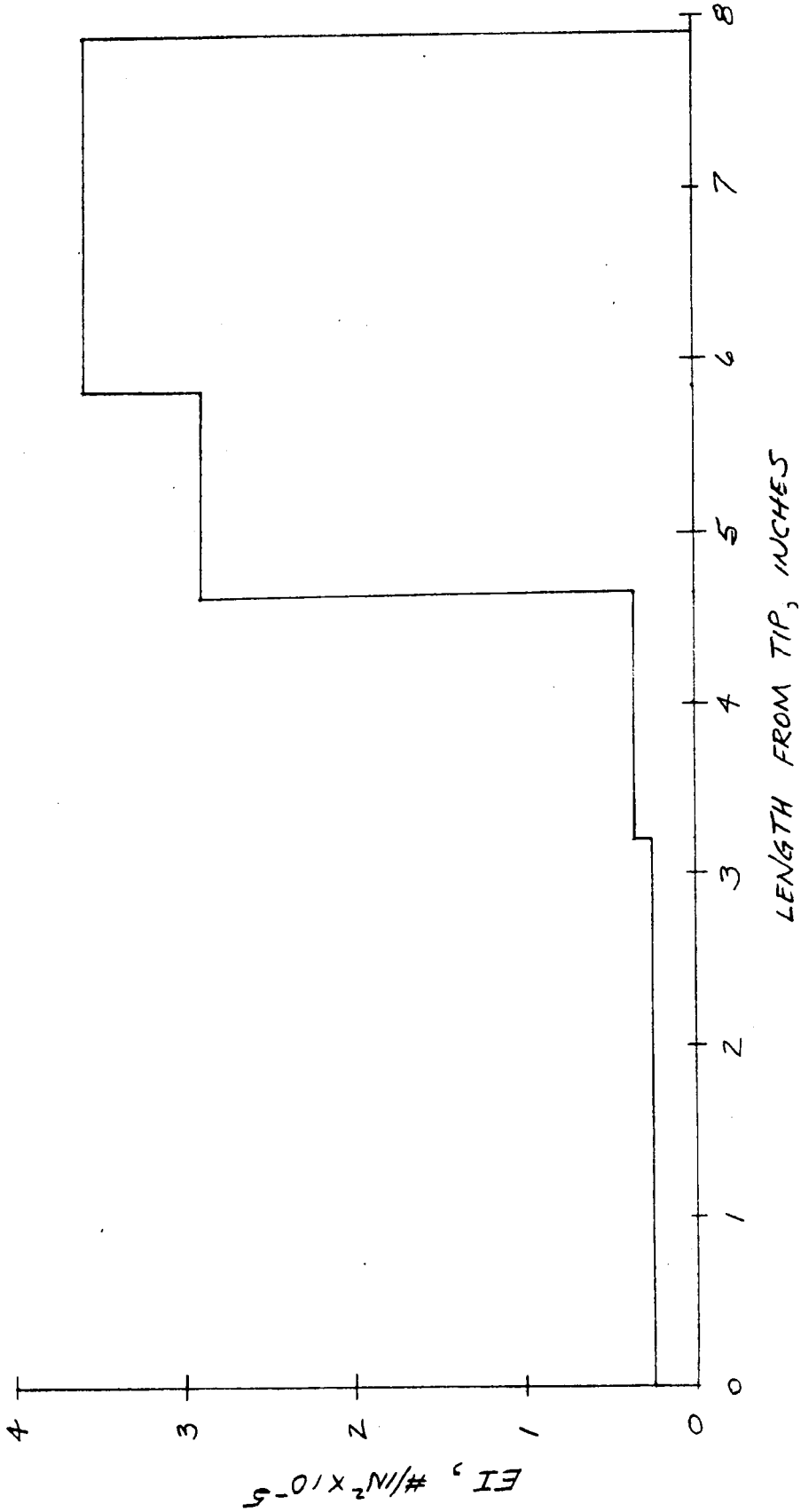

FIGURE 31
LOWER SUPPORT LUG
STIFFNESS DISTRIBUTION